

Biomedical Optics (BIOMED)

28 April - 2 May 2012, Miami, Florida, United States

There are few basic biological science studies that are not touched by biomedical optics. Optical methods play a critical role in biotechnologies ranging from genomics to cell-based assays to *in vivo* imaging and therapies. In light of this, the importance of biomedical optics has never been greater. The upcoming Biomedical Optics meeting covers the diversity of cutting edge biomedical research and brings together leading scientists, engineers and physicians engaged in biological and medical research using optical methods. With over 400 attendees, this *must-attend* meeting affords attendees the opportunity to interact one-on-one with oral presenters, along with multiple poster sessions allowing for lively discussions of the latest research.

[Online Access to Technical Digest Now Available!](#)

Full Technical Attendees now have an alternate way to access the digest papers at the meeting. Access the papers through [Optics InfoBase](#) using the same login email address and password provided during the meeting registration process. Access is currently limited to Biomedical Optics and Three-Dimensional Imaging Full Technical Attendees only. If you need assistance with your login information, please use the forgot password utility or "Contact Help" link.

NEW! [Recorded Technical Sessions on Demand](#)

We are excited to announce a new enhancement to the value of your registration to this year's conference! Selected sessions (including all plenary talks) from the Biomedical Optics Topical Meeting as well as the Joint BIOMED/DH Plenary will be recorded. This content is presented as audio-recording synched with the speakers' power point presentations. All registered full technical attendees will have complimentary access to the program content for a period of 60 days post conference. Recorded content will be available 24 hours following its presentation.

Congratulations to the following Biomedical Optics Student Award Winners:

1st Place Award Winners

Qiaoya Lin, *Univ. Health Network, Canada*

Paper: "In vivo near infrared fluorescence imaging of efficient systemic siRNA delivery with HDL-mimicking peptide lipid nanoparticles"

Ludguier Montejó, *Columbia Univ., USA*

Paper: "Classification of OT Images of Arthritic Joints Using Spatial-Fourier Frequency Coefficients"

Tracy Liu, *Univ. of Toronto/Ontario Cancer Inst., Canada*

Paper: "Photodynamic Molecular Beacons: An Image -Guided Therapeutic Approach for Vertebral Metastases"

Kelly Michaelsen, *Dartmouth College, USA*

Paper: "Using Partial Frequency Domain Data to Improve Reconstruction Accuracy in Continuous Wave Breast Tomosynthesis Guided Diffuse Optical Spectroscopy"

Lingling Chen, *Photonics Group, Department of Physics, Imperial College London, UK*

Paper: "Improved OPT Reconstructions Based on the MTF and Extension to FLIM-OPT"

Yu Wang, *Washington Univ. in St. Louis, USA*

Paper: "Spectrally Encoded Photoacoustic Microscopy Using a Digital Mirror Device"

Thomas Klein, *Ludwig-Maximilians-Universität München, Germany*

Paper: "Multi-MHz retinal OCT imaging using an FDML laser"

Yan Zeng, *Hong Kong Univ. of Science of Technology, Hong Kong*

Paper: "In vivo Cytometry using Two-photon Autofluorescence Microscopy"

Dam Glaser, *Dartmouth College, USA*

Paper: "Cherenkov Emission Spectroscopy for Tissue Oxygen Saturation Assessment"

Andrew Gomes, *Northwestern Univ., USA*

Paper: "In Vivo Measurement of Carcinogenesis-Associated Shape Alterations of the Refractive Index Correlation Function"

2nd Place Award Winners

Jonathan Elliott, *Univ. of Western Ontario, Canada*

Paper: "Cerebral blood flow quantification during ischemia using a multi-distance moments-based time-resolved technique"

Georgios Mallas, *Northeastern Univ. & MGH, USA*

Paper: "Combined Image Deconvolution and Attenuation Correction for Intravascular Near Infrared Fluorescence Imaging"

Mahlega Hassanpour, *Washington Univ. in St. Louis, USA*

Paper: "Optimizing statistical analysis for DOT to image rapid brain function events"

Rabah Al abdi, *SUNY D.M.C., USA*

Paper: "Carbogen Inspiration Enhances Hemodynamic Contrast in the Cancerous Breast"

Sarah Erickson, *Florida Inst. of Technology, USA*

Paper: "In vivo Breast Imaging Using a Gen-2 Hand-Held Optical Imager"

Behnoosh Tavakoli, *Univ. of Connecticut, USA*

Paper: "Solving Inverse Problem of Diffuse Optical Tomography with Global Optimization"

Hector Basevi, *Univ. of Birmingham, UK*

Paper: "Application of Compressive Sensing to Bioluminescence Tomography"

Elizabeth Huynh, *Univ. Health Network, Canada*

Paper: "Generation of Photonic Shell Microbubbles"

Chi Zhang, *Washington Univ. in St. Louis, USA*

Paper: "Reflection-mode submicron-resolution photoacoustic microscopy in vivo"

Adeel Ahmad, *Univ. of Illinois at Urbana Champaign*

Paper: "Magnetomotive Contrast in Optical Coherence Tomography for Detecting Early-stage Atherosclerosis Using Targeted Microspheres"

Stefan Zotter, *Medical Univ. of Austria, Austria*

Paper: "Wide-field, High-speed Polarization Sensitive Spectral Domain OCT for Measuring Retardation, Birefringence and Retinal Nerve Fiber Layer Thickness"

Jiefeng Xi, *Johns Hopkins Univ., USA*

Paper: "Real-time Three-Dimensional Dynamic Imaging of Lower Airway Using Swept Source Optical Coherence Tomography"

Taewoo Kim, *Univ. of Illinois at Urbana Champaign, USA*

Paper: "Phase Derivative Microscopy for Label-free Imaging of Dynamic Biological Structures"

Louis Gagnon, *Harvard Univ., USA*

Paper: "Computation of Baseline Flow Across the Mouse Cortex Using Two-photon Microscopy and Vascular Anatomical Network Modeling"

David Busch, *Univ. of Pennsylvania, USA*

Paper: "Microvascular Blood Flow Changes in Human Breast During Simulated Mammography"

Ilaria Bargigia, *Politecnico di Milano, Italy*

Paper: "Optical Spectroscopy up to 1700 nm: a Time-Resolved Approach Combined with an InGaAs/InP Single-Photon Avalanche Diode"

Timothy Baran, *Univ. of Rochester, USA*

Paper: "Image-Guided Treatment Planning and Dosimetry for Interstitial Photodynamic Therapy"

Plenary and Invited Speakers



The Invention and Early History of the CCD

[George Smith](#)

Recipient of 2009 Nobel Prize in Physics

[Special Events](#)

The congress has a variety of special events throughout the meeting including the OIDA Rump session, Congress Reception and special presentations. For more detailed information, view our [Special Events](#) page.

Topic Categories

BIO 1: Biomedical Applications of Digital Holography

BIO 2: BioNanophotonic and Molecular Probes

- Novel Molecular and Functional Contrast Agents
- Metal Nanoparticles
- Quantum Dots
- Inorganic/Organic Hybrid Materials
- Multifunctional Nanoparticles
- Surface Enhanced Raman Scattering and Surface Enhanced Fluorescence
- Single Molecule Techniques
- Molecular and Functional Imaging Applications
- Photodynamic Therapy
- *In vitro*, *in vivo* and Clinical Applications of Molecular Probes

BIO 3: Optical Microscopy Techniques

- Microscopy *in vivo*
- Spectral Microscopy
- Multiphoton/Nonlinear Microscopy
- Super Resolution Microscopy
- Novel Forms of Microscopy
- Endoscopic Microscopy
- Multimodal Microscopy
- *In vivo* Applications and Clinical Translation

BIO 4: Photoacoustic Imaging and Spectroscopy

- Photoacoustic Tomography
- Photoacoustic Microscopy
- Functional Photoacoustic Imaging
- Ultrasound Modulated Optical Imaging
- Photoacoustic Endoscopy
- Multimodal Photoacoustic Imaging
- Photoacoustic Molecular Imaging
- *In vivo* and Clinical Applications of Photoacoustic Techniques

BIO 5: Optical Coherence Tomography

- OCT Technology Development
- OCT Light Source Development
- Ultrahigh Resolution and Ultrahigh Speed OCT
- Functional OCT (Doppler, Polarization Sensitive and Others)
- Contrast Enhancement Techniques in OCT
- Optical Coherence Microscopy
- Phase Sensitive OCT Technology
- Multimodal Techniques
- Biomedical and Clinical Applications of OCT

BIO 6: Optical Imaging and Tomography

- Diffuse Imaging and Spectroscopy: Clinical and *in vivo* Applications
- Instrumentation for Diffuse Optical Imaging
- Theoretical Methods and Image Reconstruction for Optical Tomography
- Diffuse Fluorescence Tomography
- Fluorescence Lifetime Tomography and Imaging
- Diffuse Correlation Spectroscopy
- Transport-Regime Modeling and Imaging
- Optical Imaging within Multimodal Neuroimaging
- Functional Imaging Techniques in Neuroscience
- Multi-Spectral Imaging

BIO 7: Optical Spectroscopy

- Fluorescence Spectroscopy and Imaging
- Phosphorescence Spectroscopy and Imaging
- Reflectance Spectroscopy and Imaging
- Mie Scattering Spectroscopy and Imaging
- Raman Spectroscopy and Imaging
- Multi-Modal Spectroscopy and Imaging
- Multi-Spectral Imaging
- Tissue Biochemistry
- Spectroscopy and Imaging in Tissue Engineering
- In vivo and Clinical Applications of Optical Spectroscopy
- Low Level Laser Therapy
- Laser Tissue Ablation and Optical Breakdown

OSA is pleased to announce that a special issue of [Biomedical Optics Express](#) will be dedicated to material presented at the meeting. More information on this will appear in early 2012 on the journal's [Feature Issue page](#).

General Chair

Claude Albert Boccara, *ESPCI, France*, General Chair
 Xingde Li, *Johns Hopkins Univ., USA*, General Chair
 Lev T. Perelman, *Harvard Univ., USA*, General Chair

Sponsor:



Biomedical Optics and 3D Imaging

29 April - 2 May 2012, Miami Hilton Downtown, Miami, Florida, USA

[Online Access to Technical Digest Now Available!](#)

Full Technical Attendees now have an alternate way to access the digest papers at the meeting. Access the papers through [Optics InfoBase](#) using the same login email address and password provided during the meeting registration process. Access is currently limited to Biomedical Optics and Three-Dimensional Imaging Full Technical Attendees only. If you need assistance with your login information, please use the forgot password utility or "Contact Help" link.

NEW! [Recorded Technical Sessions on Demand](#)

We are excited to announce a new enhancement to the value of your registration to this year's conference! Selected sessions (including all plenary talks) from the Biomedical Optics Topical Meeting as well as the Joint BIOMED/DH Plenary will be recorded. This content is presented as audio-recording synched with the speakers' power point presentations. All registered full technical attendees will have complimentary access to the program content for a period of 60 days post conference. Recorded content will be available 24 hours following its presentation.

Congress Joint Plenary Speakers:



[Byounggho Lee](#), *Seoul National Univ., South Korea*
3D Display - Where We Are and Where to Go



[George Smith](#)
Recipient of 2009 Nobel Prize in Physics
The Invention and Early History of the CCD

A general scope for the two meetings in the congress is listed below, and more detailed information (including the list of topics for consideration) for each topical meeting is available by following the meeting link.

[Biomedical Optics](#)

The Biomedical Optics meeting covers the diversity of cutting edge biomedical research topics and brings together leading scientists, engineers and physicians engaged in forefront biological and medical research using optical methods. Advances in biological and drug delivery imaging, optical coherence tomography, microscopy, optical probe development, and the application of bio-optical techniques in clinical environments will be covered. Optical bio/medical imaging is now established as offering unique capabilities that compliment and in several cases exceed the capabilities of related imaging approaches such as PET and CT imaging. This optical technology is being developed for image guided surgery, imaging of bio-markers, drug delivery studies

and shallow tissue imaging with research trying to extend the range to deep tissue. In multiple laboratories, optical nano-technologies are being studied for enhanced molecular probing to examine cell function as well as early disease detection and monitoring. Optical technologies also offer the promise of improved therapies for several medical problems. This meeting will present comprehensive review of the latest important advances in biomedical optical field.

Digital Holography and 3D Imaging

This topical meeting consists of two closely interrelated topics; 3D display and digital holography. The aspect of the meeting covering digital holography provides a forum for disseminating the latest research results in the field of holographic and digital methods and its use in the solution of difficult optical imaging problems in research and field application. The other principal topic covered relates to the latest advances in the technological development of 3D display technology for research as well as commercial applications. Digital holographic topics cover recent advances in the development of holographic devices and material used therein, compressive holographic approaches, readout and holographic formation for volume storage, and uses of the technology to solve problems in laser radar and communications, phase error correction, imaging through turbidity, and tissue imaging using non-linear holographic microscopic technologies to mention a few.

Topics included in the 3D display section of the meeting illustrate advances that are leading to commercialization of this technology. The latest advances in display technology including 3D sensing, 3D visualization, stereoscopic 3D technologies, lens-less image projection, volumetric displays using holography, multiple projector displays, etc will be reviewed by well known experts in this field. This meeting as a whole provides the attendees a comprehensive picture of the state of the art in 3D display and digital holography.

Special Events

The congress has a variety of special events throughout the meeting including the OIDA Rump session, Congress Reception and special presentations. For more detailed information, view our [Special Events](#) page.

Corporate Sponsor:



Sponsor:



Biomedical Optics (BIOMED)

28 April - 2 May 2012, Miami, Florida, United States

Conference Program

About Biomedical Optics

Biomedical Optics (BIOMED): There are few basic biological science studies that are not touched by biomedical optics. Optical methods play a critical role in biotechnologies ranging from genomics to cell-based assays to in vivo imaging and therapies. In light of this, the importance of biomedical optics has never been greater. The upcoming Biomedical Optics meeting covers the diversity of cutting edge biomedical research and brings together leading scientists, engineers and physicians engaged in biological and medical research using optical methods.

Plenary Speakers

Joint Plenary



[George Smith](#), Recipient of 2009 Nobel Prize in Physics
Monday, 30 April
08:00-08:45 a.m., Symphony I & II

The Invention and Early History of the CCD

Abstract: As the first practical solid state imaging device, the invention of the Charge Coupled Device has profoundly affected image sensing technology. They are used in a wide range of applications both as area and linear imaging devices starting with the replacement of imaging tubes used in commercial TV cameras and cam-corders. The rapid rise of their use in digital cameras has initiated the demise of film photography and created vast new markets with great economic benefit for many. Other uses include a wide variety of scientific, medical, surveillance and scanning applications. The inception of the device at Bell Labs by Willard S. Boyle and George E. Smith in 1969 was strongly influenced by several unique factors existing both within Bell Labs and the current world state of technology. These factors and their relevance will be discussed along with the train of thought leading to the invention. Early experimental devices and their initial applications were vigorously pursued and will be described. Mention of current applications will be given.



[Byoungho Lee](#),

Seoul National Univ., South Korea

Monday 30 April

08:45 – 09:30 a.m., Symphony I & II

3D Display - Where We Are and Where to Go

Abstract: An overview of history and present state of three-dimensional display is given, covering technical and market aspects. Possible research directions that will be considered important in the future are also discussed.

BIOMED Plenary



[Mathias Fink](#),

Langevin Institute ESPCI ParisTech, France

Sunday, 29 April

08:45 - 09:30, Symphony I & II

BIOMEDical Applications of Ultrasonic Time-reversal

Abstract: An overview on research conducted on ultrasonic time-reversal methods medical applications. Time-reversal focuses wave through complex and heterogeneous media and shows exciting results both in ultrasound therapy and ultrasonic imaging.



[Bruce J. Tromberg](#),

Beckman Laser Institute and Medical Clinic, University of California, Irvine, USA

Tuesday, 1 May

08:00 - 08:45, Symphony I & II

Diffuse Optical Spectroscopy: Technology Development and Clinical Translation

Abstract: This talk describes the development of Diffuse Optical Spectroscopy (DOS) using spatially- and temporally-modulated sources and model-based analyses. DOS methods are capable of dynamic in vivo functional imaging with variable, but limited, spatial localization. Multiple optical contrast elements such as absorption, scattering, fluorescence, and speckle are detectable at relatively low cost. Quantitation of these signals can be achieved using methods for controlling optical path length in conjunction with computational models and visualization techniques.



[Lihong Wang](#),

Washington Univ. in St. Louis, USA

Sunday, 29 April
08:00 - 08:45, Symphony I & II

Photoacoustic Tomography: Ultrasonically Breaking through the Optical Diffusion Limit

Abstract: PAT, embodied in the forms of scanning photoacoustic microscopy or photoacoustic computed tomography, is the only modality capable of imaging across the length scales of organelles, cells, tissues, and organs with consistent contrast.



[Xiaowei Zhuang](#),
Howard Hughes Medical Inst., Harvard Univ., USA
Tuesday, 1 May
08:45 - 09:30, Symphony I & II

Bioimaging at the nanoscale: Single-molecule and super-resolution fluorescence microscopy

Abstract: Optical microscopy is an essential tool in biological research. However, the spatial resolution of optical microscopy, classically limited by diffraction to several hundred nanometers, is substantially larger than typical molecular length scales in cells, leaving many biological structures unresolvable. We recently developed a new form of super-resolution light microscopy, stochastic optical reconstruction microscopy (STORM), that surpasses the diffraction limit. STORM uses single-molecule imaging and photoswitchable fluorescent probes to temporally separate the spatially overlapping images of individual molecules. This approach allows the localization of fluorescent probes with nanometer precision and the construction of sub-diffraction-limit images. Using this method, we have achieved multicolor and three-dimensional (3D) imaging of living cells with nanometer-scale resolution. In this talk, I will discuss the general concept, recent technical advances and biological applications of STORM.

Special Events

The congress has a variety of special events throughout the meeting including the OIDA Rump session, Congress Reception and special presentations. For more detailed information, view our [Special Events](#) page

Biomedical Optics (BIOMED)

28 April - 2 May 2012, Miami, Florida, United States

Invited Speakers

Plenary



[George Smith](#)

Recipient of 2009 Nobel Prize in Physics

The Invention and Early History of the CCD

Abstract: As the first practical solid state imaging device, the invention of the Charge Coupled Device has profoundly affected image sensing technology. They are used in a wide range of applications both as area and linear imaging devices starting with the replacement of imaging tubes used in commercial TV cameras and cam-corders. The rapid rise of their use in digital cameras has initiated the demise of film photography and created vast new markets with great economic benefit for many. Other uses include a wide variety of scientific, medical, surveillance and scanning applications. The inception of the device at Bell Labs by Willard S. Boyle and George E. Smith in 1969 was strongly influenced by several unique factors existing both within Bell Labs and the current world state of technology. These factors and their relevance will be discussed along with the train of thought leading to the invention. Early experimental devices and their initial applications were vigorously pursued and will be described. Mention of current applications will be given.



[Mathias Fink](#), *Langevin Institute ESPCI ParisTech, France*

Time Reversal in Biomedical Methods

Abstract: This talk will present an overview of the research conducted on ultrasonic time-reversal methods in the field of medical applications. Time-reversal is a very powerful method for focusing wave through complex and heterogeneous media and shows exciting results both in ultrasound therapy and ultrasonic imaging. In the field of therapy we will first describe iterative time-reversal techniques that allow tracking and focusing ultrasonic waves on strong reflectors in tissues (kidney stones, micro-calcifications). Spatio-temporal focusing of ultrasonic waves in reverberating cavities will be described to obtain very intense focused shock waves (ultrasonic bazookas !!). This is the field of lithotripsy and histotripsy. Because time reversal is also able to correct for the strong distortions induced by the skull bone on ultrasonic propagation, this adaptive focusing technique allows non-invasive therapy of brain diseases and high resolution brain neurostimulation. We will show that time-reversal focusing does not need the presence of bright reflectors but it can be achieved only from the speckle noise generated by random distributions of non-resolved scatterers. We will describe the applications of this concept to correct distortions and aberrations in ultrasonic imaging.



[ByoungHo Lee](#), *Seoul National Univ., South Korea*
3D Display - Where We Are and Where to Go

Abstract: An overview of history and present state of three-dimensional display is given, covering technical and market aspects. Possible research directions that will be considered important in the future are also discussed.



[Bruce J. Tromberg](#), *Beckman Laser Institute and Medical Clinic, University of California, Irvine, USA*
Diffuse Optical Spectroscopy: Technology Development and Clinical Translation

Abstract: Although NIR light penetrates tissue to depths of several centimeters, quantifying the magnitude and origin of biological processes in specific tissue compartments remains a significant challenge. At depths of approximately 1 mm and greater, multiple-scattering dominates light propagation in tissue. Under these conditions, optical phase relationships become randomized and coherent properties of light are generally not detectable. In this regime, light transport can be described using mathematical models where photons behave as stochastic particles that move in proportion to a gradient, much like the diffusive movement of molecules or heat. Several experimental approaches, generally referred to as "Diffuse Optics" methods, have been developed to quantify multiple scattering and measure thick tissue function.

This talk describes the development of Diffuse Optical Spectroscopy (DOS) using spatially- and temporally-modulated sources and model-based analyses. DOS methods are capable of dynamic in vivo functional imaging with variable, but limited, spatial localization. Multiple optical contrast elements such as absorption, scattering, fluorescence, and speckle are detectable at relatively low cost. Quantitation of these signals can be achieved using methods for controlling optical path length in conjunction with computational models and visualization techniques. This allows formation of 2 and 3D images of various optical and physiological properties such as blood flow, vascular density, extracellular matrix composition, and cellular metabolism. Particular emphasis is placed on determining the tissue concentration of oxy- and deoxyhemoglobin, lipid, and water, as well as tissue scattering parameters. Clinical study results will be shown highlighting the sensitivity of broadband DOS to breast tumor metabolism with sufficient sensitivity for cancer detection and therapeutic drug monitoring. Broadband spatial frequency-domain imaging is used in pre-clinical animal models to dynamically map intrinsic brain signals, monitor the efficacy of chemotherapeutic agents, and form depth-resolved tomographic images of fluorescence and hemodynamics. These findings will be placed in the context of conventional imaging methods in order to assess the current and future role of diffuse optics in medical imaging.



[Lihong Wang](#), *Washington Univ. in St. Louis, USA*
Photoacoustic Tomography: Ultrasonically Breaking through the Optical Diffusion Limit

Abstract: Photoacoustic tomography (PAT), combining optical and ultrasonic waves via the photoacoustic effect, provides in vivo multiscale non-ionizing functional and molecular imaging. Light offers rich tissue contrast but does not penetrate biological tissue in straight paths as x-rays do. Consequently, high-resolution pure optical imaging (e.g., confocal microscopy, two-photon microscopy, and optical coherence tomography) is limited to depths within the optical diffusion limit (~1 mm in the skin). Ultrasonic imaging, on the contrary, provides good image resolution but suffers from poor contrast in early-stage tumors as well

as strong speckle artifacts. In PAT, pulsed laser light penetrates the tissue and generates a small but rapid temperature rise, which induces emission of ultrasonic waves due to thermoelastic expansion. The ultrasonic waves, ~1000 times less scattering than optical waves in tissue, are then detected to form high-resolution images at depths up to 7 cm, breaking through the optical diffusion limit. Further depths can be reached by using microwaves or RF waves as the excitation source. PAT, embodied in the forms of scanning photoacoustic microscopy or photoacoustic computed tomography, is the only modality capable of imaging across the length scales of organelles, cells, tissues, and organs with consistent contrast. Such a technology has the potential to enable multiscale systems biology and accelerate translation from microscopic laboratory discoveries to macroscopic clinical practice. PAT may also hold the key to the earliest detection of cancer by in vivo label-free quantification of hypermetabolism, the quintessential hallmark of cancer. The technology is commercialized by several companies.



[Xiaowei Zhuang](#), *Howard Hughes Medical Inst., Harvard Univ., USA*

Bioimaging at the nanoscale: Single-molecule and super-resolution fluorescence microscopy

Abstract: Optical microscopy is an essential tool in biological research. However, the spatial resolution of optical microscopy, classically limited by diffraction to several hundred nanometers, is substantially larger than typical molecular length scales in cells, leaving many biological structures unresolvable. We recently developed a new form of super-resolution light microscopy, stochastic optical reconstruction microscopy (STORM), that surpasses the diffraction limit. STORM uses single-molecule imaging and photoswitchable fluorescent probes to temporally separate the spatially overlapping images of individual molecules. This approach allows the localization of fluorescent probes with nanometer precision and the construction of sub-diffraction-limit images. Using this method, we have achieved multicolor and three-dimensional (3D) imaging of living cells with nanometer-scale resolution. In this talk, I will discuss the general concept, recent technical advances and biological applications of STORM.

BIO 1: Biomedical Applications of Digital Holography

BIO 2: BioNanophotonic and Molecular Probes

Imaging RNA in Single Living Cells: Recent Advances and Future Outlook, Andrew Tsourkas, *Univ. of Pennsylvania, USA*

Molecular Probes in Photodynamic Therapy, Tayyaba Hasan, *Harvard Medical School, USA*

BIO 3: Optical Microscopy Techniques

ePetri: Self-imaging Petri Dish Platform for Autonomous Cell Culture Tracking, Changhui Yang, *Caltech, USA*

BIO 4: Photoacoustic Imaging and Spectroscopy

Sound and Light Catheters, Ton van der Steen, *Erasmus MC, Netherlands*

Detecting Circulating Tumor Cells (CTCs) with Integrated Photoacoustic/Ultrasonic Imaging, Matthew O'Donnell, *Univ. of Washington, USA*

BIO 5: Optical Coherence Tomography

Intraoperative OCT for Vitreoretinal Surgery, Joseph Izatt, *Duke Univ., USA*

Applying OCT to Dermatology: Technology, Clinical Applications, and the Translational Process, Jon Holmes, *Michaelson Diagnostics Ltd., UK*

BIO 6: Optical Imaging and Tomography

Wide-field Time Resolved Optical Tomography, Xavier Intes, *RPI Rensselaer Polytechnic Inst., USA*

Functional Imaging Techniques in Neuroscience, Mark Pflieger, *Source Signal Imaging, Inc., USA*

Near-infrared Imaging of Breast Cancer Using Intrinsic and Extrinsic Contrast Agents, Alexander Poellinger, *Charité, Germany*

Bed-side Neuro-critical Monitoring with Hybrid Diffuse Optics, Turgut Durduran, *ICFO, Spain*

BIO 7: Optical Spectroscopy

Multi-spectral Morphology Scanning for Margin Detection in Breast Surgery, Brian W. Pogue, *Dartmouth College, USA*

Quantitative Monitoring of Apoptosis in Viable Cells with Elastic Scattering Spectroscopy, Irving Bigio, *Boston University, USA*

Two-photon Excited Blood Autofluorescence for In Vivo Imaging and Flow Cytometry, Jianan Y. Qu, *The Hong Kong University of Science & Technology, China*

Biomedical Optics and 3D Imaging

29 April - 2 May 2012, Miami Hilton Downtown, Miami, Florida, USA

Special Events

[Nirfast Pre-Conference Training Workshop](#)

27 – 28 April, 2012

Separate registration required for this workshop

This nirfast workshop is prior to the OSA Biomedical and 3D Imaging Congress. The goal of this workshop is to provide hands-on instruction with NIRFAST for modeling light transport in tissue. The workshop will cover basic aspects of Nirfast and will include user driven examples on modeling light transport in tissues and performing tomographic image reconstruction.

Plenary Sessions

BIOMED Plenary I - BSu1A

Sunday, 29 April

08:00 - 09:30

Symphony I & II

Don't miss the opening BIOMED plenary session features for the following speakers:



[Lihong Wang](#), *Washington Univ. in St. Louis, USA*

Photoacoustic Tomography: Ultrasonically Breaking through the Optical Diffusion Limit



[Mathias Fink](#), *Langevin Institute ESPCI ParisTech, France*

Time Reversal in Biomedical Methods

Joint Biomed and DH Plenary

Monday, 30 April

08:00 - 09:30

Symphony I & II

Joint Plenary features world-renown leaders in their fields, Nobel Prize Winner, George Smith and ByoungHo Lee.



[George Smith](#)

Recipient of 2009 Nobel Prize in Physics

The Invention and Early History of the CCD



[Byoungho Lee](#), *Seoul National Univ., South Korea*

3D Display - Where We Are and Where to Go

Biomed Plenary II - **BTu1A**

Tuesday, 1 May

08:00 - 09:30

Symphony I & II

This Biomed Plenary features these two exciting speakers:



[Bruce J. Tromberg](#), *Beckman Laser Institute and Medical Clinic, University of California, Irvine, USA*

Diffuse Optical Spectroscopy: Technology Development and Clinical Translation



[Xiaowei Zhuang](#), *Howard Hughes Medical Inst., Harvard Univ., USA*

Bioimaging at the nanoscale: Single-molecule and super-resolution fluorescence microscopy

Conference Reception

Monday, 30 April
18:30 - 20:00
Overture Foyer & Concerto Ballroom

Complimentary to technical attendees! This Reception brings together all the attendees including exhibitors from the Biomedical Optics and Digital Holography & 3D Imaging Congress for a fun evening of networking with light appetizers and drinks.

DH Tutorials

DH Tutorial - DTu1C.1



Myung K. Kim, *Univ. of South Florida, USA*
8:00 - 8:45
Symphony IV

Title to be announced.

DH Tutorial - DTu2C.1



[Partha P. Banerjee](#), *Univ. of Dayton, USA*
Tuesday, 1 May
10:00-10:45
Symphony IV

Digital Holographic Interferometry - Principles and Applications to Deformation Measurement

Abstract: Starting from basic principles of holography and digital holography, we discuss its application to digital holographic interferometry for 3D object deformation. Dual wavelength holography, digital holographic microscopy and single beam holographic tomography are also discussed

Poster Sessions

Sunday, 29 April, 13:00-15:00, BSu3A
Monday, 30 April, 13:30-15:00, JM3A
Tuesday, 1 May, 13:00-15:00, BTu3A
Concerto Ballroom and Overture Foyer

The poster sessions are an integral part of the technical program and offer a unique networking opportunity, where presenters can discuss their results one-to-one with interested parties. Each author is provided with board on which to display the summary and results of his or her paper.

Postdeadline Papers Sessions

BIOMED Postdeadline Session

Sunday, 29 April

18:30-20:40

Symphony I & II

DH Postdeadline Session

Sunday, 29 April

18:30-19:45

Symphony IV

The postdeadline papers sessions will give participants the opportunity to hear new and significant material in rapidly advancing areas. Only those papers judged to be truly excellent and compelling in their timeliness were accepted. More information, including the schedule, will be posted in the weeks preceding the conference.

OIDA Networking Reception and Rump Session

Sponsored by Hamamatsu Photonics K.K.

Tuesday, 1 May

18:00 - 20:00,

Symphony IV

Complimentary to Congress Technical Attendees

OSA's 2012 Biomedical Optics and 3-D Imaging Congress will include a special event hosted by the [Optoelectronics Industry Development Association \(OIDA\)](#) and **Hamamatsu Photonics K.K.** This session will be a unique opportunity to exchange ideas in an energized and fun environment and *we look forward to your joining in!*

Program Description: An early evening reception and session that engages research and industry attendees in a fast-paced, highly participatory discussion of a topic of key interest to both the academic and applied communities. Guest speakers will make brief presentations on "Growth opportunities for photonics companies in healthcare" followed by an "open microphone" segment where attendees are asked to address the audience with their

Program Schedule

Networking Reception: 30 minutes

Session: 5-Minute

Guest Presentations: 20-30 minutes

Open microphone: 30+ minutes

RUMP Session Planning Committee

Adam Wax, *Duke University*

Tom Baer, *Stanford University*

Ken Kauffman, *Hamamatsu, USA*

Irene Georgakoudi, *Tufts University*

Thank You Program Sponsor & OIDA Member



Biomedical Optics and 3-D Imaging Congress: Topical Meeting Exhibit 2012

- **Biomedical Optics (BIOMED)**
- **Digital Holography and Three-Dimensional Imaging (DH)**

28 April – 2 May, 2012 ♦ Miami Hilton Downtown, Miami, Florida, USA

Welcome!

We are glad you will be joining us in Sunny Miami! This packet should include what you need to prepare for the meeting. If you have any questions or need more information, please contact Melissa Lanham, Meeting and Exhibits Coordinator, at topicalexhibits@osa.org or +1 202.416.1928.

Exhibitor Service Manual

Please provide this information to anyone who will be attending the meeting and staffing your company's table.

All exhibit space will be assigned on-site based on the order of when a space contract was received.

Deadlines Summary

Date	Deadline
19 March 2012	75 word description of company due for exhibitor listing (See Buyers Guide Submission Instructions form)
19 March 2012	Exhibitor Response Form Due (included in packet)
19 March 2012	Registration forms due (fax to +1 202.416.6100 or email topicalexhibits@osa.org) (See Exhibitor Registration Form included in packet)
29 March 2012	Housing reservations due
29 March 2012	Final day to order electrical power, internet or other services from the Hotel. (See order form included in this packet)
26 April 2012	The Miami Hilton Downtown begins accepting shipments from exhibitors; shipments received any earlier will incur storage charges. (See Shipping Guidelines included in this packet)

Exhibit Schedule

(For a complete schedule of the meeting, visit the Agenda of Sessions on the [OSA Congress website](#))

Sunday, 29 April

Event	Time
Registration Open	7:00 – 18:00
Exhibitor Set-Up	7:00 – 13:00 15:30 – 18:00
Exhibit and Poster Session	13:00 – 15:00
Optional Coffee Break	15:00 – 15:30

(Exhibitor's note – it is optional to exhibit this day, but recommended as there are "set" exhibit hours planned that coincide with the Poster Session)

Monday, 30 April

Event	Time
Registration Open	7:00 – 18:30
Exhibitor Set-Up	7:00 – 9:00
Exhibit and Poster Session	13:00 – 15:00
Exhibit and Reception	18:30 – 20:00
Optional Coffee Break	9:30 – 10:00 15:00 – 15:30

All exhibitors must be ready and have their displays set no later than 9:00.

Tuesday, 1 May

Event	Time
Registration Open	7:30 – 18:00
Exhibit and Poster Session	13:00 – 15:00
Optional Coffee Breaks	9:30 – 10:00 15:00 – 15:30
Exhibit Break Down (if you are not staying for the optional Coffee Breaks on Wednesday)	15:30 – 18:00

Do not dismantle displays before Coffee Break is over.

Wednesday, 2 May

Event	Time
Registration Open	7:30 – 17:00
Optional Coffee Breaks	10:00 – 10:30 15:30 – 16:00
Exhibit Break Down (if you are staying for the optional Coffee Breaks)	10:30 – 15:00 16:00 – 17:00

Do not dismantle displays before Coffee Break is over.

IMPORTANT EXHIBITOR NOTE:

* We do not require that you remain at your display for the entire conference. **However, tables should be staffed during Exhibit and Poster Session hours listed above.** Attendee traffic patterns vary for each meeting. Most attendees will leave the technical sessions for the coffee breaks that are located in the exhibit hall, but will then return to the sessions. If you decide to not staff your display during coffee breaks, please secure all belongings as attendees will have access to displays due to being in the same room as the coffee breaks. Exhibit traffic is limited during other times. Reach out to attendees and schedule meetings, extend yourself for extra time and/or go to the sessions. If you are interested in scheduling appointments over a meal, Unopposed Lunch and/or Dinner times are as follows:

Sunday, 29 April

Lunch	12:00 – 13:00
Dinner	17:30 – 18:30 After 20:00

Monday, 30 April

Lunch	12:00 – 13:00
Dinner	After 20:00

Tuesday, 1 May

Lunch	12:00 – 13:00
Dinner	After 19:00

Wednesday, 2 May

Lunch	12:30 – 13:30
Dinner	After 16:15

- For more information contact Melissa Lanham at topical Exhibits@osa.org or +1 202.416.1928.

Exhibit Details

The exhibit, coffee break, conference reception and a majority of the scheduled poster session(s) will be held in **Concerto ABC**.

Exhibitors will be provided with a draped table and 2 chairs. A table display sign with company name will be provided. Your display must fit completely within display space no larger than 6' wide x 2' deep x 8' tall. Decorations and signage may not be attached to or hung from any permanent structure. OSA highly encourages you to remove valuables from your exhibit when it is unattended, or bring a cover due to the location not being in a locked room or secure area. Exhibitors will be assigned location placement by OSA management.

Tabletop: Your display must fit completely on the surface of the table for a total display space no larger than 6' x 2' x 8'. Decorations and signage may not be attached to or hung from any permanent structure. The total height of all materials, including the table, must be no higher than 8 feet (approx. 2.5m).

Booths: Your display must fit completely within a 10' x 10' area which will be marked. Decoration and signage may not be attached to or hung from any permanent structure. In the front half of the booth (from aisle), the total height of all materials must not exceed 4 feet; in the back half, the total height must be no higher than 8 feet.

Exhibitors will not receive the following items that will need to be ordered separately.

- Electrical Service
- Internet Service
- Portage

Electrical Service - Deadline: Thursday, 29 March 2012

Standard 120v/60Hz voltage electricity is used in the United States.

Cost: up to 10 amps is USD \$115. 00 advanced ordering price not including labor.

Please see the enclosed order form for more information and pricing.

Electrical Service must be ordered directly from the hotel. Please fill out the Exhibitor form below and send to the hotel. Hotel contact is listed on the form.

NOTE: Electrical orders CAN NOT be placed on-site. Exhibitors may bring their own extension cords, power strips and surge protectors, but these items might also be available through the hotel for a charge. Power converters are not available and international exhibitors should bring these items. Electrical circuits may be non-exclusive and may be shared with other exhibitors.

Internet Service - Deadline: Thursday, 29 March 2012

Wireless internet is complimentary in all meeting spaces for those exhibitors who book within the official Congress hotel block.

Wired Internet service is available upon request. Cost: USD \$125/day per line not including labor.

Please see the enclosed order form for more information and pricing.

Note that the exhibit hours are flexible, and there will be time during the day to leave the exhibit area to utilize the wireless service in a guest room or meeting areas.

Exhibitor Registration

Exhibitors may pick up their badges on-site at the registration desk during meeting registration hours:

Date	Hours
Sunday, 29 January	7:00 – 18:00
Monday, 30 January	7:00 – 18:30
Tuesday, 31 January	7:30 – 18:00
Wednesday, 1 February	7:30 – 17:00

Exhibitor Badges – Deadline: Monday, March 19 2012

Exhibitors – Do not use online registration. Fax the completed registration form to +1 202.416.6100 ATTN: Cathryn Wanders by Monday, 19 March 2012

http://www.osa.org/Meetings/optics_and_photonics_congresses/Biomedical_Optics_Congress/Registration.aspx#1

Each person attending the meeting must have a badge. Each exhibiting company will receive three complimentary badges. A completed form must be submitted for each.

One Exhibitor Technical Badge – includes access to all technical sessions and receptions; one copy of technical digest on CD-ROM; one copy of conference program

Two Exhibitor Personnel Badge – access to the exhibit hall only

If an additional registration is needed, that person must purchase a technical registration. The registration form is included with this packet. Please note, by signing up to exhibit you are NOT automatically registered for the conference. A form must be submitted.

Exhibitor Listing – *Deadline: Monday, 19 March 2012*

If you have not already done so, please email the completed Buyers' Guide submission form (**form is included in this packet**) that includes a 50-75 word description of your company (including complete contact information). To have your description included in the Exhibitor Listings, it must be received by Melissa Lanham, topical Exhibits@osa.org no later than 19 March. This listing will be distributed to each registrant at the meeting. Please make sure the company contact information that you have listed is the information you want attendees to receive.

Security

The exhibit will be held in the **Concerto ABC** at the hotel that will be locked at night. The hotel has security on the property; however security will not be specifically designated to monitor the room. It is strongly recommended that you take any valuable equipment (i.e. laptops, small components, other materials) with you or secure them each night. It is also recommended that you bring a drape or cloth to cover your table each night. Each exhibitor is required to have adequate insurance levels, and basic precautions should be taken. Please do not store valuables under the table, or leave valuables objects such as phones, cameras, etc. on your table unless the booth is staffed. Management is not responsible for lost or stolen items. If you decide to not staff your display during coffee breaks, the same guidelines apply as the coffee breaks will be in the same room as the exhibit hall.

Travel

For more information about transportation to the hotel, including airline and rental car discounts and links to public transportation, please visit our [Travel Information Website](#).

Area Airport

Miami is served by [Miami International Airport](#).(MIA) It is approximately 8 miles or 15 minutes east of Hilton Miami Downtown.

Airline Discount

[American Airlines](#)

For your convenience, OSA management has arranged discounted air travel with the American Airlines. You may visit the American Airlines website at www.aa.com to search for available flights and use the authorization code **A8142AX** to receive your discount. You may also call the American Airlines Meeting Services Desk directly at 1 800.433.1790 for assistance with reservations and ticket purchases.

By Ground

SuperShuttle is the nation's leading shared-ride airport shuttle, providing door-to-door ground transportation and provides service to and from 28 major airports in 23 cities. Shared van service is available at Miami International Airport (MIA) to Hilton Miami Downtown for approximately US\$16 one-way per person. Reservations may be made by phone at 1 800.BLUE VAN (258.3826) or +1

305.871.2000. SuperShuttle does not except on-line reservations for the Miami International Airport.

Taxi

US\$22 – Miami International Airport (MIA) to Hilton Miami Downtown.
All prices are estimates, and taxis are metered fares.

Bus and Rail

[Miami-Dade Transit](#) provides service daily to thousands of regular, first-time, and occasional public transit customers. [Click Here](#) for more information on Metrobus, Metrorail, Metromover and other forms of public transportation. [Metro Mover Map](#)

Rental Car

Avis Rent-a-Car is pleased to offer low rates with unlimited mileage to participants attending OSA Biomedical and 3-D Congress. For reservations call 1 800.331.1600 and refer to Avis Worldwide Discount # **D004076**. Reservations may also be made on the [Avis website](#) or by [phone \(World Wide Telephone Numbers\)](#). Additional [car rentals](#) are available at Miami International Airport.

Parking

24-hour Valet Parking is provided through the hotel and allows for unlimited in-out privileges. Self-Parking is also available through an unaffiliated company but allows for no in-out privileges.

Housing – Deadline: Thursday, 29 March 2012

Miami Hilton Downtown

1601 Biscayne Blvd
Miami, Florida, United States 33132

Rates will be honored 3 days prior and post conference dates

Single/Double	US\$169
Extra Person	US\$20
State and Local Taxes	13% (taxes are subject to change)

For the latest currency exchange [click here](#).

All reservations must be guaranteed with a major credit card. Hotel will charge one night's room and tax at the time of reservation. This amount will be refundable up to 72 hours prior to scheduled arrival date. In the event of a no show, one night's room and tax will be charged and the reservation will be canceled.

Stay within the block!

[Book your Hotel Reservation](#)

- [ONLINE](#)
Please note that our online system will only accept reservations that are within the contracted dates. Any guests requesting to extend their stay outside of the block must call our reservation's team
- Call Toll free: + 1 800.HILTONS (445. 8667) or +1 305.374.000
The reservations desk is opened 24 hours
Request: 2012 OSA Biomedical and 3-D Imaging Congress.
If you book within the block, the following services are complimentary to make your stay more enjoyable:
- High Speed Internet Access in All Guest Rooms and Meeting Rooms
- Daily bottle water in your guest room.

Check-in: 16:00
Check-out: 11:00

For more information, special offers and visitor information; go to the conference travel page:
http://www.osa.org/Meetings/optics_and_photonics_congresses/Biomedical_Optics_Congress/Housing_and_Travel.aspx#hotel

Shipping & Material Handling

Upon arrival contact hotel security for any materials shipped to Hilton Miami Downtown to be delivered to the assigned location. In order for this to be expedited, it is essential that all shipments reflect the name of the exhibitor, as well as the name of the group that is hosting the exhibit show and show dates. Failure to do so may result in a delay in receipt of exhibit materials.

Due to limited storage areas, the hotel cannot accept any exhibit drayage packages for an exhibit company. Such packages need to be shipped via private carrier Exhibitors who have arranged for delivery direct to the Exhibit via must notify such carrier this will be an inside delivery, the carrier is expected to provide all labor and equipment necessary to load-in their shipments. The hotel accepts no responsibility for the movement of these materials. Freight insurance is highly suggested.

Regardless of carrier utilized, please address all shipments to:

Your Name/ EXHIBITOR
2012 OSA conference (28 April – 2 May)
Concerto ABC
Hilton Miami Downtown
1601 Biscayne Blvd
Miami, FL 33132
CSM: Domingo Sanchez

Shipping INSTRUCTIONS

For any boxes that are to be sent to the hotel – The delivery of small packages (50 lbs. or less) will be accepted two (2) days prior to meeting date, with the first three boxes complimentary and any package after that a \$5.00 per box or carton service charge in and out. Packages received over two (2) days prior to delivery will be subject to an additional \$2.00 per box or carton storage fee per day. Please Contact your convention services manager for more details.

No deliveries can be made through the public areas of the hotel.
Please deliver all materials through the Shipping and Receiving entrance only.

The hotel will not be liable for safe or timely arrival of packages sent to the hotel by or for the group.

It is the group's responsibility to check that the contents are intact. The hotel accepts no liability for lost, stolen or damaged goods.

The hotel will not accept cash delivery shipments. Due to limited storage areas, the hotel cannot accept any exhibit drayage packages for an exhibit company. Should an exhibitor send packages, they will not be accepted.

Delivery Driving Directions:

Coming from North Miami going south:

Take Biscayne Blvd. to 17th Court and make a right, the entrance to the loading dock area will be on your right hand side.

Coming from South Miami going north:

Take Biscayne Blvd. to 17th Court and make a left, the entrance to the loading will be on your right hand side.

**A charge of \$100.00 per day is to be applied to any vehicle that needs to be parked overnight.

Banding equipment **IS NOT** available. For billing purposes, each exhibitor must record their Shipper billing number (FedEx and UPS) on the request form / air bill. Only if exhibitor has issued a "Call Tag" through his/her Home Office prior to arrival at Hilton Miami Downtown. Arrangements for pick up via Air Freight/Truck Line should be made prior to arrival. Please schedule pick up on the day following the show. Exhibitor must provide completed "Bill of Lading" for each destination. The hotel will not be responsible for any packages left behind without proper documentation/information and payment.

Shipping Information:

Regardless of carrier utilized, please address all shipments to:

Your Name/ EXHIBITOR

2012 OSA conference (28 April – 2 May)

Concerto ABC

Hilton Miami Downtown

1601 Biscayne Blvd

Miami, FL 33132

CSM: Domingo Sanchez

Payment

All shipments are to be pre-paid by sender regardless of origin or shipment method UPS. The hotel will not accept cash delivery shipments.

Unclaimed Materials

Any conference materials, posters, banners, etc., left in meeting rooms or in our Shipping Department after departure, without direction as to disposal, will be held for a period of 30 days following the group's departure. At that time the materials will be discarded.

Disclaimer

Hilton Miami Downtown is not responsible for any delay in receipt or delivery of conference materials, nor any special handling fees assessed by a carrier, due to inadequate or improper labeling of conference materials. Packages bearing insufficient information to identify the conference or use dates once received will be held in our Receiving Department for a period not to exceed 30 days, Hilton Miami Downtown will not assume responsibility or liability for damage or loss of any merchandise or articles brought into any function room and left unattended.

Deliveries and Storage

Exhibit and display materials cannot be accepted for storage prior to the set up day without express prior approval of Convention Services. The hotel reserves the right to refuse delivery of any such materials

shipped without prior consent. The hotel will not be liable for any additional costs for shipments that are refused due to lack of prior approval. .

Deliveries and storage of materials that are accepted prior to set up day will be handled by the Business Services department at Hilton Miami Downtown. Conference materials are to be shipped to the hotel and must be clearly labeled as to conference/function name, function room, date of event and client's contact name. For further information, contact Convention Services prior to shipping. Charges will be applicable for receipt and storage of any materials.

Return Shipments

If you need to ship any packages at the end of your conference, please contact your preferred carrier, fill out all proper documentation forms and provide method of payment to carrier. Hilton Miami Downtown will assist you in collection of your packages and hold them in our Storage Room. You must pre-arrange a pick-up time with your shipper. A processing and storage fee is applied to packages held for pick up. Please do not leave packages in the Function Room at the conclusion of the event for security reasons. All packages must be shipped off property within 24 hours of completion of meeting.

Air Freight/ Cargo – Domestic Shipments

STS Air Cargo is available to assist those companies who need to ship exhibit materials to San Diego. For more information, please contact:

Mike Carver
STS Air
PO Box 998
Millbrae, CA 94030
stsair@stsair.com
Phone: +1 800.692.6116
Fax: +1 650.692.6175

Customs & International shipments

All shipments which will be traveling internationally (i.e. to and from San Diego to and from another country) **MUST** use a customs broker. Management is not responsible for any shipments that may be stopped at customs or for any additional charges that may be incurred for international shipments. Below is a suggested customs broker.

TWI Global will assist those companies which need to ship exhibit materials to Miami. All materials shipped through TWI will be delivered to the hotel no later than Friday, 27 April. For more information, please contact:

Sarah Kucsma
TWI Group, Inc.
Tel: +1 702.691.9074
SKucsma@twiglobal.com
4480 South Pecos Road
Las Vegas, Nevada 89121

Promotional Opportunities

Take advantage of the opportunity to maximize your company's meeting presence through the unique sponsorships available at Biomedical and 3-D Imaging Congress. Increase your company's visibility among qualified attendees while utilizing a cost-effective way to gain a competitive advantage. Don't miss your chance to reach hundreds of attendees!

To take advantage of a sponsorship opportunity, please call +1 202.416.1474 or email Regan Pickett at rpickett@osa.org.

Biomedical Optics (BIOMED) ■ Digital Holography (DH)
29 April - 2 May 2012 ♦ Miami, Florida, United States
 One registrant per form

SECTION A: BADGE INFORMATION – PLEASE PRINT CLEARLY

Do you want all OSA correspondence and subscriptions sent to the address listed below? Yes No

Last (Family) Name	First (Given) Name	Middle Initial
Professional Affiliation/Institution		Title
Mailing Address		
City	State/Province	ZIP/Postal Code
Country	Email	
Telephone with Country Code	Fax with Country Code	
Emergency Contact (In case of emergency)		Phone with Country Code

SOCIETY MEMBERSHIP INFORMATION: Optical Society of America (OSA) ID# _____

SECTION B: CONFERENCE REGISTRATION

I. Full Technical Registration – Includes admission to all BIOMED/DH 2012 technical sessions, exhibit, refreshments, the conference reception, and one copy of the BIOMED/DH 2012 Conference Program and Technical Digest on CD-ROM. Students must provide valid student I.D. to receive the discounted registration. Forms received without payment will not be processed. Forms received after the deadline of 2 April 2012 will be charged the higher fee. Short Course admittance is not included.

CHECK THE MEETING YOU ARE PRIMARILY INTERESTED IN ATTENDING (for statistical purposes only): BIOMED DH

	On or before	After
	2 April 2012	2 April 2012
OSA Member	<input type="checkbox"/> US\$ 585	<input type="checkbox"/> US\$ 700
Non-member	<input type="checkbox"/> US\$ 765	<input type="checkbox"/> US\$ 880
Emeritus / OSA Student Member	<input type="checkbox"/> US\$ 200	<input type="checkbox"/> US\$ 300
Student Non-member	<input type="checkbox"/> US\$ 265	<input type="checkbox"/> US\$ 370

II. Exhibit Only Registration - Only includes admission to the exhibit hall for attendees. US\$ 0 US\$ 0

III. Exhibitor Technical Registration – One complimentary technical badge per Tabletop Space or 10x10. Includes admission to all BIOMED/DH technical sessions, exhibit, refreshments, conference reception, and one copy of the BIOMED/DH Congress Program and Technical Digest on CD-ROM. Short Course admittance is not included.

Complimentary Technical Badge US\$ 0 US\$ 0

IV. Exhibit Personnel Only – Only includes admission to the exhibit hall for exhibitor staff. US\$ 0 US\$ 0

SECTION B PAYMENT \$ _____

SECTION C: Conference Publications

One copy of the BIOMED/DH Conference Program and Technical Digest on CD-ROM is included in the Full Technical and Exhibitor Technical Registration fee. Additional copies are available for purchase.

BIOMED/DH Program and Technical Digest on CD-ROM _____ x US\$ 100.

SECTION C PAYMENT \$ _____

SECTION D: EXTRA ITEMS AVAILABLE

Extra Congress Reception Ticket No. of Guests _____ x US\$ 75 Paid Registrant – No Charge

OSA Foundation Donation US\$25

Attendee Bonus Special 6-month OSA Member Offer International – US \$30 US or Canada - \$30

[] Yes, I plan to attend the **FREE OIDA Reception & RUMP Session**. Tuesday, 1 May (directly following the technical sessions-Miami Hilton Downtown). The program will feature guest presentations about growth opportunities for photonics companies in healthcare and an “open microphone” for audience participation!

SECTION D PAYMENT \$ _____

TOTAL PAYMENT \$ _____

SECTION F: PAYMENT INFORMATION

One registrant per form. This form can be copied for additional registrants. **PAYMENT MUST ACCOMPANY FORM TO COMPLETE PROCESSING.**

Your name and full address must be typed or printed clearly on your check or bank draft.

Method of Payment: (Make check payable to the **Optical Society of America** in US dollars on a US bank)

Check No. _____ Money Order No. _____ Bank Name _____ Date of Transfer _____

I authorize the Optical Society of America to charge my: VISA Master Card AMEX Diner's Club Discover JCB Card

Card Number _____ Exp. Date _____ Name on Card _____

I authorize the Optical Society of America to charge the total payment indicated on this form to my credit card. If the registration form is received by OSA after 2 April 2012, I authorize OSA to charge the on-site registration rate as stated in Section B. Payment amount subject to membership verification.

Signature _____

Refund Policy for pre-registration: A \$75 service charge will be assessed for processing refunds. A letter requesting the refund should state the registrant's name and to whom the refund should be made payable. Requests for refunds must be received in writing no later than 16 April 2012 to be honored. Details should be mailed to OSA Meetings and Exhibits, 2010 Massachusetts Ave., NW, Washington, DC, 20036-1012, emailed to custserv@osa.org or faxed to +1.202.416.6140.

For Special Assistance while attending this meeting, call 1.202.416.1907. Registration implies consent that any picture taken during OSA sponsored events can be used for meeting and promotional purposes without remuneration and that your name will be placed on an attendee list which is distributed to BIOMED/DH meeting attendees.

THREE WAYS TO REGISTER

Fax: +1.202.416.6140

Mail: OSA Finance Department
 c/o BIOMED Congress 2012 Registration
 PO Box 55480, Boston MA 02205-9923

Express Mail: OSA Finance Dept.
 c/o BIOMED Congress 2012 Registration
 2010 Massachusetts Ave., NW / Washington, DC 20036-1012



Biomedical Optics and 3-D Imaging Congress: Topical Meeting Exhibit 2012

Exhibitor Response Form

Fax response to +1 202.416.6100 ATTN: Melissa Lanham or email topicalexhibits@osa.org.

DEADLINE: No later than 19 March 2012

Company: _____

Contact: _____

Phone: _____ Email: _____

We have ordered electricity through the hotel:

- Yes
- No

We have ordered internet through the hotel:

- Yes
- No

We have read and understand all shipping rules and regulations:

- Yes
- No



Biomedical Optics and 3-D Imaging Congress: Topical Meeting Exhibit 2012

Buyers' Guide Submission Instructions

- Fax: +1 202.416.6100 Attn: Melissa Lanham – mlanham@osa.org**

- Please provide the following information for inclusion in the Buyers' Guide, which will be provided to all attendees. One listing per company is provided. Should a company miss this deadline, you will not be listed in the Guide.
- Provide all information as it is to be published. Please write **legibly** in dark ink or email to mlanham@osa.org.*

- Company Name _____
- Address 1 _____
- Address 2 _____
- City _____ State/Province _____
- ZIP/Postal Code _____ Country _____
- Phone _____ Fax _____
- Web site _____
- Email _____

- 50-75 word description** (*any descriptions over 75 words may be edited*):

ELECTRICAL RENTAL ORDER FORM

MAIL WITH 100% Remittance to:

Tri-City Electric Co., Inc.

625 NW 16th Avenue • Miami, Florida 33125-4611

Phone: (305) 691-4900 • Fax: (305) 693-3546

Email: mmendez@tricity-electric.com



TRI-CITY ELECTRIC CO., INC.
TRADE SHOW & CONVENTION SERVICES DIVISION

SHOW NAME		LOCATION		DATES	
COMPANY NAME		BOOTH #		DISCOUNT DEADLINE DATE	
CARDHOLDER'S BILLING ADDRESS		CITY		STATE	
ORDERED BY (PLEASE PRINT)		PHONE #		FAX #	
CREDIT CARD INFORMATION		ACCOUNT #		CVV2	
<input type="checkbox"/> M/C <input type="checkbox"/> VISA <input type="checkbox"/> AMEX		PRINT LEGIBLY		SECURITY CODE	
EXPIRATION DATE		CARD HOLDER'S SIGNATURE		(PLEASE PRINT)	

ELECTRICAL OUTLETS Approximately 120/208v a/c/ 60 cycle - PRICES ARE FOR ENTIRE EVENT.

	QUANTITY (For show hours only)	QUANTITY (For 24hrs/day- Double price)	14 DAY ADVANCE PAYMENT PRICE	REGULAR PRICE	TOTAL COST
120 VOLTS					
0-1000 WATTS (10 AMPS)	_____	_____	115.00	155.00	_____
1001-1500 WATTS (15 AMPS)	_____	_____	135.00	180.00	_____
1501-2000 WATTS (20 AMPS)	_____	_____	160.00	220.00	_____
120/208 VOLTS SINGLE PHASE					
10 AMPS	_____	_____	190.00	292.50	_____
15 AMPS	_____	_____	225.00	330.00	_____
20 AMPS	_____	_____	280.00	415.00	_____
30 AMPS	_____	_____	330.00	475.00	_____
60 AMPS	_____	_____	460.00	665.00	_____
100 AMPS	_____	_____	675.00	915.00	_____
120/208 VOLTS THREE PHASE					
10 AMPS	_____	_____	260.00	360.00	_____
15 AMPS	_____	_____	295.00	410.00	_____
20 AMPS	_____	_____	360.00	520.00	_____
30 AMPS	_____	_____	425.00	465.00	_____
60 AMPS	_____	_____	620.00	680.00	_____
100 AMPS	_____	_____	880.00	1320.00	_____
TRANSFORMERS TO BOOST 208V TO 230V- \$3.00 PER AMP WITH 20 AMP MINIMUM					

LIGHTING EQUIPMENT (Including Current Consumed) Provide Drawing Showing Light Location(s).

120W QUARTZ FLOOD LIGHT ¹	_____	_____	68.00	102.00	_____
120W FLOOD LIGHT ON STANCTION ¹	_____	_____	84.00	126.00	_____
300W ARM HALOGEN LIGHT ²	_____	_____	95.00	135.00	_____
1000W OVERHEAD PAR LIGHT ³	_____	_____	275.00	350.00	_____

1. Inline Booths Only/Light on 8ft. Pole. 2. Hardwall Booths Only.
3. Additional Charge for Time and Material will apply when lift required to mount overhead.

MATERIAL (Electricity Not Included) (120 Volt Only)

EXTENSION CORD	_____	19.00	_____
MULTI OUTLET POWER STRIP	_____	25.00	_____

LABOR (Require for ALL island booths, 208V & higher connections and non-standard installations-see back)

ST-MON-FRI(Except Holidays) (8 am- 4:30 pm)	_____	72.00	_____
OT-MON-FRI 4:30 pm- 8 am (All Day Sat/Sun/Holidays)	_____	140.00	_____

MAKE CHECKS PAYABLE TO TRI-CITY ELECTRIC CO., INC.

SALES TAX DUE ON ALL ORDERS UNLESS FLORIDA DR-13 OR DR-14 TAX EXEMPTION CERTIFICATE ACCOMPANIES ORDER.	Sub-Total \$	_____
	Add FL 7% Sales Tax \$	_____
	TOTAL PAYMENT \$	_____

FOR ADVANCE PAYMENT PRICE

We must receive your order, payment and a floor plan showing main power location and distribution points 14 days prior to show

SEE REVERSE SIDE FOR ADDITIONAL TERMS AND CONDITIONS

ISLAND BOOTHS

There is a minimum labor charge for (1) one hour to deliver power to all island booths & 1/2 hour for removal plus materials. All additional distribution is done by Tri-City electricians on a time & material basis.

A legible, scaled floor plan, with orientation, is required for all island booths. A suitable location must be shown for Tri-City's distribution panel(s).

208V & HIGHER VOLTAGES

There is a minimum labor charge of (1) one hour for installation & 1/2 hour for removal of all high voltage services. Material charges may apply. If you require services not listed on this form, please call for a quote.

DEDICATED OUTLETS

Dedicated outlet require 20 amp outlet.

24 HOUR SERVICE

Electricity will be turned on within 30 minutes of show opening and off within 30 minutes of show closing each show day. If you require power at any other time, order 24 hour power.

TCE RESERVES THE RIGHT TO CORRECT ORDERS FIGURED INCORRECTLY. *ALL FOREIGN CHECKS MUST BE DRAWN ON U.S.BANKS ONLY*



COMMUNICATION INSTALLATION REQUEST

DATE OF REQUEST: _____

Group Name: _____
Contact Name: _____
Address: _____ City: _____ State: _____ Zip: _____
Telephone: _____ Fax: _____

Installation Date: _____ Installation Time: _____
Disconnect Date: _____ Disconnect Time: _____
Location of installation: _____ Booth Number: _____
Installation to be billed to: _____
Toll Charges to be billed to: _____
Special Instructions: _____

PHONE OPTIONS:

DID PHONE – LOCAL OR LOCAL/L.D. \$125.00 (per line, per day) X _____ = \$ _____

DID FOR LAPTOP \$125.00 (per line, per day) X _____ = \$ _____

DSL (Hardwired) \$750.00 (one time charge) X _____
= \$ _____

HOUSE PHONE \$ 0.00 X _____ = \$ _____

***Wireless internet Complimentary in Meeting Spaces

CONDITIONS AND REGULATIONS

1. Above prices refer to rental and installation only. Calls will be billed separately at prevailing Hotel rates.
2. Above prices are one time only, unless otherwise specified.
3. Request must be received in advance with a minimum of three (3) days prior to installation date; otherwise a 25% increase for late charges will apply.
4. Rates quoted for installations apply to installation day Monday through Friday 8:00 am to 4:00 pm. Saturday, Sunday and Holidays have a surcharge of 100%.

****Please forward this form along with credit card authorization from info to: domingo.sanchez2@hiltoncom**

I agree that I will be responsible for all calls made from the above listed phone(s) during the period indicated above.
(Installation to Removal)
Signature: _____ Date: _____

Biomedical Optics & 3D Imaging: OSA Optics & Photonics 2012

Biomedical Optics (BIOMED)
Digital Holography and Three-Dimensional Imaging (DH)

28 April-2 May, 2012
Miami Hilton Downtown,
Miami, Florida, USA

Conference Program

Welcome to Miami, Florida, and to the 10th biennial **Biomedical Optics Topical Meeting**. We hope you enjoy all the opportunities that Miami offers, and take full advantage of the scientific sessions before you. This meeting has been a favorite over the years because of its focused topics, quality peer-reviewed presentations, and pleasant surroundings.

There are ample opportunities for networking between sessions, and the multiple poster sessions allow for lively discussions of the latest research. Despite the popularity of the meeting, we have strived to maintain a “small meeting” feel with only two parallel oral sessions. The meeting has grown in size and scope, ranging from basic technology development to clinical studies. We received a record number of paper submissions for this year’s meeting. The diversity of topics allows plenty of room for physicists and engineers to rub shoulders with biologists and clinicians. You will see the latest cutting edge optical technologies, and also see how these technologies can be applied. We believe that it is critical to create as many forums as possible for technical and applied interactions to occur in order to facilitate the next advances in medical care and research.

We have a busy four days ahead of us twenty invited and plenary talks, and 137 contributed talks. Because there are only two parallel sessions, there are far more poster papers than oral papers—247 poster papers altogether. You will find many outstanding papers in the poster sessions, some of which may win our poster awards; so don’t miss them.

We hope you enjoy the meeting!

Sincerely,



Xingde Li
Johns Hopkins University, USA
General Chair



Claude Boccara,
Institut Langevin, France
General Chair



Lev T. Perelman
Harvard Univ., USA
General Chair

Digital Holography and Three-Dimensional Imaging (DH)

28 April-2 May 2012

Miami, Florida

Welcome to the **6th Digital Holography and Three-Dimensional Imaging (DH) Topical Meeting** in Miami, Florida. The DH Topical Meeting is the world's premier forum for disseminating the science and technology geared towards 3-D information processing. Since the meeting's inception in 2007, it has steadily and healthily grown to 103 presentations this year.

The four-day program includes a plenary speaker, 2 tutorials, 16 invited speakers, 65 contributed oral presentations, and 19 poster presentations. At this meeting, expect to hear about the latest research on 3-D imaging, digital holographic microscopy, digital/electronic holography, 3-D displays and systems, integral photography and imaging, and holographic interferometry/modulators/filters/materials as well as applications in BIOMEDical imaging, optical processing, and metrology.

We look forward to meeting you in Miami, Florida.

Sincerely,



Myung K. Kim
Univ. of South Florida, USA
General Chair



George Barbastathis
MIT, USA
General Co-Chair

BIOMEDICAL Optics Program Committee

General Chairs

Claude Boccard, *Institut Langevin, France*

Xingde Li, *Johns Hopkins Univ., USA*

Lev T. Perelman, *Harvard Univ., USA*

BIOMED 1: Joint DH

No BIOMED subcommittee members were selected.

BIOMED 2: BioNanophotonics and Molecular Probes

Samuel Achilefu, *Washington Univ. in St Louis, USA, Co-Chair*

Gang Zheng, *Univ. of Toronto, Canada, Co-chair*

Stephen A. Boppart, *Univ of Illinois at Urbana-Champaign, USA*

Shawn Chen, *National Instit. Of Biomedical Imaging and Bioengineering, USA*

Christopher Contag, *Stanford Univ., USA*

Ute Resch-Genger, *BAM Federal Institute for Materials Research and Testing, Germany*

Andrew Tsourkas, *Univ. of Pennsylvania, USA*

Yasuteru Urano, *Univ. of Tokyo, Japan*

Itamar Willner, *Hebrew Univ. of Jerusalem, Israel*

BIOMED 3: Optical Microscopy Techniques

Peter So, *MIT, USA, Co-Chair*

Tony Wilson, *Univ. of Oxford, UK, Co-Chair*

Adela Ben-Yakar, *Univ. of Texas at Austin, USA*

Paul J Campagnola, *Univ. of Wisconsin-Madison, USA*

Kristen Carlson Maitland, *Texas A&M Univ., USA*

Ji-Yen Cheng, *Center for Applied Sciences/Academia Sinica, Taiwan*

Wonshik Choi, *Korea Univ., South Korea*

Alberto Diaspro, *Italian Institute of Technology, Italy*

David L. Dickensheets, *Montana State Univ., USA*

Melike Lakadamyali, *Instit. of Photonic Science, ICFO, Spain*

Dan Oron, *Weizmann Institute of Science, Israel*

Jianan Y. Qu, *Hong Kong Univ. of Science & Technology, Hong Kong*

BIOMED 4: Photoacoustic Imaging and Spectroscopy

Lihong V. Wang, *Washington Univ. in St Louis, USA, Co-Chair*

Wiendelt Steenbergen, *Universiteit Twente/MIRA Institute, Netherlands, Co-Chair*

Mark A. Anastasio, *Washington Univ. in St Louis, USA*

Paul C. Beard, *Univ. College London, UK*

Stanislav Emelianov, *Univ. of Texas at Austin, USA*

Martin Frenz, *Universitat Bern, Inst. of Applied Physics, Switzerland*

Jan Laufer, *Univ. College London, UK*

Pai-Chi Li, *National Taiwan Univ., Taiwan*

Alexander A. Oraevsky, *Fairway Medical Technologies Inc, USA*

Guenther Paltauf, *Karl-Franzens-Universitaet Graz, Austria*

Roger J Zemp, *Univ. of Alberta, Canada*

BIOMED 5: Optical Coherence Tomography

James G. Fujimoto, *MIT, USA, Co-Chair*

Christoph K. Hitzenberger, *Medizinische Universität Wien, Austria, Co-Chair*

Iwona Maria Gorczynska, *Nicolaus Copernicus Univ., Poland*
Robert Huber, *Ludwig-Maximilians-Universität München, Germany*

Michael W Jenkins, *Case Western Reserve Univ., USA*

Michael Pircher, *Medical Univ. of Vienna, Austria*

Guillermo J. Tearney, *Harvard Medical School, USA*

Alex Vitkin, *Ontario Cancer Institute, Canada*

Ruikang K. Wang, *Univ. of Washington, USA*

Yoshiaki Yasuno, *Univ. of Tsukuba, Japan*

BIOMED 6: Optical Imaging and Tomography

Stefan Andersson-Engels, *Lunds Universitet, Sweden, Co-Chair*

Brian W. Pogue, *Dartmouth College, USA, Co-Chair*

Randall L. Barbour, *SUNY Downstate Medical Center, USA*

David Cuccia, *Modulated Imaging, USA*

Hamid Dehghani, *Univ. of Birmingham, UK*

Jeremy C. Hebden, *Univ. College London, UK*

Huabei Jiang, *Univ. of Florida, USA*

Robert J. Nordstrom, *NIH/NCI, USA*

Eiji Okada, *Keio Univ., Japan*

Michael S. Patterson, *Juravinski Cancer Centre, Canada*

Antonio Pifferi, *Politecnico di Milano, Italy*

Nirmala Ramanujam, *Duke Univ., USA*

Ilya Turchin, *Institute of Applied Physics, Russia*

Arjun Yodh, *Univ. of Pennsylvania, USA*

Quing Zhu, *Univ. of Connecticut, USA*

BIOMED 7: Optical Spectroscopy

Vadim Backman, *Northwestern Univ., USA, Co-Chair*

Valery V. Tuchin, *Saratov State Univ., Russia, Co-Chair*

Jennifer Barton, *Univ. of Arizona, USA*

Irving J. Bigio, *Boston Univ., USA*

Nada Boustany, *Rutgers University, USA*

Rinat Esenaliev, *Univ. of Texas Medical Branch Galveston, USA*

Bob Filkins, *General Electric, USA*

Kirill Larin, *Univ. of Houston, USA*

Martin Leahy, *Univ. of Limerick, Ireland*

Qingming Luo, *Huazhong Univ. of Science and Technology, China*

Igor Meglinsky, *Univ. of Otago, New Zealand*

Herbert Schneckenburger, *Hochschule Aalen, Germany*

Dick Sterenberg, *Univ. Hospital Rotterdam-Daniel den Hoed Cancer Center, The Netherlands*

Bruce Tromberg, *Univ. of California, Irvine, USA*

Urs Utzinger, *Univ. of Arizona, USA*

Martin Wolf, *Univ. Hospital of Zurich, Switzerland*

Digital Holography and Three-Dimensional Imaging (DH) Program Committee

General Chairs

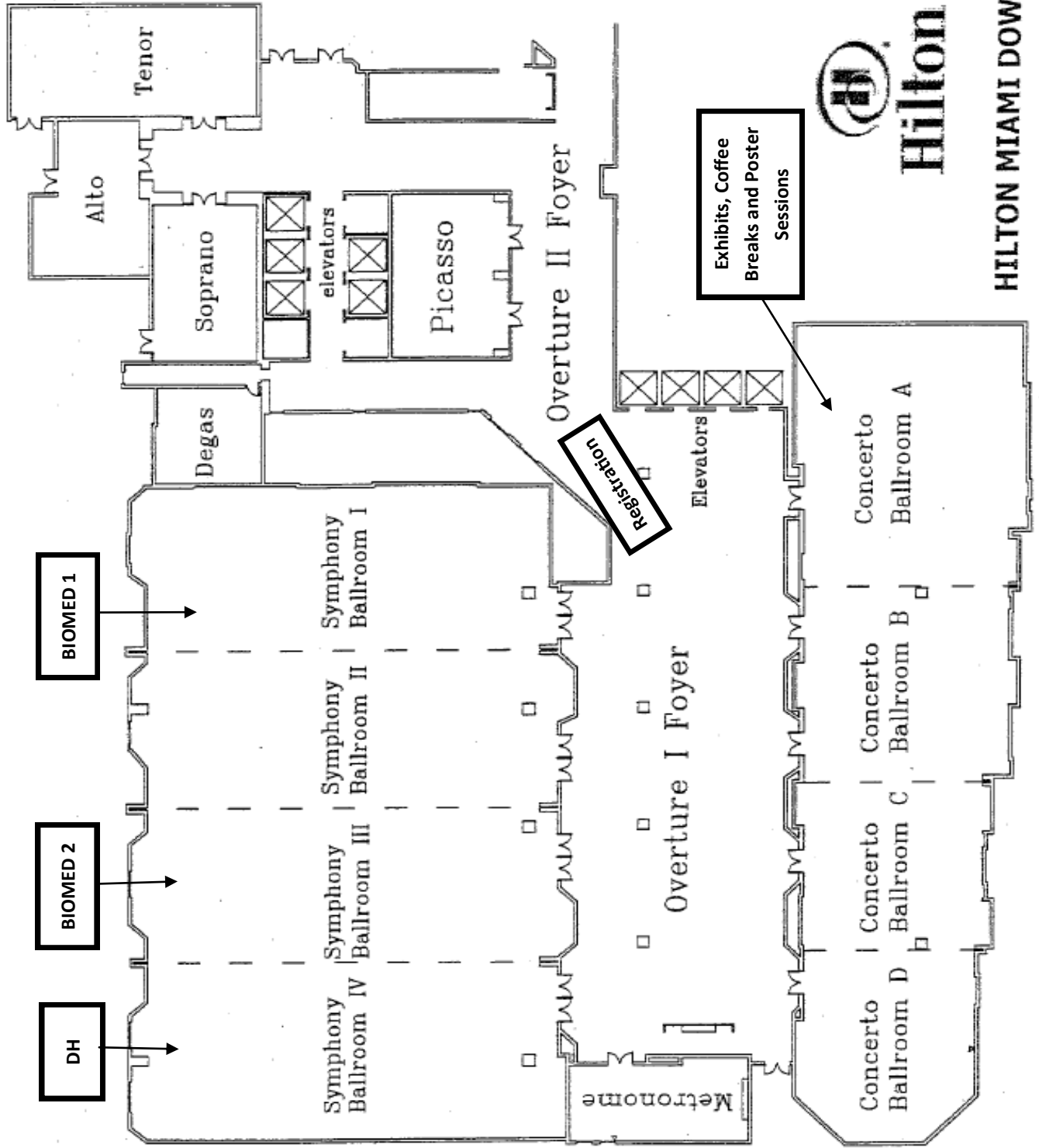
Myung K. Kim, *Univ. of South Florida, USA, General Chair*
George Barbastathis, *Massachusetts Inst. of Technology, USA, General Co-Chair*

Advisory Committee

Ting-Chung Poon, *Virginia Tech, USA, Chair*
Partha P. Banerjee, *University of Dayton, USA*
Byoung-ho Lee, *Seoul National Univ., South Korea*
Kehar Singh, *IIT Delhi, India*
Ichirou Yamaguchi, *Gunma Univ., Japan*
Toyohiko Yatagai, *Utsunomiya Univ., Japan*

Committee Members

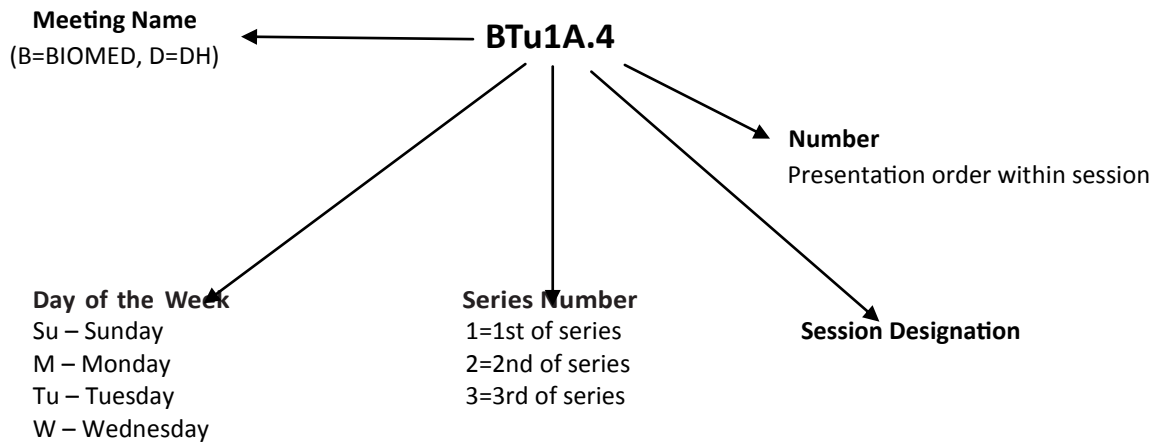
Anand Asundi, *Nanyang Tech University, Singapore*
Michael Bove, *MIT, USA*
Chau-Jern Cheng, *National Taiwan Normal Univ., Taiwan*
Gary Cook, *AFRL, USA*
Pietro Ferraro, *INO, Italy*
James W. Fleischer, *Princeton Univ., USA*
Yoshio Hayasaki, *Utsunomiya Univ., Japan*
Thomas Kreis, *BIAS, USA*
Nickolai Kukhtarev, *Alabama A&T Univ., USA*
Jung-Ping Liu, *Feng Chia Univ., Taiwan*
Takanori Nomura, *Wakayama Univ., Japan*
Aydogan Ozcan, *UCLA, USA*
Nasser Peyghambarian, *Univ. of Arizona, USA*
Pascal Picart, *Lemans Univ., France*
Joseph Rosen, *Ben Gurion Univ., Israel*
Yasuhiro Takaki, *Tokyo Univ. A&T, Japan*
Hiroshi Yoshikawa, *Nihon Univ., Japan*
Changhe Zhou, *Academia Sinica, China*



Hilton

HILTON MIAMI DOWNTOWN

Explanation of Session Codes



The first letter of the code designates the meeting (For instance, A=BIOMED, D=DH). The second element denotes the day of the week (Monday=M, Tuesday=Tu, Wednesday=W). The third element indicates the session series in that day (for instance, 1 would denote the first parallel sessions in that day). Each day begins with the letter A in the fourth element and continues alphabetically through a series of parallel sessions. The lettering then restarts with each new series. The number on the end of the code (separated from the session code with a period) signals the position of the talk within the session (first, second, third, etc.). For example, a presentation coded BTu1A.4 indicates that this paper is part of BIOMED meeting (B) and is being presented on Tuesday (Tu) in the first series of sessions (1), and is the first parallel session (A) in that series and the fourth paper (4) presented in that session.

Exhibits

The exhibits will be taking place during the Conference Reception and most Poster Sessions in Concerto Ballroom. Please note: Coffee breaks will take place in the same location.

Date	Coffee Breaks*	Poster Sessions
Sunday, 29 April*	15:00 – 15:30	13:00 – 15:00
Monday, 30 April	9:30 – 10:00 15:00 – 15:30	13:00 – 15:00 18:30 – 20:00 (Conference Reception)
Tuesday, 1 May	9:30 – 10:00 15:00 – 15:30	13:00 – 15:00
Wednesday 2 May*	10:00 – 10:30 15:30 – 16:00	

- *Optional for Exhibitors to be present during Sunday and Wednesday times and for all coffee breaks.*

Agenda of Sessions

Saturday, 28 April 2012

15:00 – 18:00	Registration, Overture Foyer
----------------------	-------------------------------------

Agenda of Sessions

Sunday, 29 April 2012

ROOM	SYMPHONY I & II	SYMPHONY III	SYMPHONY IV
	BIOMED 1	BIOMED 2	DH
07:00 – 18:00	<i>Registration, Overture Foyer</i>		
07:50 – 08:00	BIOMED Opening Remarks		DH Opening Remarks
08:00 – 09:30	BSu1A: BIOMED Plenary Speakers I: Lihong Wang and Mathias Fink ▶		DSu1C: Three- Dimensional Display I
09:30 – 10:00	<i>Coffee Break, Concerto Ballroom</i>		
10:00 – 12:00	BSu2A: Brain Imaging ▶	BSu2B: Microscopy Imaging: Novel Fluorescence Contrast	DSu2C: Special Techniques of Digital Holography I
12:00 – 13:00	Lunch on Your Own		
13:00 – 15:00	BSu3A: BIOMED Poster Session I and Exhibits <i>Overture I Foyer & Concerto Ballroom</i> ▶		DSu3C: Digital Holographic Microscopy I (ends at 14:45)
15:00 – 15:30	<i>Coffee Break, Concerto Ballroom</i>		
15:30 – 17:30	BSu4A: Brain Signals I ▶	BSu4B: Microscopy Imaging: Novel Contrast Mechanisms	DSu4C: Biomedical Applications of Digital Holography I
18:30 – 20:00	BIOMED Postdeadline Papers, <i>Symphony I & II</i> ▶		DH Postdeadline Papers, <i>Symphony IV</i>

▶ Session is being recorded

Agenda of Sessions



Monday, 30 April 2012

ROOM	SYMPHONY I & II	SYMPHONY III	SYMPHONY IV
	BIOMED I	BIOMED 2	DH
07:00 – 18:30	<i>Registration, Overture Foyer</i>		
08:00 - 09:30	JM1A: Joint Plenary Speakers: George Smith and Byoung-ho Lee, <i>Symphony I & II</i>		
09:30 - 10:00	<i>Coffee Break, Concerto Ballroom</i>		
10:00 – 12:30	BM2A: BioNanophotonics and Molecular Probes	BM2B: Photoacoustic Tomography	DM2C: Three- Dimensional Digital Display II (until 11:45)
12:00 – 13:00	<i>Lunch on Your Own</i>		
13:00 – 15:00	JM3A: BIOMED/DH Joint Poster Session and Exhibits, <i>Overture Foyer and Concerto Ballroom</i>		
15:00 – 15:30	<i>Coffee Break, Concerto Ballroom</i>		
15:30 – 17:30	BM4A: Brain Signals II	BM4B: Microscopy Imaging: Novel Techniques and Applications	DM4C: Digital Holographic Optical Processing
17:30 - 18:30			
18:30 – 20:00	<i>Conference Reception, Overture Foyer & Concerto Ballroom</i>		

 **Session is being recorded**

Agenda of Sessions





Tuesday, 1 May 2012

ROOM	SYMPHONY I & II	SYMPHONY III	SYMPHONY IV
	BIOMED 1	BIOMED 2	DH
07:30 – 18:00	<i>Registration, Overture Foyer</i>		
08:00 - 09:30	BTu1A: BIOMED Plenary Speakers II: Bruce Tromberg and Xiaowei Zhuang 		DTu1A: Digital Holographic Microscopy II
09:30 - 10:00	<i>Coffee Break, Concerto Ballroom</i>		
10:00 – 12:00	BTu2A: Imaging of Vascular Dynamics 	BTu2B: Optical Coherence Tomography in Ophthalmology	DTu2C: Novel Applications of Digital Holography I
12:00 – 13:00	Lunch on Your Own		
13:00 – 15:00	BTu3A: BIOMED Poster Session II and Exhibits, Overture Foyer and Concerto A,B,C		DTu3C: Special Techniques of Digital Holography II
15:00 – 15:30	<i>Coffee Break, Concerto Ballroom</i>		
15:30 – 17:30	BTu4A: Fluorescence Imaging	BTu4B: Optical Coherence Tomography: Clinical Applications	DTu4C: Three-Dimensional Display III (ends 17:15)
18:00 - 20:00	OIDA Rump Session, <i>Symphony IV</i>		

 **Session is being recorded**

Agenda of Sessions

Wednesday, 2 May 2012

ROOM	SYMPHONY I & II	SYMPHONY III	SYMPHONY IV
	BIOMED 1	BIOMED 2	DH
07:30 – 17:00	<i>Registration, Overture Foyer</i>		
08:00 – 10:00	BW1A: Nevel Techniques and Models 	BW1B: Non-linear and Fluorescence Spectroscopy	DW1C: Novel Applications of Digital Holography II
10:00 – 10:30	<i>Coffee Break, Concerto Ballroom</i>		
10:30 – 12:30	BW2A: Optical Coherence Tomography: Technology and Applications 	BW2B: Spectroscopy of Elastic Light Scattering I	DW2C: Biomedical Applications of Digital Holography II
12:30 – 13:30	Lunch on Your Own		
13:30 – 15:30	BW3A: Breast Cancer Imaging 	BW3B: Spectroscopy of Elastic Light Scattering II	DW3C: Digital Holographic Microscopy III (ends 15:15)
15:30 – 16:00	<i>Coffee Break, Concerto Ballroom</i>		
16:00 – 18:00	BW4A: Tomography 	BW4B: New Spectro- scopic Techniques and Applications	DW4C: Special Techniques of Digital Holography III
18:00 – 18:15	BIOMED Closing Remarks		DH Closing Remarks

 **Session is being recorded**

Biomedical Optics (BIOMED) and Digital Holography and Three-Dimensional Imaging (DH) Joint Plenary Speakers



The Invention and Early History of the CCD, George Smith, Recipient of 2009 Nobel Prize in Physics
Monday, 30 April
08:00—08:45, *Symphony I & II*

George E. Smith was born in White Plains, New York, in 1930. He received the B. A. in Physics from the University of Pennsylvania in 1955, the M. S. and Ph. D. in Physics from the University of Chicago in 1956 and 1959 respectively. Following graduation, he joined Bell Laboratories (1959) where he initially studied the electrical properties and band structures of semimetals, mostly bismuth and bismuth antimony alloys. These studies were largely microwave resonance experiments and investigations of a variety of magnetothermoelectric and galvanomagnetic effects. In 1964 he became Head of the Device Concepts Department, a group formed to devise next generation solid state devices. In this capacity, he was involved in a variety of investigations including junction lasers, semiconducting ferroelectrics, electroluminescence, transition metal oxides, the silicon diode array camera tube and Charge-Coupled Devices. In April 1986 he retired from his position at Bell Laboratories as Head of the VLSI Device Department where his responsibilities covered the physics of devices made with submicron lithography and their use in high performance digital and analog circuits. He then started a world cruise aboard his 9.5 meter sailing vessel APOGEE which was completed in 2003 after 55,000 miles of ocean sailing. He is now living in Barnegat, New Jersey. Smith's major technical accomplishment was the inception of the Charge Coupled Device with Willard S. Boyle. They hold the basic patent (US 3,858,232) and published the first paper disclosing the device concept accompanied by a paper on its experimental verification. A following invention of the Buried Channel Charge Coupled Device (US patent 3,792,322) significantly improved the performance of the original CCD. Their accomplishment has been recognized in a number of awards, the most notable of which is the 2009 Nobel Prize in Physics.



3D Display - Where We Are and Where to Go, Byoung-ho Lee, *Seoul National Univ., South Korea*
Monday, 30 April
08:45—9:30, *Symphony I & II*

Byoung-ho Lee received his PhD degree from EECS, University of California at Berkeley in 1993. Since September 1994, he has been with the School of Electrical Engineering, Seoul National University, Korea as a faculty member, where he became a full professor in 2005. He is a fellow of OSA and SPIE and a member of the Korean Academy of Science and Technology. He received many awards including the Presidential Young Scientist Award of Korea (2002) and the Scientist of the Month Award of Korea (Sep. 2009). He served as a Director-at-Large of OSA and is currently serving as the chair of MES Council of OSA and chair of the Holography and Diffractive Optics Technical Group of OSA. He has also served as a topical editor of Applied Optics for six years, and was a co-founder of DH topical meeting. His research fields are digital holography, 3D display and plasmonics. His research group has published more than 290 international journal papers and presented more than 500 international conference papers including more than 80 invited talks.

Biomedical Optics (BIOMED) Plenary Speakers



Time Reversal in Biomedical Methods, Mathias Fink, *Langevin Institute ESPCI ParisTech, France*

Sunday, 29 April

08:45—09:30, *Symphony I & II*

Mathias Fink is a professor of physics at the Ecole Supérieure de Physique et de Chimie Industrielles de la Ville de Paris (ESPCI ParisTech), Paris, France. In 1990 he founded the Laboratory Ondes et Acoustique at ESPCI that became in 2009 the Langevin Institute. In 2002, he was elected at the French Academy of Engineering, in 2003 at the French Academy of Science and in 2008 at the Collège de France on the Chair of Technological Innovation. Mathias Fink's area of research is concerned with the propagation of waves in complex media and the development of numerous instruments based on this basic research. His current research interests include time-reversal in physics, super-resolution, metamaterials, medical ultrasonic imaging, ultrasonic therapy, multiwave imaging, acoustic smart objects, underwater acoustics, geophysics and telecommunications. He has developed different techniques in medical imaging (ultrafast ultrasonic imaging, transient elastography, supersonic shear imaging), wave control and focusing in complex media with time-reversal mirrors. He holds more than 55 patents, and he has published more than 350 peer reviewed papers and book chapters. 4 start-up companies have been created from his research (Echosens, Sensitive Object, Supersonic Imagine and Time Reversal Communications)



Diffuse Optical Spectroscopy: Technology Development and Clinical Translation, Bruce J. Tromberg,

Beckman Laser Institute and Medical Clinic, University of California, Irvine, USA

Tuesday, 1 May

08:00—08:45, *Symphony I & II*

Dr. Tromberg is the Director of the Beckman Laser Institute and Medical Clinic (BLI) at the University of California, Irvine (UCI) and principal investigator of the Laser Microbeam and Medical Program (LAMMP), an NIH National BIOMEDical Technology Center. He is a Professor in the departments of Biomedical Engineering and Surgery, co-leads the Onco-imaging and Spectroscopy Program in UCI's Chao Family Comprehensive Cancer Center, and has been a member of the BLI faculty since 1990. His research interests are in Biophotonics and Biomedical Optics, including diffuse optics, non-linear microscopy, cancer imaging, and photodynamic therapy.



Photoacoustic Tomography: Ultrasonically Breaking through the Optical Diffusion Limit, Lihong Wang,

Washington Univ. in St. Louis, USA

Sunday, 29 April

08:00—08:45, *Symphony I & II*

Lihong Wang is a Gene Beare Distinguished Professor at Washington Univ. His book entitled, *BIOMEDical Optics: Principles and Imaging*, won the J. Goodman Award. He has published more than 280 peer-reviewed journal articles with an h-index of 57 and delivered more than 31 keynote/plenary/invited talks. He has received 31 research grants as PI with a cumulative budget of more than \$34M. He is the Editor-in-Chief of the Journal of Biomedical Optics. He chairs the annual conference on Photons plus Ultrasound, and chaired the 2010 Gordon Conference on Lasers in Medicine and Biology and the 2010 OSA Topical Meeting on Biomedical Optics. Wang serves as the founding chairs of the scientific advisory boards for two companies commercializing photoacoustic tomography. He was awarded OSA's C.E.K. Mees Medal and IEEE's Technical Achievement Award for seminal contributions to photoacoustic tomography and Monte Carlo modeling of photon transport in biological tissues and for leadership in the international biophotonics community.

Digital Holography and Three-Dimensional Imaging (DH) Tutorial Speakers



Title Not Available, George Barbastathis, *MIT, USA*

Tuesday, 1 May

8:00—8:45, *Symphony IV*

George Barbastathis is Professor of Mechanical Engineering at MIT and holds the Singapore Research Professorship in Optics for the year 2011. Between December 2010 - August 2011 he is Faculty Resident with the Singapore-MIT Alliance for Research and Technology (SMART) Centre. He received the Diploma in Electrical and Computer Engineering from the National Technical University of Athens in 1993, and the M.Sc. and Ph.D. in Electrical Engineering from Caltech in 1994 and '97, respectively. Between 1997-99 he was a Post-doctoral Research Associate with the Beckman Institute at the University of Illinois, Urbana-Champaign. Between 2006-2007 he was Visiting Scholar with the School of Engineering and Applied Science at Harvard University. He has been the recipient of the Nikolaos Kritikos award in Mathematics, the 3M Innovation Award, the NSF Young Investigator Award, and the Esther & Harold E. Edgerton junior chair at MIT. His research is centered on the physics and engineering of 3D optical systems, in particular digital holography, volume holography, gradient-index media, and transformation optics.



Digital Holographic Interferometry - Principles and Applications to Deformation Measurement, Partha P. Banerjee, *Univ. of Dayton, USA*

Tuesday, 1 May

10:00—10:45, *Symphony IV*

Partha P. Banerjee is Professor of Electro-Optics and Electrical and Computer Engineering at the University of Dayton, where he was Chair of the ECE department from 2000-2005. Prior to that, he was with the Electrical and Computer Engineering department at the University of Alabama in Huntsville from 1991-2000, and Syracuse University from 1984-2001. He received his BTech from the Indian Institute of Technology in 1979, and his MS and PhD from the University of Iowa in 1980 and 1983, respectively. His areas of interest include optical processing, nonlinear optics, photorefractive materials and acousto-optics. He has authored/coauthored 5 books, several book chapters, over 120 refereed journal articles, and over 120 conference papers/presentations. He is a Fellow of the OSA and the SPIE, and a senior member of the IEEE. He received the NSF Presidential Young Investigator Award in 1987.

Special Events

Postdeadline Session

BIOMED Postdeadline Session

Sunday, 29 April

18:30—20:00, *Symphony I & II*

DH Postdeadline Session

Sunday, 29 April

18:30—20:00., *Symphony IV*

The postdeadline sessions will give participants the opportunity to hear new and significant material in rapidly advancing areas. Only those papers judged to be truly excellent and compelling in their timeliness were accepted. More information, including the schedule, will be posted in the weeks preceding the conference.

Conference Reception

Monday, 30 April

18:30—20:00, *Overture Foyer & Concerto Ballroom*

This Reception brings together the Biomedical Optics and Digital Holography & 3D Imaging meetings for a fun evening of networking with light appetizers and drinks. This event will take place in the Overture Foyer and the Concerto Ballroom.

OIDA Rump Session

Tuesday, 1 May

18:00—20:00, *Symphony IV*

OSA's 2012 Biomedical Optics and 3-D Imaging Congress will include a special event hosted by the Optoelectronics Industry Development Association (OIDA) and sponsored by OIDA Member **Hamamatsu Photonics K.K.** This session will be a unique opportunity to exchange ideas in an energized and fun environment and *we look forward to your joining in!*

Program Description: An early evening reception and session that engages research and industry attendees in a fast-paced, highly participatory discussion of a topic of key interest to both the academic and applied communities. Guest speakers will make brief presentations on "Growth opportunities for photonics companies in healthcare" followed by an "open microphone" segment where attendees are asked to address the audience with their comments and ideas.

This session is free to all BIOMED and DH registrants!

Poster Sessions

Sunday, 29 April, 13:00—15:00, *Concerto Ballroom and Overture Foyer*

Monday, 30 April, 13:30 – 15:30, *Concerto Ballroom and Overture Foyer*

Tuesday, 1 May, 13:00 – 15:00, *Concerto Ballroom and Overture Foyer*

The poster sessions are an integral part of the technical program and offer a unique networking opportunity, where presenters can discuss their results one-to-one with interested parties. Each author is provided with a 4 ft. x 8 ft. (1.22 m x 2.44 m) board on which to display the summary and results of his or her paper. The poster sessions will be held in the Concerto Ballroom and Overture Foyer.



Indicates that the session is being recorded

REGISTRATION, *Overture Foyer*

7:50—8:00

BIOMED Opening Remarks

08:00 - 09:30

BSu1A • BIOMED Plenary

Xingde Li; *John Hopkins Univ., USA, Presider*

7:50—8:00

DH Opening Remarks

08:00 - 09:30

DSu1C • Three—Dimensional Display I

Yasuhiro Takaki; *Tokyo Univ. of Agriculture & Technology, Japan, Presider*

BSu1A.1 • 08:00

Plenary

Photoacoustic Tomography: Ultrasonically Breaking through the Optical Diffusion Limit, Lihong V. Wang¹; ¹*Department of Biomedical Engineering, Washington Univ. in St. Louis, USA*. PAT, embodied in the forms of scanning photoacoustic microscopy or photoacoustic computed tomography, is the only modality capable of imaging across the length scales of organelles, cells, tissues, and organs with consistent contrast.

DSu1C.1 • 08:00

Invited

Enhanced Dynamic Holography in Organic-Inorganic Hybrid Devices, Dean Evans¹; ¹*US Air Force Research Laboratory, USA*. We describe dynamic holographic coupling in a hybridized photorefractive device. Ferroelectric nanoparticles incorporated in hybrids, resulted in improved coupling efficiency. Nanoparticles fabrication and characterization will be discussed, including techniques to separate strong and weak dipoles.

DSu1C.2 • 08:30

Off-axis integral floating system using concave mirror, Young Min Kim¹, Sung-Wook Min¹, Byoung-Sub Song¹; ¹*Kyung Hee Univ., Republic of Korea*. Off-axis integral floating display system using concave mirror is proposed for the simple structure and the high optical efficiency. The image distortion due to the off-axis optics is resolved using the compensated integrated image.

BSu1A.2 • 08:45

Plenary

Biomedical Applications of Ultrasonic Time-reversal, Mathias Fink¹; ¹*Langevin Inst., Ecole Sup Physique Chimie Industrielles, France*. An overview on research conducted on ultrasonic time-reversal methods medical applications. Time-reversal focuses wave through complex and heterogeneous media and shows exciting results both in ultrasound therapy and ultrasonic imaging.

DSu1C.3 • 08:45

The Fast Calculation Method for Computer-Generated Holograms Compatible with Self Occlusion, Yusuke Sando¹, Daisuke Barada¹, Toyohiko Yatagai¹; ¹*Center for Optical Research and Education, Utsunomiya Univ., Japan*. We have proposed the fast calculation method of computer-generated holograms compatible with self occlusion by the occlusion process and the extraction of spectrum with respect to each direction. This method has been verified by simulation.

DSu1C.4 • 09:00

Optical block module for autostereoscopic three-dimensional display, Youngmin Kim^{1,2}, Keehoon Hong¹, Jiwoon Yeom¹, Jisoo Hong¹, Byoung-ho Lee¹; ¹*School of Electrical Engineering, Seoul National Univ., Republic of Korea*; ²*Realistic Media Platform Research Center, Korea Electronics Technology Inst., Republic of Korea*. Optical block module for autostereoscopic three-dimensional display is presented. By using a polarizer and a quarter-wave retarding film, the proposed method can be incorporated in frontal projection-type parallax barrier display.

DSu1C.5 • 09:15

Depth-fused Display with Enhanced Viewing Region, Soon-gi Park¹, Jae-Hyun Jung¹, Youngmin Kim², Byoung-ho Lee¹; ¹*School of Electrical Engineering, Seoul National Univ., Republic of Korea*; ²*Realistic Media Platform Research Center, Korea Electronics Technology Inst., Republic of Korea*. We propose a viewing region enhanced depth-fused display (DFD) system. Combination of multi-view rear image and transparent front image reduces the mismatching problem of conventional DFD system. We demonstrate the feasibility with experiment.

Symphony I & II

Symphony III

Symphony IV

BIOMED I

BIOMED 2

DH

9:30—10:00

COFFEE BREAK, Concerto A,B,C

10:00 - 12:00 ▶

BSu2A • Brain Imaging

Brian Pogue; *Dartmouth College, USA, Presider*

BSu2A.1 • 10:00 Invited ▶

Multimodal Integration of fMRI, EEG, and NIRS, Mark E. Pflieger¹, Randall L. Barbour²; ¹*Source Signal Imaging, Inc., USA*; ²*Department of Pathology, SUNY Downstate Medical Center, USA*. Multimodal integration in the field of human brain mapping has evolved from structural-functional co-registrations toward functional-functional combinations. This paper briefly reviews fMRI-EEG, fMRI-NIRS, EEG-NIRS, and fMRI-EEG-NIRS combinations.

BSu2A.2 • 10:30 ▶

Investigating Hemodynamics in Scalp and Brain Using High-resolution Diffuse Optical Tomography in Humans, Christina Habermehl¹, Christoph Schmitz^{1,2}, Stefan P. Koch¹, Jan Mehnert^{1,3}, Jens Steinbrink^{1,4}; ¹*Neurology, Charité Berlin, Germany*; ²*Nirx Medizintechnik, Germany*; ³*Neurology, Max Planck Inst. for Human Cognitive and Brain Sciences, Germany*; ⁴*Center for Stroke Research Berlin (CSB), Charité Berlin, Germany*. We investigate prerequisites for developing a cw-NIRS brain perfusion monitor. Based on the separation of superficial and cortical layers using HR-DOT we investigate the power and distribution of low frequency oscillations in the brain and scalp.

BSu2A.3 • 10:45 ▶

Quantification of Cerebral Blood Flow and Oxygen Metabolism by Combining Time-Resolved Near-Infrared Spectroscopy and Diffuse Correlation Spectroscopy, Kyle Verdecchia^{1,2}; ¹*Imaging Division, Lawson Health Research Inst., Canada*; ²*Medical Biophysics, Univ. of Western Ontario, Canada*. A time-resolved near-infrared and diffuse correlation spectroscopy hybrid method to measure absolute cerebral blood flow and oxygen metabolism measurements dynamically. Arterial and venous blood samples are drawn for validation in newborn piglets.

10:00 - 12:00

BSu2B • Microscopy Imaging: Novel Fluorescence Contrast

Paul Campagnola; *Univ. of Wisconsin, USA, Presider*

BSu2B.1 • 10:00

Multiphoton Microscopic (MPM) Endoscopy Imaging within Lung Tissue for Medical Diagnostics, Watt W. Webb¹, Ina Pavlova¹; ¹*Applied & Engineering Physics, Cornell Univ., USA*. Elusive lung cancer diagnostics have motivated evolution of in situ benign spectroscopic nano-imaging by newly evolved multiphoton microscopic (MPM) endoscopy offering internal tissue diagnostics.

BSu2B.2 • 10:15

In Vivo, Deep Tissue Three-Photon Imaging at the 1700-nm Spectral Window, Nicholas G. Horton¹, Demirhan Kobat¹, Ke Wang¹, Chris Xu¹; ¹*Cornell Univ., USA*. We demonstrate deep tissue three-photon microscopy at the new spectral window of 1700 nm. We imaged vasculature and RFP-tagged neurons up to 1 mm below the cortical surface, and RFP-tagged neurons below an unthinned skull.

BSu2B.3 • 10:30

High-Speed Simultaneous in vivo Multiphoton Microscopy and Fluorescence Lifetime Microscopy, Scott Howard¹, Adam Straub², Chris Xu²; ¹*Electrical Engineering, Univ. of Notre Dame, USA*; ²*Applied and Engineering Physics, Cornell Univ., USA*. We present full-frame (256x500 pixel) simultaneous MPM and FLIM imaging, in vivo. Parallel excitation and collection on a single element detector allows for a two orders of magnitude increase in pixel rate over serial scanning and deep imaging.

BSu2B.4 • 10:45

Nonlinear Imaging of Intrinsic Tissue Contrast with a Fiber-optic Scanning Endomicroscope, Yuying Zhang¹, Kartikeya Murari¹, Wenxuan Liang¹, Kristine Glunde², Ming-Jun Li³, Xingde Li¹; ¹*Department of Biomedical Engineering, Johns Hopkins Univ. School of Medicine, USA*; ²*Department of Radiology, Johns Hopkins Univ. School of Medicine, USA*; ³*Science and Technology, Corning Incorporated, USA*. We present a fiberoptic scanning endomicroscope with a 2-mm diameter and a 32-mm rigid length capable of imaging two-photon excitation fluorescence from intrinsic fluorophors and second harmonic generation from non-centrosymmetric molecules.

10:00 - 12:00

DSu2C • Special Techniques of Digital Holography I

David Nolte; *Purdue Univ., USA, Presider*

DSu2C.1 • 10:00 Invited

Digital Holographic Interferometry and ESPI at Long Infrared Wavelengths with CO₂ Lasers, Marc Georges¹, Jean-François Vandenrijt¹, Cedric Thizy¹, Frank Dubois², Patrick Queeckers², Dominic Doyle³, Igor Alexeenko⁴, Giancarlo Pedrini⁴, Wolfgang Osten⁴; ¹*Centre Spatial de Liege, Université de Liege, Belgium*; ²*Microgravity Research Center, Université Libre de Bruxelles, Belgium*; ³*ESTEC, ESA, Netherlands*; ⁴*Institut für Technische Optik, Universität Stuttgart, Germany*. Holography and speckle techniques for various metrology and non destructive applications were developed in the 10 μm wavelength range allowing large displacements measurement. Other specific advantages are emphasized like combining temperature and displacement measurement.

DSu2C.2 • 10:30

Path-independent phase unwrapping using phase derivative and total-variation (TV) denoising, Yuanhao Huang¹, Lei Tian², Z. Zhang¹, Yi Liu², George Barbastathis^{1,2}; ¹*Singapore MIT Alliance for Research and Technology (SMART) Center, Singapore*; ²*Mechanical Engineering, Massachusetts Inst. of Technology, USA*. A path-independent method for phase unwrapping is proposed and demonstrated in the case of a noisy wrapped phase map obtained from a shearography experiment.

DSu2C.3 • 10:45

Spatial Phase Calibration Used to Improve Holographic Optical Trapping, David Engström¹, Martin Persson¹, Mattias Goksör¹; ¹*Department of Physics, Univ. of Gothenburg, Sweden*. We demonstrate that a spatial phase calibration strongly improves the trapping pattern generated by a holographic optical trapping setup. The main advantage is the decreased power in the zeroth order.

BSu2A • Brain Imaging—Continued

BSu2A.4 • 11:00

Performance Assessment of Time-Domain Optical Brain Imagers: The nEUROPT Protocol, Heidrun Wabnitz¹, Alexander Jelzow¹, Mikhail Mazurenka¹, Oliver Steinkellner¹, Rainer Macdonald¹, Antonio Pifferi^{2,3}, Alessandro Torricelli², Davide Contini², Lucia Zucchelli², Lorenzo Spinelli³, Rinaldo Cubeddu^{2,3}, Daniel Milej⁴, Norbert Zolek⁴, Michal Kacprzak⁴, Adam Liebert⁴, Salavat Magazov⁵, Jeremy Hebden⁵, Fabrizio Martelli⁶, Paola Di Ninni⁶, Giovanni Zaccanti⁶; ¹Physikalisch-Technische Bundesanstalt, Germany; ²Dipartimento di Fisica, Politecnico di Milano, Italy; ³Consiglio Nazionale delle Ricerche-Istituto di Fotonica e Nanotecnologie, Italy; ⁴Inst. of Biocybernetics and BIOMEDical Engineering, Poland; ⁵Department of Medical Physics and Bioengineering, Univ. College London, UK; ⁶Dipartimento di Fisica e Astronomia, Università degli Studi di Firenze, Italy. A novel protocol to determine sensitivity, spatial resolution and quantification of absorption changes in optical brain imaging was applied to assess time-domain instruments and methods of data analysis.

BSu2A.5 • 11:15

Combining and optimizing NIRS and EEG to study inter-ictal epileptic discharges, Robert J. Cooper¹, Meryem A. Yucel¹, Louis Gagnon^{1,2}, Nao Suzuki¹, Naoaki Tanaka¹, Claus Reinsberger^{1,3}, David Boas¹, Steve Stufflebeam¹; ¹Martinos Center for BIOMEDical Imaging, MGH, USA; ²Division of Health Sciences and Technology, Harvard-MIT, USA; ³Department of Neurology, Brigham and Women's Hospital, USA. We describe our ongoing application of NIRS-EEG to the study of inter-ictal discharges in adult epilepsy. We discuss optimizing NIRS-EEG data acquisition and analysis and we present preliminary NIRS-EEG results for an epileptic patient.

BSu2A.6 • 11:30

Fast multispectral diffuse optical tomography system for in vivo imaging of seizure dynamics, Tao Zhang¹; ¹BIOMEDical Engineering, Univ. of Florida, USA. We report a multispectral continuous-wave diffuse optical tomography system for real time noninvasive 3D imaging of hemodynamic changes. The system is validated by tissue-like phantoms, and further demonstrated by in vivo animal seizure model.

BSu2A.7 • 11:45

Potential Use of Low-Frequency Oscillations of Cortical Hemodynamics in Pediatric Epilepsy Surgery, Yinchen Song¹, Sanjiv Bhatia², John Ragheb², Prasanna Jayakar², Wei-Chiang Lin¹; ¹Department of BIOMEDical Engineering, Florida International Univ., USA; ²Neurosurgery Department, Miami Children's Hospital, USA. Low-frequency oscillations in cortical hemodynamics were observed from the cortex of pediatric patients undergoing epilepsy surgery; they may be used to identify the functional and/or the epileptic cortex intraoperatively.

BSu2B • Microscopy Imaging: Novel Fluorescence Contrast—Continued

BSu2B.5 • 11:00

Multifocal multiphoton endoscope, David R. Rivera¹, Christopher M. Brown¹, Dimitre G. Ouzounov¹, Watt W. Webb¹, Chris Xu¹; ¹AEP, Cornell Univ., USA. We report a miniaturized resonant/non-resonant multi-fiber raster scanner that is paired with a gradient-index assembly to achieve a compact (3 mm OD) multifocal multiphoton endoscope capable of transverse and longitudinal parallel image acquisition.

BSu2B.6 • 11:15

Non-invasive Optical Detection of Cell Differentiation Status Using Endogenous Sources of Optical Contrast, Kyle P. Quinn¹, Rebecca S. Hayden¹, David L. Kaplan¹, Irene Georgakoudi¹; ¹BIOMEDical Engineering, Tufts Univ., USA. Two-photon fluorescence and second harmonic generation images of mesenchymal stem cells undergoing osteoblastic differentiation demonstrate the cell redox ratio of FAD/(NADH+FAD) can serve as non-invasive biomarker of cell differentiation status

BSu2B.7 • 11:30

Monolithic Micro-Structures Fabricated by Wide Field Two Photon Polymerization, Yun-Ho Jang^{1,2}, Daekeun Kim^{2,3}, Peter So^{2,4}; ¹Femtofab, Inc., USA; ²Biological Engineering, MIT, USA; ³Biological Engineering, Dankook Univ., Republic of Korea; ⁴Mechanical Engineering, MIT, USA. We examined the feature size of micro-structures and demonstrated microfluidic channels based on wide field two photon polymerization for the applications requiring monolithic three-dimensional micro-structures such as microfluidic devices or tissue engineered scaffolds.

BSu2B.8 • 11:45

9.6-mm diameter femtosecond laser microsurgery probe, Christopher L. Hoy¹, Onur Ferhanoglu¹, Murat Yildirim¹, Wibool Piyawattanametha², Hyejun Ra², Olav Solgaard², Adela Ben-Yakar¹; ¹Mechanical Engineering, The Univ. of Texas at Austin, USA; ²Electrical Engineering, Stanford Univ., USA. We present a 9.6-mm fiber-coupled probe for femtosecond laser microsurgery and nonlinear imaging. Towards enabling clinical use, we successfully reduced the volume of our earlier 18-mm surgery probe by 5 times, while improving optical performance.

DSu2C • Special Techniques of Digital Holography I—Continued

DSu2C.4 • 11:00

Digital in-line holography with a spatially partially coherent beam, Clément Remacha^{2,1}, Jean-Marc Dorey², Franck David², Denis Lebrun¹, Sébastien Coëtmellec¹; ¹G2O, CORIA, France; ²MFEF, EDF, France. We propose in this paper an analytical solution to the problem of scalar diffraction of a partially coherent beam by an opaque disk. This analytical solution is applied in digital in-line holography of particles.

DSu2C.5 • 11:15

3D relative locations and diameters measurements of spherical particles by Fourier Interferometry Imaging (FII), Paul Briard¹, Gérard Gréhan¹, Xue Cheng Wu², Ling Hong Chen², Siegfried Meunier-Guttin-Cluzel¹, Sawatree Saengkaew¹; ¹Coria, France; ²Zhejiang Univ., China. This paper presents the possibility to measure the diameters and relative locations of a set of spherical particles. The method is based on the analysis of the interference patterns in the 2D associated Fourier space.

DSu2C.6 • 11:30

Dynamic Hologram Recording on an Azo-Containing Polymer-Liquid Crystal Hybrid System, Sarfaraz Baig¹, Pengfei Wu², Qunhui Sun², Michael R. Wang¹; ¹Dept. of Electrical and Computer Engineering, Univ. of Miami, USA; ²New Span Opto-Technology Inc., USA. Holograms with significantly improved diffraction efficiency are recorded on a new Azo-containing polymer-liquid crystal hybrid composite film, allowing dynamic recording and readout. Local heating can facilitate hologram erasure for re-recording.

DSu2C.7 • 11:45

Withdrawn

Concerto Ballroom and Overture Foyer

BIOMED

12:00—13:00
LUNCH ON YOUR OWN

13:00—15:00

BSu3A: BIOMED Poster Session I

BSu3A.1

Axial displacement and position measurement of single particle using optical tweezers, Mary-Clare C. Dy¹, Tadao Sugiura¹, Kotaro Minato¹; ¹*Information Science, Nara Inst. of Science and Technology, Japan*. A simple yet sensitive scheme is developed to transport a particle using optical tweezers and measure the particle displacement in the axial direction. This technique can be applied to axial force measurement of cells.

BSu3A.5

Development of a Highly Sensitive Label-Free Nucleic Acid Biosensor, Bailin Zhang¹, Shatha Dallo¹, Ralph Peterson¹, Syed Hussain¹, Tao Weita¹, Jing Yong Ye¹; ¹*Univ. of Texas at San Antonio, USA*. We have demonstrated the development of a highly sensitive label-free nucleic acid biosensor based on a unique open optical micro-cavity using a photonic crystal structure in a total-internal-reflection configuration.

BSu3A.9

Porphysomes: Multifunctional Nanovesicles to Treat Hypoxic Tumour by Photothermal Therapy, Cheng Jin^{1,2}, Jonathan F. Lovell^{1,3}, Gang Zheng^{2,3}; ¹*Pharmaceutical Sciences, Univ. of Toronto, Canada*; ²*Inst. for Biomaterials and Bioengineering, Univ. of Toronto, Canada*; ³*Ontario Cancer Inst., Univ. Health Network, Canada*. Porphysomes are multifunctional nanovesicles and potent photothermal agents. Their photothermal efficiency was compared to Photofrin PDT on normoxic and hypoxic tumors. Porphysomes were investigated to treat hypoxic tumor by photothermal therapy.

BSu3A.2

Development of a vertically and horizontally applicable multi-frequency alternating-magnetic-field device for hyperthermia of glioma in rodent model using iron oxide based nanoparticles, Daqing Piao¹, Kelvin Le², Debra Saunders³, Nataliya Smith³, Jessica Goddard², Daniel Figueroa², Jerzy Krasinski¹, Rheel A. Towner³; ¹*School of Electrical and Computer Engineering, Oklahoma State Univ., USA*; ²*Department of Engineering and Physics, Univeristy of Central Oklahoma, USA*; ³*Advanced Magnetic Resonance Center, Oklahoma Medical Research Foundation, USA*. We developed an alternating-magnetic-field (AMF) device of operating either vertically for in vitro or horizontally for animal study, with frequency ranging from 0.209-1.1MHz. Heating of 10nm-core iron-oxide nanoparticles was demonstrated in vivo.

BSu3A.6 Photodynamic diagnosis model for depth evaluation of basal cell carcinomas

Irene Salas-García¹, Félix Fanjul-Vélez¹, Noé Ortega-Quijano¹, Jose L. Arce-Diego¹; ¹*TEISA, Univ. of Cantabria, Spain*. The present work is devoted to the development of a diagnostic model based on photodynamic therapy to obtain an estimation of a skin tumor depth from the measurement of the photosensitizer fluorescence emission.

BSu3A.10

From random lasing to single-nanoparticle detection, Seung Ho Choi¹, Zhengbin Xu¹, Qinghai Song², Young Kim¹; ¹*Purdue Univ., USA*; ²*Harbin Inst. of Technology, China*. We review our recent studies on random lasers for spectroscopic and biosensing approaches, using the unique combination of its intriguing physical principle, its simplicity of realization, and its sensitivity to nanoscale perturbations.

BSu3A.3

In vivo near infrared fluorescence imaging of efficient systemic siRNA delivery with HDL-mimicking peptide lipid nanoparticles, Qiaoya Lin^{1,3}, Juan Chen¹, Zhihong Zhang^{1,3}, Gang Zheng^{1,2}; ¹*Campbell Family Cancer Research Inst. and Ontario Cancer Inst., Univ. Health Network, Canada*; ²*Department of Medical Biophysics, Univ. of Toronto, Univ. of Toronto, Canada*; ³*Britton Chance Center for BIOMEDical Photonics, Wuhan National Laboratory for Optoelectronics-Huazhong Univ. of Science & Technology, China*. The big challenge for RNAi therapeutics is systemic delivery of siRNA. Here, we report the successful in vivo targeted delivery of siRNA using HDL-Mimicking Peptide Phospholipid Scaffold (HPPS) nanoparticle proved by near infrared fluorescence imaging.

BSu3A.7

Withdrawn

BSu3A.11

Withdrawn

BSu3A.4

Raman-Coded Nanoparticles for Multiplexed Molecular Endoscopy of the Esophagus, Anushree Srivastava¹, Jack Zhou², Danni Wang¹, Steven Y. Leigh¹, Ye Chen¹, Jonathan T. Liu¹; ¹*BIOMEDical Engineering, State Univ. of New York (SUNY) at Stony Brook, USA*; ²*Ward Melville High School, USA*. In order to perform quantitative molecular imaging of a large panel of disease biomarkers in a rat model of esophageal cancer, a rigid endoscopic probe is being developed to image molecularly targeted SERS nanoparticles.

BSu3A.8

Optically Controlled Opening of Self-Sealing Giant Unilamellar Vesicles, Elizabeth Huynh^{1,2}, Jonathan F. Lovell³, Gang Zheng^{1,2}; ¹*Univ. of Toronto, Canada*; ²*Univ. Health Network, Canada*; ³*Univ. at Buffalo, State Univ. of New York, USA*. Micron-scale giant unilamellar vesicles were readily opened using a focused laser beam in situ. These giant unilamellar vesicles have potential use as versatile microreactors possessing temporally and spatially controlled optical opening.

BSu3A.12

Study on the Cytosolic delivery mechanism of HDL-mimicking Peptide-Phospholipid Scaffold (HPPS) By Confocal Microscopy, Qiaoya Lin^{1,2}, Juan Chen¹, Zhihong Zhang^{1,2}, Gang Zheng^{1,3}; ¹*Campbell Family Cancer Research Inst. and Ontario Cancer Inst., Univ. Health Network, Canada*; ²*Britton Chance Center for BIOMEDical Photonics, Wuhan National Laboratory for Optoelectronics-Huazhong Univ. of Science & Technology, China*; ³*Department of Medical Biophysics, Univ. of Toronto, Canada*. The cytosolic drug delivery mechanism is a key advantage for the delivery of intracellular active cancer agents. Here, we use confocal microscopy to investigate the cytosolic delivery mechanism of HDL-mimicking peptide-phospholipid scaffold (HPPS).

BSu3A: BIOMED Poster Session I—Continue

BSu3A.13

Optical Fiber Biosensor with Self-Assembled Nanoscale Coatings for Rapid Detection of Methicillin-Resistant Staphylococcus Aureus, James R. Heflin¹, Ziwei Zuo¹, Abey Bandara², Anne Hyman², Thomas Inzana², Siddharth Ramachandran³; ¹Physics, Virginia Tech, USA; ²BIOMED-ical Sciences and Pathobiology, Virginia Tech, USA; ³Electrical Engineering, Boston Univ., USA. A turnaround point long-period grating with an ionic self-assembled multilayer film and monoclonal antibody on the cladding surface can detect methicillin-resistant staphylococcus aureus at a level of 450 cells/ml in under an hour.

BSu3A.14

Exploring the Multifunctional Capabilities of Porphysomes for Prostate Cancer Imaging, Tracy W. Liu¹, Thomas D. MacDonald¹, Cheng Jin¹, Brian C. Wilson¹, Gang Zheng¹; ¹Medical Biophysics, Univ. of Toronto/Ontario Cancer Inst., Canada. We explore the multimodal imaging capacity of porphysomes beyond bionanophotonics. Porphysomes demonstrate PET treatment planning capabilities for prostate cancer that can be translated onto the surgical table by fluorescence guided therapy.

BSu3A.15

Gold nanocages as contrast agents for two-photon luminescence endomicroscopy, Yongping Chen¹, Yuying Zhang¹, Xingde Li¹; ¹Johns Hopkins Univ., USA. We reported the contrast agents based on structured Au nanocages for enhancing TPL endomicroscopic imaging. Cancer cells and tissues TPL endomicroscopy imaging with the Au nanocages were performed, demonstrating significant contrast enhancement.

BSu3A.16

Modeling AlGaInP-Au Lasers in Photodynamic Therapy for Tumors and Cancers, Meng-Mu Shih¹; ¹Univ. of Florida, USA. This work develops multi-parametric models to compute coupling coefficients of semiconductor-metal lasers at around 633 nm for photodynamic therapy. Numerical results computed by the photonic and the optical methods have excellent agreements.

BSu3A.17

An Edge Detection Approach for Mapping of the Human Cone Photoreceptor Mosaic using Adaptive Optics Scanning Laser Ophthalmoscope, Shahab Chitchian^{1,2}, Adam R. Borretsky¹, Frederik J. van Kuijk³, Massoud Motamedi^{1,2}; ¹Center for BIOMEDical Engineering, Univ. of Texas Medical Branch, USA; ²Department of Ophthalmology, Univ. of Texas Medical Branch, USA; ³Department of Ophthalmology, Univ. of Minnesota, USA. In this study, a novel edge detection algorithm and an adaptive optics scanning laser ophthalmoscopy were applied to visualize the cone photoreceptor mosaic from approximately 4° to 8° eccentricities in the vertical, superior retina.

BSu3A.18

Confocal Retinal Imaging using Scanning Laser Ophthalmoscopy with Annular Beams, Brian Vohnsen¹, Benjamin Lochocki¹, Carmen Vela-Garcia¹, Diego Rativa¹; ¹School of Physics, Univ. College Dublin, Ireland. The human retina has been imaged in-vivo using scanning laser ophthalmoscopy employing annular incident beams adapted for resolution optimization. The pros and cons of the approach are discussed and the importance of coherence is explored.

BSu3A.19

Influence of Wavefront Slope on Effective Retinal Images Using a Spatial Light Modulator, Sara Castillo¹, Brian Vohnsen²; ¹School of Physics, Univ. college dublin, Ireland; ²School of Physics, Univ. college dublin, Ireland. A spatial light modulator has been used to project two coherent Maxwellian point sources on to the eye and study the Stiles-Crawford effect dependence on the wavefront slope create at the retina.

BSu3A.20

In vivo cytometry using two-photon autofluorescence microscopy, Yan Zeng¹, Jin Xu², Dong Li¹, Li Li², Zilong Wen², Jianan Y. Qu¹; ¹Department of Electronic and Computer Engineering, Hong Kong Univ. of science and technology, Hong Kong; ²Department of Biochemistry, Hong Kong Univ. of Science and Technology, Hong Kong. We demonstrate an in vivo cytometry based on two-photon excited autofluorescence in zebrafish blood vessels. The plasma and NADH fluorescence provide contrasts for visualizing and counting of red blood cells and white blood cells, respectively.

BSu3A.21

Lensed Fiber Raster Scanner for a Large Field-of-View, High-Resolution Microendoscope, David R. Rivera¹, Christopher M. Brown¹, Dimitre G. Ouzounov¹, Watt W. Webb¹, Chris Xu¹; ¹AEP, Cornell Univ., USA. A lensed fiber is used in a miniaturized fiber-raster scanner for a microendoscope with large field-of-view and high-resolution. Paired with a miniature lens, the scanner achieves a 1.1-um lateral resolution with a 440-um-diameter FOV.

BSu3A.22

Optical Microfluidics for Cell Studies, Sanhita S. Dixit¹, Hanyoung Kim¹, Kanaka Hettiarachchi¹, Gregory W. Faris¹; ¹Molecular Physics Laboratory, SRI International, USA. We apply optical microfluidic methods to cell studies including: nanoliter polymerase chain reaction amplification of DNA/RNA, useful for circulating tumor cells; and preparing artificial bilayers, useful for transmembrane protein function.

BSu3A.23

Extended depth of field microscopy by using digital optics, Yung Lin Chen¹; ¹ITRI, Taiwan. The shallow depth of field (DOF) of the microscope is the inherent problem due to its high numerical aperture (NA), the paper proposed a method to extend the DOF by using spherical phase coding, DOF can be extended 2 times

BSu3A.24

Two-photon volume imaging with a nondiffracting beam: a simulation study based on a scalar diffraction method, Juanjuan Zheng¹, Yanlong Yang¹, Ming Lei¹, Baoli Yao¹, Peng Gao¹, Tong Ye¹; ¹State Key Laboratory of Transient Optics and Photonics, Xi'an Inst. of Optics and Precision Mechanics, Chinese Academy of Sciences, China. A two-photon excitation fluorescence volume imaging method is proposed with a non-diffracting and self-reconstructing Bessel beam and investigated with a simulation approach based on a scalar diffraction method.

BSu3A: BIOMED Poster Session I—Continue

BSu3A.25
Study on vibration characteristics of two nodal wedges controlled NSOM probe submerged partially in water, Wonjun Lee¹, Dae-Chan Kim¹, Seung Gol Lee²; ¹*Inha Univ., Republic of Korea*. Vibration characteristics of a dithering NSOM probe being controlled mechanically with two nodal wedges, whose tip end was partially submerged in water, was studied. The optimum controlling condition was found for measuring samples in water.

BSu3A.29
Aberration correction of sub-10-fs pulse focusing with high-numerical-aperture microscope objective, Miaochan Zhi¹, Holly Gibbs¹, Alvin Yeh¹; ¹*BIOMEDical Engineering, Texas A&M Univ., USA*. Deformable mirror is used to correct radially varying group delay in a nonlinear optical microscopy setup aiming to improve signal generation and image resolution. Simulations and experiments which support the efficacy of our method are presented.

BSu3A.33
Elucidating metabolic, subcellular, and tissue-level changes induced by HPV-related oncoproteins, Joanna Xylas¹, Margaret McLaughlin-Drubin², Karl Münger², Irene Georgakoudi¹; ¹*BIOMEDical Engineering, Tufts Univ., USA*; ²*Brigham and Women's Hospital, USA*. We use tissue engineering and a Human papillomavirus (HPV) model of carcinogenesis to associate specific molecular changes to optical precancerous biomarkers.

BSu3A.26
Needle-free Microscopy for Malaria Diagnostics, Jennifer Burnett¹, Rebecca Richards-Kortum¹; ¹*Bioengineering, Rice Univ., USA*. This is a proof-of-concept study to assess whether in vivo confocal microscopy coupled with topical proflavine staining can be used to recognize malaria-infected RBCs. Results from a chicken embryo model indicate this may be feasible.

BSu3A.30
Phase derivative microscopy for label-free imaging of dynamic biological structures, Taewoo Kim¹, Gabriel Popescu¹; ¹*Electrical and Computer Engineering, Univ. of Illinois, Urbana-Champaign, USA*. Laplace and gradient field microscopy use a spatial light modulation in the Fourier plane of a microscope image to measure the intensity of field derivatives which is valuable in studying the dynamics of biological samples.

BSu3A.34
Polarization Imaging System for Colposcopy, Victor Chernomordik¹, Alexander Sviridov^{2,1}, Moinuddin Hassan¹, Jana M. Kainerstorfer¹, Laleh Najafzadeh¹, Paul D. Smith³, Amir Gandjbakhche¹; ¹*Program in Physical Biology, Lab. of Integrative and Medical Biophysics, National Inst. of Child Health and Human Development, National Inst.s of Health, USA*; ²*Inst. for Laser and Information Technologies of Russian Academy of Sciences, Russian Federation*; ³*Ecole Supérieure de Physique et de Chimie Industrielle de Paris, France*. The designed polarization adapter is incorporated into a colposcope, provides illumination with polarized light and capturing of orthogonally polarized images, using liquid crystal retarder and polarizer.

BSu3A.27
 Withdrawn

BSu3A.31
Computation of baseline flow across the mouse cortex using two-photon microscopy and vascular anatomical network modeling, Louis Gagnon^{1,2}, Emiri T. Mandeville³, Mohammad A. Yaseen², Vivek J. Srinivasan², Eng Lo³, Emmanuel Roussakis⁴, Sergei A. Vinogradov⁴, Anna Devor⁵, David Boas^{2,1}, Sava Sakadzic²; ¹*Harvard-MIT Division of Health Sciences and Technology, USA*; ²*Athinoula A. Martinos Center for BIOMEDical Imaging, Department of Radiology, Massachusetts General Hospital, Harvard Medical School, USA*; ³*Departments of Radiology and Neurology, Massachusetts General Hospital, Harvard Medical School, USA*; ⁴*Department of Biochemistry and Biophysics, Univ. of Pennsylvania, USA*; ⁵*Departments of Neurosciences and Radiology, Univ. of California San Diego, USA*. We demonstrate the feasibility of computing baseline flow in the mouse cortex using vascular anatomical network constructed from two-photon microscopy measurements. The values obtained are in good agreement with values reported in the literature.

BSu3A.35
Fiber-optic Second Harmonic Generation Endomicroscopy: A Potential tool for Diagnosis of Preterm Birth, Yuying Zhang¹, Meredith L. Akins², Kartikeya Murari¹, Ming-Jun Li⁴, Katherine Luby-Phelps³, Mala Mahendroo², Xingde Li¹; ¹*Department of BIOMEDical Engineering, Johns Hopkins Univ. School of Medicine, USA*; ²*Department of Obstetrics and Gynecology, UT Southwestern Medical Center, USA*; ³*Department of Cell Biology, UT Southwestern Medical Center, USA*; ⁴*Science and Technology, Corning Incorporated, USA*. We present a fiber-optic scanning second harmonic generation (SHG) endomicroscopy system that can detect the morphological changes in cervical collagen fiber during gestation with sub-micrometer resolution.

BSu3A.28
A simple, cost efficient fiber amplifier wavelength extension unit for broadly tunable, femtosecond pulse Ti-sapphire lasers for CARS microscopy, Attila Kolonics^{1,2}, Dániel Csáti¹, Péter Antal¹, Róbert Szipöcs^{1,2}; ¹*Research Inst. for Solid State Physics and Optics, Hungary*; ²*R&D Ultrafast Lasers Ltd, Hungary*. An inherently synchronized Yb-fiber amplifier based extension unit for femtosecond pulse, broadly tunable Ti-sapphire lasers is introduced, which is well suited for coherent anti-Stokes Raman scattering microscopy.

BSu3A.32
In Vivo Imaging of Unstained Rat Tissue Using a Multiphoton Microendoscope, Christopher M. Brown¹, David R. Rivera¹, Dimitre G. Ouzounov¹, Ina Pavlova¹, Watt W. Webb¹, Chris Xu¹; ¹*AEP, Cornell Univ., USA*. Unstained liver, kidney, and colon tissue from an anesthetized rat was imaged in vivo using a compact and flexible raster scanning endoscope. Endoscopic image acquisition was guided using a wide field infrared imaging system.

BSu3A.36
Lissajous Scanning Fiber-optic Nonlinear Endomicroscope with Precise Position Calibration, Kartikeya Murari¹, Wenxuan Liang¹, Yuying Zhang¹, Jiefeng Xi¹, Xingde Li¹; ¹*Johns Hopkins Univ., USA*. Using an acousto-optic modulator that froze beam positions on frames captured by an ordinary CCD camera, we were able to calibrate the Lissajous scanning pattern on a fiber-optic nonlinear endomicroscope quickly and precisely.

BSu3A: BIOMED Poster Session I—Continue

BSu3A.37

White Light Diffraction Phase Microscopy (wDPM) for quantitative phase imaging, Basanta Bhaduri¹, Gabriel Popescu¹; ¹*Electrical and Computer Engineering, Univ. of Illinois at Urbana Champaign, USA*. We present white-light diffraction phase microscopy (wDPM) as a fast and sensitive quantitative phase imaging method and a successive derivatives based phase reconstruction method. We illustrate the utility of wDPM with measurements on live cells.

BSu3A.38

Response to Optical Trapping by Red Blood Cells (RBCs) from a Transfused Sickle Cell Patient, Daniel Erenso¹, Aline Pellizzaro³, Gabriel Welker¹, Omar Mohammed¹, Anthony Farone³, Mary Farone³, Maria del Pilar Aguinaga²; ¹*Physics & Astronomy, Middle Tennessee State Univ, USA*; ²*Obstetrics and Gynecology3, Meharry Sickle Cell Center, Meharry Medical College, USA*; ³*Biology, Middle Tennessee State Univ, USA*. The response of RBCs from a transfused sickle cell anemia (Hb S and Hb A) patient has been studied in comparison with RBCs from a healthy person (Hb AA) when directly trapped by a laser.

BSu3A.39

Stimulated Emission Depletion Microscopy with a Single Ultrafast Laser, Tong Ye¹, Yuhua Zhang², Xun Ai³, Lucas Pozzo-Miller¹, Kent Keyser⁴; ¹*Department of Neurobiology, Univ. of Alabama at Birmingham, USA*; ²*Ophthalmology, Univ. of Alabama at Birmingham, USA*; ³*Medicine, Univ. of Alabama at Birmingham, USA*; ⁴*Vision Science, Univ. of Alabama at Birmingham, USA*. We present a stimulated emission depletion microscopy system that has been built around a single ultrafast laser system. Excitation beams are provided by a supercontinuum generation with the same laser.

BSu3A.40

Selective Sampling in Hyperspectral Raman Micro-Spectroscopy: Obtaining Maximum Data with Minimal Sampling Time, Christopher Rowlands^{1,2}, Ioan Nottingher¹; ¹*Physics, Univ. of Nottingham, UK*; ²*Biological Engineering, MIT, USA*. We present a new method for selectively sampling hyperspectral Raman maps in order to maximize the information that can be obtained for a given sample time. Example maps and comparisons with alternative methods are provided.

BSu3A.41

Infrared Cholangiography in open surgery and its projection to minimally invasive surgery, Patricio E. Fluxa^{1,3}, Carlos Castilla², Mario Garavaglia^{1,3}, Jannick Rolland⁴; ¹*CIOp Centro de Investigaciones Opticas, Argentina*; ²*Fac. de Ciencias Medicas, Universidad Nacional de La Plata, Argentina*; ³*Dpto. de Fisica, Universidad Nacional de La Plata, Argentina*; ⁴*The Inst. of Optics, Univ. of Rochester, USA*. This paper describes an alternative method for imaging the bile ducts during Cholecystectomy. X-Rays are not needed. Positive results in open cholecystectomy are shown and the design of an IR endoscope is evaluated.

BSu3A.42

Reflection-mode submicron-resolution photoacoustic microscopy in vivo, Chi Zhang¹, Konstantin Maslov¹, Song Hu¹, Ruimin Chen², Qifa Zhou², Kirk Shung², Lihong V. Wang¹; ¹*BIOMEDical Engineering, Washington Univ. in St. Louis, USA*; ²*BIOMEDical Engineering, Univ. of Southern California, USA*. We developed the first reflection-mode submicron-resolution photoacoustic microscopy system. With a lateral resolution of ~0.5 μm and a maximum penetration depth of ~0.42 mm in soft tissue, it is suitable for in vivo high-resolution imaging.

BSu3A.43

Ring-shaped confocal photoacoustic computed tomography for small-animal whole-body imaging, Jun Xia¹, Muhammad Chatni¹, Konstantin Maslov¹, Zijian Guo¹, Rebecca Sohn¹, Jeffrey Arbeit¹, Mark Anastasio¹, Quing Zhu², Lihong V. Wang¹; ¹*BIOMEDical Engineering, Washington Univ. in St. Louis, USA*; ²*Electrical Engineering, Univ. of Connecticut, USA*. We developed a new photoacoustic tomography system for small-animal whole-body imaging. With the novel design of ring-shaped light delivery and full-ring ultrasonic array detection, the system can generate a cross-sectional image in 1.6 seconds.

BSu3A.44

Finite-element-method based reconstruction of heterogeneous conductivity distribution under point-illumination in trans-rectal imaging geometry for thermoacoustic tomography, Sovanlal Mukherjee¹, Charles F. Bunting¹, Daqing Piao¹; ¹*Oklahoma State University, USA*. We simulate trans-rectal thermo-acoustic tomography by using a convex-array of ultrasound transducer and a point microwave illuminator. Tissue conductivity distribution is reconstructed by decoupling the electrical field from the power loss density.

BSu3A.45

FEM model based optimization of transducer geometry for photoacoustic imaging, Wenfeng Xia¹, Daniele Piras¹, Spiridon van Veldhoven², Christian Prins², Ton G. van Leeuwen^{1,3}, Wiendelt Steenbergen¹, Srirang Manohar¹; ¹*BIOMEDical Photonic Imaging, Netherlands*; ²*Oldelft Ultrasound B.V., Netherlands*; ³*BIOMEDical Engineering and Physics, Netherlands*. We optimize the design of an ultrasound transducer for photoacoustic breast imaging using FEM analysis. We arrive at a detector design which shows significant improvement in image quality when used in photoacoustic tomographic simulations.

BSu3A.46

Iterative Algorithm for Multiple Illumination Photoacoustic Tomography using Transducer Channel Data, Roger J. Zemp¹, Peng Shao¹; ¹*Electrical & Computer Engineering, Univ of Alberta, Canada*. We present an algorithm for quantitative photoacoustic tomography based on minimizing an error functional between measured photoacoustic channel data and a calculated forward model. Simulations using multiple illuminations show improved conditioning over single illumination.

BSu3A.47

Toward quantitative fluorescence by using ultrasound modulation of light, Khalid Daoudi¹, Wiendelt Steenbergen¹; ¹*BIOMEDical Photonic Imaging group, Univ. of Twente MIRA Inst. for BIOMEDical Technology and Technical Medicine, Netherlands*. We propose a method to quantify fluorophore absorption coefficient by combining acousto-optics and fluorescence. Using Monte Carlo simulations we explain a methodology and we show a possibility to estimate absorption coefficient within 10% accuracy

BSu3A.48

Intraoperative photoacoustic tumor imaging, Lei Xi¹, Stephen Grobmyer¹, Lei Wu¹, Ruimin Chen², Guangyin Zhou¹, Luke Gutwein¹, Jingjing Sun¹, Wenjun Liao¹, Qifa Zhou², Huikai Xie¹, Huabei Jiang¹; ¹*Univ. of Florida, USA*; ²*Department of BIOMEDical Engineering, Univ. of Southern California, USA*. We report a microelectromechanical systems based intraoperative PAT technique, and demonstrate its ability for accurately mapping tumors in three-dimension and inspecting the completeness of tumor resection during surgery in an animal model.

BSu3A: BIOMED Poster Session I—Continue

BSu3A.49

Spectrally Encoded Photoacoustic Microscopy Using a Digital Mirror Device, Yu Wang¹, Konstantin Maslov¹, Lihong Wang¹; ¹*Dept. of BIOMEDical Engineering, Washington Univ. in St. Louis, USA*. We developed a spectrally encoded photoacoustic microscope system using a digital mirror device. Using spectrally encoded PA measurement, the imaging system can recover chromophore absorption spectra at a low laser pulse energy.

BSu3A.50

Quantitative photoacoustic tomography assisted by diffuse optical tomography: A simulation study, Xiaoqi Li¹, Huabei Jiang¹; ¹*BIOMEDical Engineering, Univ. of Florida, USA*. We present a new method that can enhance quantitative recovery of optical absorption coefficient in heterogeneous media from photoacoustic data by considering inhomogeneous scattering coefficient distribution provided by diffuse optical tomography.

BSu3A.51

Modeling GaAs/AlGaAs/Ag Lasers for Photoacoustic Diagnosis of Bone Density by Photonic and Optical Methods, Meng-Mu Shih¹; ¹*Univ. of Florida, USA*. This work develops models to compute coupling coefficients of semiconductor-metal lasers for photoacoustic diagnosis of bone density variations. Numerical results computed by the photonic and the optical methods have close values.

BSu3A.52

Photoacoustic detection of iron oxide nanoparticles in resected rat lymph nodes, Diederik J. Grootendorst¹, Jithin Jose¹, Raluca Fratila³, Martijn Visscher³, Aldrik Velders², Bennie Ten Haken³, Ton G. van Leeuwen^{1,5}, Wiendelt Steenberg¹, Srirang Manohar¹, Theo J. Ruers⁴; ¹*BIOMEDical Photonic Imaging, Univ. of Twente, Netherlands*; ²*BIO-MEDical Chemistry, Univ. of Twente, Netherlands*; ³*Neuro IMaging, Univ. of Twente, Netherlands*; ⁴*Nanobiophysics, Univ. of Twente, Netherlands*; ⁵*BIOMEDical Engineering and Physics, Academic Medical Center Univ. of Amsterdam, Netherlands*. Photoacoustic detection of superparamagnetic iron oxide nanoparticles was performed in resected rat lymph nodes opening up possibilities for intra-operative nodal staging in oncology.

BSu3A.53

In-vivo Imaging of Embedded Surgical Sutures and the Surrounding Physiology with Photoacoustic Microscopy, Alexia Giannoula¹, Lutz Funk², Christine Weis², Pau Turon², Turgut Durduran¹; ¹*Inst. of Photonic Sciences, Spain*; ²*BBraun Surgical SA, Spain*. We image surgical sutures embedded in tissue and the surrounding tissue physiology using photoacoustic microscopy (PAM). PAM can be used to monitor the suture integrity, the healing process, infections and bleeding non-invasively at high-resolution.

BSu3A.54

Water-Immersible MEMS Scanning Mirror Enhanced Optical-Resolution Photoacoustic Microscopy, Junjie Yao¹, Chih-Hsien Huang², Konstantin Maslov¹, Lidai Wang¹, Liang Gao¹, Jun Zou², Lihong V. Wang¹; ¹*BIOMEDical Engineering, Washington Univ. in St. Louis, USA*; ²*Department of Electrical and Computer Engineering, Texas A&M Univ., USA*. A fast scanning optical-resolution photoacoustic microscopy has been developed using a water-immersible MEMS mirror. A B-scan rate of 400 Hz over a 3 mm scanning range has been demonstrated in phantom studies.

BSu3A.55

Generation of Photonic Shell Microbubbles, Elizabeth Huynh^{1,2}, Jonathan F. Lovell³, Brandon Helfield^{1,4}, Chulhong Kim³, David Goertz^{1,4}, Gang Zheng^{1,2}; ¹*Univ. of Toronto, Canada*; ²*Univ. Health Network, Canada*; ³*Univ. at Buffalo, State Univ. of New York, USA*; ⁴*Sunnybrook Health Sciences Center, Canada*. Photonic shell microbubbles demonstrated unique physical properties including enhanced serum stability, superior size monodispersity and increased microbubble yield. They are also suitable for both ultrasound and photoacoustic imaging.

BSu3A.56

Fiber Laser Based Realtime Optical-Resolution Photoacoustic Microscopy and Microendoscopy, Roger J. Zemp¹, Wei Shi¹, Peng Shao¹, Parsin Hajireza¹; ¹*Electrical & Computer Engineering, Univ. of Alberta, Canada*. We present an OR-PA microendoscope system based on an image-guide fiber, a high-repetition-rate fiber laser, and a fast-scanning mirror system. The system is capable of imaging 800 micron field of views in realtime.

BSu3A.57

Photoacoustic detection of small volume of tissue and cell clusters targeted with modified gold nanorods, Anton Liopo¹, Andre Conjusteau¹, Sergey Ermilov¹, Alexander Oraevsky¹; ¹*Tomowave Laboratories Inc., USA*. We propose the use of surface-modified gold nanorods (GNR) as a contrast agent for photoacoustic detection into small volume of tissue or cell clusters. Accumulation of targeted GNR in cells will yield increased, selective laser-cell interactions.

BSu3A.58

Multispectral imaging as a potential predictor of treatment efficacy for Kaposi's sarcoma skin lesions, Jana M. Kainerstorfer^{1,2}, Mark N. Polizzotto¹, Thomas S. Ulrick¹, Moinuddin Hassan¹, Rafa Rahman¹, Laleh Najafizadeh¹, Kathleen M. Wyvill¹, Karen Aleman¹, Paul D. Smith¹, Robert Yarchoan¹, Amir Gandjbakhche¹; ¹*National Inst.s of Health, USA*; ²*Department of BIOMEDical Engineering, Tufts Univ., USA*. Assessment of the response of Kaposi's sarcoma lesions to therapy is challenging. We propose diffuse multispectral imaging for lesion follow-up as an objective measure for treatment efficacy.

BSu3A.59

Time-bin Optimization in Time-resolved Near Infrared Fluorescence Tomography, Hamid Dehghani¹, Qun Zhu¹, Fredric Leblond², Kenneth M. Tichauer², Robert Holt², Brian Pogue²; ¹*Univ. of Birmingham, UK*; ²*Thayer School of Engineering, Dartmouth College, USA*. In this work we present a general method for the optimization of time-bins for accurate recovery of fluorophores in NIR tomography, which provide both high resolution and contrast, particularly in the presence of multiple targets.

BSu3A.60

Whole body optical imaging without a scattering background, Kevin J. Webb¹, Vaibhav Gaiind¹, Hsiao-rho Tsai¹, Brian Bentz¹, Venkatesh Chelvam¹, Philip Low¹; ¹*Purdue Univ., USA*. An imaging method that utilizes a laser topography scan and a multigrid reconstruction based on a diffusion model avoids the scattering emulsion background. Image reconstructions for a tissue phantom and fluorescence in a mouse are shown.

BSu3A: BIOMED Poster Session I—Continue

BSu3A.61

Model-based demonstration of spectral tomographic imaging, Shikhar Uttam¹, Sergey Alexandrov¹, Rajan K. Bista¹, Yang Liu¹; ¹*Univ. of Pittsburgh, USA*. Simulation results for a novel optical diffraction tomography approach using spectral diversity to access Fourier components of the sample permittivity contrast are presented. Structure characterization of the sample reconstruction is also presented.

BSu3A.62

3D localization and tracking of gold particles in biological environment using digital holography, Michel Gross¹, Frédéric Verpillat¹, Pierre Desbiolles¹; ¹*Laboratoire Charles Coulomb - UMR 5221 CNRS-UM2, France*. By using the dark field holographic microscopy technique described in Opt. Express, 19 pp26044-26055 (2011) we have track gold particles in brownian motion in living cells. First results are presented.

BSu3A.63

An fMRI based Method for Characterizing Superficial Layer Contribution to fNIRS Signals, Sinem B. Erdogan¹, Turan D. Nevsehirli¹, Yasemin Keskin-Ergen¹, Ata Akin¹; ¹*BIOMEDICAL Engineering, Bogazici Univ., Turkey*. This study aims at extracting scalp and gray matter fMRI data obtained during breathhold and mental arithmetic tasks to quantify the degree and pattern of systemic fluctuations that are hypothesized to contaminate the fNIRS signal.

BSu3A.64

Application of Compressive Sensing to Bioluminescence Tomography, Hector R. Basevi^{1,2}, James A. Guggenheim^{1,2}, Hamid Dehghani^{1,2}, Iain B. Styles²; ¹*PSIBS, Univ. of Birmingham, UK*; ²*School of Computer Science, Univ. of Birmingham, UK*. Bioluminescence Tomography characteristics suggest its suitability to Compressive Sensing-based reconstruction. Numerical simulations examining reconstruction quality in the presence of noise demonstrate improved robustness and compactness.

BSu3A.65

Cell Life Cycle Characterization Based on Generalized Morphological Parameters for Interferometric Phase Microscopy, Pinhas Girshovitz¹, Natan Shaked¹; ¹*BIOMEDICAL Engineering, Tel Aviv Univ., Israel*. We developed new biological cell analysis tools for interferometric phase microscopy based directly on the quantitative phase profile and used them to characterize cancer-cell life cycle, and uniquely distinguish and predict the cell life phases.

BSu3A.66

Parametric level-set method for diffuse optical tomography with a hard l1 norm sparsity constraint, Fridrik Larusson¹, Pamela G. Anderson², Roni Cantor-Balan², Geethika Weliwitigoda², Angelo Sassaroli², Sergio Fantini², Eric Miller¹; ¹*Electrical and Computer Engineering, Tufts Univ., USA*; ²*BIOMEDICAL Engineering, Tufts Univ., USA*. We implement a parametric level-set (PaLS) method to reconstruct images for diffuse optical tomography (DOT). The method uses a large dictionary matrix with a hard l1 norm constraint allowing for accurate recovery of a wide array of shapes.

BSu3A.67

The Effect of Instrumentation on the Experimental Reduction of Photon Scatter in Time-Resolved Diffuse Fluorescence Tomography, Niksa Valim¹, Mark Nieder¹; ¹*Electrical and Computer Engineering, Northeastern Univ., USA*. Time-resolved detection of transmitted photons through diffusive media can be used to reduce scatter, but experimentally this is limited by instrument design. We investigate the impact of geometry, temporal response and sensitivity on this effect.

BSu3A.68

Tomographic reconstruction of absorption and diffusion coefficient maps in biological media using time-dependent parabolic simplified spherical harmonics equations, Jorge Bouza Dominguez¹, Yves Bérubé-Lauzière¹; ¹*Electrical Engineering, Université de Sherbrooke, Canada*. We present a diffuse optical tomography algorithm based on the time-dependent parabolic simplified spherical harmonics equations and adjoint variables for reconstructing images of absorption and diffusion coefficient distributions.

BSu3A.69

The transport of intensity equation and partially coherent fields, Jonathan Petrucci¹, Lei Tian¹, George Barbastathis^{1,2}; ¹*Massachusetts Inst. of Technology, USA*; ²*Singapore-MIT Alliance for Research and Technology (SMART) Centre, Singapore*. We examine the physical meaning of the phase recovered from the transport of intensity equation (TIE) with partially coherent illumination and verify experimentally a modification of the TIE which removes effects of nonuniform illumination from measurements of sample thickness.

BSu3A.70

Assessments of cerebral blood volume and oxygenation asymmetry in neonatal cardiopulmonary bypass by near infrared spectroscopy, Fenghua Tian¹, Joshua Koch², Joseph M. Forbess³, Katrina Vandebuinhorst², Dorothy Kelly², Hanli Liu¹; ¹*Bioengineering, Univ. of Texas at Arlington, USA*; ²*Pediatrics, Univ. of Texas Southwestern Medical Center at Dallas, USA*; ³*Cardiovascular and Thoracic Surgery, Univ. of Texas Southwestern Medical Center at Dallas, USA*. We use a NIRS device to monitor the neonatal brain during cardiopulmonary bypass. The focus is to assess the blood and oxygenation asymmetry caused by selective cerebral perfusion that has become standard of care.

BSu3A.71

Optimizing statistical analysis for DOT to image rapid brain function events, Mahlega Hassanpour¹, Brian R. White¹, Adam T. Eggebrecht², Silvina L. Ferradal³, Joseph P. Culver^{2,1}; ¹*Department of Physics, Washington Univ. in St. Louis, USA*; ²*Department of Radiology, Washington Univ. School of Medicine, USA*; ³*Department of BIOMEDICAL Engineering, Washington Univ. in St. Louis, USA*. A general linear model was used to statistically analyze HD-DOT data during rapid, event-related brain activation. Spatial and temporal properties of data were evaluated and used in the response modeling and statistical inference.

BSu3A.72

Capturing Task-Evoked Functional Brain Connectivity Using Combined NIRS/EEG, Nader Shahni Karamzadeh^{1,3}, Andrei Medvedev², Atieh Bakhtiar¹, Jana M. Kainerstorfer¹, Amir Gandjbakhche¹, Laleh Najafizadeh^{1,3}; ¹*Eunice Kennedy Shriver National Inst. of Child Health and Human Development, NIH, USA*; ²*Center for Functional and Molecular Imaging, Georgetown Univ., USA*; ³*Center for Neuroscience and Regenerative Medicine, Henry M. Jackson Foundation, USA*. To capture the dynamics of brain interactions subjects were exposed to an auditory and a visual task while their EEG/NIRS data were simultaneously being collected. Data analysis highlighted connectivity between multiple parts of the brain.

BSu3A: BIOMED Poster Session I—Continue

BSu3A.73

Registration and Analysis of Multi-spectral Images Acquired During Uterine Transplantation Surgery, Neil T. Clancy^{1,2}, Vincent Sauvage^{1,2}, Srdjan Saso³, Danail Stoyanov⁴, David J. Corless⁵, Michael Boyd⁶, David Noakes⁶, Guang-Zhong Yang^{1,7}, Sadaf Ghaem-Maghami⁸, J. R. Smith⁸, Daniel S. Elson^{1,2}; ¹*Hamlyn Centre for Robotic Surgery, Imperial College London, UK*; ²*Department of Surgery and Cancer, Imperial College London, UK*; ³*Inst. of Reproductive and Developmental Biology, Hammersmith Hospital, Imperial College London, UK*; ⁴*Centre for Medical Image Computing, Department of Computer Science, Univ. College London, UK*; ⁵*Department of Surgery, Leighton Hospital, UK*; ⁶*Royal Veterinary College, UK*; ⁷*Department of Computing, Imperial College London, UK*; ⁸*Gynaecological Oncology, West London Gynaecological Cancer Centre, Hammersmith Hospital, Imperial College London, UK*. Organ transplant success is dependent on blood supply health. A multispectral imaging laparoscope has been used to monitor tissue oxygenation during a rabbit uterine transplant. A feature tracking algorithm was used to compensate for movement.

BSu3A.77

Widefield Mesh-based Monte Carlo method in time-domain FMT, Jinchun¹; ¹*RPI, USA*. We evaluated the potential of mesh-based Monte Carlo method for widefield time-resolved fluorescence tomography in pre-clinical settings. The in silico results established that this method is computationally efficient for optical tomography.

BSu3A.74

Flexible Gen-2 Hand-held Optical Imager: Flat and Curved Phantom Studies, Manuela Roman¹, Sarah J. Erickson¹, Jean Gonzalez¹, Pallavi Joshi¹, Anuradha Godavarty¹; ¹*BIO-MEDical Engineering, Florida International Univ., USA*. A gen-2 hand-held based optical imager is developed with a flexible probe head to contour to different curved breast tissues. Targets are imaged within slab and curved breast phantoms, and resolution studies are ongoing.

BSu3A.78

A frequency domain near-infrared spectroscopy oximeter using high-speed, direct analog to digital conversion, Bernhard Zimmermann^{1,2}, Juliette Selb¹, Stefan Carp¹, Qianqian Fang¹, Joe Stadtmiller³, Robert Dewsnap³, Ron Altman³, David Boas¹; ¹*Athinoula A. Martinos Center for BIOMedical Imaging, Massachusetts General Hospital, USA*; ²*Department of Electrical Engineering and Computer Science, Massachusetts Inst. of Technology, USA*; ³*TechEn, Inc., USA*. A frequency-encoded frequency domain near-infrared spectroscopy (FD-NIRS) oximeter with two wavelengths has been constructed. The system digitizes the 67.5MHz and 75MHz waveforms using a high speed (180MSPS) 16-bit analog to digital converter.

BSu3A.75

Handheld near infrared imaging device for hemorrhage detection, Jason D. Riley¹, Franck Amyot¹, Tom Pohida¹, Randall Pursley¹, Yasaman Ardeshipour¹, Jana M. Kainerstorfer¹, Laleh Najafizadeh¹, Victor Chernomordik¹, Paul D. Smith¹, James Simrniotopoulos², Eric Wassermann¹, Amir Gandjbakhche¹; ¹*SAFB/PPITS/NICHD, NIH, USA*; ²*Uniformed Service Univ., USA*. We present a Near-infrared handheld device for imaging subsurface hemorrhage such as hematomas. The device uses novel motion-based measurement techniques to detect inclusions in real-time. We present phantom studies to demonstrate the technique.

BSu3A.79

Using few-mode fiber to improve the signal-to-noise ratio of DCS flow-oximeter measurements, Lian He¹, Yu Lin¹, Yu Shang¹, Guoqiang Yu¹; ¹*Center for BIOMedical Engineering, Univ. of Kentucky, USA*. Single-mode and few-mode fibers are used and compared for exploring the possibility to improve the signal-to-noise ratio of diffuse correlation spectroscopy (DCS) flow-oximeter measurements.

BSu3A.76

Real-time in vivo visualization of tissue oxygenation and autofluorescence with a snapshot hyperspectral camera for detection of precancerous lesions, Noah Bedard¹, Tomasz Tkaczyk¹; ¹*Bioengineering, Rice Univ., USA*. A new type of snapshot hyperspectral camera shows promising preclinical results for real-time in vivo detection of oral and esophageal cancers. Maps of hemoglobin content, tissue oxygenation and autofluorescence are presented for oral cavity tissue.

BSu3A.80

Design of a Multi-Wavelength Time-Domain Imager Based on a Supercontinuum Laser, Juliette Selb¹, Bernhard Zimmermann¹, Mark Martino¹, David Boas¹; ¹*The Optics Division at the Athinoula A. Martinos Center for BIOMedical Imaging, Massachusetts General Hospital, USA*. We developed a multi wavelength time domain imager for baseline hemoglobin measurements and functional imaging. A multiplexed supercontinuum pulsed laser and gated parallel detection on an intensified CCD camera allow for multi channel imaging.

BSu3A: BIOMED Poster Session I—Continue

BSu3A.81

Time-resolved spectral imaging of fluorescent inclusions in optically turbid medium: a phantom study, Daniel Milej¹, Marcin Botwicz¹, Anna Gerega¹, Norbert Zolek¹, Adam Liebert¹; ¹*IBBE PAS, Poland*. Time-resolved measurements of diffuse reflectance and fluorescence carried out on polyurethane phantom with ICG inclusions confirm that fluorescence data may allow for depth selective detection of inclusions in the turbid medium.

BSu3A.85

NIRS Captured Changes in Resting State Functional Connectivity after Performing a Working Memory Task, Laleh Najafizadeh^{1,2}, Fatima Chowdhry², Nader Shahni karamzadeh², Jana M. Kainerstorfer^{2,3}, Franck Amyot², Jason D. Riley², Amir Gandjbakhche²; ¹*Center for Neuroscience and Regenerative Medicine, Henry M. Jackson Foundation, USA*; ²*Section on Analytical and Functional BioPhotonics/PPITS, Eunice Kennedy Shriver National Inst. of Child Health and Human Development/NIH, USA*; ³*Department of BIOMEDical Engineering, Science & Technology Center, Tufts Univ., USA*. We investigate changes in the resting-state functional connectivity (RSFC) in the prefrontal cortex before and after executing a working memory task, using NIRS. Preliminary results demonstrate changes in RSFC after executing a working memory task.

BSu3A.89

Bioluminescence Tomography With A PDE-Constrained Algorithm Based On The Equation Of Radiative Transfer, Hyun K. Kim^{1,2}, Andreas H. Hielscher^{1,2}; ¹*BIOMEDical Engineering, Columbia Univ., USA*; ²*Radiology, Columbia Univ., USA*. We present the first bioluminescence tomography algorithm that makes use of the PDE-constrained concept, which has shown to lead to significant savings in computation times in similar applications.

BSu3A.82

A novel method for measurement of dynamic light scattering phase function of particles utilizing laser-Doppler power density spectra, Stanislaw Wojtkiewicz¹, Adam Liebert¹, Herve Rix², Piotr Sawosz¹, Roman Maniewski¹; ¹*IBBE PAS, Poland*; ²*IS CNRS, France*. We developed a novel method of measurement of the dynamic light scattering phase function of particles utilizing laser Doppler technique. We show: theoretical background, validation carried out on Monte Carlo and proposition of measurement setup.

BSu3A.86

Solving Inverse Problem of Diffuse Optical Tomography with Global Optimization, Behnoosh Tavakoli¹, Quing Zhu¹; ¹*ECE, Univ. of connecticut, USA*. A new imaging reconstruction based on a global optimization approach is presented. Simulation and phantom results have demonstrated superior performance in accurately mapping absorption distribution compared with that of conjugate-gradient method.

BSu3A.90

Methods For Simultaneous Optical And Electrical Measurement Of Neurovascular Coupling in Awake Rats, Jason Sutin¹, Weicheng Wu¹, Lana Ruvinskaya¹, Maria Angela Franceschini¹; ¹*Athinoula A. Martinos Center for BIOMEDical Imaging, Massachusetts General Hospital / Harvard Medical School, USA*. Development of an implantable EEG and diffuse optical imaging probe for longitudinal measurements in awake rats to investigate neurovascular coupling.

BSu3A.83

Photodynamic Molecular Beacons: An Image -Guided Therapeutic Approach for Vertebral Metastases, Tracy W. Liu¹, Margarete K. Akens^{1,2}, Juan Chen¹, Lisa Wise-Milestone², Brian C. Wilson¹, Gang Zheng¹; ¹*Medical Biophysics, Univ. of Toronto/Ontario Cancer Inst., Canada*; ²*Sunnybrook Health Science Centre, Univ. of Toronto, Canada*. We demonstrate the metastatic-specific activation of photodynamic molecular beacons by MMPs as a useful image-guidance tool with an unprecedented level of PDT selectivity for the therapeutic management of breast cancer spinal metastases.

BSu3A.87

Target Tumor Hypoxia with 2-nitroimidazole-ICG dye Conjugate, Yan Xu¹, Quing Zhu¹; ¹*ECE, UCONN, USA*. We systemically evaluated the sensitivity of the hypoxia targeted 2-nitroimidazole-ICG conjugate using piperazine linker in in-vivo tumor models, which showed hypoxia can be targeted with twice higher signal strength than that of untargeted ICG.

BSu3A.91

Breast Cancer Detection by Optomechanical Imaging, Rabah M. Al abdi¹, Harry L. Graber^{1,2}, Yong Xu^{1,2}, Randall L. Barbour^{1,2}; ¹*Pathology, SUNY Downstate Medical Center, USA*; ²*NIRx Medical Technologies, USA*. A new functional imaging system, which combines precise mechanical articulation and dynamic optical tomography for the detection breast cancer, is presented. Results obtained indicate that a wealth of new contrast features is accessible.

BSu3A.84

Depth sensitivity in multi-distance NIRS measurements in humans, Christina Habermehl¹, Christoph H. Schmitz^{1,4}, Stefan P. Koch¹, Jan Mehnert^{1,3}, Jens Steinbrink^{1,2}; ¹*Neurology, Charité Berlin, Germany*; ²*Center for Strokeresearch Berlin (CSB), Charité Berlin, Germany*; ³*Neurology, Max Planck Inst. for Human Cognitive and Brain Sciences, Germany*; ⁴*Nirx Medizintechnik, Germany*. We review different experiments using HR-DOT to monitor functional activation or brain perfusion in humans. We show the demand of an objective depth correction algorithm, especially when intrinsic contrast agents are used.

BSu3A.88

An Anatomical Atlas-Based Method for fNIRS Imaging of the Rhesus Macaque, Yong Xu^{1,4}, Tigran Gevorgyan^{1,3}, Douglas Pfeil¹, Daniel C. Lee^{2,3}, Randall L. Barbour^{1,3}; ¹*Pathology, SUNY Downstate Medical Center, USA*; ²*Surgery, SUNY Downstate Medical Center, USA*; ³*Surgery, Interfaith Medical Center, USA*; ⁴*NIRx Medical Technologies LLC., USA*. An anatomical atlas-based method for rhesus monkey brain imaging is presented. Numerical simulation, phantom experiment, and animal studies show that the method is computation-efficient in the generation and registration of 3D image findings.

BSu3A.92

Optomechanical Imaging: Biomechanical and Hemodynamic Responses of the Breast to Controlled Articulation, Rabah M. Al abdi¹, Gavriel Feuer¹, Harry L. Graber^{1,2}, Subrata Saha¹, Randall L. Barbour^{1,2}; ¹*Pathology, SUNY D.M.C., USA*; ²*NIRx Medical Technologies LLC., USA*. The optomechanical response of the breast was explored during fine articulation as a function of the applied force protocol. Comparisons between calculated internal pressure or stress maps and reconstructed hemodynamic images show strong correlations.

BSu3A: BIOMED Poster Session I

BSu3A.93

A Programmable Laboratory Testbed in Support of Evaluation of Functional Brain Activation, Randall L. Barbour^{1,3}, Harry L. Graber^{1,3}, Yong Xu^{1,3}, Yaling Pei³, Christoph H. Schmitz⁴, Douglas Pfeil¹, Anandita Tyagi¹, Randall Andronica¹, Daniel C. Lee^{2,5}, San-Lian S. Barbour³, John D. Nichols⁶, Mark E. Pflieger⁶; ¹*Pathology, SUNY Downstate Medical Center, USA*; ²*Surgery, SUNY Downstate Medical Center, USA*; ³*NIRx Medical Technologies LLC., USA*; ⁴*NIRx Medizintechnik GmbH, Germany*; ⁵*Interfaith Medical Center, USA*; ⁶*Source Signal Imaging, Inc., USA*. Near infrared spectroscopy and electroencephalography are well suited to explore the brain's response to neuroactivation. We have established a stable, programmable testbed that provides for experimental measures and analysis of neuroactivation-linked bioelectric and hemodynamic responses

BSu3A.94

Carbogen Inspiration Enhances Hemodynamic Contrast in the Cancerous Breast, Rabah M. Al abdi¹, Harry L. Graber^{1,2}, Randall L. Barbour^{1,2}; ¹*Pathology, SUNY D.M.C., USA*; ²*NIRx Medical Technologies LLC., USA*. We have explored the vascular response of the breast to inspiration of Carbogen. Results show greater changes in vasoconstriction and HbSat in the tumor-bearing breast compared to the healthy contralateral breast of the same patient.

BSu3A.95

Brain Connectivity via Traffic Engineering Approach, Serdar Aslan¹, Yasemin Keskin-Ergen¹, Ata Akin¹; ¹*Inst. of BIOMEDical Engineering, Bogazici Univ., Turkey*. Brain connectivity via fNIRS multi-channel data collected during s Stroop task is investigated via traffic engineering approach. Right lateralized increase in "brain traffic" was detected for incongruent condition compared to neutral one.

BSu3A.96

Quantitative diffuse optical tomography using a mobile phone camera and automatic 3D photo stitching, Qianqian Fang¹; ¹*Radiology, Massachusetts General Hospital, USA*. We show proof-of-concept for using an ultra-portable mobile-phone-based imaging system for quantitative 3D diffuse optical tomography. Phantom images were successfully recovered using a photo-stitched 3D model and near-infrared images, both acquired from a mobile-phone camera.

BSu3A.97

Monte Carlo simulation of realistic transmission breast optical tomography data for optimization of finite element image reconstruction, Mark Martino¹, Qianqian Fang¹, David Boas¹, Stefan Carp¹; ¹*Massachusetts General Hospital, USA*. We use mesh based Monte Carlo simulations to generate a realistic dataset for transmission breast diffuse optical tomography. We use these controlled conditions to test the impact of data degradation on finite element diffusion based image reconstructions.

Symphony IV

DH

13:00 - 14:45

DSu3C • Digital Holographic Microscopy I

T.-C. Poon; Virginia Tech, USA, Presider

DSu3C.1 • 13:00

Invited

Analysis and Experimental Achievement of High Resolution Imaging in Digital Holography, Jianlin Zhao¹; ¹*Department of Applied Physics, School of Science, Northwestern Polytechnical Univ., China*. Based on optical information theory, the propagation, recording and numerical reconstruction of the object wave are analyzed in a digital holographic image system, and several methods are presented to improve the resolution of reconstructed image.

DSu3C.2 • 13:30

Dual wavelength digital holographic imaging of cells with phase background subtraction, Alexander Khmaladze¹, Rebecca Matz¹, Joshua Jasensky¹, Emily Seeley¹, Mark M. Banaszak Holl¹, Zhan Chen¹; ¹*Univ. of Michigan, USA*. We describe a simple dual wavelength phase imaging method, which allows three dimensional measurements of a wide variety of biological systems and microstructures. Additionally, an effective method of removing phase background curvature is presented.

DSu3C.3 • 13:45

A Simple Lensless Digital Holographic Microscope, Shakil Rehman^{1,2}, Kiyofumi Matsuda³, Makoto Yamauchi³, Mikiya Muramatsu⁴, George Barbastathis^{1,5}, Colin Sheppard^{1,2}; ¹*BioSym, SMART, Singapore*; ²*Bioengineering, National Univ. of Singapore, Singapore*; ³*BIOMEDical Imaging, AIST, Japan*; ⁴*Institue of Physics, Univ. of Sao Paolo, Brazil*; ⁵*Chemical Engineering, MIT, USA*. Transparent objects can be imaged with high resolution along the optical axis by numerical reconstruction of digitally recorded holograms. A simple lensless digital holographic microscope is demonstrated to image optically transparent phase objects.

DSu3C.4 • 14:00

Iterative zero-order suppression from an off-axis hologram based on the 2D Hilbert transform, Florian B. Soulard¹, Alan Purvis¹, Richard McWilliam¹, Joshua Cowling¹, Gavin Williams², Jose J. Toriz-Garcia², N. Luke Seed², Peter A. Ivey³; ¹*School of Engineering and Computing Sciences, Durham Univ., UK*; ²*Department of Electronic and Electrical Engineering, Univ. of Sheffield, UK*; ³*Innotec Ltd, UK*. The two-dimensional demodulation of a hologram using the 2D Hilbert transform requires the suppression of the background illumination beforehand. We propose an iterative algorithm based on a spiral phase function for this purpose.

DSu3C.5 • 14:15

Image formation of digital holographic microtomography, Chau-Jern Cheng¹; ¹*Inst. of Electro-Optical Science and Technology, Taiwan*. We describe a three-dimensional image formation based on the digital holographic microtomography. The refractive index distribution inside a sample can be determined by the technique. Experiments and simulation results are presented and discussed.

DSu3C.6 • 14:30

Tracking of micrometer-sized objects with high-numerical aperture lensless digital holographic microscopy, Jorge Garcia-Sucerquia¹, Jhon F. Restrepo¹; ¹*Physics, Universidad Nacional de Colombia Sede Medellin, Colombia*. We present a method to track automatically micrometer-sized objects with high numerical aperture lensless holographic microscopy. The method is tested with modeled in-line holograms and real experiments to track bubbles in cubic millimeters of soda.

Symphony I & II

Symphony III

Symphony IV

BIOMED I

BIOMED 2

DH

15:00—15:30

COFFEE BREAK, *Overture Foyer*

15:30 - 17:30

BSu4A • Brain Signals 1

Stefan Andersson-Engels; Lund Univ., Sweden, *Presider*

BSu4A.1 • 15:30

Invited

Bed-side Neuro-critical Monitoring with Hybrid Diffuse Optics, Turgut Durduran¹; ¹*ICFO, Spain*.

Transcranial, non-invasive monitoring of cerebral hemodynamics, autoregulation and metabolism at the neuro-intensive care has a great deal of potential. I present the latest advances in hybrid diffuse optical and correlation spectroscopies as neuro-monitors.

BSu4A.2 • 16:00

A quantitative spatial comparison of high-density diffuse optical tomography and fMRI cortical mapping, Adam T. Eggebrecht¹, Brain R. White^{1,2}, Silvina L. Ferradal^{1,3}, Yuxuan Zhan⁴, Abraham Z. Snyder^{1,5}, Hamid Dehghani⁴, Joseph P. Culver^{1,2}; ¹*Radiology, Washington Univ. School of Medicine, USA*; ²*Physics, Washington Univ., USA*; ³*BIOMEDICAL Engineering, Washington Univ., USA*; ⁴*Computer Science, Univ. of Birmingham, UK*; ⁵*Neurology, Washington Univ. School of Medicine, USA*. Image-quality of high-density diffuse optical tomography is evaluated against fMRI using functional maps of visual cortex as a benchmark. Co-registered subject-specific light models have an average localization error of 4.4 +/- 1 mm.

BSu4A.3 • 16:15

Characterization of post-Occlusion Oxygen Tension in Cortical Arterioles in vivo, S. M. Shams Kazmi¹; ¹*BIOMEDICAL Engineering, The Univ. of Texas at Austin, USA*. Depth-resolved pO₂ and blood flow in descending arterioles after occlusion is characterized with two-photon lifetime imaging in the mouse brain. Oxygen tension decreases rapidly in depth with branches supplementing pO₂ levels after occlusion.

15:30 - 17:30

BSu4B • Microscopy Imaging: Novel Contrast Mechanisms

Adela Ben-Yakar; Univ. of Texas at Austin, USA, *Presider*

BSu4B.1 • 15:30

SHG imaging of Cancer, Paul Campagnola¹, Molly A. Brewer⁴, Visar Ajeti¹, Patricia Keely^{2,1}, Kevin Eliceiri¹, Manish Patankar³, Karissa Tilbury¹; ¹*BIOMEDICAL Engineering, Univ. of Wisconsin, USA*; ²*Department of Cell and Regenerative Biology, Univ. of Wisconsin-Madison, USA*; ³*Obstetrics and Gynecology, Univ. of Wisconsin-Madison, USA*; ⁴*Obstetrics and Gynecology, Univ. of Connecticut Health Center, USA*. SHG imaging microscopy is used to quantitatively study structural changes in the collagen organization in the ECM in ovarian and breast cancers using in vitro models, animal models and ex vivo human tissues.

BSu4B.2 • 15:45

In Vivo Pump-Probe Microscopy of Eumelanin, Pheomelanin in Melanoma, Tanya Mitropoulos¹, Jesse W. Wilson¹, Simone Degan¹, M. Angelica Selim², Jennifer Y. Zhang³, Warren S. Warren^{1,4}; ¹*Chemistry, Duke Univ., USA*; ²*Pathology, Duke Univ., USA*; ³*Dermatology, Duke Univ., USA*; ⁴*BIOMEDICAL Engineering, Duke Univ., USA*. We employ pump-probe microscopy to highlight eumelanin versus pheomelanin content of in vivo pigmented skin lesions, and combine it with confocal reflectance and fluorescence microscopies to gain a more complete illustration of the skin.

BSu4B.3 • 16:00

Coherent Confocal Light Absorption and Scattering Spectroscopic Microscopy, Le Qiu¹, Vladimir Turzhitsky¹, Edward Vitkin¹, Lianyu Guo¹, Eugene Hanlon¹, Irving Itzkan¹, Lev T. Perelman¹; ¹*Center for Advanced BIOMEDICAL Imaging and Photonics, Harvard Univ., USA*. We report development of coherent CLASS microscopy which provides dramatically higher spectral contrast compared to the existing incoherent technique. It can non-invasively monitor subcellular dynamics without the need for exogenous agents.

BSu4B.4 • 16:15

Third-Harmonic Generation Microscopy For Label-Free Brain Imaging, Stefan Witte^{1,3}, Nikolay V. Kuzmin^{1,3}, Adrian Negrean^{2,3}, Johannes C. Lodder^{2,3}, Guilherme T. Silva^{2,3}, Christiaan P. de Kock^{2,3}, Huibert D. Mansvelde^{2,3}, Marloes L. Groot^{1,3}; ¹*LaserLab, VU Univ., Netherlands*; ²*CNCR, VU Univ., Netherlands*; ³*Neuroscience Campus Amsterdam, VU Univ., Netherlands*. We demonstrate high-resolution live brain tissue imaging without fluorescent dyes, using third-harmonic generation. Targeted patching of living neurons is demonstrated, and label-free images of fixed human brain tissue have been obtained.

15:30 - 17:30

DSu4C • BIOMEDICAL Applications of Digital Holography I

Chau-Jern Cheng; Inst. of Electro-Optical Science and Technology, Taiwan, *Presider*

DSu4C.1 • 15:30

Invited

Albert-Claude Boccaro¹; ¹*Ecole Sup Physique Chimie Industrielles*. We will discuss how wave control using OCT improves the possibility to correct wavefronts in optical microscopy and tomography and that controlling a large number of modes opens the path to imaging in highly scattering media.

DSu4C.2 • 16:00

Invited

Digital Holography of Cellular Motions in Live Tissue, David Nolte¹; ¹*Purdue Univ., USA*. Subcellular motions inside live tissue are sensitive indicators of cellular health and cellular response to applied drugs. Digital holography volumetrically captures these motions in a tissue dynamics spectroscopy approach to live-tissue drug screening.

17:30—19:30

BIOMED Postdeadline Papers

17:30—19:30

DH Postdeadline Papers

Symphony I & II

BIOMED I

BSu4A • Brain Signals 1—Continue

BSu4A.4 • 16:30

Histopathological and Radiological Validation of Continuous Wave (CW) Near Infrared Spectroscopy (NIRS) Recordings During Cerebral Intravascular Manipulations, Tigran Gevorgyan^{2,6}, Douglas Pfeil¹, Harry L. Graber^{1,7}, Yong Xu^{1,7}, Sundeep Mangla³, Frank C. Barone⁴, Jenny Libien¹, Jean Charchafli⁵, Randall L. Barbour^{1,7}, Daniel C. Lee^{2,6}; ¹Pathology, SUNY Downstate Medical Center, USA; ²Surgery, SUNY Downstate Medical Center, USA; ³Interventional Neuroradiology, SUNY Downstate Medical Center, USA; ⁴Neurology, SUNY Downstate Medical Center, USA; ⁵Anesthesiology, SUNY Downstate Medical Center, USA; ⁶Interfaith Medical Center, USA; ⁷NIRx Medical Technologies, LLC., USA. An experimental animal stroke model, complicated with subarachnoid hemorrhage, was monitored using CW-NIRS DOT. Comparison of results with histopathology and radiology findings demonstrate the utility of CW-NIRS for functional imaging and monitoring.

BSu4A.5 • 16:45

Assessments of posttraumatic stress disorder by functional near infrared spectroscopy: A preliminary report, Fenghua Tian¹, Alexa Smith-Osborne², Amarnath Yennu¹, Hanli Liu¹; ¹Bioengineering, Univ. of Texas at Arlington, USA; ²School of Social work, Univ. of Texas at Arlington, USA. Post-traumatic stress disorders (PTSD) affect up to 20% of service members in the global war on terror. We use a portable multi-channel fNIRS device to assess student veterans with PTSD; preliminary results are reported.

BSu4A.6 • 17:00

Regional and hemispheric asymmetries of cerebral hemodynamic and oxygen metabolism in newborns, Pei-Yi Lin¹, Mathieu Dehaes², Nadege Roche-Labarbe¹, Angela Fenoglio¹, P. Ellen Grant², Maria Angela Franceschini¹, Athinola A. Martinos¹; ¹Center for BIOMEDical Imaging, Massachusetts General Hospital, USA; ²Fetal-Neonatal Neuroimaging and Developmental Science Center, Children's Hospital Boston, USA. By using noninvasive optical techniques, we presented higher cerebral hemoglobin oxygenation and metabolism in the temporal and parietal than in the frontal region and higher metabolism in the right than in the left in newborns.

BSu4A.7 • 17:15

Functional connectivity mapping in hospitalized infants using diffuse optical tomography, Silvina L. Ferradal^{1,2}, Steve M. Liao³, Adam T. Eggebrecht², Terrie E. Inder^{2,3}, Joseph P. Culver^{1,2}; ¹BIOMEDical Engineering, Washington Univ. in St. Louis, USA; ²Radiology, Washington Univ. in St. Louis, USA; ³Pediatrics, Washington Univ. in St. Louis, USA. Resting-state functional connectivity is an attractive tool for studying brain function in neonates. Here, we present fCDOT maps of multiple networks detected in premature infants at the bedside.

Symphony III

BIOMED 2

BSu4B • Microscopy Imaging: Novel Contrast Mechanisms—Continue

BSu4B.5 • 16:30

Ratiometric Molecular Microscopy: Towards Real-Time Quantitative Delineation of Brain Tumor Margins, Steven Y. Leigh¹, Danni Wang¹, Ye Chen¹, Michael J. Mandella², Henry Haeberle², Olav Solgaard³, Christopher Contag², Jonathan T. Liu¹; ¹BIOMEDical Engineering, State Univ. of New York (SUNY) at Stony Brook, USA; ²Clark Center, Stanford Univ. School of Medicine, USA; ³Electrical Engineering, Stanford Univ., USA. An achromatic version of a micro-mirror-scanned surgical dual-axis confocal microscope has been developed for ratiometric quantification of biomarker expression as revealed by the topical application of fluorescent contrast agents.

BSu4B.6 • 16:45

Fallopian Tube Imaging Using An Articulating Confocal Microlaparoscope, Tzu-Yu Wu^{1,2}, Arthur F. Gmitro^{1,2}, Andrew R. Rouse²; ¹College of Optical Sciences, University of Arizona, USA; ²Radiology, Univ. of Arizona, USA. A confocal microlaparoscope for in-vivo imaging of early stage cancer inside the fallopian tube is presented. Feasibility is demonstrated using a rigid microlaparoscope and preliminary in-vivo results with the new articulating catheter are expected.

BSu4B.7 • 17:00

Epi-Detected Stimulated Raman Scattering Microscopy Using Long-Wavelength Excitation, Terumasa Ito^{1,2}, Minbiao Ji¹, Gary Holtom¹, X. Sunney Xie¹; ¹Chemistry and Chemical Biology, Harvard Univ., USA; ²Core Device Development Group, Sony Corporation, Japan. Epi-detected stimulated Raman scattering microscopy using a high NA objective and long-wavelength excitation is presented. The increased NA and reduced scattering loss allow for high resolution imaging with deeper tissue penetration.

BSu4B.8 • 17:15

Coherent Super-Resolution Structured Illumination Microscopy of Non-Fluorescent Samples, Shwetadwip Chowdhury¹, Al-Hafeez Dhalla¹, Joseph Izatt¹; ¹Duke Univ., USA. We introduce a framework for coherent structured illumination, which may extend advantages of far-field super-resolution microscopy to non-fluorescent samples. Experimental confirmation is obtained in a target at moderate numerical aperture.

Symphony IV

DH

DSu4C • BIOMEDical Applications of Digital Holography I—Continue

DSu4C.3 • 16:30

Automated 3D detection of particles using digital holographic microscopy with partially coherent source - Applications in environmental monitoring, El Mallahi Ahmed¹, Minetti Christophe¹, Frank Du-bois¹; ¹Université libre de Bruxelles, Belgium. We investigate the automated 3D detection of particles by digital holographic microscopy (DHM) with a partial coherent light source. We have successfully applied the developed process to several particles of interest for the environmental monitoring.

DSu4C.4 • 16:45

Quantitative Phase Imaging Flow Cytometry, Sai Siva Gorthi¹, Ethan Schonbrun¹; ¹Rowland Institute at Harvard Univ., USA. This paper introduces a fluidics based focus-stack collecting microscope. Images from the focus stacks are used to reconstruct the quantitative phase of red blood cells in flow with the Transport-of-Intensity-Equation method.

DSu4C.5 • 17:00

Elastic Depth Profiling of Soft Tissue by Holographic Imaging of Surface Acoustic Waves, Karan Mohan¹, William Sanders¹, Amy Oldenburg^{1,2}; ¹Department of Physics & Astronomy, Univ. of North Carolina at Chapel Hill, USA; ²BIOMEDical Research Imaging Center, Univ. of North Carolina at Chapel Hill, USA. Digital holography is used to image surface acoustic waves in tissue-mimicking silicone phantoms. Elastic depth profiles, at depths up to 30mm, are then obtained from the phase velocity dispersion curves by solving the inverse problem.

DSu4C.6 • 17:15

Quantitative imaging of surface deformation on substrata due to cell motility by digital holography, Xiao Yu¹, Michael Cross¹, Changgeng Liu¹, David C. Clark¹, Donald Haynie¹, Myung K. Kim¹; ¹Physics, Univ. of South Florida, USA. Quantitative phase microscopy by digital holography (QPM-DH) is introduced for quantitatively imaging surface deformation on soft material for cellular adhesion.

Symphony I & II

Joint BIOMED and DH

REGISTRATION, *Overture Foyer*

08:00 - 09:30

JM1A • BIOMED/DH Joint Plenary Session

Lev Perelman; Harvard Univ., USA, and George Barbastathis,; MIT, USA, Presiders

JM1A.1 • 08:00

Plenary

The Invention and Early History of the CCD, George Smith; Recipient of 2009 Nobel Prize in Physics, USA. As the first practical solid state imaging device, the invention of the Charge Coupled Device has profoundly affected image sensing technology. They are used in a wide range of applications both as area and linear imaging devices starting with the replacement of imaging tubes used in commercial TV cameras and camcorders. The rapid rise of their use in digital cameras has initiated the demise of film photography and created vast new markets with great economic benefit for many. Other uses include a wide variety of scientific, medical, surveillance and scanning applications. The inception of the device at Bell Labs by Willard S. Boyle and George E. Smith in 1969 was strongly influenced by several unique factors existing both within Bell Labs and the current world state of technology. These factors and their relevance will be discussed along with the train of thought leading to the invention. Early experimental devices and their initial applications were vigorously pursued and will be described. Mention of current applications will be given.

JM1A.2 • 08:45

Plenary

3D Display - Where We Are and Where to Go, ByoungHo Lee¹; ¹School of Electrical Engineering, Seoul National Univ., Republic of Korea. An overview of history and present state of three-dimensional display is given, covering technical and market aspects. Possible research directions that will be considered important in the future are also discussed.

Notes

Horizontal lines for taking notes.

Symphony I & II

BIOMED 1

Symphony III

BIOMED 2

Symphony IV

DH

9:30—10:00

COFFEE BREAK, *Concerto A,B,C & Overture Foyer*

10:00 - 12:30

BM2A • BioNanophotonics and Molecular Probes
Gang Zheng; *Univ. of Toronto, Canada, Presider***BM2A.1 • 10:00** Invited

Molecular probes in Photodynamic Therapy, Tayyaba Hasan¹; ¹*Harvard Medical School, USA*. Advances in optical technologies combined with targeted molecular probes enable therapeutics optimization by earlier disease detection or by therapy monitoring. Photodynamic therapy (PDT) is exceptional in that the same molecule may serve as the therapeutic and diagnostic agent. Development and use of targeted probes in DT will be discussed. PDT will be discussed.

BM2A.2 • 10:30 Invited

Imaging RNA in Single Living Cells: Recent Advances and Future Outlook, Xuemei Zhang¹, Antony Chen¹, Andrew Tsourkas¹; ¹*Department of Bioengineering, Univ. of Pennsylvania, USA*. Recently, we developed an oligonucleotide-based probe for imaging RNA in living cells, i.e. Ratiometric BiMolecular Beacons (RBMBs). RBMBs are highly sensitive, exhibit little/no false-positives, and can be used for prolonged imaging of single RNA transcripts.

BM2A.3 • 11:00

In vivo assessment of HER2 Receptors Expression, Using NIR Fluorescence Imaging with Affibody-DyLight Probe, Victor Chernomordik¹, Moinuddin Hassan¹, Yasaman Ardeshirpour¹, Rafal Zielinski^{3,2}, Jacek Capala², Amir Gandjbakhche¹; ¹*Program in Physical Biology, Lab. of Integrative and Medical Biophysics, National Inst. of Child Health and Human Development, National Inst.s of Health, USA*; ²*National Cancer Inst., National Inst.s of Health, USA*; ³*UT MD Anderson Cancer Center, USA*. Her2 overexpression in different carcinoma types is assessed in vivo (mouse model), using time sequences of fluorescence images after injection of HER2-specific fluorescent probes with fast pharmacokinetics.

10:00 - 12:30

BM2B • Photoacoustic Tomography
Wiendelt Steenbergen; *Univ. of Twente / Inst. MIRA, Netherlands, Presider***BM2B.1 • 10:00** Invited

Detecting Circulating Tumor Cells (CTCs) with Integrated Photoacoustic/Ultrasonic Imaging, Matthew O'Donnell¹, Chen-wei Wei¹, Jinjun Xia¹, Ivan Pelivanov^{2,1}, Xiaohu Gao¹, Xiaoge Hu¹; ¹*Department of Bioengineering, Univ. of Washington, USA*; ²*Physics Faculty, of M.V. Lomonosov, Moscow State Univ., Russian Federation*. Magnetic trapping and manipulation of polystyrene beads mimicking magnetically targeted circulating tumor cells (CTCs) has been demonstrated using magnetomotive photoacoustic (mmPA) imaging. These techniques appear promising for the detection of rare CTCs in the vasculature.

BM2B.2 • 10:30 Invited

Sound and Light Catheters
Ton van der Steen¹; ¹*Erasmus MC, Netherlands*. Abstract not available.

BM2B.3 • 11:00

Preclinical photoacoustic imaging using all-optical detection and time-reversal image reconstruction. Paul Beard¹; ¹*UCL, UK*. 3D photoacoustic images of the vasculature in mice were obtained in vivo using a photoacoustic scanner based on a Fabry Perot polymer film ultrasound sensor and an attenuation compensated acoustic time reversal image reconstruction method.

10:00 - 11:45

DM2C • Three-Dimensional Display II
Kenji Yamamoto; *NICT, Japan, Presider***DM2C.1 • 10:00** Invited

Adaptive Liquid Crystal Lens(LC Lens) Array for 3D Display and Capturing, Yi-Pai Huang^{1,2}, Yu-Cheng Chang¹, Chi-Wei Chen¹, Lin-Yao Liao¹, Po-Tuan Shieh¹, Tai-Hsien Jen¹, Tsu-Han Chen²; ¹*Department of Photonics/Display Inst., National Chiao Tung Univ, Taiwan*; ²*School of Electrical and Computer Engineering, Cornell Univ., USA*. A low driving voltage with fast response LC lens was developed. By implementing the LC-lens as an array structure, it can be adaptively used for 2D/3D switching and 3D rotation on autostereoscopic display. Additionally, it also can be utilized as a depth sensor for 3D capturing.

DM2C.2 • 10:30

Fully Updatable Three-dimensional Holographic Display Device Using a Monolithic Compound, Naoto Tsutsumi¹, Kenji Kinashi¹, Wataru Sakai¹, Junichi Nishide², Yutaka Kawabe², Hiroyuki Sasabe²; ¹*Kyoto Inst. of Technology, Japan*; ²*Chitose Inst. of Science and Technology, Japan*. Paper shows the updatable three-dimensional holographic display with capability of recording and displaying new images within a few seconds using a non-electric field photorefractive device of monolithic compound doped transparent polymer film.

DM2C.3 • 10:45

Enhanced Layered 3D with a Lens, Stefan Muenzel¹, Laura A. Waller¹, Jason Fleischer¹; ¹*Electrical Engineering, Princeton Univ., USA*. We augment layered 3D displays using optical elements placed in front of or in between attenuation layers, which improves resolution or field-of-view of the display. We also significantly reduce memory requirements for layer calculations.

DM2C.4 • 11:00

Multiplexed holographic display based on a fast response liquid crystal film, Hongyue Gao^{1,2}, Xiao Li¹, Zhenghong He¹, Yikai Su¹, Ting-Chung Poon²; ¹*Center for Opto-electronic Materials and Devices, Shanghai Jiao Tong Univ., China*; ²*Bradley Department of Electrical and Computer Engineering, Virginia Tech, USA*. Real-time holographic display with angularly multiplexed holograms is presented with holographic response time of ~1ms in a liquid crystal thin film, showing the possibility of a color holographic three-dimensional display with this film.

Symphony I & II

BIOMED I

BM2A • BioNanophotonics and Molecular Probes—Continue

BM2A.4 • 11:15

In Vivo Fluorescence Lifetime Detection of a Catepsin-Activatable Probe in Infarcted Myocardium, Craig J. Goergen¹, Howard H. Chen², Alexei Bogdanov³, David E. Sosnovik^{1,2}, Anand T. Kumar¹; ¹*Martinos Center for BIOMEDical Imaging, Massachusetts General Hospital, USA*; ²*Center for Molecular Imaging Research, Massachusetts General Hospital, USA*; ³*Department of Radiology, Univ. of Massachusetts Medical School, USA*. Using a protease-activatable near-infrared probe, we demonstrate that lifetime-based time domain imaging can improve fluorescence contrast useful for detecting myocardial infarctions in vivo and for isolating the non-specific signal from the liver.

BM2A.5 • 11:30

Porphysomes: Intrinsically Multifunctional Nanovesicles for Photothermal Therapy, Cheng Jin^{1,2}, Jonathan F. Lovell^{2,3}, Gang Zheng^{2,3}; ¹*Pharmaceutical Sciences, Univ. of Toronto, Canada*; ²*Inst. for Biomaterials and Bioengineering, Univ. of Toronto, Canada*; ³*Ontario Cancer Inst., Univ. Health Network, Canada*. Porphysomes are intrinsically multifunctional nanovesicles with unique structure-dependent fluorescence self-quenching and photothermal properties. We investigated imaging and photothermal effect on subcutaneous and orthotopic prostate tumor models.

BM2A.6 • 11:45

Multimodal video-rate fluorescence DOT and SPECT/CT for small animals, Metasebya Solomon^{1,2}, Ralph Nothdurft², Walter Akers², W. Barry Edwards², Kexian Liang², Baogang Xu², Hamid Dehghani⁴, Yuan-Chuan Tai², Sam Achilefu^{1,3}, Joseph P. Culver^{1,2}; ¹*BIO-MEDical Engineering, Washington Univ. in Saint Louis, USA*; ²*Department of Radiology, Washington Univ. School of Medicine, St. Louis, MO, USA*; ³*Biochemistry and Molecular Biophysics, Washington Univ. School of Medicine, St. Louis, MO, USA*; ⁴*School of Computer Science, The Univ. of Birmingham Birmingham, UK, UK*. We integrated our fiber-based video-rate fluorescence diffuse optical tomography with a preclinical NanoSPECT/CT. This design permits visualization of anatomically co-registered physiological events with combined optical-nuclear platforms.

Symphony III

BIOMED 2

BM2B • Photoacoustic Tomography—Continue

BM2B.4 • 11:15

Volumetric Photoacoustic Endoscopy, Joon-Mo Yang¹, Christopher Favazza¹, Ruimin Chen², Junjie Yao¹, Xin Cai¹, Konstantin Maslov¹, Qifa Zhou², Kirk Shung², Lihong V. Wang¹; ¹*BIOMEDical Engineering, Washington Univ. in St. Louis, USA*; ²*BIOMEDical Engineering, Univ. of Southern California, USA*. Photoacoustic endoscopy provides unique functional information through its broad spectroscopic imaging capability. The imaging results presented here suggest its potential for use as a comprehensive endoscopic tool in various medical applications.

BM2B.5 • 11:30

Quantitative Photoacoustic Imaging by Acoustically Measured Light Fluence, Altaf Hussain¹, Khalid Daoudi¹, Erwin Hondebrink¹, Wiendelt Steenbergen²; ¹*BIOMEDical Photonic Imaging group, Univ. of Twente, MIRA Inst. for BIOMEDical Technology and Technical Medicine, Netherlands*. We propose a methodology to measure the absolute local absorption coefficient in biological tissue using photoacoustics in combination with reflection mode acousto-optics. We provide proof of the concept with numerical simulations and experiments.

BM2B.6 • 11:45

Simultaneous in vivo imaging of dual molecular contrasts in the retina with multimodal photoacoustic ophthalmoscopy, Shuliang Jiao¹, Hao F. Zhang²; ¹*Ophthalmology, Univ. of Southern California, USA*; ²*BIOMEDical Engineering, Northwestern Univ., USA*. We combined photoacoustic ophthalmoscopy with autofluorescence imaging for simultaneous in vivo imaging of dual molecular contrasts in the retina using single light source. The dual molecular contrasts come from melanin and lipofuscin in the RPE.

Symphony IV

DH

DM2C • Three-Dimensional Display II—Continue

DM2C.5 • 11:15

Development of a Holographic Display Module Using a 4k2k-SLM Based on the Resolution Redistribution Technique, Yasuhiro Takaki¹, Junya Nakamura¹; ¹*Tokyo Univ. of Agriculture and Technology, Japan*. A holographic display module with a viewing zone angle of 10.5° and a screen size of 2" was developed using a 4k2k-SLM. This module has a frameless screen so that multiple modules can be arranged seamlessly.

DM2C.6 • 11:30

Two-dimensional and three-dimensional see-through screen using holographic optical elements, Keehoon Hong¹, Jisoo Hong¹, Jiwoon Yeom¹, ByoungHo Lee¹; ¹*Seoul National Univ., Republic of Korea*. In this paper, we propose two-dimensional and three-dimensional see-through screen using lens-array holographic optical element (HOE). Recording scheme for HOE is presented and the proposed see-through screen is experimentally verified.

Symphony I & II

Symphony III


Symphony IV

BIOMED I


BIOMED 2

DH

Monday, 30 April

BM2A • BioNanophotonics and Molecular Probes—Continue**BM2A.7 • 12:00** 

Comparative Study on Photothermal Therapy of Cancer Cells with Different Localizations of Gold Nanorods, Varun Pattani¹, James Tunnell¹; ¹BIO-MEDical Engineering, The Univ. of Texas at Austin, USA. Photothermal therapy was performed by targeting gold nanorods to two locations on cancer cells. We demonstrated a fluence rate threshold difference during therapy, suggesting certain damage pathways are more

BM2A.8 • 12:15 

Plasmonic Gold Nanostars: A Potential Agent for Molecular Imaging and Cancer Therapy, Hsiangkuo Yuan¹, Christopher Khoury¹, Andrew Fales¹, Christy Wilson¹, Gerald Grant¹, Tuan Vo-Dinh¹; ¹Duke Univ., USA. Gold nanostars, with tunable plasmon in the near infrared tissue optic window, generate intense two-photon photoluminescence capable of in vitro cell labeling and in vivo particle tracking. Efficient photothermal ablation therapy is demonstrated.

BM2B • Photoacoustic Tomography—Continue**BM2B.7 • 12:00**

Feasibility of Contrast-Enhanced Photoacoustic Liver Imaging at a Wavelength of 1064 nm, Yun-Sheng Chen^{1,2}, Kimberly Homan¹, David Xu¹, Wolfgang Frey¹, Stanislav Emelianov^{1,2}; ¹BIOMEDical Engineering, The Univ. of Texas at Austin, USA; ²Electrical and Computer Engineering, The Univ. of Texas at Austin, USA. The feasibility of photoacoustic imaging in ex-vivo liver tissue was demonstrated. Studies were performed using a pulsed laser at 1064 nm to reduce background noise. Gold nanorods resonant at 1064 nm were visualized in the blood-laden liver.

BM2B.8 • 12:15

Dichroism optical-resolution photoacoustic microscopy, Song Hu¹, Konstantin Maslov¹, Ping Yan², Jin-Moo Lee², Lihong V. Wang¹; ¹Department of BIO-MEDical Engineering, Washington Univ. in St. Louis, USA; ²Department of Neurology, Washington Univ. School of Medicine, USA. We developed dichroism photoacoustic microscopy capable of imaging polarization-dependent optical absorption with excellent specificity. This innovation enriches photoacoustic contrasts and holds potential for detecting amyloid-associated diseases.

DM2C • Three-Dimensional Display II—Continue

12:30—13:00

LUNCH ON YOUR OWN

11:30—3:00

LUNCH ON YOUR OWN

Concerto Ballroom & Overture Foyer

BIOMED and DH

13:00—15:00

JM3A—Joint BIOMED/DH Poster Session

JM3A.1

Detection of hemoglobin variants using surface enhanced Raman scattering, Maria Navas-Moreno¹, Josef T. Prchal¹, Valy Vardeny²; ¹*Physics and Astronomy, Univ. of Utah, USA*; ²*Hematology and Pathology, Univ. of Utah, USA*. Hemoglobin variants are abnormal hemoglobin molecules and some of them elude current methods of detection, making proper diagnosis rather difficult. We investigate SERS as an alternative for hemoglobin variant detection.

JM3A.2

A Novel Optical Property Recovery Algorithm for Use in the Optical Biopsy of Brain Tissue, Derek J. Cappon¹, Zhaojun Nie², Thomas J. Farrell¹, Qiyan Fang^{2,3}, Joseph E. Hayward^{1,3}; ¹*Department of Medical Physics & Applied Radiation Sciences, McMaster Univ., Canada*; ²*School of BIOMEDical Engineering, McMaster Univ., Canada*; ³*Department of Engineering Physics, McMaster Univ., Canada*. A novel fibre optic probe design and Monte Carlo based optical property recovery algorithm for use in the optical biopsy of brain tissue are described. The algorithm's performance is characterized when subjected to random noise.

JM3A.3

Quantitative measurement of Cerebral Blood Flow, using broad band, continuous wave near infrared spectroscopy, Hadi Zabihi Yeganeh¹, Vladislav Toronov¹, Jonathan T. Elliot², Mamadou Diop², Keith St Lawrence², Ting-Yim Lee^{3,2}; ¹*Physics, Ryerson Univ., Canada*; ²*Imaging program, Lawson Health Research Inst., Canada*; ³*Imaging Labs, Robarts Research Inst., Canada*. We present a broad-band, continuous wave spectral approach by using an algorithm based on a solution of diffusion equation to quantify cerebral blood flow of a pig model from dynamic contrast-enhanced near infrared spectroscopy technique.

JM3A.4

Wavelet synchronization index to assess variations in regional cerebral oxygenation in infants on life support, Maria Papademetriou¹, Ilias Tachtsidis¹, Aparna Hoskote², Martin J. Elliott², Clare Elwell¹; ¹*Medical Physics and Bioengineering, Univ. College London, UK*; ²*Cardiothoracic Unit, Great Ormond Street Hospital, UK*. We used synchronisation index between mean arterial pressure and oxyhaemoglobin concentration measured by optical topography to demonstrate regional variations in cerebral autoregulation in infants undergoing extracorporeal membrane oxygenation.

JM3A.5

Recipes for Organic Phantoms and Characterization by Time-Resolved Diffuse Optical Spectroscopy, Giovanna Quarto¹, Antonio Pifferi¹, Ilaria Bargigia¹, Andrea Farina¹, Rinaldo Cubeddu¹, Paola Taroni¹; ¹*Physics, Politecnico di Milano, Italy*. Three recipes for tissue constituent-equivalent phantoms of water and lipids are presented. The phantom optical characterization showed good homogeneity and reproducibility. Estimates of composition by time-resolved spectroscopy were also performed.

JM3A.6

Optimal Wavelength Combinations for Resolving in-vivo Changes of Haemoglobin and Cytochrome-c-oxidase Concentrations with NIRS, Tingting Zhu¹, Stuart Faulkner³, Tushaar Madaan¹, Alan Bainbridge², David Price², David Thomas⁴, Ernest Cady², Nicola Robertson³, Xavier Golay⁴, Ilias Tachtsidis¹; ¹*Medical Physics and Bioengineering, Univ. College London, UK*; ²*Medical Physics and Bioengineering, Univ. College London Hospitals, UK*; ³*Inst. for Women's Health, Univ. College London Hospitals, UK*; ⁴*Inst. of Neurology, Univ. College London Hospitals, UK*. Novel method used to identify the optimal three and four wavelength combinations (out of 120, 780-900nm) to accurately resolve the concentration changes in haemoglobin and cytochrome-c-oxidase during hypoxic-ischaemia in a neonatal pre-clinical model.

JM3A.7

Spectral Distortions in Time-Resolved Diffuse Optical Spectroscopy Due to AOTFs, Andrea Farina², Antonio Pifferi^{1,2}, Paola Taroni¹, Ilaria Bargigia¹; ¹*Physics, Politecnico di Milano, Italy*; ²*Consiglio Nazionale delle Ricerche-Istituto di Fotonica e Nanotecnologie, CNR-IFN, Italy*. This work discusses the spectral distortions occurring when time-resolved diffuse spectroscopy is performed by a system based on supercontinuum generation of radiation spectrally filtered by a prism and by an acousto-optics tunable filter.

JM3A.8

Noninvasive Optical Quantification of Absolute Blood Flow and Oxygen Consumption Rate in Exercising Skeletal Muscle, Katelyn Gurley¹, Yu Shang¹, Guoqiang Yu¹; ¹*Center for BIOMEDical Engineering, Univ. of Kentucky, USA*. Diffuse optical technologies (NIRS/DCS) are combined with a novel gating algorithm to continuously and noninvasively quantify absolute blood flow, blood oxygenation, and oxygen consumption rate in exercising skeletal muscle for the first time.

JM3A.9

Optical Spectroscopic Properties of Brown Fat Reveal Pathophysiological Conditions, Lianyu Guo¹, Wanzhu Jin¹, Le Qiu¹, Vladimir Turzhitsky¹, Edward Vitkin¹, Eugene Hanlon¹, Irving Itzkan¹, Lev T. Perelman¹; ¹*Center for Advanced BIOMEDical Imaging and Photonics, Harvard Univ., USA*. A double-integrating-sphere system measures the absorption and scattering coefficients of brown and white fat. The optical spectroscopic properties of the fat tissue are sensitive to the pathophysiological conditions of mice.

JM3A.10

Color of Human Tissues as Viewed in a Higher Range of Spectra, Igor Meglinski¹, Alexander Doronin¹, Harry T. Whelan², Georgi I. Petrov³, Vladislav V. Yakovlev³; ¹*Department of Physics, Univ. of Otago, New Zealand*; ²*Department of Neurology, Medical College of Wisconsin, USA*; ³*Department of BIOMEDical Engineering, Texas A&M Univ., USA*. The near-IR transmittance spectra obtained for various parts of human body in vivo are analyzed in framework of CIE L*a*b* color space and the regularities of the color variation are examined by Monte Carlo simulation.

JM3A.11

Development of a wireless near-infrared tissue oxygen monitor system with high sampling rate, Takashi Watanabe¹, Toshihiko Mizuno^{1,2}, Takahiro Shikayama¹, Mitsuharu Miwa¹; ¹*Optical Diagnostic Technology Group, Development Center, Hamamatsu Photonics K.K., Japan*; ²*DynaSense Inc., Japan*. We developed a portable near-infrared tissue oxygen monitor having both wireless data communication capability and high sensitivity. This device is able to measure relative changes in oxy- and deoxyhemoglobin concentrations in real time.

JM3A.12

Diffuse Spectroscopy for Tissue Characterization: Application to Skin Tests Reading, Anne Koenig¹, Amir Nahas², Anne Planat-Chrétien¹, Vincent Poher¹, Jean-Marc Dinten¹; ¹*DTBS/STD/LISA, CEA Grenoble, France*; ²*Institut Langevin ESPCI, France*. In this paper, we present a low-cost optical instrument, usable in a clinical environment, to enable early skin tests reading before the onset of visual signs. Results on an ongoing clinical study are presented.

JM3A—Joint BIOMED/DH Poster Session - Continue

JM3A.13

Microvascular Blood Flow Changes in Human Breast During Simulated Mammography, David R. Busch¹, Regine Choe², Turgut Durduran³, Wesley B. Baker¹, Ellen K. Foster¹, Tiffany A. Alverna¹, Daniel Friedman¹, Mark A. Rosen¹, Michael D. Schnall¹, Arjun G. Yodh¹; ¹Univ. of Pennsylvania, USA; ²Univ. of Rochester, USA; ³ICFO-Institut de Ciències Fotòniques, Spain. We employ Diffuse Correlation Spectroscopy to measure microvascular blood flow in human breast during mammographic-like compression. Our results suggest that blood flow is reduced significantly by mild and ~90% by mammographic compression.

JM3A.17

Image-Guided Treatment Planning and Dosimetry for Interstitial Photodynamic Therapy, Timothy M. Baran¹, Thomas H. Foster^{1,2}, Daryl P. Nazareth³; ¹Inst. of Optics, Univ. of Rochester, USA; ²Imaging Sciences, Univ. of Rochester, USA; ³Department of Radiation Medicine, Roswell Park Cancer Inst., USA. The treatment scenario for photodynamic therapy (PDT) can vary between patients. We present a method that combines clinical images, radiation therapy planning contours, and Monte Carlo simulation in order to design individualized PDT treatment plans.

JM3A.21

Light reflectance spectroscopy and auto-fluorescence lifetime: potential tools for intra-operative breast cancer margin detection, Vikrant Sharma¹, Shivarjanji Shivalingaiah¹, Yan Peng², David Euhus³, Hanli Liu¹; ¹Bioengineering, The Univ. of Texas at Arlington, USA; ²Pathology, The Univ. of Texas Southwestern Medical Center at Dallas, USA; ³Surgery, The Univ. of Texas Southwestern Medical Center at Dallas, USA. This paper reports the use of light reflectance spectroscopy and auto-fluorescence lifetime for detecting breast cancer in human ex vivo samples. Preliminary results show significant differences using both techniques.

JM3A.14

Long Term Monitoring of Cerebral Blood Flow in Subarachnoid Hemorrhage Patients Using Diffuse Correlation Spectroscopy, Malavika Chandra¹, David L. Minkoff¹, Steven S. Schenkel¹, Suzanne Frangos¹, Rickson C. Mesquita^{1,2}, Jennifer A. Kosty¹, Soojin Park¹, W. Andrew Kofke¹, Arjun G. Yodh¹; ¹Univ. of Pennsylvania, USA; ²Univ. of Campinas, Brazil. We used diffuse correlation spectroscopy to continuously monitor cerebral blood flow changes in subarachnoid hemorrhage patients due to interventions in the clinic, and present a novel index for assessing cerebral autoregulation in these patients.

JM3A.18

Optically-Measured Dose-Dependent Increase in Cerebral Blood Flow Caused by Sodium Bicarbonate Therapy, Erin M. Buckley^{1,2}, Jennifer M. Lynch², Donna A. Goff³, Maryam Y. Naim⁴, Susan Nicolson⁵, Lisa Montenegro⁵, Laura K. Diaz⁵, Mark Fogel³, Daniel J. Licht¹, Arjun G. Yodh²; ¹Neurology, Children's Hospital of Philadelphia, USA; ²Physics and Astronomy, Univ. of Pennsylvania, USA; ³Cardiology, Children's Hospital of Philadelphia, USA; ⁴Critical Care Medicine, Children's Hospital of Philadelphia, USA; ⁵Cardiothoracic Anesthesia, Children's Hospital of Philadelphia, USA. Sodium bicarbonate (NaHCO₃) is used to treat metabolic acidemia, despite a link between treatment and brain injury. We observe a dose-dependent increase in cerebral blood flow after NaHCO₃, possibly explaining the cause of this injury.

JM3A.22

In vivo quantification of tumor metabolic demand in pre-clinical models using optical spectroscopy, Tony Jiang¹, Narasimhan Rajaram¹, Chengbo Liu^{1,2}, Fangyao Hu¹, Nimmi Ramanujam¹; ¹BIOMEDICAL Engineering, Duke Univ., USA; ²School of Life Science and Technology, Xi'an Jiatong Univ., China. We report the dose-dependent uptake and kinetics of 2-NBDG, a fluorescent glucose analog, in pre-clinical models using intrinsic fluorescence spectroscopy. Extracted in vivo concentrations of 2-NBDG were proportional to the injected dose in tumors.

JM3A.15

Cherenkov emission spectroscopy for tissue oxygen saturation assessment, Adam Glaser¹, Johan Axelsson¹, Rongxiao Zhang², David Gladstone³, Brian Pogue^{1,2}; ¹Thayer School of Engineering, Dartmouth College, USA; ²Department of Physics and Astronomy, Dartmouth College, USA; ³Norris Cotton Cancer Center, Dartmouth College, USA. Radiation from a linear accelerator induces Cherenkov emission in tissue. The absorption and scatter of this light imparts spectral changes which can be made quantitative through the use of standard spectroscopic techniques.

JM3A.19

Auto-fluorescence lifetime spectroscopy for prostate cancer detection: an optical biopsy approach, Vikrant Sharma¹, Payal Kapur², Ephrem Olweny³, Jeffrey Cadeddu³, Claus G. Roehrborn³, Hanli Liu¹; ¹Bioengineering, The Univ. of Texas at Arlington, USA; ²Pathology, The Univ. of Texas Southwestern Medical Center at Dallas, USA; ³Urology, The Univ. of Texas Southwestern Medical Center at Dallas, USA. We report the use of auto-fluorescence lifetime as a biomarker for prostate cancer diagnosis. 23 human ex vivo prostates were measured post-prostatectomy, and compared to histology. Significant differences in cancer and benign tissue were identified.

JM3A.23

In vivo Spectroscopy of Cervical Tissue, Judith R. Mourant¹, Oana C. Marina¹, Harriet O. Smith²; ¹Bioscience, LANL, USA; ²Montefiore Medical Center, USA. We have collected in vivo spectroscopy data of cervical lesions from two separate locations. The data are analyzed to determine spectroscopic and colposcopic accuracy as compared to the gold standard of pathology.

JM3A.16

Optical Spectroscopy up to 1700 nm: a Time-Resolved Approach Combined with an InGaAs/InP Single-Photon Avalanche Diode, Ilaria Bargigia¹, Alberto Tosi², Andrea Farina³, Andrea Bassi¹, Paola Taroni¹, Andrea Bahgat Shehata², Adriano Della Frera², Alberto Dalla Mora¹, Franco Zappa², Rinaldo Cubeddu^{1,3}, Antonio Pifferi^{1,3}; ¹Physics, Politecnico di Milano, Italy; ²Elettronica e Informazione, Politecnico di Milano, Italy; ³Istituto di Fotonica e Nanotecnologie, Consiglio Nazionale delle Ricerche, Italy. Time-resolved spectroscopy has been exploited mostly up to 1100 nm: our system reaches up to 1700 nm, thanks to a supercontinuum laser source and an InGaAs/InP Single-Photon Avalanche Diode. A first in-vivo application is presented.

JM3A.20

Cerebral Oxygen Extraction Decreases with Age in Preoperative Neonates With Congenital Heart Defects, Erin M. Buckley^{1,2}, Jennifer M. Lynch², Maryam Y. Naim⁵, Donna A. Goff³, Susan Nicolson⁴, Lisa Montenegro⁴, Daniel J. Licht¹, Arjun G. Yodh²; ¹Neurology, Children's Hospital of Philadelphia, USA; ²Physics and Astronomy, Univ. of Pennsylvania, USA; ³Cardiology, Children's Hospital of Philadelphia, USA; ⁴Cardiothoracic Anesthesia, Children's Hospital of Philadelphia, USA; ⁵Critical Care Medicine, Children's Hospital of Philadelphia, USA. Diffuse optical spectroscopy is used to quantify cerebral oxygen saturation, total hemoglobin concentration, & oxygen extraction fraction in neonates with congenital heart defects. Preoperative cerebral oxygen extraction increased with day of life.

JM3A.24

Cerebral Hemodynamic Effects of Hyperoxia Linked to Severity of Pediatric Pulmonary Hypertension, Jennifer M. Lynch¹, Erin M. Buckley^{1,2}, Peter Schwab², Brian D. Hanna³, Daniel J. Licht², Arjun G. Yodh¹; ¹Physics and Astronomy, Univ. of Pennsylvania, USA; ²Neurology, Children's Hospital of Philadelphia, USA; ³Cardiology, Children's Hospital of Philadelphia, USA. We employ diffuse optical spectroscopies to measure cerebral hemodynamic effects of hyperoxia in pediatric patients treated with pulmonary vasodilators and demonstrate the potential of diffuse optics to probe severity of pulmonary hypertension.

JM3A—Joint BIOMED/DH Poster Session - Continue

JM3A.25

Gender-specific hemodynamics in prefrontal cortex during visual-verbal working memory by near-infrared spectroscopy, Ting Li^{1,2}, Qingming Luo¹, Hui Gong¹; ¹*Britton Chance Center for BIOMEDICAL Photonics, Wuhan National Laboratory for Optoelectronics, Huazhong Univ. of Science and Technology, China;* ²*Center of Neuro-Inf., Univ. of Electron. Sci. & Technol. of China, China.* A NIRS study during working memory tested the gender effect on [oxy-Hb], [deoxy-Hb], and [tot-Hb] for hemodynamic-based neuroimaging studies, and found females possess more efficient hemodynamics in PFC, emphasizing the importance of PFC in gender.

JM3A.29

Modeling InGaAs/AlGaAs/Au Lasers for Brain Surgery, Meng-Mu Shih¹; ¹*Univ. of Florida, USA.* This work develops parametric models to compute coupling coefficients of semiconductor-metal lasers at 980 nm for brain surgery. Numerical results computed by the photonic and the optical methods are close.

JM3A.33

Measuring chromophore's concentration and scattering coefficient in a turbid medium using back reflection spectroscopy, Murat Canpolat¹, Aslinur Sircan-Kucuksayan¹; ¹*Biophysics, Akdeniz Univ., Turkey.* Scattering and absorption coefficients were estimated within an error of 4.8% and 13.3% respectively using the back reflection spectral measurements and Monte Carlo simulations results from tissue phantoms consist of Intralipid and methylene blue.

JM3A.26

Raman Spectroscopy Sensor for Surgical Robotics - Instrumentation and Tissue Differentiation Algorithm, Praveen C. Ashok¹, Nikola Krstajić¹, Mario E. Giardini², Kishan Dholakia¹, Wilson Sibbett¹; ¹*School of Physics & Astronomy, Univ. of St Andrews, UK;* ²*School of Medicine, Univ. of St Andrews, UK.* A fiber Raman probe based sensor is designed to be integrated into a surgical robot. The chemical information obtained from this sensor would assist tissue margin detection and surgical guidance during laparoscopic surgical procedures.

JM3A.30

The strong influence of CO2 on cerebral hemodynamics and oxygenation during functional near-infrared spectroscopy (fNIRS) studies, Felix Scholkmann^{1,2}, Ursina Gerber¹, Martin Wolf², Sabine Klein¹, Ursula Wolf¹; ¹*Inst. of Complementary Medicine KIKOM, Univ. of Bern, Switzerland;* ²*BIOMEDICAL Optics Research Laboratory, Division of Neonatology, Univ. Hospital Zurich, Switzerland.* We employed fNIRS to investigate the relationship between cerebral hemodynamics/oxygenation (HD/OX) and end-tidal CO2 (PETCO2). We found a strong influence of PETCO2 on HD/OX during task-evoked brain activity.

JM3A.34

Diffuse Near Infrared Spectroscopy Assessment of Diabetic Foot Ulcers: A Human Study, Joshua Samuels¹, Michael Neidrauer¹, Leonid Zubkov¹, Michael S. Weingarten², David Diaz¹, Xiang Mao¹, Elisabeth S. Papazoglou¹; ¹*BIOMEDICAL Engineering, Drexel Univ., USA;* ²*Surgery, Drexel Univ. College of Medicine, USA.* Forty-six human diabetic foot ulcers were measured with Diffuse Near-Infrared Spectroscopy. The weekly change in oxy-hemoglobin concentration could distinguish healing and non-healing ulcers with a sensitivity of 0.9 and specificity of 0.86 (p<0.002)

JM3A.27

In-Vivo Measurements of Brain Haemodynamics and Energetics using Multimodal Spectroscopy in Perinatal Hypoxia-Ischaemia, Ilias Tachtsidis¹, Alan Bainbridge², Stuart Faulkner³, David Price², Elizabeth Powell³, David Thomas⁴, Ernest Cady², Nicola Robertson³, Xavier Golay⁴; ¹*Medical Physics and Bioengineering, Univ. College London, UK;* ²*Medical Physics and Bioengineering, Univ. College London Hospitals, UK;* ³*Inst. for Women's Health, Univ. College London Hospitals, UK;* ⁴*Inst. of Neurology, Univ. College London Hospitals, UK.* We report a novel multimodal spectroscopy methodology that combines broadband near-infrared spectroscopy and magnetic resonance spectroscopy to monitor brain tissue oxygenation and metabolism in a preclinical model of hypoxic-ischaemic neonatal encephalopathy.

JM3A.31

Multi-wavelength time-resolved measurements of diffuse reflectance: phantom study with dynamic inflow of ICG, Anna Gerega¹, Daniel Milej¹, Wojciech Weigl², Norbert Zolek¹, Piotr Sawosz¹, Roman Maniewski¹, Adam Liebert¹; ¹*Inst. of Biocybernetics and BIOMEDICAL Engineering PAS, Poland;* ²*Department of Anesthesiology and Intensive Care, Medical Univ. of Warsaw, Poland.* Multi-wavelength detection of time-resolved diffuse reflectance signal was carried out in phantom experiments with dynamic inflow of ICG at different depths in a turbid media.

JM3A.35

Fluorescence Suppression Using Modulated Wavelength Raman Spectroscopy for Tissue and Cell Analysis, Bavishna Balagopal¹, Praveen C. Ashok¹, Robert F. Marchington¹, Michael Mazilu¹, Alastair D. Gillies¹, Simon Herrington², Andrew Riches², Kishan Dholakia¹; ¹*School of Physics & Astronomy, Univ. of St Andrews, UK;* ²*School of Medicine, Univ. of St Andrews, UK.* Fluorescence suppression using modulated wavelength Raman spectroscopy has been investigated using a fiber Raman probe and micro-Raman spectroscopy. This may lead to enhanced differentiation between normal and cancerous tissues and cells.

JM3A.28

Cerebral vasomotor reactivity in micro- and macro-vasculature of patients with severe steno-occlusive internal carotid artery lesions, Peyman Zirak¹, Raquel Delgado-Mederos², Lavinia Dinia², Joan Marti Fabregas², Turgut Durduran¹; ¹*BIO-MEDICAL Optics group, The Inst. of Photonic Sciences, ICFO, Spain;* ²*Department of Neurology, Hospital de la Santa Creu i Sant Pau, Spain.* Cerebral-vasomotor-reactivity(CVR) is evaluated in patients with severe internal-carotid-artery steno-occlusion by diffuse optics and transcranial Doppler ultrasound. The micro- and macro-vascular CVR diverged for affected arteries/hemispheres.

JM3A.32

Individualised Optimisation of Modelled Cerebral Oxygenation Near-Infrared Spectroscopy Signals, Beth Jelfs¹, Jasmina Panovska-Griffiths¹, Ilias Tachtsidis¹, Murad Banaji², Clare Elwell¹; ¹*Department of Medical Physics & Bioengineering, Univ. College London, UK;* ²*Department of Mathematics, Univeristy of Portsmouth, UK.* Responses of NIRS signals in a healthy volunteer are predicted using a model of brain circulation. Optimisation using partial data is shown to increase the model's predictive power which can aid the interpretation of NIRS signals in individuals.

JM3A.36

A New, Modular Frequency Domain Diffuse Optical Monitor in the Digital Domain, Udo M. Weigel¹, Ruben Revilla¹, Nestor H. Oliverio¹, Alberto A. Gonzalez¹, Jose C. Cifuentes¹, Peyman Zirak¹, Ricardo Saiz¹, Daniel Mitrani¹, Jordi Ninou¹, Oscar Casellas¹, Turgut Durduran¹; ¹*BIOMEDICAL Optics, ICFO, Spain.* State-of-the-art digital electronics can be utilized to improve performance and scalability of frequency domain diffuse optical monitors. We present a new design based on an under-sampled, heterodyne approach without limitations of analog hardware.

JM3A—Joint BIOMED/DH Poster Session - Continue

JM3A.37

Hemodynamic Monitoring of Spinal Cord with Diffuse Optical & Correlation Spectroscopies, Rickson C. Mesquita^{1,2}, Angela D'Souza³, Asher Emanuel³, Steven S. Schenkel², Robert M. Galler³, Thomas V. Bilfinger³, Arjun G. Yodh², Thomas Floyd²; ¹*Inst. of Physics, Univ. of Campinas, Brazil*; ²*Department of Physics & Astronomy, Univ. of Pennsylvania, USA*; ³*Stony Brook Univ. Medical Center, USA*. We employ diffuse optics to measure spinal cord hemodynamics in response to pharmacologic and mechanical perturbations for the first time. Comparison of blood flow and blood pressure responses demonstrate robust spinal cord autoregulation.

JM3A.41

Withdrawn

JM3A.45

Chemotherapeutic Effects on Breast Malignant Cells Evaluated by Native Fluorescence Spectroscopy, Yang Pu¹, Guichen Tang¹, Wubao Wang¹, H. E. Savage², S. P. Schantz², Robert R. Alfano¹; ¹*Physics, Inst. for Ultrafast Spectroscopy and Lasers, City College of City Univ of New York, USA*; ²*Division of Head and Neck Surgery, Manhattan Eye, Ear & Throat Hospital, USA*. The decreasing relative content of tryptophan, NADH and flavin of the retinoic acid-treated breast cancerous cells were demonstrated using native fluorescence spectra. The changes may be used to evaluate the chemotherapeutic effects on cancer.

JM3A.38

Correction of shape-induced artifacts in spectroscopic imaging of biological media, Jessica C. Ramella-Roman¹; ¹*BIOMEDical Engineering, Catholic Univ., USA*. Imaging spectroscopy results are often biased by the surface structure of the imaged object. A combination of software and experimental tools has been designed to study and minimize this effect

JM3A.42

Development of a Non-Invasive Optical Method for Assessment of Skin Barrier to External Penetration, Georgios N. Stamatas¹, Elise Boireau-Adamezyk¹; ¹*R&D, Johnson & Johnson Santé Beauté France, France*. Confocal Raman Microspectroscopy was used to compute the concentration profiles of topically applied caffeine through the skin. Parameters relating to the skin barrier function were calculated from the caffeine concentration profiles.

JM3A.46

Normative database of judgment of complexity task with functional near infrared spectroscopy - Application for TBI, Franck Amyot¹, Trelawny Zimmermann², Jason D. Riley¹, Jana M. Kainerstorfer¹, Victor Chernomordik¹, Laleh Najafzadeh¹, Eric Wassermann², Amir Gandjbakhche¹; ¹*SFAB, NICHD / NIH, USA*; ²*BNU, NINDS / NIH, USA*. We construct a normative database for a simple cognitive test which can be useful in evaluating cognitive disability such as mild traumatic brain injury. Our results with fNIRS show activation from the medial frontopolar cortex

JM3A.39

Withdrawn

JM3A.43

Assessment of Breast Cancer Induced Bone Quality Changes Using Raman Spectroscopy, Xiaohong Bi¹, Julie Sterling², Daniel Perrien³, Alyssa Merkel², Jeffrey Nyman³, Barbara Rowland², Anita Mahadevan-Jansen¹; ¹*BIO-MEDical Engineering, Vanderbilt Univ., USA*; ²*Clinical Pharmacology, Vanderbilt Univ., USA*; ³*Orthopaedics and Rehab, Vanderbilt Univ., USA*. Cancer bone metastases result in bone degradation and pathologic fracture. This study investigated compositional alterations in metastatic bones from a mouse model of breast cancer and showed significant cancer induced difference in bone quality.

JM3A.47

In Vivo Measurement of Carcinogenesis-Associated Shape Alterations of the Refractive Index Correlation Function, Andrew J. Gomes¹, Sarah Ruderman¹, Mart Delacruz², Ramesh Wali², Hemant K. Roy², Vadim Backman¹; ¹*BIOMEDical Engineering, Northwestern University, USA*; ²*Internal Medicine, Northshore Univ. Health System, USA*. We employed polarization-gating spectroscopy in the azoxymethane-treated rat model of colon carcinogenesis and found differences in the shape of the refractive index correlation function that correlated with risk of neoplasia. This marker has potential in predicting tumor development.

JM3A.40

Pulsatile and static hemodynamics of human patella during rest and cuff inflation, Parisa Farzam¹, Peyman Zirak¹, Tiziano Binzoni^{2,3}, Turgtur Durduran¹; ¹*ICFO-Institut de Ciències Fotoniques, Spain*; ²*Département des Neurosciences Fondamentales, Switzerland*; ³*Imagerie et des Sciences de l'Information Médicale, Switzerland*. Pulsatile and static hemodynamics of the human patella (knee-cap) were studied at rest and at arterial cuff-occlusion. Differences in hemodynamics between the patella and the muscle were observed.

JM3A.44

Evaluation of Skin Vascular Malformations' Laser Treatment by RGB and Multi-spectral Imaging, Dainis Jakovels¹, Ilona Kuzmina¹, Anna Berzina², Janis Spigulis¹; ¹*Inst. of Atomic Physics and Spectroscopy, Biophotonics Laboratory, Univ. of Latvia, Latvia*; ²*The Clinic of Laser Plastics, Latvia*. RGB imaging system for mapping and monitoring of hemoglobin changes in skin has been tested for evaluation of vascular malformations' laser treatment. The multi-spectral imaging system was used as the reference.

JM3A.48

Frontal Activation Assessment Using Near-Infrared Spectroscopy and Electroencephalography, Jing Dong¹, Chidambaram Yegappan¹, Renzhe Bi¹, Kijoon Lee¹; ¹*SCBE/BIE, Nanyang Technological Univ., Singapore*. Here, we focus on assessing frontal activation of normal subjects in response to verbal fluency test. A multimodal instrument, combining NIRS and EEG, was used. The results lead to a better understanding of brain functionality.

JM3A—Joint BIOMED/DH Poster Session - Continue

JM3A.49

Efficient simulation of intensity profile of light through subpixel-matched lenticular lens array for auto-stereoscopic liquid crystal display, Yia-Chung Chang¹, Li-Chuan Tang¹, Chun-Yi Yin¹; ¹*The Research Center for Applied Sciences, Academia Sinica, Taiwan*. We present numerical simulation of the accumulating intensity profile of a lenticular lens array on a liquid crystal display. This efficient method allows one to adjust the parameters and crosstalks of a subpixel-matched autostereoscopic display.

JM3A.50

Portable and low-cost digital holographic microscopy using web camera, point light source LED and open-source libraries, Tomoyoshi Shimobaba¹, Yusuke Taniguchi¹, Atsushi Shiraki², Nobuyuki Masuda¹, Tomoyoshi Ito¹; ¹*Graduate school of Engineering, Chiba Univ., Japan*; ²*Department of Information and Computer Engineering, Kisarazu National College of Technology, Japan*. We report a portable and low-cost digital holographic microscopy (DHM). By adopting the Gabor hologram and using a web camera, point light source LED and open-source libraries, development costs were decreased

JM3A.51

Numerical investigation of holographic wavefront retrieval using Laplacian reconstruction, Tomoyoshi Shimobaba¹, Nobuyuki Masuda¹, Tomoyoshi Ito¹; ¹*Graduate school of Engineering, Chiba Univ., Japan*. We numerically investigated holographic wavefront retrieval using Laplacian reconstruction. We used Laplacian reconstruction as a wavefront retrieval technique in which the equation of Laplacian reconstruction was regarded as a Poisson equation.

JM3A.52

3D image enlargement without distortion based on the optical reversibility theorem, Jia Jia¹, Yongtian Wang¹, Juan Liu¹, Xin Li¹, Jinghui Xie¹; ¹*School of Optoelectronics, Beijing Inst. of Technology, China*. We propose a method to enlarge the 3D image in holographic display using a lens based on the optical reversibility theorem. The 3D image is magnified without any distortion, and the image distance is shortened.

JM3A.53

Design of Virtual Image for 360-degree Viewable Image-plane Disk-type Multiplex Holography, Yih-Shyang Cheng¹, Chih-Hung Chen¹, Zheng-Feng Chen¹; ¹*NCU, Taiwan*. In this paper, the fabrication method and the parameter design of multiplex holograms for virtual image display in walk-around viewable disk-type holography is introduced.

JM3A.54

GPU based acceleration of incoherent Fourier hologram capture using integral imaging, Kyeong-Min Jeong¹, Hee-Seung Kim¹, Sung-In Hong¹, Hyun-Eui Kim¹, Jae-Hyeung Park¹; ¹*Chungbuk National University, Republic of Korea*. GPU based acceleration of incoherent Fourier hologram capture technique using integral imaging is reported. It is demonstrated that parallel processing using GPU reduces processing time for hologram generation and numerical reconstruction.

JM3A.55

Superposition Procedure for Improvement of Digital Holographic Particle Field Reconstruction, Abhishek Nigam¹; ¹*Mechanical Engineering, IIT Kanpur, India*. The present study proposes a superposition procedure during the holographic reconstruction of 3-D particle field. Both simulated and experimental holograms have been used to demonstrate the improvement in the performance of proposed algorithm.

JM3A.56

Generation of Fresnel Complex Holograms with Packed Ray-Tracing Software, Wang-Yu Hsieh¹, Jung-Ping Liu¹, Shih-Hsin Ma¹; ¹*Department of Photonics, Feng Chia Univ., Taiwan*. We use packaged ray-tracing software to generate complex Fresnel holograms. The principle is that the wavefront can be decomposed to Gaussian beams, and the propagation of a Gaussian beam can be calculated by ray tracing.

JM3A.57

A Practical Holographic Encryption/Decryption Technique, Shaohua Tao¹; ¹*School of Physics and Electronics, Central South Univ., China*. A digital holographic decryption technique is proposed to decode holograms that are printed as gray-scale images. The technique has high security and can be conveniently applied for protecting confidential information.

JM3A.58

Dynamic holographic images using photorefractive composites, Kenji Kinashi¹, Yu Wang¹, Sho Tsujimura¹, Wataru Sakai¹, Naoto Tsutsumi¹; ¹*Department of Macromolecular Science and Engineering, Kyoto Inst. of Technology, Japan*. We have studied the effect of Mw of PVCz on dynamic holographic imaging. The appropriate performance for dynamic holographic imaging was obtained by the photorefractive polymeric composite film with Mw:23,000 PVCz.

JM3A.59

A New Hologram Generating Algorithm for Improved Control of Diffraction Spot Intensities, Martin Persson¹, David Engström¹, Mattias Goksör¹; ¹*Physics, Univ. of Gothenburg, Sweden*. We demonstrate a novel method for generating phase holograms, which compensates for interaction between adjacent pixels in liquid crystal based spatial light modulators. A method for characterizing SLMs in this aspect is also provided.

JM3A.60

Three-dimensional blood vessel imaging using integral imaging, Sung-In Hong¹, Hee-Seung Kim¹, Kyeong-Min Jeong¹, Jae-Hyeung Park¹; ¹*Chungbuk National University, Republic of Korea*. Three-dimensional imaging of blood vessel using integral imaging technique is proposed. With a near infrared illumination, a finger is imaged through a lens array and three-dimensional structure of the blood vessel in the finger is visualized.

JM3A—Joint BIOMED/DH Poster Session - Continue

JM3A.61

Biological imaging by Digital Holographic Adaptive Optics, Changgeng Liu¹, Myung K. Kim¹, ¹*Physiscs, Univ. of South Florida, USA*. The basic principles of DHAO have been presented and demonstrated in a recent paper [Opt. Lett. 36, 2710-2712(2011)]. In this paper, the application of DHAO in biological imaging is investigated.

JM3A.62

Geometrical Characterization of Micro-fiber in 3D Volume using Digital In-line Holography, Dhananjay K. Singh¹; ¹*Mechanical Engineering, I. I. T. Kanpur, India*. The present study proposes a method to determine orientation, length and location of micro fiber in 3D volume using digital in-line holography. The proposed algorithm is validated using experimental hologram of micro fiber inside object volume.

JM3A.63

Analysis of 2D Digital Holography using Synthesized Holograms, Isao Matsubara¹, Chung-Chieh Yu¹, William J. Dallas^{2,3}; ¹*Optics Research Laboratory, Research & Development Center, Canon U.S.A., Inc., USA*; ²*College of Optical Sciences, Univ. of Arizona, USA*; ³*Department of Radiology, College of Medicine, Univ. of Arizona, USA*. An algorithm to generate synthesized holograms is described, and the results are validated by comparing them with an experiment. The system's axial resolution is analyzed using the algorithm as an example of the algorithm's capabilities.

JM3A.64

A Flicker-Reduced Full-Resolution Autostereoscopic Liquid Crystal Display with Multi-Viewpoints using a Multi-Directional Backlight Unit, Hyunkyung Kwon¹, Minyoung Park¹, Hee-Jin Choi¹; ¹*Department of Physics, Sejong Univ., Republic of Korea*. The loss of resolution is one of the most important issues of autostereoscopic displays. In this paper, a method to realize an autostereoscopic LCD with full-resolution and reduced flicker using a multi-directional backlight unit is proposed.

JM3A.65

Distributed Scan SDOCT Improves Post Refractive Surgery Corneal Biometry, Ryan P. McNabb¹, Francesco LaRocca¹, Sina Farsiu^{2,1}, Anthony Kuo², Joseph Izatt^{1,2}; ¹*Biomedical Engineering, Duke University, USA*; ²*Ophthalmology, Duke University Eye Center, USA*. We report on a preliminary study comparing corneal refractive power acquired using distributed scanning OCT (DSOCT) to corneal topography and Scheimpflug photography in normal subjects both before and after refractive surgery.

JM3A.66

Holographic image acquisition and rendering for laser Doppler angiography, Michael Atlan¹, Benjamin Samson¹, Nicolas Verrier¹, Max Lesaffre¹; ¹*CNRS, France*. A brief review of acquisition and rendering methods of optically-acquired holograms in frequency-shifting and off-axis conditions is presented. Applications to laser Doppler imaging in angiography are reported, as well as our latest technical developments in image reconstruction.

JM3A.67

Intensity Based Holographic Reconstruction of Symmetric and Asymmetric Object Field, Satya P. Gupta^{1,2}, Abhishek Nigam¹, Dhananjay K. Singh¹, Pradeepta K. Panigrahi^{1,3}; ¹*Mechanical Engineering, Indian Inst. of Technology, India*; ²*Materials Science Programme, Indian Inst. of Technology, India*; ³*Center for Laser Technology, Indian Inst. of Technology, India*. The paper reports the performance of intensity based holographic reconstruction approach for characterization of symmetric and asymmetric objects. Silver particles inside cavity represent symmetric object field. Fiber and crystals inside volume represent asymmetric object field.

JM3A.68

Spectrally constrained functional diffuse optical tomography of the adult brain, Yuxuan Zhan¹, Adam T. Eggebrecht², Joseph P. Culver², Hamid Dehghani¹; ¹*School of Computer Science, The Univ. of Birmingham, The Univ. of Birmingham, UK*; ²*Department of Radiology, Washington Univ. School of Medicine, Washington Univ. School of Medicine, USA*. We present a spectrally constrained DOT image reconstruction scheme which demonstrates better imaging artifacts suppression due to poor signal to noise ratio as compared with the standard scheme.

JM3A.69

Diffuse Optical Tomography Imaging of the Hemodynamic Response to a Breath Hold for Use in Breast Cancer Detection, Molly Flexman¹, Jacqueline E. Gunther¹, Hyun K. Kim¹, Emerson Lim², Elise Desperito³, Randall L. Barbour⁴, Dawn Hershman², Andreas H. Hielscher^{1,3}; ¹*BIOMEDical Engineering, Columbia Univ., USA*; ²*Department of Oncology & Internal Medicine, Columbia Univ., USA*; ³*Department of Radiology, Columbia Univ., USA*; ⁴*Department of Pathology, State Univ. of New York - Downstate Medical Center, USA*. We discuss here a recent study using diffuse optical tomography to make simultaneous dual-breast measurements in 21 subjects during a breath hold. An exponential fit to the transient response differentiates between tumor-bearing and healthy breasts.

JM3A.70

Monitoring Tumor Response to Neoadjuvant Chemotherapy using Ultrasound-guided Near Infrared Light, Qinging Zhu¹; ¹*ECE, Univ. of Connecticut, USA*. In this paper, we show that initial tumor vascularity is a good predictor of final pathologic response. Additionally, the vascular changes during early treatment cycles assessed by %total hemoglobin can further predict final pathologic response.

JM3A.71

Multi-Color in vivo fluorescence lifetime tomography, Leilei Peng¹, Weibin Zhou², Ming Zhao¹; ¹*College of Optical Sciences, Univ. of Arizona, USA*; ²*Department of Pediatrics and Communicable Diseases, Univ. of Michigan Medical School, USA*. We present an in vivo multi-color fluorescence lifetime imaging method based on scanning laser optical tomography and Fourier fluorescence lifetime excitation-emission matrix spectroscopy. The system was tested with live transgenic zebrafish embryo.

JM3A.72

Processing of Dynamic Phase Images of Moving Organisms, Katherine Creath^{1,2}, Goldie Goldstein^{1,2}; ¹*4D Technology Corp, USA*; ²*College of Optical Sciences, The Univ. of Arizona, USA*. Recent work utilizing an interference microscope system imaging live biological samples to create phase image movies tracking dynamic motions and volumetric changes is presented. Measurement examples highlight background leveling and unwrapping phase in time.

Symphony I & II

BIOMED I

15:30 - 17:30

BM4A • Brain Signals 2

Randall Barbour, *SUNY Downstate Medical Center, USA, Presider*

BM4A.1 • 15:30

Multimodality fNIRS-EEG, fMRI-EEG and TMS Clinical Study on Cortical Response During Motor Task in Adult Volunteers and Epileptic Patients with Movement Disorders, Lorenzo Spinelli¹, Alessandro Torricelli², Davide Contini², Matteo Caffini², Lucia Zucchelli², Rinaldo Cubeddu², Erika Molteni³, Anna Maria Bianchi³, Giuseppe Baselli³, Sergio Cerutti³, Elisa Visani⁴, Isabella Gilioli⁴, Davide Rossi Sebastiano⁴, Elena Schiaffi⁴, Ferruccio Panzica⁴, Silvana Franceschetti⁴; ¹*Istituto di Fotonica e Nanotecnologie, CNR, Italy*; ²*Physics, Politecnico di Milano, Italy*; ³*Bioengineering, Politecnico di Milano, Italy*; ⁴*Unità Operativa Neurofisiopatologia ed Epilettologia diagnostica, Centro per l'Epilessia, Fondazione IRCCS Istituto Neurologico Carlo Besta, Italy*. A multimodality fNIRS-EEG, fMRI-EEG and TMS clinical study was performed on adult volunteers and epileptic patients with movement disorders to assess cortical response during motor tasks

BM4A.2 • 15:45

Biophysical Model Estimation from Multispectral Intrinsic Optical Imaging in a Rat Model of Epilepsy, Philippe Pouliot^{1,2}, Tri Truong Van^{1,3}, Cong Zhang¹, Simon Dubeau¹, Dang Khoa Nguyen³, Frédéric Lesage^{1,2}; ¹*Electrical Engineering and Biomedical Imaging, Ecole Polytechnique Montreal, Canada*; ²*Research Center, Montreal Heart Inst., Canada*; ³*Service de Neurologie, Hôpital Notre-Dame du CHUM, Canada*. The hemodynamic responses to 4-AP induced focal epileptic spikes and electrical stimulations are compared in a rat model. Nonlinearities are quantified with biophysical models. Supranormal oxygen consumption from epileptic spikes is inferred.

BM4A.3 • 16:00

Imaging of Motor Activity in Freely Moving Subjects Using a Wearable NIRS Imaging System, Arne Krüger¹, Stefan P. Koch¹, Jan Mehnert¹, Christina Habermehl¹, Sophie Piper¹, Jens Steinbrink¹, Hellmuth Obrig^{2,3}, Christoph H. Schmitz^{1,4}; ¹*Neurology, Charité Univ. Medicine Berlin, Germany*; ²*Max Planck Inst. for Human Cognitive and Brain Sciences, Germany*; ³*Clinic for Cognitive Neurology, Univ. Hospital Leipzig, Germany*; ⁴*NIRx Medizintechnik GmbH, Germany*. We present a miniaturized multi-channel NIRS imaging system for functional brain imaging in unrestrained settings suitable for any aspect of the head. Performance is demonstrated in a motor execution paradigm performed during bicycle riding.

Symphony III

BIOMED 2

15:30 - 17:30

BM4B • Microscopy Imaging: Novel Techniques and Applications

Peter So; *MIT, USA, Presider*

BM4B.1 • 15:30

Invited

ePetri: Self-imaging Petri Dish Platform for Autonomous Cell Culture Tracking, Changhui Yang¹; ¹*Electrical Engineering, California Inst. of Technology, USA*. Here we show that autonomous self-imaging bright-field and fluorescence ePetri systems can be constructed compactly and cheaply with low cost commercially available CMOS chips.

BM4B.2 • 16:00

Imaging sub-cellular structures using three-dimensional sparse deconvolution SLIM, Mustafa Mir^{1,2}, S. Derin Babacan², Michael Bednarz³, Minh N. Do^{1,2}, Ido Golding^{3,4}, Gabriel Popescu^{1,2}; ¹*Electrical Engineering, Univ. of Illinois at Urbana Champaign, USA*; ²*Beckman Inst. for Advanced Science and Technology, USA*; ³*Department of Physics, Center for the Physics of Living Cells, Univ. of Illinois at Urbana-Champaign, USA*; ⁴*Venna and Marrs McLean Department of Biochemistry and Molecular Biology, Baylor College of Medicine, USA*. We demonstrate a 2.5x resolution enhancement of three-dimensional quantitative phase maps using a novel sparse deconvolution method. This method was used to visualize and characterize two previously invisible coil-like structures in *E. coli* cells.

Symphony IV

DH

15:30 - 17:30

DM4C • Digital Holographic Optical Processing

John Sheridan; *Univ. College Dublin, Ireland, Presider*

DM4C.1 • 15:30

Invited

Optical Information Processing by Polarization-Holographic Elements, Barbara Kilosanidze¹, George Kakauridze¹; ¹*Laboratory of Holographic Recording and Processing of Information, Inst. of Cybernetics of the Georgian Technical Univ., Georgia*. A new polarimetric method of real-time complete analysis of the polarization state of light based on the integral polarization-holographic element is considered. The advantages and applications of this method in optical information processing are discussed.

DM4C.2 • 16:00

Multi-Plane Image Reconstruction Using Cascaded Phase Elements, A. Alkan Gulsues¹, B. Keith Jenkins¹; ¹*Electrical Engineering, Univ. of Southern California, USA*. Cascaded phase only holograms, designed by a deterministic iterative algorithm, are used for multi-plane image formation. Numerical results are presented. This technique could be applicable to a static micro-holographic 3D display.

BM4A • Brain Signals 2—Continue

BM4A.4 • 16:15

Evoked Hemodynamic Responses to Auditory Stimulation Following Sleep Deprivation in Humans, Jennifer L. Schei^{1,2}, Joseph E. Cahall^{3,4}, Gregory Belenky⁴, David M. Rector³; ¹*P-21 Applied Modern Physics, Los Alamos National Laboratory, USA*; ²*Physics and Astronomy, Washington State Univ., USA*; ³*Department of Veterinary, Comparative Anatomy, Pharmacology, and Physiology, Washington State Univ., USA*; ⁴*Sleep and Performance Research Center, Washington State Univ., USA*. Evoked hemodynamic responses measured following sleep deprivation were larger compared baseline and recovery sleep nights. Attention differences during sleep deprivation showed larger responses in alert individuals than sleepy individuals, suggesting differences in vascular compliance.

BM4A.5 • 16:30

Phase relationship between the low-frequency oscillatory components of cerebral [HbO] and [Hb] assessed by NIRS during sleep in human subjects, Michele L. Pierro¹, Angelo Sassaroli¹, Sergio Fantini¹, Peter Bergethon²; ¹*BME, Tufts Univ., USA*; ²*Boston Univ. School of Department of Anatomy & Neurobiology, Boston Univ. School of Medicine, USA*. We measured the phase of low-frequency oscillations (LFOs) of [Hb] and [HbO] in the human brain during sleep. We found that, on average, the phase lead of [Hb] vs [HbO] LFOs is greater during slow-wave sleep than during REM sleep.

BM4A.6 • 16:45

Noninvasive Optical Detection of Spontaneous Low Frequency Oscillations in Cerebral Blood Flow, Ran Cheng¹, Guoqiang Yu¹, Yu Shang¹; ¹*Center for BIOMEDical Engineering, Univ. of Kentucky, USA*. A diffuse correlation spectroscopy was used to quantify low frequency oscillations in cerebral blood flow of healthy volunteers at rest, during head-up-titling (HUT) and during enforced breathing. The HUT is found to be a robust and stable protocol.

BM4A.7 • 17:00

Optical intrinsic signal imaging of functional connectivity in the mouse brain, Adam Q. Bauer¹, Brian R. White¹, Abraham Z. Snyder^{1,2}, Jin-Moo Lee², Bradley L. Schlaggar^{1,2}, Joseph P. Culver^{1,3}; ¹*Radiology, Washington Univ. in Saint Louis, USA*; ²*Neurology, Washington Univ. in Saint Louis, USA*; ³*BIOMEDical Engineering, Washington Univ. in Saint Louis, USA*. We develop functional connectivity optical intrinsic signal imaging (fcOIS) for mice, with validation in acallosal mice. FcOIS provides mouse researchers with a method analogous to the new standards in resting state functional human neuroimaging.

BM4B • Microscopy Imaging: Novel Techniques and Applications—Continue

BM4B.3 • 16:15

3D Super-resolution Imaging of Microtubules with a Double Helix Point Spread Function Microscope, Ginni Grover¹, Keith DeLuca², Sean Quirin¹, Jennifer DeLuca², Rafael Piestun¹; ¹*Department of Electrical Computer and Energy Engineering, Univ. of Colorado, Boulder, USA*; ²*Department of Biochemistry and Molecular Biology, Colorado State Univ., USA*. Double Helix PSF Imaging of PtK1 cells reveals 3D intracellular structure beyond the diffraction limit. The 3D super-resolution microscope is built around a photon-efficient PSF design and phase mask matched to an optimal estimation algorithm.

BM4B.4 • 16:30

3D microfluidic microscopy using a tilted channel, Nicolas C. Pégard¹, Jason Fleischer¹; ¹*Princeton Univ., USA*. We present a 3D microfluidic microscope. Using a microfluidic channel that is tilted along the optical axis of the objective, we record and deconvolve a focal stack as the sample passes across the focal plane.

BM4B.5 • 16:45

Spectral-domain Differential Interference Contrast (SD-DIC) Microscopy for Measuring Live Cell Dynamics, Yizheng Zhu¹, Michelle R. Lyons², Anne E. West², Lisa L. Satterwhite¹, Adam Wax¹; ¹*BIOMEDical Engineering, Duke Univ., USA*; ²*Neurobiology, Duke Univ., USA*. We present spectral-domain DIC microscopy, a novel technique for high-resolution, quantitative measurement of optical pathlength gradients. Imaging and dynamic monitoring of live neurons and cardiomyocytes were demonstrated.

BM4B.6 • 17:00

Targeted Alteration of Real and Imaginary Refractive Index of Biological Cells by Histological Staining, Lusik Cherkezyan¹, Hariharan Subramanian¹, Seungmoo Yang¹, Dhwanil Damania¹, Vadim Backman¹; ¹*Northwestern Univ., USA*. Histological staining changes the intracellular refractive index due to the Kramers-Kronig relation. We present a method for creating 2-D maps of real and imaginary refractive index of stained biological cells using their thickness and absorbance.

DM4C • Digital Holographic Optical Processing—Continue

DM4C.3 • 16:15

Comparison of different digital holographic setup configurations, Daniel Claus¹, Daciana Iliescu², John Watson³, John Rodenburg¹; ¹*Univ. of Sheffield, UK*; ²*Univ. of Warwick, UK*; ³*Univ. of Aberdeen, UK*. This paper presents a comparison of the most commonly applied digital holographic setups, namely Fourier hologram, Fresnel hologram and Image-plane hologram.

DM4C.4 • 16:30

Speckle noise reduction for digital holography using longitudinal shifting, Chung-Chieh Yu¹, Isao Matsubara¹, William J. Dallas^{2,3}; ¹*Optics Research Laboratory, Research & Development Center, Canon U.S.A., Inc., USA*; ²*College of Optical Sciences, Univ. of Arizona, USA*; ³*Department of Radiology, College of Medicine, Univ. of Arizona, USA*. A method of reducing speckle noise for digital holography is developed by shifting the sample longitudinally. The averaging of phase images is achieved using numerical focusing. Significant noise reduction is observed experimentally.

DM4C.5 • 16:45

Weak-Object Image Reconstructions with Single-Shot Digital Holography, Abbie E. Tippie¹, James R. Fienup¹; ¹*Inst. of Optics, Univ. of Rochester, USA*. Weak object signals with less than one photoelectron per detector pixel can be recovered using off-axis digital holography. We show image reconstructions in simulation with a single exposure.

DM4C.6 • 17:00

Tomographic Compressive Holography, Georges Nehmetallah¹, Logan Williams²; ¹*ECE, Univ. of Dayton, USA*. Compressive holography with multiple projection tomography are applied to solve the inverse ill-posed problem of 3D reconstruction of phase as well as amplitude objects with high axial accuracy. Brief theory and experimental results are shown.

Symphony I & II

Symphony III

Symphony IV

BIOMED I

BIOMED 2

DH

BM4A • Brain Signals 2—Continue

BM4B • Microscopy Imaging: Novel Techniques and Applications—Continue

DM4C • Digital Holographic Optical Processing—Continue

BM4A.8 • 17:15

▶
Neurovascular Coupling Varies with Level of Global Cerebral Ischemia in a Rat Model, Wesley B. Baker¹, Teruyuki Hiraki², Zhenghui Sun², Mary Putt³, Martin Reivich², Arjun G. Yodh¹, Joel H. Greenberg²; ¹*Physics and Astronomy, Univ. of Pennsylvania, USA*; ²*Neurology, Univ. of Pennsylvania, USA*; ³*Biostatistics, Univ. of Pennsylvania, USA*. We employed optical imaging to study the acute effects of global cerebral ischemia on cerebral blood flow and metabolic functional responses to forepaw stimulation in rats. We compared these responses to the underlying neuronal activity.

BM4B.7 • 17:15

Phase contrast spectroscopy using spatial light modulator, Hoa Pham¹, Gabriel Popescu¹; ¹*ECE, Univ. of Illinois at Urbana-Champaign, USA*. We developed a phase contrast spectroscopy (PCS) using spatial light modulator (SLM) capable of measuring at multiple wavelengths. We demonstrate the capability of the setup by dispersion measurements of microsphere beads and red blood cells.

DM4C.7 • 17:15

Scanning Holography with Simultaneous Optical Filtering, Chieh-Cheng Lee¹, Ting-Chung Poon^{2,1}, Dao-Zheng Luo¹, Jung-Ping Liu¹; ¹*Department of Photonics, Feng Chia Univ., Taiwan*; ²*Bradley Department of Electrical and Computer Engineering, Virginia Tech., USA*. We proposed to acquire optically filtered digital holograms by using the optical scanning holography. Experimental demonstrations of the low-pass and the high-pass filtering were provided.

CONFERENCE RECEPTION

18:30—20:00, *Concerto Ballroom and Overture Foyer*

Symphony I & II

BIOMED

Symphony IV

DH

08:00 - 09:30

BTu1A • BIOMED Plenary II

Claude Boccara; Institut Langevin, France, Presider

08:00 - 09:30

DTu1C • Digital Holographic Microscopy II

Gabriel Popescu; Univ of Illinois at Urbana-Champaign USA, Presider

BTu1A.1 • 08:00

Plenary **Diffuse Optical Spectroscopy: Technology Development and Clinical Translation**

Bruce J. Tromberg¹; ¹Univ. of California Irvine, USA. This talk describes the development of Diffuse Optical Spectroscopy (DOS) using spatially- and temporally-modulated sources and model-based analyses. DOS methods are capable of dynamic in vivo functional imaging with variable, but limited, spatial localization. Multiple optical contrast elements such as absorption, scattering, fluorescence, and speckle are detectable at relatively low cost. Quantitation of these signals can be achieved using methods for controlling optical path length in conjunction with computational models and visualization techniques.

DTu1C.1 • 08:00

Tutorial

Title Not Available, George Barbastathis, MIT, USA.. Abstract not available.

BTu1A.2 • 08:45

Plenary 

Bioimaging at the Nanoscale: Single-molecule and Super-resolution Fluorescence Microscopy, Xiaowei Zhuang¹; ¹Howard Hughes Medical Inst., USA. Optical microscopy is an essential tool in biological research. However, the spatial resolution of optical microscopy, classically limited by diffraction to several hundred nanometers, is substantially larger than typical molecular length scales in cells, leaving many biological structures unresolvable. We recently developed a new form of super-resolution light microscopy, stochastic optical reconstruction microscopy (STORM), that surpasses the diffraction limit. STORM uses single-molecule imaging and photoswitchable fluorescent probes to temporally separate the spatially overlapping images of individual molecules. This approach allows the localization of fluorescent probes with nanometer precision and the construction of sub-diffraction-limit images. Using this method, we have achieved multicolor and three-dimensional (3D) imaging of living cells with nanometer-scale resolution. In this talk, I will discuss the general concept, recent technical advances and biological applications of STORM.

DTu1C.2 • 08:45

Phase Retrieval using Nonlinear Diversity, Chien-Hung Lu¹, Christopher Barsi^{1,2}, Jason Fleischer¹; ¹Electrical Engineering, Princeton Univ., USA; ²Media Laboratory, Massachusetts Inst. of Technology, USA. We extend the Gerchberg-Saxton algorithm to a nonlinear optical system. We experimentally demonstrate the technique by reconstructing an input phase distribution from two output intensity measurements taken at different values of the nonlinearity.

DTu1C.3 • 09:00

High Dynamic Range Holographic Microscopy, William J. Dallas¹, Isao Matsubara², Chung-Chieh Yu²; ¹Optical Sciences, Univ. of Arizona, USA; ²Optics Research Laboratory, Canon U.S.A., Inc., USA. A spatial-filtering method for demodulating interlace-sampled off-axis digital holograms is applied to holograms made in monochromatic illumination using a color sensor. The end results are high dynamic-range images. Includes experimental results.

DTu1C.4 • 09:15

Multi-wavelength digital in-line holographic microscopy, Jorge Garcia-Sucerquia¹, Daniel Velasquez²; ¹Physics, Universidad Nacional de Colombia Sede Medellin, Colombia; ²Basic sciences, Universidad EAFIT, Colombia. We present multi-wavelength digital in-line holographic microscopy (DIHM): the simplest approach to color holographic microscopy. As the technique is applied to study a biological sample it surpasses the performance of monochrome DIHM.

Tuesday, 1 May

Symphony I & II

BIOMED I

10:00 - 12:00

BTu2A • Imaging of Vascular Dynamics
Huabei Jiang; *Univ. of Florida, USA, Presider*

BTu2A.1 • 10:00

Simulation and Experimental Studies of Transrectal Diffuse Optical Tomography for Monitoring Laser Interstitial Thermal Therapy of Localized Prostate Cancer, Jie He^{1,2}, Robert Weersink², Israël Veilleux², Sean Davidson², John Trachtenberg^{1,2}, Brian C. Wilson^{1,2}; ¹*Univ. of Toronto, Canada*; ²*Ontario Cancer Inst., Canada*. We validate the sensitivity of changes in the diffuse reflectance optical signal to localize the photocoagulation boundary within ±1 mm in transrectal monitoring of interstitial NIR laser treatment of focal prostate cancer.

BTu2A.2 • 10:15

Small Animal Tomographic In Vivo Flow Cytometry with Diffuse Fluorescence Light, Eric Zettergren¹, Judith Runnels², Charles P. Lin², Mark Niedre¹; ¹*Electrical and Computer Engineering, Northeastern Univ., USA*; ²*Wellman Center for Photomedicine, Harvard Medical School and Massachusetts General Hospital, USA*. We have developed a new approach for fluorescence sensing, enumeration and tomographic localization of rare circulating cells with diffuse light. We validate our instrument using multiple-myeloma cells in optical phantoms and in mice in vivo.

BTu2A.3 • 10:30

Pharmacokinetic Analysis for Tumor Characterization Using MR-Guided Dynamic Contrast Enhanced Diffuse Optical Tomography, Mitchell Hsing¹, Yuting Lin¹, Gultekin Gulsen¹; ¹*Univ. of California, Irvine, USA*. Pharmacokinetic analyses for tumor characterization performed using perfectly co registered DCE-DOT and DCE-MR parameters to produce the first ever quantitative MR-DCE-DOT kinetic parameters used for tumor characterization are derived in this study.

BTu2A.4 • 10:45

Measurement of Vascular Response within the Foot Using Dynamic Diffuse Optical Tomography, Michael Khalil¹, Hyun K. Kim¹, Molly Flexman¹, In-Kyong Kim³, Rajeev Dayal³, Andreas H. Hielscher^{1,2}; ¹*BIO-MEDICAL Engineering, Columbia Univ., USA*; ²*Radiology, Columbia Univ., USA*; ³*Vascular Surgery, New York-Presbyterian Columbia Univ. Medical Center, USA*. We present case studies using dynamic diffuse optical tomographic imaging to view the vascular perfusion of patients with Peripheral Arterial Disease with and without calcifications as well as a healthy control group.

Symphony III

BIOMED 2

COFFEE BREAK
9:30—10:00, *Concerto Ballroom*

10:00 - 12:00

BTu2B • Optical Coherence Tomography in Ophthalmology
James Fujimoto; *Massachusetts Inst. of Technology, USA*; Christoph Hitzenberger; *Medical Univ. of Vienna, Austria, Presiders*

BTu2B.1 • 10:00

Invited

Intraoperative OCT for Vitreoretinal Surgery, Joseph Izatt¹; ¹*Duke Univ., USA*. We report on the design and initial clinical trials of a surgical microscope-integrated OCT system for image-guided vitreoretinal microsurgery, including real-time OCT imaging and surgical instrument tracking.

BTu2B.2 • 10:30

Extended Coherence Range Megahertz FDML Laser for Imaging the Human Anterior Segment, Wolfgang Wieser¹, Thomas Klein¹, Desmond C. Adler², Francois Trépanier³, Christoph Eigenwillig¹, Sebastian Karpf¹, Joseph M. Schmitt², Robert A. Huber¹; ¹*BMO, Univ. of Munich (LMU), Germany*; ²*LightLab Imaging, St. Jude Medical, USA*; ³*TeraXion Inc, Canada*. We present a 1300nm FDML laser for OCT application with greatly improved coherence length operating at a scan rate of 1.6 MHz and demonstrate OCT imaging of the anterior segment of the human eye.

BTu2B.3 • 10:45

Simultaneous Swept Source Optical Coherence Tomography of the Anterior Segment and Retina, Al-Hafeez Dhalla¹, Derek Nankivil¹, Theresa Bustamante¹, Anthony Kuo², Joseph Izatt^{1,2}; ¹*BIOMEDICAL Engineering, Duke Univ., USA*; ²*Ophthalmology, Duke Univ. Medical Center, USA*. We report on the implementation of swept source optical coherence tomography for simultaneous imaging of the anterior segment and retina. The system achieves depth-encoding by coherence revival heterodyning and a polarization-encoded sample arm.

Symphony IV

DH

10:00 - 12:00

DTu2C • Novel Applications of Digital Holography I
Pascal Picart; *LAUM CNRS, France, Presider*

DTu2C.1 • 10:00

Tutorial

Digital Holographic Interferometry - Principles and Applications to Deformation Measurement, Partha Banerjee¹; ¹*Univ. of Dayton, USA*. Starting from basic principles of holography and digital holography, we discuss its application to digital holographic interferometry for 3D object deformation. Dual wavelength holography, digital holographic microscopy and single beam holographic tomography are also discussed.

DTu2C.2 • 10:45

Measuring Vapour Cloud Concentrations with Digital Holography, Sam Dehaeck¹, Pierre Colinet¹; ¹*TIPS, Universite Libre de Bruxelles, Belgium*. In a Mach-Zehnder interferometer, the vapour cloud surrounding an evaporating droplet is imaged with digital holography. Using an Abel inversion, quantitative local evaporation rates can be measured precisely for the first time.

Symphony I & II

Symphony III

Symphony IV

BIOMED I

BIOMED 2

DH

BTu2A • Imaging of Vascular Dynamics—Continue

BTu2A.5 • 11:00

DCS Measurement Can Be Gated Via Monitoring Muscle Movement to Derive Accurate Blood Flow in Exercising Muscle, Guoqiang Yu¹, Katelyn Gurley¹, Yu Shang¹; ¹University of Kentucky, USA. We demonstrate that the diffuse correlation spectroscopy (DCS) measurement can be gated via monitoring muscle movement by a dynamometer to continuously derive accurate blood flow information in exercising skeletal muscle.

BTu2A.6 • 11:15

A Geometric-Differential-Sensitivity Based Reconstruction Algorithm Improves Target-Depth Localization for Trans-Luminal Outward-Imaging Diffuse Optical Tomography, Guan Xu¹, Daqing Piao¹; ¹School of Electrical and Computer Engineering, Oklahoma State Univ., USA. We demonstrate experimentally that reconstruction based on a geometric-differential-sensitivity method improves target localization in trans-luminal outward-imaging diffuse optical tomography than do with conventional depth-compensation methods.

BTu2A.7 • 11:30

Intrinsic optical imaging and Doppler OCT assessment of vascular reactivity with aging under caloric restriction, Frédéric Lesage^{1,2}, Simon Dubeau², Cong Zhang^{1,2}, Edward Baraghis^{1,2}, Guylaine Ferland³, Pierrette Gaudreau⁴, Philippe Pouliot^{1,2}; ¹Genie Electrique, Ecole polytechnique Montréal, Canada; ²Research Center, Montréal Heart Inst., Canada; ³Nutrition department, Université de Montréal, Canada; ⁴Biochemistry department, Université de Montréal, Canada. Optical imaging and Doppler OCT were used to measure vascular reactivity in old rats fed ad-libitum or put under caloric restriction. Gas challenges and Doppler OCT were used to measure vessel reactivity and pulsatility.

BTu2A.8 • 11:45

Simultaneous Morphological And Biochemical Optical Imaging Of Coronary Atherosclerotic Plaques, Paritosh Pande¹, Sebina Shrestha¹, Jesung Park¹, Fred Clubb^{1,2}, Brian E. Applegate¹, Javier A. Jo¹; ¹BIOMEDical Engineering, Texas A&M Univ., USA; ²Veterinary Pathobiology, Texas A&M Univ., USA. We demonstrated that simultaneous optical coherence tomography and fluorescence lifetime imaging microscopy imaging allows the identification of most types of coronary atherosclerotic plaques based on their morphological/biochemical characterization.

BTu2B • Optical Coherence Tomography in Ophthalmology—Continue

BTu2B.4 • 11:00

Passive Component Based Multi-Functional Jones Matrix Optical Coherence Tomography for Doppler and Polarization Sensitive Imaging of Retina, Yiheng Lim¹, Youngjoo Hong¹, Lian Duan¹, Yoshiaki Yasuno¹; ¹Univ. of Tsukuba, Japan. A fiber based multi-functional optical coherence tomography was developed based on a novel Jones matrix detection. Simultaneous in vivo measurement of intensity, phase retardation, and Doppler flow imaging of a retina is demonstrated.

BTu2B.5 • 11:15

High-speed polarization-sensitive optical coherence tomography (PS-OCT) at 1060 nm, Teresa Torzicky¹, Michael Pircher¹, Sebastian Marschall², Marco Bonesi¹, Stefan Zotter¹, Erich Götzinger¹, Thomas Klein³, Wolfgang Wieser³, Benjamin Biedermann³, Robert A. Huber³, Peter Andersen², Christoph K. Hitzenberger¹; ¹Medical Univ. of Vienna, Austria; ²DTU Denmark, Denmark; ³LMU Munich, Germany. In this work we are using a high-speed swept source PS-OCT system working at 1060 nm, for acquiring intensity, retardation, fast axis and degree of polarization uniformity images of retina, choroid and sclera in vivo.

BTu2B.6 • 11:30

Image analysis and quantification in anterior segment OCT: techniques and applications, Sergio Ortiz¹, Pablo Perez-Merino¹, Enrique Gamba¹, Susana Marcos¹; ¹Instituto de Optica (CSIC), Spain. We present a methodology to extract accurate data from OCT systems, including calibration, distortion compensation, and 3D data processing for several applications of cornea and lens (topography, aberrations analysis and geometrical changes).

BTu2B.7 • 11:45

Wide tuning range wavelength-swept laser at 1020 nm for ultra-high resolution ophthalmic FD-OCT, Sang-Won Lee^{1,2}, Hyun-Woo Song¹, Moon-Youn Jung¹, Seunghwan Kim¹; ¹BT convergence research department, Electronics and Telecommunications Research Inst., Republic of Korea, ²Center for Nano-Bio Convergence, Korea Research Inst. of Standards and Science, Republic of Korea. We demonstrated a wide tuning range wavelength-swept laser at 1020 nm for ultra-high resolution ophthalmic Fourier-domain optical coherence tomography. The swept laser using a polygon mirror had a tuning range of 142 nm at a scan speed of 18 kHz. We obtained the measured axial resolution of 4.2 μm.

DTu2C • Novel Applications of Digital Holography I—Continue

DTu2C.3 • 11:00

Angular spectrum method for different sampling rates on source and destination planes: Scaled angular spectrum method, Tomoyoshi Shimobaba¹, Nobuyuki Masuda¹, Tomoyoshi Ito¹; ¹Graduate school of Engineering, Chiba Univ., Japan. We propose a scaled angular spectrum method that calculates diffraction at different sampling rates on source and destination planes, and verify the method in a one-dimensional case. In addition, we describe the two numerical implementations.

DTu2C.4 • 11:15

Digital holographic position measurement of an optically-trapped dielectric nanosphere in water, Yoshio Hayasaki¹, Takayuki Higuchi¹, Akira Sato¹, Quang D. Pham¹, Satoshi Hasegawa¹; ¹Utsunomiya Univ., Japan. We demonstrate the three-dimensional position measurement of a nanometer-sized polystyrene sphere held in optical tweezers in water using an in-line low-coherence digital holographic microscope with three-dimensional sub-pixel estimation.

DTu2C.5 • 11:30

Time-Division Multiplexing of Iterated Holograms for Lithography on 3D Surfaces, Joshua Cowling¹, Jose J. Toriz-Garcia², Alan Purvis¹, Richard McWilliam¹, Gavin Williams², Florian B. Souillard¹, N. Luke Seed², Peter A. Ivey³; ¹Engineering and Computing Science, Durham Univ., UK; ²Department of Electronic and Electrical Engineering, Univ. of Sheffield, UK; ³Innotec Ltd, UK. A 3D substrate is lithographically patterned using a set of holograms generated by a multi-plane iterative algorithm. The substrate is exposed to multiple phase-only holograms over the duration of an exposure, thus averaging noise.

DTu2C.6 • 11:45

Real-time detection of 3-D field distribution of a single terahertz pulse based on pulsed digital holography, Xiaolei Wang¹, Lujie Li¹, Hongchen Zhai¹; ¹Inst. of modern optics, Nankai Univ., China. A pulsed digital holographic approach for real-time detecting the 3D field distribution of a single-shot terahertz pulse in time resolution of the femtosecond order based on electro-optic sampling technique is proposed and experimentally implemented.

12:00—13:00

LUNCH ON YOUR OWN

Concerto Ballroom and Overture Foyer

BIOMED

13:00 - 15:00

BTu3A • BIOMED Poster Session II

Tuesday, 1 May

BTu3A.01

A surface recognition approach for in vivo optical imaging applications using a micro-lens-array light detector, Xiaoming Jiang¹, Liji Cao¹, Wolfhard Semmler¹, Jörg Peter¹; ¹*Medical physics in Radiology, German Cancer Research Center, Germany*. A method for surface recognition is presented whereby surface information is obtained considering multiview images from an MLA detector at a low number of detector projections. Simulated and experimental phantom data are presented.

BTu3A.02

Reconstruction Algorithm for Fluorescence Tomography Using a Reduced Space of Eigenvectors and Optimized Source Permissible Region, Mohamed A. Naser¹, Michael S. Patterson²; ¹*Medical Physics & Applied Radiation Sciences, McMaster Univ., Canada*; ²*Juravinski Cancer Center, Canada*. A 3D fluorescence tomography algorithm has been developed. The ill-posedness of the problem has been reduced using a reduced space of eigenvectors and shrinking the permissible source region to find a unique solution.

BTu3A.03

Imaging of interacting nano-objects with superlenses, Timo Hakkarainen¹, Tero Setälä¹, Ari T. Friberg^{1,2}; ¹*Department of Applied Physics, Aalto Univ. School of Science, Finland*; ²*Department of Physics and Mathematics, Univ. of Eastern Finland, Finland*. Employing rigorous electromagnetic theory we show that near-field imaging of point-like objects with subwavelength resolution is achievable with superlenses. We also illustrate how the interactions among the objects and the lens affect the imaging.

BTu3A.04

Modeling Light Propagation in Tissues Using the Corrected Diffusion Approximation, Ossi Lehtikangas¹, Tanja Tarvainen^{1,2}, Arnold Kim³; ¹*Department of Applied Physics, Univ. of Eastern Finland, Finland*; ²*Department of Computer Science, Univ. College London, UK*; ³*School of Natural Sciences, Univ. of California, USA*. Recently introduced corrected diffusion approximation is numerically implemented. An additive correction term is computed for the diffusion approximation at the boundary based on asymptotic analysis of the radiative transport equation.

BTu3A.05

Approximation Errors and Model Reduction in Three-Dimensional Diffuse Optical Tomography, Ville Kolehmainen¹, Martin Schweiger², Ilkka Nissilä³, Tanja Tarvainen¹, Simon R. Arridge², Jari P. Kaipio^{4,1}; ¹*Department of Applied Physics, Univ. of Eastern Finland, Finland*; ²*Department of Computer Science, Univ. College London, UK*; ³*Department of Biomedical Engineering and Computational Science, Aalto Univ. (School of Science), Finland*; ⁴*Department of Mathematics, Univ. of Auckland, New Zealand*. We apply the Bayesian approximation error model for treatment of model reduction by domain truncation and coarse computation mesh in diffuse optical tomography. The approach is tested with a three-dimensional example using experimental data.

BTu3A.06

Fully Automatic Ultrasound Guided Diffuse Optical Tomography (US-DOT) System for Whole Breast Imaging, Zixin Deng¹, Yuting Lin¹, Judith Zimmermann¹, Gultekin Gulsen¹; ¹*Tu and Yuen Center for Functional Oncology Imaging and Department of Radiological Sciences, Univ. of California, Irvine, USA*. A priori information can be used to guide near-infrared diffuse optical tomography reconstruction and improve quantification. The goal of this study is to develop a hands-free, fully automatic US-DOT system for quantitative whole breast imaging.

BTu3A.07

Versatile Picosecond Laser Sources for Time-Resolved Fluorescence Microscopy and Diffuse Optical Imaging, Thomas Schoenau¹, Dietmar Klemme¹, Romano Haertel¹, Kristian Lauritsen¹, Rainer Erdmann¹, Thorsten Siebert¹; ¹*PicoQuant GmbH, Germany*. Picosecond laser sources operating over an order of magnitude in repetition rates and pulse energies at selected emission wavelengths from the UV to IR range are presented for time-correlated single-photon counting in demanding imaging applications.

BTu3A.08

Time-resolved optical imaging for monitoring response of breast cancer patients to therapy, Louise Enfield¹, Jeremy Hebden¹, Michael Douek², Adam P. Gibson¹; ¹*Dept. of Medical Physics and Bioengineering, Univ. College London, UK*; ²*Dept. of Research Oncology, Kings College London, UK*. The use of optical tomography to monitor changes in the uncompressed breast in response to neoadjuvant treatment of breast cancer. An investigation of the reproducibility of data and images from healthy volunteers was also conducted.

BTu3A.09

One-Click Mesh Generation: Going From Multi-Region 2D Images to Tetrahedral Mesh, Hamid R. Ghadyani¹, Brian Pogue¹, Keith D. Paulsen¹; ¹*Thayer School of Engineering, Dartmouth College, USA*. '1click' toolbox for tetrahedral mesh generation is presented that uses stack of 2D images with multiple regions. GUI-based approach to quality inspection and optimization of mesh bridges the gap from volume imaging to mesh generation.

BTu3A.10

Using Gold Nanoparticles to Enhance the Contrast in Optical Imaging using Short-Pulse Laser, Amir Y. Sajjadi¹, Kunal Mitra¹, Michael Grace²; ¹*Mechanical and Aerospace Engineering, Florida Inst. of Technology, USA*; ²*Biological Sciences, Florida Inst. of Technology, USA*. Intravenously administration of spherical gold nanoparticles, which accumulate in tumors due to the leakiness of their vasculature, enhances the resolution of laser-based cancer detection system by increasing the contrast of the images.

BTu3A.11

Influences of Tissue Optical Properties on Diffuse Correlation Spectroscopy Blood Flow Measurements, Lixin Dong¹; ¹*Center for Biomedical Engineering, Univ. of Kentucky, USA*. The influences of optical property assumptions on DCS flow index measurements were evaluated by phantom experiments, computer simulation and in vivo measurements. The results suggest tissue scattering influence is greater than that of absorption.

BTu3A.12

Noninvasive diffuse optical monitoring of hemodynamic changes in head and neck tumor during radiation delivery, Lixin Dong¹; ¹*Center for Biomedical Engineering, Univ. of Kentucky, USA*. A remote-operated DCS flow-oximeter was built to monitor hemodynamic changes in head and neck tumors during radiation delivery. The results indicate instant hemodynamic responses can be optically detected without being overly burdensome on patients.

BTu3A.13

Feasibility of a Simple and Cost-Effective Wide-Angle Corneal Topography Method for Placido-based Videokeratographs, Luis A. Carvalho^{1,2}; ¹Grupo de Óptica, Universidade de Sao Paulo, Brazil; ²Ophthalmology, Federal Univ. of Sao Paulo, Brazil. The instrumentation and software for wide-angle corneal topography using a Placido based videokeratographer was developed. Measurement of the entire area of the cornea using a simple adaptation to the Placido mire is possible

BTu3A.17

Estimating Hemoglobin Changes with an Extended Fusion Model Incorporating DOT, BOLD and ASL Data, Meriem A. Yucel¹, Theodore Huppert², David Boas^{1,3}, Louis Gagnon^{1,3}; ¹MGH/MIT/HMS Athinoula A. Martinos Center for BIOMEDical Imaging, Department of Radiology, Massachusetts General Hospital, Harvard Medical School, USA; ²Department of Radiology and Bioengineering, Univ. of Pittsburg, USA; ³Harvard-MIT Division of Health Sciences and Technology, USA. Combining arterial spin labeling (ASL), diffuse optical tomography (DOT) and blood oxygen level dependent (BOLD) recordings, we obtained better estimates of changes in hemoglobin species and BOLD calibration factor M without a hypercapnia challenge.

BTu3A.21

Integrated diffuse optical tomography and photoacoustic tomography, Xiaohu Li¹, Lei Xi¹, Ruixin Jiang¹, Lei Yao¹, Huabei Jiang¹; ¹BIOMEDical Engineering, Univ. of Florida, USA. We designed, fabricated and tested a novel imaging system that fuses DOT and PAT in a single platform which can potentially provide dual-modality two dimensional functional and cellular images of the breast quantitatively.

BTu3A.14

Elliptically Polarized Light for Depth Resolved Optical Imaging, Anabela Da Silva¹, Carole Deumié¹, Ivo Vanzetta²; ¹Institut Fresnel CNRS UMR 6133, France; ²Institut des Neurosciences Cognitives CNRS UMR 6193, France. Using elliptically polarized light allows performing a selection of a well defined subsurface volume in a turbid medium. This offers the possibility to probe biological tissues in depth. The method and preliminary results are presented.

BTu3A.18

A deconvolution method for recovering tissue impulse response from time-resolved measurements, Mamadou Diop^{1,2}, Keith St Lawrence^{1,2}; ¹Imaging Division, Lawson Health Research Inst., Canada; ²Department of Medical Biophysics, Univ. of Western Ontario, Canada. A deconvolution method for extracting tissue impulse response (TIR) from time-resolved measurements is presented. The algorithm is stable and can recover TIR with high fidelity, even from noisy data.

BTu3A.22

Comparison of L1 and L2 Regularizations in Diffuse Optical Tomography, Venkaiah C. Kavuri¹, Zi-Jing Lin¹, Hanli Liu¹; ¹Department of Bioengineering, Univ. of Texas at Arlington, USA. We compare L1 versus L2 regularizations in diffuse optical tomography (DOT). Both methods were applied after the application of DCA (Depth compensation algorithm). L1 regularization clearly shows improvement in the spatial resolution of DOT images.

BTu3A.15

An FFT-based Software Autocorrelator in Diffuse Correlation Spectroscopy System, Jing Dong¹, Renzhe Bi¹, Kijoon Lee¹; ¹School of Chemical and BIOMEDical Engineering/Division of Bioengineering, Nanyang Technological Univ., Singapore. We present an FFT-based software autocorrelator which was controlled by LabVIEW for DCS. Without much compromise in speed, the minimum decay time is in μ -second scale. Not only is it cost-effective, but also is flexible for raw signal processing.

BTu3A.19

Confocal Fluorescence Microscopy for Evaluation of Breast Cancer in Human Breast Tissue, Jessica L. Dobbs¹, Hao Ding¹, Ana Benveniste², Henry Keurer³, Savitri Krishnamurthy⁴, Wei Yang², Rebecca Richards-Kortum¹; ¹Bioengineering, Rice Univ., USA; ²Diagnostic Radiology, U.T. M.D. Anderson Cancer Center, USA; ³Surgical Oncology, U.T. M.D. Anderson Cancer Center, USA; ⁴Pathology, U.T. M.D. Anderson Cancer Center, USA. Abstract: Confocal fluorescence microscopy can be used to rapidly acquire high resolution images of normal, benign, and neoplastic breast cellular features in ex vivo human breast tissue.

BTu3A.23

Improved OPT reconstructions based on the MTF and extension to FLIM-OPT, Lingling Chen¹, James McGinty¹, Harriet B. Taylor², Laurence Bugeon², Jonathan R. Lamb², Margaret J. Dallman^{2,3}, Paul French¹; ¹Photonics Group, Department of Physics, Imperial College London, UK; ²Division of Cell and Molecular Biology, Department of Life Sciences, Imperial College London, UK; ³Centre for Integrative Systems Biology, Department of Life Sciences, Imperial College London, UK. We demonstrate the improved reconstruction of OPT datasets by incorporating the measured MTF in the reconstruction process. We also extend OPT to FLIM-OPT and demonstrate its use for imaging live zebrafish embryos displaying autofluorescence.

BTu3A.16

Efficiently "seeded" perturbation Monte Carlo Method for photon migration, Angelo Sassaroli¹; ¹Tufts Univ., USA. We present a perturbation Monte Carlo method which can be used for light propagation in heterogeneous diffusive media. The method is based on the correspondence between the seed of a random number generator and the sequence of random numbers.

BTu3A.20

Assessment of brain perfusion disorders by ICG bolus tracking with time-resolved fluorescence monitoring, Adam Liebert¹, Daniel Milej¹, Wojciech Weigl², Anna Gerega¹, Michal Kacprzak¹, Ewa Mayzner-Zawadzka², Roman Maniewski¹; ¹Nalecz Inst. of Biocybernetics and BIOMEDical Engineering, Poland; ²Department of Anesthesiology and Intensive Care, Medical Univ. of Warsaw, Poland. Time resolved measurements were carried out on the surface of the head during inflow of indocyanine green (ICG) in patients with severe brain perfusion disorders. Advantages of fluorescence light detection over diffuse reflectance was presented.

BTu3A.24

Detection of Specific Binding to HER2 Receptors by in vivo Fluorescence Lifetime Imaging, Yasaman Ardeshirpour¹, Victor Chernomordik¹, Moinuddin Hassan¹, Rafal Zielinski², Gary Griffiths³, Olga Vasalatiy³, Aleksandr Smirnov⁴, Jay Knutson⁴, Sam Achilefu⁵, Jacek Capala², Amir Gandjbakhche¹; ¹Eunice Kennedy Shriver National Inst. of Child Health and Human Development, National Inst.s of Health, USA; ²National cancer Inst., National Inst.s of Health, USA; ³Imaging Probe Development Center, National Inst.s of Health, USA; ⁴National Inst.s of Lung and Blood, National Inst.s of Health, USA; ⁵School of Medicine, Washington Univ., USA. In this study we have shown that in-vivo fluorescence lifetime imaging can be used for early detection of specific probe binding to HER2 receptors, providing information on HER2 overexpression.

BTu3A • BIOMED Poster Session II—Continue

BTu3A.25

A Pilot study of Multispectral Digital Colposcopy (MDC) for Detection of Clinical Cervical Intraepithelial Neoplasia, Michele Follen¹, Sylvia F. Lam², Martial Guillaud², Deanna Ceron², Jessica N. McAlpine³, Tom Ehlen³, Dianne Miller³, Dennis D. Cox⁴, E. N. Atkinson⁵, Roderick Price¹, Dirk van Niekerk⁶, Timon Buys², Pierre Lane², Calum E. MacAulay²; ¹Department of Obstetrics & Gynecology, Drexel Univ. College of Medicine, USA; ²Integrative Oncology, BC Cancer Research Centre, Canada; ³Department of Obstetrics & Gynecology, Univ. of British Columbia, Canada; ⁴Department of Statistics, Rice Univ., USA; ⁵Department of Biostatistics, The Univ. of Texas M. D. Anderson Cancer Center, USA; ⁶Department of Pathology and Laboratory Medicine, British Columbia Cancer Agency, Canada. We report clinical imaging results for an MDC that has been applied to more than 50 patients with suspected cervical pre-cancer and analyze against matched histopathology results. For high grade dysplasia: sensitivity ~90%, specificity ~55%.

BTu3A.29

Hemodynamic monitoring of repeated cerebral ischemia in mice using diffuse optical spectroscopies, Yu Shang¹, Lei Chen², Michal Toborek², Guoqiang Yu¹; ¹Center for BIOMEDICAL Engineering, Univ. of Kentucky, USA; ²Department of Neurosurgery, Univ. of Kentucky, USA. Cerebral hemodynamics were monitored using diffuse optical spectroscopies in mice undergoing 5-day repeated transient fore-brain ischemia. The results indicate that mouse adaptation to cerebral ischemia could be influenced by repeated preconditioning.

BTu3A.33

Novel method to improve 2D DOT spatial resolution using l1-regularization and noise-normalization, Jixing Yao¹, Fenghua Tian², Soontorn Oraintara¹, Hanli Liu²; ¹Electrical Engineering, Univ. of Texas at Arlington, USA; ²Bioengineering, Univ. of Texas at Arlington, USA. The data used for reconstructing sparse DOT images are often with a large range of noise taken from different channels. A novel and effective reconstruction approach is developed by combining l1-regularization and noise normalization.

BTu3A.26

Time-resolved spectroscopy method for breast cancer detection, Yukio Ueda¹, Kenji Yoshimoto¹, Etsuko Yamaki¹, Toshihiko Suzuki¹, Takeshi Yamanaoka¹, Daisuke Yamashita¹, Hiroyuki Ogura², Hatsuko Nasu³, Emiko Imi³, Harumi Sakahara³, Motoki Oda¹, Yutaka Yamashita¹; ¹Central Research Laboratory, Hamamatsu Photonics K.K., Japan; ²Department of Breast Surgery, Hamamatsu Univ. School of Medicine, Japan; ³Department of Radiology, Hamamatsu Univ. School of Medicine, Japan. We have been developing time-resolved spectroscopy (TRS) systems for breast cancer diagnosis. Its principle is based on the optical properties of the patient's breast obtained by TRS measurements.

BTu3A.30

Comparison of diffuse optical spectroscopies and electroencephalogram for cerebral monitoring during carotid endarterectomy, Yu Shang¹, Ran Cheng¹, Lixin Dong¹, Stephen J. Ryan², Sibub P. Saha³, Guoqiang Yu¹; ¹Center for BIOMEDICAL Engineering, Univ. of Kentucky, USA; ²Department of Neurology, Univ. of Kentucky, USA; ³Division of Cardiothoracic Surgery, Univ. of Kentucky, USA. The cerebral blood flow responses to arterial clamping measured by near-infrared diffuse optical spectroscopies were found to be significantly faster, larger and more sensitive than electroencephalogram (EEG) responses during carotid endarterectomy.

BTu3A.34

Measurement of brain activations to examine gender-specific risk decision making using functional near infrared spectroscopy (fNIRS), Lin Li¹, Zi-Jing Lin¹, Mary Cazzell², Hanli Liu¹; ¹Bioengineering, Univ. of Texas at Arlington, USA; ²College of Nursing, Univ. of Texas at Arlington, USA. We utilized fNIRS to examine gender differences in brain activation at the prefrontal cortex of forty healthy adults while performing the Balloon Analogue Risk Task (BART). It shows promises of fNIRS to study risk decision-making.

BTu3A.27

Diffuse optical detecting hemodynamic responses during fatiguing exercise in women with fibromyalgia, Yu Shang¹, Katelyn Gurley¹, Brock Symons², Douglas Long³, Jonah Lee³, Ratchakrit Srikueta³, Leslie Crofford⁴, Charlotte Peterson³, Guoqiang Yu¹; ¹Center for BIOMEDICAL Engineering, Univ. of Kentucky, USA; ²Department of Gerontology, Univ. of Kentucky, USA; ³College of Health Sciences, Univ. of Kentucky, USA; ⁴College of Medicine, Univ. of Kentucky, USA. Muscle hemodynamics and oxygen metabolism were monitored by diffuse optical spectroscopies in women with and without fibromyalgia throughout fatiguing exercise. Less oxygen extraction was found in fibromyalgia women during fatiguing exercise.

BTu3A.31

Analysis of Vasoactive Optical Imaging of Breast Cancer, Sanhita S. Dixit¹, Hanyoung Kim¹, Christopher Comstock², Gregory W. Faris¹; ¹Molecular Physics Laboratory, SRI International, USA; ²Moore's Cancer Center, UC San Diego, USA. We describe analysis of data acquired with near infrared transillumination imaging of breast cancer during inhalation of vasoactive gases. Detailed contrast signatures are obtained from multiwavelength cw image sets versus time.

BTu3A.35

Adaptive Algebraic Reconstruction Technique Optimized for Fast Robust Bio-luminescence Tomography: Optical/CT Dual Modality In vivo Studies, Ali Behrooz^{1,2}, Heng Xu¹, Chauncy Kuo¹, Brad Rice¹; ¹Caliper, a PerkinElmer Company, USA; ²Electrical and Computer Engineering, Georgia Inst. of Technology, USA. An optimized adaptive algebraic reconstruction technique for fast robust 3D bio-luminescence tomography is presented. Speed and performance of the algorithm in depth and flux quantification are examined by in silico, phantom and in vivo studies.

BTu3A.28

Two-Photon Microscopy of Oxygen Distributions in Mouse Cerebral Microvasculature, Sava Sakadzic¹, Emiri T. Mandeville^{1,2}, Louis Gagnon¹, Anna Devor³, Mohammad A. Yaseen¹, Joe Musacchia¹, Emmanuel Roussakis⁴, Katharina Ekermann-Haerter^{1,2}, Vivek J. Srinivasan¹, Cenk Ayata^{1,2}, Eng Lo^{1,2}, Anders M. Dale³, Sergei A. Vinogradov⁴, David Boas¹; ¹Radiology, Massachusetts General Hospital / Harvard Medical School, USA; ²Neurology, Massachusetts General Hospital, Harvard Medical School, USA; ³Neurosciences and Radiology, Univ. of California San Diego, USA; ⁴Biochemistry and Biophysics, Univ. of Pennsylvania, USA. The two-photon microscopy imaging was used to obtain high-density PO2 maps in cortical microvasculature in anesthetized mice. The detailed PO2 distributions were presented as functions of various microvascular morphological parameters.

BTu3A.32

Diffuse optical tomography to study ischemic stroke in pre-clinical rat models, Zi-Jing Lin¹, Ming Ren², Lin Li¹, Shaohua Yang², Hanli Liu¹; ¹Bioengineering, Univ. of Texas at Arlington, USA; ²Pharmacology & Neuroscience, Univ. of North Texas Health Science Center, USA. We investigated hyperacute cerebral ischemia using diffuse optical tomography with the depth compensation algorithm (DCA) in rat models. Results suggest that this methodology has a great potential to monitor the effect of antistroke therapies.

BTu3A.36

The Influence of Source-Detector Separation and Superficial Channel Choice upon NIRS Signal Correction, Andrew Berger¹, James R. Goodwin², Chantel R. Gaudet³; ¹The Inst. of Optics, Univ. of Rochester, USA; ²Queensland Univ. of Technology, Australia; ³Univ. of Rochester, USA. Near-infrared spectroscopy (NIRS) sensing of cerebral hemodynamics can be made more brain-specific by regressing against superficially-sensitive channels. Different distances and single channels versus global averages are discussed.

BTu3A.37

Heterogeneous Hierarchical Segmentation Method for Improved Prostate Cancer Imaging In Diffuse Optical Tomography: Simulation Study, Venkai-ah C. Kavuri¹, Zi-Jing Lin¹, Hanli Liu¹,
¹*Department of Bioengineering, Univ. of Texas at Arlington, USA.* We report a heterogeneous hierarchical segmentation method to image prostate cancer without prior cancer information, using combined Trans-rectal ultrasound and diffuse optical tomography. The method is validated by computer simulations

BTu3A.38

Classification of OT Images of Arthritic Joints Using Spatial-Fourier Frequency Coefficients, Ludguier D. Montejó¹, Hyun K. Kim^{1,2}, Jingfei Jia¹, Andreas H. Hielscher^{1,2},
¹*BIOMEDical Engineering, Columbia Univ., USA;* ²*Radiology, Columbia Univ., USA.* Fourier Transform coefficients of absorption and scattering distributions, reconstructed from OT scans of PIP joints II-IV, are used in conjunction with discriminate analysis to diagnose rheumatoid arthritis (91.0% sensitivity and 90.0% specificity).

BTu3A.39

Fast-Fluorescence Camera (FFC) - A Consumer-Grade Digital Camera to Capture Endogenous Tissue Fluorescence, Pierre Lane^{1,2}, Sylvia F. Lam¹, Jessica N. McAlpine², Thomas G. Ehlen², Catherine Poh¹, Michele Follen³, Calum E. MacAulay¹,
¹*BC Cancer Agency, Canada;* ²*Univ. of British Columbia, Canada;* ³*Drexel Univ. College of Medicine, USA.* Imaging of endogenous tissue fluorescence can be challenging. We have developed a flash-excited fluorescence imaging system based on a consumer-grade digital camera to overcome the challenges associated with depth-of-field and motion artifact.

BTu3A.40

Corrected Diffusion Approximation in Layered Tissues, Shelley B. Rohde¹, Arnold Kim¹,
¹*School of Natural Sciences, UC Merced, USA.* We present the corrected diffusion approximation for a thin beam incident on a layered medium. This model improves upon the diffusion approximation for small source-detector separation distances and is computationally efficient.

BTu3A.41

Utilising Approximation Error Modelling in Linear Reconstruction in Diffuse Optical Tomography, Tanja Tarvainen^{1,2}, Ville Kolehmainen¹, Simon R. Arridge², Jari P. Kaipio^{1,3},
¹*Univ. of Eastern Finland, Finland;* ²*Univ. College London, UK;* ³*Univ. of Auckland, New Zealand.* The relationship between conventional reference measurement correction and approximation error modelling in linear reconstruction in diffuse optical tomography is considered.

BTu3A.42

Compact & Portable In Vivo Multiphoton GRIN Endoscope, David Huland¹, Christopher M. Brown¹, Dimitre G. Ouzounov¹, Ina Pavlova¹, David R. Rivera¹, Watt W. Webb¹, Chris Xu¹,
¹*School of Applied and Engineering Physics, Cornell Univ., USA.* We present a compact, portable, multiphoton GRIN endoscope system capable of imaging a field of view of 200 μm at 4 frames/s. In vivo images of unstained rat kidney, colon and liver are shown.

BTu3A.43

Photo-Magnetic Imaging: Optical Imaging at MRI resolution, Yuting Lin¹, David A. Thayer¹, Alex T. Luk¹, Gultekin Gulsen¹,
¹*Center for functional onco imaging, UC Irvine, USA.* In this paper, we present a novel imaging technique, namely Photo-Magnetic Imaging (PMI), which overcomes the limitation of pure optical imaging and provides optical contrast at MRI spatial resolution.

BTu3A.44

Time-Resolved Reflectance Diffuse Optical Tomography by using Mellin-Laplace Transform, Lionel Hervé¹, Agathe Puszka¹, Anne Koenig¹, Anne Planat-Chrétien¹, Jean-Marc Dinten¹,
¹*DTBS, CEA-LETI, Minatoc, France.* In this paper, we show how the Mellin-Laplace Transform helps to obtain robust and relevant reconstructions of deep optical heterogeneity from time-resolved diffuse optical tomography measurements.

BTu3A.45

Dynamic Imaging of Cerebral Blood Flow Using Laser Speckle During Epileptic Events, Max Jiang¹, Ruixin Jiang¹, Junli Zhou¹, Lijun Ji¹, Paul Carney¹, Huabei Jiang¹,
¹*Univ. of Florida, USA.* We present a method that is capable of imaging cerebral blood flow (CBF) using laser speckle imaging. In vivo images of dynamic relative CBF during seizure onset are obtained using a single-spectral system.

BTu3A.46

Toward Compressive Architecture for Image Acquisition in Optical Tomography: An Application of Compressed Sensing in Wavelet Compression of Fluorescence Tomography Data, Ali Behrooz¹, Ali A. Eftekhar¹, Ali Adibi¹,
¹*Electrical and Computer Engineering, Georgia Inst. of Technology, USA.* Inspired by compressed sensing, we present and study a cost-effective compressive architecture for fast image acquisition in optical tomography that exploits wavelet compressibility of data. Theoretical results validated by experimental studies.

BTu3A.47

Simultaneous EEG-Correlated Noninvasive Imaging of Epilepsy Using Fast Diffuse Optical Tomography, Ruixin Jiang¹, Lijun Ji¹, Junli Zhou¹, Max Jiang¹, Zhen Yuan¹, Qizhi Zhang¹, Paul Carney¹, Huabei Jiang¹,
¹*Univ. of Florida, USA.* We present a dynamic, noninvasive and functional diffuse optical brain imaging method that is done simultaneously with hippocampus CA1 LFP recordings for anesthetized rats under resting conditions and during acute chemoconvulsant provoked seizures.

BTu3A.48

Confocal Reflectance/ Auto-Fluorescence Tomography (CRAFT) for Early Skin Cancer Diagnosis, Tong Peng^{1,2}, Hao Xie¹, Yichen Ding¹, Weichao Wang³, Zhiming Li⁴, Dayong Jin⁵, Yuanhe Tang², Qiushi Ren^{1,3}, Peng Xi¹,
¹*Department of BIOMEDical Engineering, Peking Univ., China;* ²*Department of Physics, Xi'an Univ. of Technology, China;* ³*Department of BIOMEDical Engineering, College of Life Sciences and Biotechnology, Shanghai Jiao Tong Univ., China;* ⁴*Department of Dermatology and Venereology, First Affiliated Hospital of Wenzhou Medical College, China;* ⁵*Advanced Cytometry Labs, MQphotonics Research Centre, Macquarie Univ., Australia.* Through the combination of confocal reflectance imaging and confocal autofluorescence imaging in our system, both the morphological and pathological information can be obtained, yielding a clear separation of the cancerous sites from control sites.

BTu3A • BIOMED Poster Session II – Continue

BTu3A.49

Speckle contrast at deviations from best focus in microfluidic and in vivo, Yaaseen Atchia^{1,2}, Hart Levy^{1,2}, Suzie Dufour¹, Ofer Levi^{1,2}; ¹*Electrical Engineering, Univ. of Toronto, Canada*; ²*BIOMEDical Engineering, Univ. of Toronto, Canada*. Speckle contrast values with depth increments of 50 μm to 600 μm from best focus was analysed in microfluidic and in vivo. We show depth deviations are allowed for $|\Phi| \leq 200\text{mm}$ while conserving velocity change to less than 20 %.

BTu3A.50

Development of an optical non-contact time-resolved diffuse reflectance scanning imaging system, Mikhail Mazurenka¹, Heidrun Wabnitz¹, Alberto Dalla Mora², Davide Continii², Antonio Pifferi², Rinaldo Cubeddu², Alberto Tosi³, Franco Zappa^{3,4}, Rainer Macdonald⁴; ¹*Physikalisch-Technische Bundesanstalt, Germany*; ²*Dipartimento di Fisica, Politecnico di Milano, Italy*; ³*Dipartimento di Elettronica e Informazione, Politecnico di Milano, Italy*; ⁴*Micro Photon Devices Srl, Italy*. We report on the development and proof-of-principle tests of a scanning non-contact tissue imaging system for time-domain NIRS applications. The system is based on the null source-detector separation approach and a state-of-the-art fast-gated SPAD.

BTu3A.51

Analysis of Light Propagation in a Realistic Head Model Including Frontal Sinus, Kazuki Kurihara¹, Hiroshi Kawaguchi², Yosuke Takahashi¹, Takayuki Obata², Hiroshi Ito², Kaoru Sakatani³, Eiji Okada¹; ¹*Department of Electronics and Electrical Engineering, Keio Univ., Japan*; ²*Molecular Imaging Center, National Inst. of Radiological Sciences, Japan*; ³*Department of Neurological Surgery, Nihon Univ., Japan*. The light propagation in a head model including a frontal sinus was predicted to investigate the influence of the frontal sinus on NIRS measurements. The influence of the frontal sinus was not consistent across source-detector positions.

BTu3A.52

A dual-step steady state reflectance method for determination of the optical properties of turbid media, Florian Foschum¹, Alwin Kienle¹; ¹*Institut für Lasertechnologien in der Medizin und Messtechnik an der Universität Ulm, Germany*. In the presented dual-step reflectance method we combine the measurements of the spatially resolved reflectance and of the total reflectance to determine the optical properties of semi-infinite turbid media with high spectral resolution.

BTu3A.53

Cerebral blood flow quantification during ischemia using a multi-distance moments-based time-resolved technique, Jonathan T. Elliott^{1,2}, Mamadou Diop², Ting-Yim Lee^{1,3}, Keith St Lawrence^{1,2}; ¹*Department of Medical Biophysics, Univ. of Western Ontario, Canada*; ²*Imaging Division, Lawson Health Research Inst., Canada*; ³*Imaging Program, Robarts Research Inst., Canada*. We present a time-resolved moments-based bolus-tracking technique to determine blood flow, blood volume and mean transit time in scalp and brain. Measurements from an adult pig before and during ischemia agree with CT perfusion.

BTu3A.54

Low-cost diffuse optical tomography for the classroom, Taisuke Minagawa¹, Peyman Zirak¹, Udo M. Weigel¹, Anna Kristoffersen¹, Nicolas Mateos¹, Alejandra Valencia¹, Turgut Durduran¹; ¹*ICFO, Spain*. We have developed simple tomographic image scanner utilizing LEGO Mindstorms NXT. This could be introduced to students in BIOMEDical optics class to help them understand concept of photon propagation in tissue and new imaging modality.

BTu3A.55

Accelerating finite-element-based 3D optical imaging reconstruction by graphic processing units, Tao Zhang¹; ¹*BIOMEDical Engineering, Univ. of Florida, USA*. We report an implementation of GPU to accelerate 3D image reconstruction in DOT. Using CUDA programming model, we parallelized our DOT algorithm and achieved a speed of more than 300x over the CPU based computation.

BTu3A.56

Optical Imaging of Hemodynamic Changes in Exposed Cortex of Awake Mice, Takahiro Kikuchi¹, Masashi Kusano¹, Hiroyuki Takuwa², Kazuto Masamoto^{2,3}, Iwao Kanno², Eiji Okada¹; ¹*Electronics and Electrical Engineering, Keio Univ., Japan*; ²*Molecular Imaging Center, National Inst. of Radiological Sciences, Japan*; ³*Center for Frontier Science and Engineering, Univ. of Electro-Communications, Japan*. The hemodynamic change in the cortex of awake mice is measured by optical imaging. The movement of the awake mice during the measurement tends to affect the hemodynamic changes in somatosensory area.

BTu3A.57

Spectral encoding of spatial frequency approach for quantitative visualization and characterization of 3D structures, Sergey Alexandrov¹, Shikhar Uttam¹, Rajan K. Bista¹, Yang Liu¹; ¹*Univ. of Pittsburgh, USA*. We present spectral encoding of spatial frequency approach to form color map, where wavelengths correspond to object's dominant 3D spatial frequencies, and to reconstruct 3D Fourier components of the scattering potential for each image point.

BTu3A.58

Temporal Mapping and Connectivity Using NIRS for Language Related Tasks, Michael Hall¹, Ujwal Chaudhary¹, Gustavo Rey², Anuradha Godavarty¹; ¹*BIOMEDical Engineering, Florida International Univ., USA*; ²*The Brain Inst., Miami Children's Hospital, USA*. NIRS was employed in 15 healthy adults to understand functionality of the temporal cortex in response to language related tasks. Herein, activation, functional connectivity, and lateralization in the temporal cortex are correlated.

BTu3A.59

Using Partial Frequency Domain Data to Improve Reconstruction Accuracy in Continuous Wave Breast Tomosynthesis Guided Diffuse Optical Spectroscopy, Kelly Michaelsen¹, Venkataramanan Krishnaswamy¹, Brian Pogue¹, Keith D. Paulsen¹; ¹*Dartmouth College, USA*. Limited frequency domain data measured with a handheld probe provides scattering information for a continuous wave multimodal system. Phantom measurements are used to quantify chromophore recovery and characterize the instrument performance.

BTu3A.60

Cognitive Response to Motor Tasks Using NIRS: Pilot Studies of Adults With And Without Spastic Cerebral Palsy, Ujwal Chaudhary¹, Michael Hall¹, Leonard Elbaum¹, Martha Bloyer¹, Anuradha Godavarty¹; ¹*BIOMEDical Engineering, Florida International Univ., USA*. Near-infrared optical spectroscopy is employed to investigate the cognitive response to motor tasks in the prefrontal cortex of adults with and without cerebral palsy.

BTu3A.61

Absolute optical measurements of cerebral optical coefficients and hemoglobin concentrations in aging and younger human subjects, Bertan Hal-lacoglu¹, Angelo Sassaroli¹, Michael Wysocki², Elizabeth Guerrero-Baruah², Michal Beer², Vahram Hartounian², Merav Shaul³, Irwin Rosenberg³, Aron M. Troen⁴, Sergio Fantini¹; ¹Department of BIOMEDical Engineering, Tufts Univ., USA; ²Department of Psychiatry, Mount Sinai School of Medicine, USA; ³Nutrition and Neurocognition Laboratory, Jean Mayer USDA Human Nutrition Research Center on Aging at Tufts Univ., USA; ⁴Inst. of Biochemistry, The Hebrew Univ. of Jerusalem, Israel. We report non-invasive, absolute near-infrared spectroscopy measurements of optical coefficients and hemoglobin concentration/saturation on the forehead of aging and younger human subjects. Significant differences were found between the two groups.

BTu3A.65

Investigation of frontopolar cortex under noxious pain stimuli using functional near infrared spectroscopy, Amarnath S. Yennu¹, Sabin Khadka¹, Pritam Gautam¹, Fenghua Tian¹, Hanli Liu¹; ¹Bio-engineering, Univ. of Texas at Arlington, USA. We report fNIRS signals from the human frontopolar cortex to investigate the hemodynamic responses under noxious pain stimuli. This study shows the potential role of frontopolar cortex in cognitive evaluation of pain by experimental evidence.

BTu3A.62

Combined Image Deconvolution and Attenuation Correction for Intravascular Near Infrared Fluorescence Imaging, Georgios Mallas^{1,2}, Dana H. Brooks¹, Farouc A. Jaffer², Vasilis Ntziachristos³; ¹Electrical and Computer Engineering, Northeastern Univ., USA; ²Cardiovascular Research Center, Massachusetts General Hospital, USA; ³Inst. for Biological and Medical Imaging, Technische Universität München, Germany. Intravascular near-infrared fluorescence imaging detects fluorescent biomarkers through blood but the imaging resolution and imaged intensity degrades with target distance. We present a distance-dependent deconvolution/correction scheme.

BTu3A.66

In vivo Breast Imaging Using a Gen-2 Hand-Held Optical Imager, Sarah J. Erickson¹, Manuela Roman¹, Jean Gonzalez¹, Richard Kiszona², Cristina Lopez-Penalver³, Anuradha Godavarty¹; ¹BIOMEDical Engineering, Florida International Univ., USA; ²Breast Imaging, Sylvester Comprehensive Cancer Center, USA; ³Advanced Medical Specialties, USA. A portable gen-2 hand-held based optical imager has been developed toward breast cancer diagnosis. In vivo diffuse optical imaging studies are carried out in healthy subjects and breast cancer patients.

BTu3A.63

Comparison of Monte Carlo and Diffusion Approximation Light Modeling in Small Animal Fluorescence Tomography, Jonathan T. Elliott², Kenneth M. Tichauer¹, Robert Holt¹, Stephen C. Kanick¹, Keith St Lawrence², Brian Pogue¹, Fredric Leblond¹; ¹Engineering, Dartmouth College, USA; ²Department of Medical Biophysics, Univ. of Western Ontario, Canada. A comparison of the Diffusion approximation and a Monte Carlo approach in the context of small animal fluorescence tomography is presented, forming a foundation for hybrid approaches to improve accuracy of fluorescence tomography.

BTu3A.67

Time-domain photon diffusions evaluated on concave and convex cylindrical medium-applicator interfaces show opposite trends of the time to reaching the peak-fluence rate---An analytic model, Daqing Piao¹; ¹Oklahoma State Univ., USA. The peak-fluence rate evaluated on the medium-applicator interface is reached sooner in a concave geometry and later in a convex geometry, when comparing to that on a semi-infinite interface, for the same line-of-sight source-detector distance.

BTu3A.64

Design and Characterization of a Hybrid Frequency Domain - Continuous Wave Breast Imaging System, Fadi El-Ghoussein¹, Shudong Jiang¹, Brian Pogue¹, Keith D. Paulsen¹; ¹Thayer School of Engineering, Dartmouth College, USA. The design of a new hybrid breast optical imaging signal detection system is described using photodiodes together with PMTs. The goal of this design is to better quantify chromophores in tissue with a wider wavelength band.

BTu3A.68

Automated image analysis of in vivo microendoscopic images for quantitative diagnosis of esophageal squamous cell carcinoma, Dongsuk Shin¹, Marion-Anna Protano², Mark C. Pierce³, Alexandros Polydorides⁴, Fan Zhang⁵, Rebecca Richards-Kortum¹; ¹Bioengineering, Rice Univ., USA; ²Gastroenterology, Mount Sinai Medical Center, USA; ³BIOMEDical Engineering, Rutgers Univ., USA; ⁴Pathology, Mount Sinai Medical Center, USA; ⁵Gastrointestinal Medicine, First Hospital of Jilin Univ., China. This study introduces an approach for quantitative analysis of microendoscopic images to identify esophageal neoplasia. The approach quantifies morphologic parameters which distinguish esophageal neoplasia accurately in an independent validation set.

BTu3A • BIOMED Poster Session II—Continue

BTu3A.69

Analytical and numerical examinations of continuous-wave photon fluence rate along unique spiral paths on a long concave or convex cylindrical medium-applicator interface when the medium contains heterogeneity, Anqi Zhang¹, Daqing Piao¹; ¹*School of Electrical and Computer Engineering, Oklahoma State Univ., USA.* CW photon remission along a unique set of spiral paths on long cylindrical applicator-medium interface could be macroscopically indistinguishable from the remission along a straight line on a semi-infinite interface for single anomaly cases.

BTu3A.73

Retinal OCT Image Enhancement via Wavelet Denoising, Shahab Chitchian^{1,2}, Markus A. Mayer³, Adam R. Boretsky¹, Frederik J. van Kuijk⁴, Massoud Motamedi^{1,2}; ¹*Center for BIOMEDical Engineering, Univ. of Texas Medical Branch, USA;* ²*Department of Ophthalmology, Univ. of Texas Medical Branch, USA;* ³*Pattern Recognition Lab, Erlangen Graduate School in Advanced Optical Technologies (SAOT), Germany;* ⁴*Department of Ophthalmology, Univ. of Minnesota, USA.* A denoising algorithm using dual-density dual-tree complex wavelet transform is applied to 2-frame OCT images of the retina to provide a comparable image quality in less acquisition time compared to commonly used multiple-frame averaging technique.

BTu3A.77

Detecting Glioma Tumor Features in Human Ex Vivo Samples Using Swept-Source OCT, Carmen Kut¹, Jiefeng Xi¹, Shaan Raza², Jessica Mavadia¹, Hugo Guerrero-Cazares², Elliot McVeigh¹, Alfredo Quinones-Hinojosa², Xingde Li¹; ¹*BIOMEDical Engineering, Johns Hopkins School of Medicine, USA;* ²*Neurosurgery, Johns Hopkins School of Medicine, USA.* Ex vivo human brain tissues from 8 glioma patients and 5 controls are imaged using SS-OCT, with higher glioma attenuation values and easily detectable and specific tumor features (microcyst, necrosis and pallisading) for intraoperative resections.

BTu3A.70

Hybrid PET/CT and Frequency-Domain Based NIRF Optical Tomography Modality for Preclinical Studies, Chinmay D. Darne¹, Yujie Lu¹, I-Chih Tan¹, Eva M. Sevick-Muraca¹; ¹*Inst. for Molecular Medicine, The Univ. of Texas Health Science Center at Houston, USA.* We present the development of miniaturized system for performing preclinical NIRF optical tomography using frequency-domain approach suitable for incorporation in a preclinical hybrid PET/CT scanner.

BTu3A.74

Extracting Diagnostic Information from Optical Coherence Tomography Images of Diabetic Retinal Tissues Using Depth-dependent Attenuation Rate and Fractal Analysis., Delia Cabrera DeBuc¹, Wei Gao¹, Erika Tatrai², Lenke Laurik², Boglarka Varga², Vera Olvedy², William Smiddy¹, Robert Tchintga³, Aniko Somogyib⁴, Gabor Somfai²; ¹*Ophthalmology, Univ. of Miami, USA;* ²*Ophthalmology, Semmelweis Univ., Hungary;* ³*Physics, Univ. of Dschang, Congo;* ⁴*Internal Medicine, Semmelweis Univ., Hungary.* The sensitivity of OCT images to sample diabetic morphology is tested by calculating attenuation coefficients and fractal dimension. Fractal analysis provided a better sensitivity to early predict diabetic retinopathy.

BTu3A.78

Investigation of Bacterial Biofilms in the Human Middle Ear using OCT Techniques and Acoustic Measurements, Cac T. Nguyen^{1,2}, Woonggyu Jung¹, Sarah Robinson^{1,2}, Jont B. Allen^{1,2}, Stephen Boppart^{1,2}; ¹*Beckman Inst. for Advanced Science and Technology, UIUC, USA;* ²*Electrical and Computer Engineering, UIUC, USA.* We investigate biofilms in human middle ear using OCT and acoustic measurements. OCT images visualize structure of the middle ear and confirm the biofilm. The acoustic measurements provide sound characteristics of the middle ears.

BTu3A.71

Imaging of retinal lesions in age related macula degeneration using wide field polarization sensitive optical coherence tomography, Michael Pircher¹, Stefan Zotter¹, Philipp Roberts^{1,2}, Erich Götzinger¹, Teresa Torzicky¹, Hirofumi Yoshida³, Futoshi Hirose³, Mathias Bolz², Ursula Schmidt-Erfurth², Christoph K. Hitzenberger¹; ¹*Center for Med. Physics and BIOMED. Engineering, Medical Univ. of Vienna, Austria;* ²*Department of Ophthalmology and Visual Sciences, Medical Univ. of Vienna, Austria;* ³*Canon Inc., Japan.* We present results of a newly developed wide-field polarization sensitive spectral domain OCT system for imaging retinal lesions in dry and wet age related macula degeneration (AMD).

BTu3A.75

Tissue elasticity imaging using Full-Field Optical Coherent Tomography, Amir Nahas^{1,2}, Claude Boccard^{1,2}; ¹*Institut Langevin, ESPCI, France;* ²*LLTech, France.* FF-OCT setup includes a static elastography system for multi-parameter images that could complement histopathology diagnostics. The setup creates various levels of compression. From stack of images one deduces displacements and elastic modulus maps.

BTu3A.79

Design and Characterization of MEMS Based Optical Coherence Tomography Endoscopic Probe, Jingjing Sun¹, Can Duan¹, Sean Samuelson¹, Huikai Xie¹; ¹*Electrical and computer engineering, Univ. of Florida, USA.* This study focused on the effects of the MEMS mirror, plastic housing and the variations in the assembly process on the performance of the MEMS-OCT imaging probes. Simulation and experimental results are shown and compared.

BTu3A.72

Shear-wave generation using acoustic radiation force detected by Optical Coherence Elastography(OCE), Marjan Razani¹, Adrian Mariampillai², Cuiru Sun², Victor .X.D Yang², Michael C Kolios¹; ¹*physics, Ryerson Univ., Canada;* ²*Electrical and Computer Engineering, Ryerson Univ., Canada.* Optical Coherence Elastography measures tissue displacement and utilizes the high resolution of OCT to generate high resolution stiffness maps. We explored the potential of measuring shear wave propagation and mechanical properties of tissue using OCE

BTu3A.76

Wide-field, high-speed polarization sensitive spectral domain OCT for measuring retardation, birefringence and retinal nerve fiber layer thickness, Stefan Zotter¹, Michael Pircher¹, Philipp Roberts^{1,2}, Erich Götzinger¹, Teresa Torzicky¹, Hirofumi Yoshida³, Futoshi Hirose³, Clemens Vass², Ursula Schmidt-Erfurth², Christoph K. Hitzenberger¹; ¹*Center for Medical Physics and BIOMEDical Engineering, Medical Univ. of Vienna, Austria;* ²*Department of Ophthalmology and Optometry, Medical Univ. of Vienna, Austria;* ³*Canon Inc., Japan.* We present a newly developed high-speed, wide-field polarization sensitive spectral domain OCT system for measuring retardation, birefringence and retinal nerve fiber layer thickness in healthy and glaucoma eyes.

BTu3A.80

Tissue Surface as the Reference Arm in Fourier Domain Optical Coherence Tomography, Nikola Krstajić¹, Praveen C. Ashok¹, Wilson Sibbett¹, Christian T. Brown¹, Kishan Dholakia¹, Mario E. Giardini²; ¹*SUPA - School of Physics & Astronomy, Univ. of St Andrews, UK;* ²*School of Medicine, Univ. of St Andrews, UK.* We present a method to use the tissue surface as reference in common-path Fourier domain optical coherence tomography. This allows a very long sample arm. The sensitivity is 94dB for 50 μs CCD integration time.

BTu3A.81

Hybrid Optical Coherence Tomography and Low-coherence Enhanced Backscattering Imager, Renzhe Bi¹, Jing Dong¹, Maria Winarni¹, Kijoon Lee¹; ¹*Nanyang Technological Univ., Singapore*. We present a dual modality device for both low-coherence enhanced backscattering (LEBS) measurement and optical coherence tomography (OCT). They provide complementary information with different resolutions, various applications are demonstrated.

BTu3A.82

Extended depth of focus adaptive optics spectral domain optical coherence tomography, Kazuhiro Sasaki¹, Kazuhiro Kurokawa¹, Shuichi Makita¹, Yoshiaki Yasuno¹; ¹*Computational optics group, Univ. of Tsukuba, Japan*. Adaptive optics spectral domain optical coherence tomography (AO-SDOCT) with a long focal range was developed by modulating the phase distribution of pupil using AO technology. The higher resolution human retinal imaging can be achieved.

BTu3A.83

Measuring known aberrations in rat brain slices with Coherence-Gated Wavefront Sensor based on a Linnik interferometer, Jinyu Wang^{1,2}, Jean-François Léger^{1,2}, Jonas Binding^{5,6}, Claude Boccard⁴, Sylvain Gigan⁴, Laurent Bourdieu^{1,3}; ¹*Ecole Normale Supérieure, Institut de Biologie de l'ENS, IBENS, France*; ²*Inserm, U1024, France*; ³*CNRS, UMR 8197, France*; ⁴*Institut Langevin, ESPCI ParisTech, CNRS UMR 7587, ESPCI, France*; ⁵*Fondation Pierre-Gilles de Gennes pour la Recherche, France*; ⁶*Max Planck Inst. for Medical Research, Germany*. Using a coherence-gated wavefront sensing scheme based on Linnik interferometer, we measured a known defocus up to 400µm into the highly scattering rat brain. The performances with objectives of different NA and magnification are compared.

BTu3A.84

New Design Options for Polarization-Sensitive Optical Coherence Tomography, Kristen Lurie¹, Audrey Ellerbee¹; ¹*Electrical Engineering, Stanford Univ., USA*. We present a framework for designing polarization-sensitive optical coherence tomography (OCT) systems that yield analytical expressions for optic axis and retardance. The new designs have features amenable to adaptation into many OCT configuration.

BTu3A.85

Magnetomotive contrast in optical coherence tomography for detecting early-stage atherosclerosis using targeted microspheres, Adeel Ahmad¹, Jong S. Kim¹, Li Joanne¹, Jonathan Rasio², Zita Hubler¹, Eric J. Chaney¹, Marina Marjanovic¹, Kenneth Suslick¹, Stephen Boppart¹; ¹*Univ. of Illinois at Urbana Champaign, USA*. We show molecularly-sensitive contrast in OCT using targeted multifunctional magnetic microspheres. Microspheres were perfused through the aorta inside the flow chamber and magnetomotive OCT was performed on the ex-vivo aorta specimens.

BTu3A.86

Fourier Domain Mode Locked laser for Optical Coherence Tomography Based on Dispersion-Shifted Fiber, Jianbing Xu¹, Rui Zhu¹, Po Ching Chui¹, Kenneth K. Wong¹; ¹*Electrical and Electronic Engineering, The Univ. of Hong Kong, China*. We report a Fourier domain mode locked laser (FDML) for OCT based on dispersion-shifted fiber. Axial resolution and coherence length compared with the case without dispersion engineering is improved by 38% and 68%, respectively.

BTu3A.87

Registration of optical coherence tomography datasets with dermoscopy images, Thomas Richardson¹, Alexis Guyot², Raj Mallipeddi³, Nisith Sheth³, Andrew Coleman¹, Graeme Penney²; ¹*Medical Physics Department, Guy's and St Thomas' Foundation Trust, UK*; ²*Division of Imaging Sciences, King's College London, UK*; ³*Dermatological Surgery and Laser Unit, St John's Inst. of Dermatology, UK*. A method of registering an OCT image data set with a dermoscopic image of a skin lesion is presented. This dual-modality system is shown to have value in delineating pre-surgical margins.

BTu3A.88

Inverse spectroscopic Optical Coherence Tomography (ISOCT): non-invasively quantifying the complete optical scattering properties from weak scattering tissue, Ji Yi¹, Andrew J. Radosevich¹, Jeremy D. Rogers¹, Vadim Backman¹; ¹*BIOMEDical Engineering, Northwestern Univ., USA*. The complete set of the scattering properties of tissue including the phase function can be locally quantified by ISOCT. The method inversely quantifies the tissue refractive index (R.I.) correlation function to deduce the optical properties.

BTu3A.89

Vernier-Tuned Single-Chip Semiconductor Laser for Optical Coherence Tomography Applications, Dennis Derickson¹, Chris Chiccone¹, David Gilbert¹, Michael Crawford², Michael Minneman², Jason Ensher²; ¹*Electrical Engineering, California Polytechnic, USA*; ²*Insight Photonic Solutions, USA*. Vernier-Tuned Distributed Bragg Reflector lasers were initially designed for telecommunications. VT-DBR laser adaptations for OCT at 1550 nm and 1300 nm are described. 200 kHz sweep rates and coherence length are key OCT contributions.

BTu3A.90

Multi-MHz retinal OCT imaging using an FDML laser, Thomas Klein¹, Wolfgang Wieser¹, Raphael André¹, Christoph Eigenwillig¹, Robert A. Huber¹; ¹*BioMolekulare Optik, Ludwig-Maximilians-Universität München, Germany*. We demonstrate multi-MHz OCT for ultrawide-field imaging in less than a second, using a 1050nm FDML laser at a sweep rate of up to 3.35MHz, doubled by a two-spot setup to 6.7MHz.

BTu3A.91

Polarization Sensitive Spectral Domain Optical Coherence Tomography of Cataract Lenses, Erich Götzinger¹, Matthias Bolz², Stefan Zotter¹, Teresa Torzicky¹, Michael Pircher¹, Philipp Roberts², Ferdinand Schlanitz², Ursula Schmidt-Erfurth², Christoph K. Hitzenberger¹; ¹*center for medical physics, medical Univ. of vienna, Austria*; ²*Department of Ophthalmology and Optometry, Medical Univ. of vienna, Austria*. We used a fiber based polarization sensitive spectral domain optical coherence tomography system using two CMOS line scan cameras to image the lens of healthy volunteers and cataract patients

BTu3A.92

Effects of Reduced Bit-Depth on Phase Data in Common-Path Optical Coherence Tomography, William Ling¹, Audrey Ellerbee¹; ¹*Electrical Engineering, Stanford Univ., USA*. Abstract We report the effects of reduced digitization resolution on phase data in a common-path SD-OCT system. Nuances of common-path systems lead to different responses to bit-depth than in non-common-path systems.

BTu3A • BIOMED Poster Session II—Continue

BTu3A.93

Real-time Three-Dimensional Dynamic Imaging of Lower Airway Using Swept Source Optical Coherence Tomography, Jiefeng Xi¹, Wayne Mitzner², Robert Brown³, Rex Yung⁴, Xingde Li¹; ¹*Department of BIOMEDical Engineering, Johns Hopkins Univ., USA*; ²*Department of Environmental Health Sciences, School of Public Health, Johns Hopkins Univ., USA*; ³*Departments of Anesthesiology, Environmental Health Sciences, Medicine, and Radiology, Johns Hopkins Univ., USA*; ⁴*Department of Medicine/Oncology, Johns Hopkins Univ. School of Medicine, USA*. We investigated the feasibility of high-speed SS-OCT system along with a miniature side-viewing catheter to dynamically assess structures of the bronchus in vivo. Excellent correlations were achieved between OCT images and the corresponding histology

BTu3A.97

Gold nanoparticles for improving contrast in Optical Coherence Tomography images, Yenisey Ponce de Leon¹, Juan L. Pichardo-Molina¹, Noe Alcalá-Ochoa¹, Jorge A. Lopez-Rios²; ¹*Centro de Investigaciones en Óptica, Mexico*; ²*División de Ciencias Naturales y Exactas, Universidad de Guanajuato, Mexico*. Gold nanoparticles of two different morphologies and sizes were tested as contrast agents for OCT images at a central wavelength of 1325nm. OCT images of the nanoparticles in water are shown.

BTu3A.94

The first scattering-dominant structured gold nanoparticles for enhancing OCT backscattering and imaging contrast, Yongping Chen¹, Jiefeng Xi¹, Jessica C. Ramella-Roman², Xingde Li¹; ¹*Department of BIOMEDical Engineering, Johns Hopkins Univ., USA*; ²*Department of BIOMEDical Engineering, The Catholic Univ. of America, USA*. We reported the first scattering-dominant agent based on structured Au nanocages for enhancing OCT imaging contrast. Animal tumor imaging with the Au nanocages was performed, demonstrating significant in vivo contrast enhancement for the first time

BTu3A.98

Dental parodontium evaluation by spectral OCT, Cosmin Sinescu¹, Meda Lavinia Negrutiu¹, Stefan Ioan Stratul¹, Florin Ionel Topala¹, Raluca Mioara Cosoroaba¹, Mihai Rominu¹, Adrian Bradu², Adrian G. Podoleanu²; ¹*Dental Materials and Dental Technology Department, Univ. of Medicine and Pharmacy Victor Babes from Timisoara, Faculty of Dentistry, Romania*; ²*Univ. of Kent, UK*. Optical coherence tomography in spectral mode was used to evaluate normal and affected dental parodontium as a noninvasive method. The results were validated by usual clinical evaluation procedures.

BTu3A.95

In vivo and in vitro diagnostics using Full Field Optical Coherence Tomography, Osnath Assayag¹, Fabrice Harms^{2,1}, Eugénie Dalimier², Bertrand de Poly², Claude Boccara^{1,2}; ¹*LLTech, France*; ²*Institut Langevin, France*. Full Field OCT has found to be useful in helping both pathologists and surgeons in their per-operative diagnosis. We describe, here, applications to breast, brain and skin cancers and demonstrate ex and in vivo capability.

BTu3A.99

Comparison of Measured and Simulated Optical Coherence Tomography Images of Human Enamel, Alwin Kienle¹, Jan Schäfer¹; ¹*Inst. of Laser Technologies, Germany*. Simulations of optical coherence tomography images based on the microstructure of enamel were performed using the Monte Carlo method and analytical solutions of Maxwell equations. A good agreement between calculated and measured images was obtained.

BTu3A.96

A New Method to Improve Image Contrast in Full Field Holographic Coherence Domain Imaging, Haibo Lin¹, Ping Yu¹; ¹*Univ. of Missouri, USA*. We propose a new method based on speckle statistics to improve image contrast in full field holographic optical coherence imaging. Theoretical analysis is compared with experimental results to validate the new method.

Symphony IV

DH

Tuesday, 1 May

13:00 - 15:00

DTu3C • Special Techniques of Digital Holography II

Adrian Stern; Ben Gurion Univ. of the Negev, Israel, Presider

DTu3C.1 • 13:00

Invited

Recent Progresses in Digital Holographic Microscopy with Spatial Partial Coherent Light and Applications

Frank Dubois¹, El Mallahi Ahmed¹, Minetti Christophe¹, Yourassowski Catherine¹; ¹Universite Libre de Bruxelles, Belgium.

We investigate the use of partially coherent source for digital holographic microscopes (DHM). Recent progresses and applications will be presented as the automated 3D detection and classification of particles or the analysis of vesicle suspension.

DTu3C.2 • 13:30

Invited

Opto-numeric systems: lenses and pixels

John Sheridan¹, Damien P. Kelly²; ¹Electrical, Electronic & Communications Engineering, UCD, Ireland; ²Institut für Mikro- und Nanotechnologien, Macro-Nano, Technische Universität Ilmenau, Germany. In this manuscript we discuss the effect of filtering a signal in a generalized phase space domain and this viewpoint can be used to better understand the imaging performance of modern optical systems.

DTu3C.3 • 14:00

Holographic imaging and interferometry with non-Bragg diffraction orders in the volume gratings, Nikolai Kukhtarev¹, Tatiana Kukhtareva¹, Partha Banerjee², Georges Nehmetallah²; ¹Physics, Alabama A&M Univ., USA; ²ECE/EOP, Univ. of Dayton, USA. Recording of holographic volume gratings lead to Bragg and non-Bragg diffracted beams with transformed images in each beam. In real-time mode fringes appear with a proper phase shift resulting in one shot phase shifting interferometry.

DTu3C.4 • 14:15

Long-depth three-dimensional object profilometry with low-coherent digital holography,

Quang D. Pham¹, Satoshi Hasegawa¹, Akihiro Kiire¹, Daisuke Barada¹, Toyohiko Yatagai¹, Yoshio Hayasaki¹; ¹Center for Optical Research and Education (CORE), Utsunomiya Univ., Japan. We proposed a new method of digital holography with an ultra-broad band light source, coherence scanning method and a continuous chromatic phase-shifter to characterize the unlimited depth object with very high resolution.

DTu3C.5 • 14:30

Experimental observation of 4D Wigner and Ambiguity distribution functions, Guohai Situ¹, Laura A. Waller¹, Jason Fleischer¹; ¹Princeton Univ., USA. We present a technique for measuring the 4D Wigner distribution function and Ambiguity function of 2D signals using a windowed Fourier transform. The method is demonstrated by numerical and experimental results.

DTu3C.6 • 14:45

Design of Volume Holographic Imaging Point Spread Functions Using Multiple Point Deformations, Hanhong Gao¹, George Barbastathis^{2,3}; ¹Department of Electrical Engineering and Computer Science, Massachusetts Inst. of Technology, USA; ²Department of Mechanical Engineering, Massachusetts Inst. of Technology, USA; ³Singapore-MIT Alliance for Research and Technology (SMART) Centre, Singapore. We present an analysis and design procedure for engineering the point-spread-function (PSF) of a volume hologram by deforming its exterior using a superposition of point indenters.

Symphony I & II

Symphony III

Symphony IV

BIOMED 1

BIOMED 2

DH

15:00—15:30

COFFEE BREAK, *Concerto Ballroom*

15:30 - 17:30

BTu4A • Fluorescence Imaging

Robert Nordstrom; National Inst. of Health, USA, President

BTu4A.1 • 15:30

Improving the Sensitivity and Specificity of Tumor Contrast in Fluorescence Imaging by Employing an Untargeted Fluorescent Reporter, Kenneth M. Tichauer¹, Kimberley S. Samkoe^{2,1}, Kristian J. Sexton¹, Jason R. Gunn¹, Tayyaba Hasan³, Brian Pogue^{1,2}; ¹Thayer School of Engineering, Dartmouth College, USA; ²Department of Surgery, Dartmouth Medical School, USA; ³Wellman Center for Photomedicine, Massachusetts General Hospital, USA. A dual-reporter fluorescence imaging approach is presented that can quantify biomarker expression in vivo. The approach was also demonstrated to provide better tumor contrast compared to targeted fluorescence uptake alone.

BTu4A.2 • 15:45

In Vivo Image-Guided Therapy of Oral Carcinoma using Topical Photodynamic Molecular Beacons, Tracy W. Liu¹, Eduardo H. Moriyama¹, Nicolas E. Wolter¹, Juan Chen¹, Brian C. Wilson¹, Gang Zheng¹; ¹Medical Biophysics, Univ. of Toronto/ Ontario Cancer Inst., Canada. We demonstrate the capability of topical photodynamic molecular beacons as useful image-guidance tools during surgical resection to improve the identification of surgical margins surrounding oral cancer using a hamster cheek pouch carcinoma model.

BTu4A.3 • 16:00

High Signal-to-Noise Ratio Voltage Imaging: A Powerful Tool for Determining Electrophysiological Properties of CNS Axons, Amanda J. Foust¹, Amanda E. Casale¹, Dejan Zecevic², David A. McCormick¹; ¹Neurobiology, Yale Univ., USA; ²Cellular and Molecular Physiology, Yale Univ., USA. Although axons play a key role in neuronal computation, the small size of CNS axons precludes direct characterization with electrical recordings. We implement high signal-to-noise ratio VSD imaging to determine cortical axon functional properties.

BTu4A.4 • 16:15

Frequency-domain Fluorescence-enhanced Optical Tomography for Primary Prostate Cancer with PET Validation in Siemens Inveon Scanner: A Preliminary Result, Yujie Lu¹, I-Chih Tan¹, Chinmay D. Darne¹, Nathaniel Wilganowski¹, Holly Robinson¹, John Rasmussen¹, Shikui Yan², Anne M. Smith², Eva M. Sevick-Muraca¹; ¹UTHSC-Houston, USA; ²Molecular Imaging, Siemens Medical Solutions USA, Inc., USA. With a dual-labeled imaging agent, Optical/CT/PET primary prostate cancer imaging was performed in a Siemens Inveon scanner. PET-based imaging validation shows the potential of the developed fluorescence tomography for preclinical research.

15:30 - 17:30

BTu4B • Optical Coherence Tomography: Clinical Applications

Michael Jenkins; Case Western Reserve Univ., USA, President

BTu4B.1 • 15:30

Invited

Applying OCT to Dermatology: Technology, Clinical Applications, and the Translational Process, Jon Holmes¹; ¹Michelson Diagnostics Ltd., UK. The application of Optical Coherence Tomography (OCT) imaging to clinical dermatology is discussed, with reference to experience gained with in bringing a novel OCT scanner into the clinical setting on a commercial basis

BTu4B.2 • 16:00

Microvascular Imaging of Skin Lesions with High Speed Doppler extended focus OCT, Cedric Blatter¹, Jessica Weingast², Branislav Grajciar¹, Rainer A. Leitgeb¹; ¹Center Medical Physics and BIOMEDICAL Engineering, Medical Univ. Vienna, Austria; ²Univ. Clinics of Dermatology, Medical Univ. Vienna, Austria. We employ high speed swept source OCT with Bessel beams at 1300nm for microvascular imaging of skin diseases including basal cell carcinoma. The lesions show characteristic vascular patterns significantly different for healthy skin.

BTu4B.3 • 16:15

Forward-Imaging Needle OCT Probe for Stereotactic Neurosurgery, Chia-Pin Liang¹, Jeremiah Wierwille¹, Thais Moreira³, Gary Schwartzbauer², Samir Samir Jafri^{2,3}, Cha-Min Tang^{2,3}, Yu Chen¹; ¹Bioengineering, Univ. of Maryland, College Park, USA; ²Univ. of Maryland School of Medicine, USA; ³VA Medical Center, USA. We developed a forwarding-imaging needle-type OCT probe for avoiding the hemorrhage and guiding neurosurgeries. The feasibility of vessel detection and neurosurgical guidance were demonstrated on sheep brain in vivo and human brain ex vivo.

15:30 - 17:30

DTu4C • Three-Dimensional Display III

Hiroshi Yoshikawa; Nihon Univ., Japan, President

DTu4C.1 • 15:30

Invited

Multiplex Holography for Walk-around Viewing, Yih-Shyang Cheng¹; ¹Department of Optics and Photonics, National Central Univ., Taiwan. Cylindrical, conical, and disk-type multiplex holograms can all generate 3D images for walk-around viewing. The pathway which led us to the development of image-plane disk-type multiplex holography is described.

DTu4C.2 • 16:00

Invited

3D data acquisition using ray-based image sensors and 3D display using electronic holography, Kenji Yamamoto¹; ¹NICT, Japan. This paper introduces challenges and two prototype systems using ray-based image sensors and electronic holography display toward ultra-realistic communication. The first one uses integral photography, and the second one uses 300-camera array.

Symphony I & II

Symphony III

Symphony IV

BIOMED I

BIOMED 2

DH

BTu4A • Fluorescence Imaging—Continue

BTu4A.5 • 16:30

Experimental Demonstration of Angled Fluorescent Laminar Optical Tomography for Tissue Engineering, Chao-Wei Chen^{1,2}, Andrew B. Yeatts¹, Emily E. Coates¹, John P. Fisher¹, Yu Chen¹; ¹Fischell department of Bio-engineering, Univ. of Maryland, USA; ²Department of Electrical and Computer Engineering, Univ. of Maryland, USA. We developed an angled fluorescent laminar optical tomography, which enables 3D imaging of stem cell distribution within engineered tissue scaffold. Depth-resolved imaging in weakly- and highly-scattering tissue scaffolds is demonstrated.

BTu4A.6 • 16:45

Molecular Laminar Optical Tomography of Thick Tissue Engineered Constructs, Lingling Zhao¹, Vivian Lee¹, Guohao Dai¹, Xavier Intes¹; ¹BIOMEDICAL Engineering, Rensselaer Polytechnic Inst., USA. We integrated a mesoscopic fluorescence molecular tomography system, and visualized both the fluid flow and fluorescent-labeled living cells of vascular construct within thick scaffold at high-frame rates, with high sensitivity and accuracy.

BTu4A.7 • 17:00

Time Domain Diffuse Fluorescence Tomography Can Increase Small-Animal Imaging Throughput, Robert Holt¹, Kenneth M. Tichauer², Qun Zhu³, Hamid Dehghani³, Fredric Leblond², Brian Pogue²; ¹Physics and Astronomy, Dartmouth College, USA; ²Thayer School of Engineering, Dartmouth College, USA; ³School of Computer Science, Univ. of Birmingham, UK. Employing multiple time-bins in the image reconstruction of a time-domain fluorescence tomography dataset provides improved spatial resolution and contrast. Furthermore, these gains can be used to minimize tissue sampling and reduce imaging duration

BTu4A.8 • 17:15

Fluorescence Tomography using Temperature Modulation, Yuting Lin¹, Linden Bolinsay², Michael Ghijsen¹, Tiffany C. Kwong¹, Gultekin Gulsen¹; ¹Center for functional onco imaging, Department of Radiological Sciences, UC Irvine, USA; ²InnoSense LLC, USA. We describe a novel approach termed "temperature-modulated fluorescence tomography" that can acquire fluorescence images at focused ultrasound resolution by utilizing recently emerged temperature sensitive fluorescence contrast agents.

BTu4B • Optical Coherence Tomography: Clinical Applications—Continue

BTu4B.4 • 16:30

Flexible and rigid endoscopy for high-resolution in-depth imaging with Full-Field OCT, Anne Latrive^{1,2}, Claude Boccara^{1,2}; ¹Institut Langevin, ESPCI, France; ²LLTech, France. We propose a novel method for in situ cellular imaging of biological tissues using a full-field OCT setup with an entirely passive probe. Ex vivo results on human breast and first in vivo results on human skin are presented

BTu4B.5 • 16:45

Single-shot Stent Segmentation in Intravascular OCT Pullbacks, Zhao Wang¹, Michael W. Jenkins¹, Hiram Bezerra², Marco Costa², David Wilson¹, Andrew Rollins¹; ¹BIOMEDICAL Engineering, Case Western Reserve Univ, USA; ²Harrington McLaughlin Heart & Vascular Inst., Univ. Hospitals Case Medical Center, USA. We propose a novel method that can detect hundreds/thousands of stent struts in an entire OCT pullback at once. The method utilizes global object information and is potentially more robust than conventional 2D methods.

BTu4B.6 • 17:00

Dynamic imaging of in vitro human airway epithelium using optical coherence tomography, Amy Oldenburg^{1,2}, Raghav K. Chhetri¹, Brian M. Button³, David B. Hill³, Richard C. Boucher³; ¹Physics and Astronomy, Univ. of North Carolina at Chapel Hill, USA; ²BIOMEDICAL Research Imaging Center, Univ. of North Carolina at Chapel Hill, USA; ³Cystic Fibrosis Center, Univ. of North Carolina at Chapel Hill, USA. Ultrahigh-resolution optical coherence tomography (OCT) is employed to depth-resolve mucociliary transport on human bronchial epithelial cell cultures. This has relevance for monitoring airway mucus in lung diseases such as cystic fibrosis and COPD.

BTu4B.7 • 17:15

All-Fiber-Optic Based Catheter System for Simultaneous Endoscopic Optical Coherence Tomography and Fluorescence Imaging, Jessica Mavadia¹, Jiefeng Xi¹, Yongping Chen¹, Xingde Li¹; ¹BIOMEDICAL Engineering, Johns Hopkins Univ., USA. An all-fiber-optically based balloon catheter for simultaneous fluorescence imaging and OCT has been implemented. The performance of this multimodal catheter is demonstrated on tissue phantom, ex vivo pig esophagus and mouse tumor imaging.

DTu4C • Three-Dimensional Display III—Continue

DTu4C.3 • 16:30

Computer-generated cylindrical holographic stereogram made from 300-camera array images, Hiroshi Yoshikawa¹, Takeshi Yamaguchi¹, Kenji Yamamoto², Taiichiro Kurita²; ¹Dpt. Electronics and Computer Science, Nihon Univ., Japan; ²National Inst. of Information and Communications Technology, Japan. We have investigated computer-generated holographic stereogram of cylindrical shape. An input image array is taken by 300-camera system and digitally processed to improve the image quality. The reconstructed image is observed with LED illumination.

DTu4C.4 • 16:45

Expression of Refractive Objects for Computer-Generated Hologram Using Ray Tracing Method, Tsubasa Ichikawa¹, Yuji Sakamoto¹; ¹Graduate School of Information Science and Technology, Hokkaido Univ., Japan. In computer-generated hologram, researches on rendering techniques are inadequate. The study expressing photorefractive phenomena are not especially established. We propose a method to display transparent objects using the ray tracing method.

DTu4C.5 • 17:00

Simultaneous Color Doppler Phase-Shifting Digital Holography, Tomohiro Kiire¹, Daisuke Barada^{2,1}, Jun-ichiro Sugisaka¹, Yoshio Hayasaki¹, Toyohiko Yatagai¹; ¹Center for Optical Research and Education, Utsunomiya Univ., Japan; ²Graduate School of Engineering, Utsunomiya Univ., Japan. Holograms of three color components in the color image are recorded simultaneously using single monochromatic camera. A reconstruction images in the color components obtained by the Doppler phase-shifting technique are combined to one color image.

16:00—20:00

OIDA RUMP SESSION, Symphony IV

Symphony I & II

Symphony III

Symphony IV

BIOMED I

BIOMED 2

DH

08:00 - 10:00

BW1A • Nevel Techniques and Models

David Cuccia; Modulated Imaging Inc., USA, President

BW1A.1 • 08:00

Time-Reversed Ultrasonically Encoded (TRUE) Optical Focusing into Soft Biological Tissue, Xiao Xu¹, Puxiang Lai¹, Honglin Liu¹, Lihong V. Wang¹; ¹BIO-MEDical Engineering, Washington Univ. in St. Louis, USA. Optical imaging of soft biological tissue has limited depth due to strong light scattering. Our novel technique—Time-Reversed Ultrasonically Encoded (TRUE) optical focusing—can dynamically focus light into tissue. Experimental results are presented.

BW1A.2 • 08:10

Time-Resolved Reflectance DOT: Experimental Results for Imaging Absorption Contrast in Depth, Agathe Puszka¹, Mathieu Debourdeau¹, Lionel Hervé¹, Anne Planat-Chrétien¹, Anne Koenig¹, Jacques Derouard², Jean-Marc Dinten¹; ¹DTBS/STD/LISA, CEA-LETI Minatec, France; ²LIPhy, Université Joseph Fourier, France. Detecting and localizing precisely contrast in depth is the major challenge of reflectance Diffuse Optical Tomography. We present a dedicated time-resolved instrumentation and first experimental results using a Mellin-Laplace Transform based method.

BW1A.3 • 08:30

Development of near-infrared swept laser based diffuse optical tomography system, Jaedu Cho¹, Yuting Lin², Gultekin Gulsen², Orhan Nalcioğlu^{1,2}, Myung Yung Jeong¹, Chang-Seok Kim¹; ¹Cogno-Mechatronics Engineering, Pusan National Univ., Republic of Korea; ²Tu and Yuen Center for Functional Onco-Imaging, Univ. of California Irvine, USA. We have introduced a NIR swept source based diffuse optical tomography (DOT) system. We also demonstrate the capabilities of the NIR swept laser for multi-spectral DOT application with a turbid gelatin phantom measurement.

BW1A.4 • 08:40

Noncontact diffuse correlation spectroscopy probe for deep tissue blood flow measurement, Yu Lin¹, Lian He¹, Yu Shang¹, Guoqiang Yu¹; ¹Center for BIO-MEDical engineering, Univ. of Kentucky, USA. A noncontact diffuse correlation spectroscopy probe for deep tissue blood flow measurements has been designed and calibrated against a validated contact probe; flow changes measured concurrently are highly correlated in phantom and real-tissue tests.

08:00 - 10:00

BW1B • Non-linear and Fluorescence Spectroscopy

Rinat Esenaliev; Univ. of Texas Medical Branch, USA, President

BW1B.1 • 08:00

Invited

Two-photon Excited Blood Autofluorescence for In Vivo Imaging and Flow Cytometry, Jianan Y. Qu¹; ¹Electrical and Computer Engineering, Hong Kong Univ. of Science and Technology, Hong Kong. We report our recent discovery of two-photon autofluorescence from blood including red/white blood cells, platelets and plasma. We demonstrate the applications of blood autofluorescence for label-free in vivo imaging of microvasculature and flow cytometry.

BW1B.2 • 08:30

Fluorescence goggle for surgical navigation, Yang Liu¹, Walter Akers¹, Adam Q. Bauer¹, Gail Sudlow¹, Kexian Liang¹, Joseph P. Culver¹, Sam Achilefu¹; ¹Washington Univ. in St. Louis, USA. We developed a fluorescence goggle system for intraoperative imaging and surgical navigation. This system enables visualization of fluorescence information directly from the eyepieces in real time, which improves surgical accuracy.

BW1B.3 • 08:45

Label-Free Multimodal Nonlinear Optical Microscopy for In Vivo Diagnosis of Precancerous Squamous Epithelia, Seng Khoon Teh¹, Wei Zheng², Shuxia Li³, Dong Li², Yan Zeng², Yanqi Yang³, Jianan Y. Qu²; ¹Division of Bioengineering, Hong Kong Univ. of Science and Technology, Hong Kong; ²Department of Electronic and Computer Engineering, Hong Kong Univ. of Science and Technology, Hong Kong; ³School of Dentistry, The Univ. of Hong Kong, Hong Kong. We explore in vivo diagnostic utility of an in-house developed multimodal nonlinear optical microscopy for detection of squamous epithelia precancer. Our results reveal all epithelial sublayers and stroma provide significant diagnostic information.

08:00 - 10:00

DW1C • Novel Applications of Digital Holography II

Yashio Hayasaki; Utsunomiya Univ., Japan, President

DW1C.1 • 08:00

Invited

Digital Holographic Three-Dimensional Imaging Spectrometry, Kyu Yoshimori¹; ¹Iwate Univ., Japan. This paper presents a brief review of the recent progress in a fully interferometric technique to obtain a set of spectral components of three-dimensional images for usual polychromatic objects.

DW1C.2 • 08:30

Quantitative Evaluation of Skin Vibration Induced by a Bone-Conduction Device Using Holographic Recording in a Quasi-Time-Averaging Regime, Mathieu Leclercq¹, Mayssa Karray¹, Vincent Isnard¹, François Gautier¹, Pascal Picart¹; ¹LAUM CNRS, France. This paper proposes a first attempt to visualize and analyze sound propagating at the surface of a human skin induced by a bone conduction device. The proposed method is based on a so-called “quasi-time-averaging regime”.

DW1C.3 • 08:45

When holography meets coherent diffraction imaging, Tatiana Latychevskaia¹, Jean-Nicolas Longchamp¹, Hans-Werner Fink¹; ¹Physics Inst., Univ. of Zurich, Switzerland. There are two well-known solutions to the phase problem: holography and coherent diffraction imaging (CDI). We show how holography and CDI can be merged into one superior technique: holographic coherent diffraction imaging (HCIDI).

Symphony I & II

BIOMED I

BW1A • Nevel Techniques and Models—Continue

BW1A.5 • 09:00

3D near-infrared imaging based on a single-photon avalanche diode array sensor: A new perspective on reconstruction algorithms, Juan Mata Pavia^{1,2}, Edoardo Charbon^{2,3}, Martin Wolf¹; ¹BIOMEDical Optics Research Laboratory(BORL), Division of Neonatology, Department of Obstetrics and Gynecology, Univ. Hospital Zurich, Switzerland; ²Quantum Architecture Group(AQUA), Ecole Polytechnique Fédérale de Lausanne (EPFL), Switzerland; ³TU Delft, Netherlands. Recently, we demonstrated the potential of single-photon imagers in diffuse optical tomography (DOT). We present the advances of a new algorithm based on optical setups using this kind of sensors.

BW1A.6 • 09:15

Inter-Laboratory Comparison of Optical Properties Performed on Intralipid and India Ink, Lorenzo Spinelli¹, Marcin Botwicz², Norbert Zolek², Michal Kacprzak², Daniel Milej², Adam Liebert², Udo Weigel³, Turgut Durdur³, Florian Foschum⁴, Alwin Kienle⁴, François Baribeau⁵, Sébastien Leclair⁵, Jean-Pierre Bouchard⁵, Isabelle Noiseux⁵, Pascal Gallant⁵, Ozzy Mermut⁵, Antonio Pifferi^{1,6}, Alessandro Torricelli⁶, Rinaldo Cubeddu^{1,6}, Hsin-Chia Ho^{7,8}, Mikhail Mazurenka⁸, Heidrun Wabnitz⁸, Katy Klauenberg⁸, Olha Bodnar⁸, Clemens Elster⁸, Magali Bénazech-Lavoué⁹, Yves Bérubé-Lauzière⁹, Frédéric Lesage¹⁰, Paola Di Ninni¹¹, Fabrizio Martelli¹¹, Giovanni Zaccanti¹¹; ¹Consiglio Nazionale delle Ricerche - Istituto di Fotonica e Nanotecnologie, Italy; ²IBIB, Nalecz Institute of Biocybernetics and BIOMEDICAL Engineering, Polish Academy of Sciences, Poland; ³ICFO, Institut de Ciències Fotòniques, Parc Mediterrani de la Tecnologia, Spain; ⁴ILM, Institut für Lasertechnologien in der Medizin und Messtechnik an der Universität Ulm, Germany; ⁵INO, National Optics Institute, Canada; ⁶POLIMI, Politecnico di Milano-Dipartimento di Fisica, Italy; ⁷ITRI, Industrial Technology Research Institute, Taiwan; ⁸PTB, Physikalisch-Technische Bundesanstalt, Germany; ⁹TomOptUS, Département de génie électrique, Université de Sherbrooke, Canada; ¹⁰Département de génie électrique, École Polytechnique de Montréal, Canada; ¹¹UNIFI, Dipartimento di Fisica e Astronomia, Università degli Studi di Firenze, Italy. Intrinsic reduced scattering coefficient of Intralipid and intrinsic absorption coefficient of Indian ink at NIR wavelengths are accurately assessed in a multi-center study involving different techniques, instrumental set-ups, and analysis methods.

Symphony III

BIOMED 2

BW1B • Non-linear and Fluorescence Spectroscopy—Continue

BW1B.4 • 09:00

Development and Characterization of a Multi-Modal Probe for Early Skin Cancer Detection using Raman, Reflectance and Fluorescence Spectroscopies, Manu Sharma¹, Liang Lim¹, Eric Marple², William Riggs³, James Tunnell¹; ¹BIOMEDical Engineering, The Univ. of Texas at Austin, USA; ²EmVision LLC, USA; ³DermDx, USA. The development and characterization of a probe utilizing Raman, reflectance and fluorescence spectroscopies, towards providing a high-level of accuracy for early skin cancer detection, is described.

BW1B.5 • 09:15

Ex vivo multispectral multiphoton imaging of peripheral nerve regeneration, Dimitrios S. Tzeranis¹, Eric Soller¹, Rebecca Lin², Ioannis V. Yannas^{1,2}, Peter So^{1,2}; ¹Mechanical Engineering, MIT, USA; ²Biological engineering, MIT, USA. Multispectral multiphoton microscopy of ex vivo transected peripheral nerves treated with collagen scaffolds of varying cross-linking is applied to quantify how biomaterial properties modulate the wound healing response and induce regeneration.

Symphony IV

DH

DW1C • Novel Applications of Digital Holography II—Continue

DW1C.4 • 09:00

Digital Color Holography as A Tool for the Detection of Premature Cracks in Composite Materials, Mayssa Karray¹, Christophe Poilane¹, Denis Mounier², Pascal Picart¹; ¹LAUM CNRS, France; ²LPEC CNRS, France. This paper proposes a three-color holographic interferometer for the early crack detection in composite materials submitted to a shear test. Evaluation of shear strains at the surface provides a pertinent parameter to detect premature crack.

DW1C.5 • 09:15

Time-dependent Surface Response of Fluid to Transmission Optical Pressure Impulse, David C. Clark¹, Myung K. Kim¹; ¹Physics, Univ. of South Florida, USA. Dynamic response to an optical pressure pulse can be a useful indicator of the mechanical properties of a fluid surface or membrane. We have mapped the time-dependent response of the water surface using precise measurement and timing techniques.

Symphony I & II

Symphony III

Symphony IV

BIOMED I

BIOMED 2

DH

BW1A • Nevel Techniques and Models—Continue

BW1B • Non-linear and Fluorescence Spectroscopy—Continue

DW1C • Novel Applications of Digital Holography II—Continue

BW1A.7 • 09:30 ▶

A User-Enabling Visual Workflow for Near-Infrared Light Transport Modeling in Tissue, Michael Jermyn¹, Brian Pogue¹, Hamid R. Ghadyani¹, Scott Davis¹, Michael A. Mastanduno¹, Hamid Dehghani^{1,2}; ¹Thayer Engineering, Dartmouth College, USA; ²Computer Science, University of Birmingham, United Kingdom. The components of a user-enabling visual workflow for clinically-relevant quantitative imaging with light in tissue are demonstrated, including new tools for integration of segmentation, meshing, reconstruction & simulation, and visualization.

BW1A.8 • 09:45

Phase Function Corrected Diffusion Approximation for Light Transport in Turbid Media, Edward Vitkin¹, Vladimir Turzhitsky¹, Le Qiu¹, Lianyu Guo¹, Eugene Hanlon¹, Irving Itzkan¹, Lev T. Perelman¹; ¹Center for Advanced BIOMEDical Imaging and Photonics, Harvard University, USA. Many optical imaging and spectroscopy applications require understanding how light propagates in turbid media near point-of-entry. We report an analytic solution to this problem that demonstrates excellent agreement with simulations and experiments.

BW1B.6 • 09:30

Stokes Shift Spectroscopy and imaging for highlighting the difference of breast cancerous and normal tissues, Yang Pu¹, Wubao Wang¹, Yuanlong Yang¹, Laura Sordillo¹, Yury Budansky¹, Robert R. Alfano¹; ¹Physics, Inst. for Ultrafast Spectroscopy and Lasers, City College of City Univ of New York, USA. Stokes Shift Spectroscopy (S3) and imaging offer a novel way to rapidly measure spectral fingerprints of fluorophores in tissue, which highlights the difference of cancerous and normal tissues.

BW1B.7 • 09:45

Using Raman Spectroscopy to Characterize Bone Metastasis and to Evaluate Treatment Response in Prostate Cancer Patients, Xiaohong Bi¹, Jeffrey Nyman², Colm Morrissey³, Martine Roudier³, Alexander Dowell³, Anita Mahadevan-Jansen¹; ¹BIOMEDical Engineering, Vanderbilt Univ., USA; ²Orthopaedics and Rehab, Vanderbilt Univ., USA; ³Urology, Univ. of Washington, USA. Raman spectroscopy was applied in this study to investigate the structure and composition of metastatic bone from prostate patients. The ultimate goal is to identify spectral features related to cancer and treatment induced bone changes.

DW1C.6 • 09:30

Three-dimensional scanning microscopy through turbid media, Xin Yang¹, Chia-Lung Hsieh^{1,2}, Ye Pu¹, Demetri Psaltis¹; ¹Optics Laboratory, École Polytechnique Fédérale de Lausanne, Switzerland; ²Electrical Engineering, California Inst. of Technology, USA. We demonstrate three-dimensional imaging through turbid medium with digital phase conjugation of second harmonic signal emitted from a nanoparticle. Accurate three-dimensional images of a fluorescent sample placed behind a turbid medium are obtained.

DW1C.7 • 09:45

A Proposal for Astronomical Adaptive Optics by Incoherent Digital Holography, Myung K. Kim¹; ¹Physics, Univ of South Florida, USA. A new type of adaptive optics system is proposed for astronomical imaging. It replaces the wavefront sensing and modulation hardware of conventional adaptive optics with numerical processing capabilities of digital holography of incoherent sources.

Symphony I & II

Symphony III

Symphony IV

BIOMED I

BIOMED 2

DH

10:00—10:30

COFFEE BREAK, *Concerto A,B,C*

10:30 - 12:30

BW2A • Optical Coherence Tomography: Technology and Applications

Robert Huber; Ludwig-Maximilians-Universität München Germany; Michael Pircher; Medical Univ. of Vienna, Austria, Presiders

BW2A.1 • 10:30

Interferometric Synthetic Aperture Microscopy with Computational Adaptive Optics for High-Resolution Tomography of Scattering Tissue, Steven Adie¹, Adeel Ahmad², Nathan Shemonski¹, Benedikt Graf¹, Heeseok Kim¹, Wen-Mei Hwu¹, P. Scott Carney¹, Stephen Boppart¹; ¹University of Illinois at Urbana-Champaign, USA. We demonstrate interferometric synthetic aperture microscopy (ISAM) with post-acquisition computational aberration correction in scattering tissue, GPU-based 2D ISAM at 75 frames per second and pseudo-3D ISAM without the use of phase correction.

BW2A.2 • 10:45

Dual-Band FDML laser for Swept Source Spectroscopic OCT, Rui Zhu¹, Jianbing Xu¹, Edmund Y. Lam¹, Kenneth K. Wong¹; ¹Electrical and Electronic Engineering, The Univ. of Hong Kong, Hong Kong. We report a synchronized dual-band-swept, Fourier domain mode locking (FDML) laser with sweeping rate of 97.6 kHz. It is the first time to achieve spectroscopic OCT based on dual-band FDML swept laser.

BW2A.3 • 11:00

Pump-probe optical coherence tomography imaging of Zenopus tadpole vasculature ex vivo, Oscar Carrasco-Zevallos¹, Ryan L. Shelton¹, Brian E. Applegate¹; ¹BIOMEDICAL Engineering, Texas A&M, USA. We present a novel Pump-Probe Optical Coherence Tomography (PPOCT) system, capable of imaging both methylene blue and hemoglobin. Ex vivo images of Zenopus tadpole vasculature were obtained using hemoglobin as the contrast agent.

BW2A.4 • 11:15

Monitoring Electric Current in Biological Tissues by Optical Coherence Tomography, Krzysztof Wawrzyn¹, Barry Vuong², Mark K. Harduar², Victor X. D. Yang^{2,3}, Valentin Demidov¹, Vladislav Toronov¹, Yuan Xu¹; ¹Department of Physics, Ryerson Univ., Canada; ²Department of Electrical and Computer Engineering, Ryerson Univ., Canada; ³Division of Neurosurgery, Univ. of Toronto, Canada. The capability of optical coherent tomography (OCT) to detect changes induced by physiological level electric field in biological tissue is demonstrated. The suggested method can potentially image the electro-kinetic properties of tissues with OCT.

10:30 - 12:30

BW2B • Spectroscopy of Elastic Light Scattering I

Vadim Backman; Northwestern Univ., USA, Presider

BW2B.1 • 10:30

Invited

Quantitative Monitoring of Apoptosis in Viable Cells with Elastic Scattering Spectroscopy, Irving J. Bigio¹, Christine Mulvey¹; ¹Boston Univ., USA. Programmed cell death, apoptosis, entails a sequence of subcellular ultrastructure changes, which are monitored with elastic scattering spectroscopy. Changes are sensed earlier than possible by standard assays, invoking structures beneath the optical resolution limit.

BW2B.2 • 11:00

Measurement of the spatial backscattering impulse-response in colon field carcinogenesis using enhanced backscattering spectroscopy, Andrew J. Radosevich¹, Nikhil N. Mutyal¹, Jeremy D. Rogers¹, Sudeep Upadhye², Andrej Bogojevic², Hemant K. Roy², Vadim Backman¹; ¹BIOMEDICAL Engineering, Northwestern Univ., USA; ²Department of Gastroenterology, Northshore Univ. Healthsystems, USA. Optical tissue characterization in field carcinogenesis elucidates the mechanisms behind cancer development. Here we compute the backscattering impulse-response at subdiffusion lengthscales in colon biopsies with enhanced backscattering spectroscopy.

BW2B.3 • 11:15

Determination of Tissue Optical Properties by Interstitial Spectroscopy Using a Custom Fiber Optic Probe, Timothy M. Baran¹, Thomas H. Foster^{1,2}; ¹Inst. of Optics, Univ. of Rochester, USA; ²Imaging Sciences, Univ. of Rochester, USA. We demonstrate a means for determination of tissue optical properties using a single interstitial optical probe. The probe contains a helical array of six side-firing fibers in an assembly that fits through an 18-gauge needle.

10:30 - 12:30

DW2C • BIOMEDICAL Applications of Digital Holography II

Claude Boccara; Institut Langevin, France, Presider

DW2C.1 • 10:30

Invited

Cell Dynamics Studied by Quantitative Phase Imaging, Gabriel Popescu¹; ¹Beckman Inst., Univ of Illinois at Urbana-Champaign, USA. We examine intracellular traffic using spatial light interference microscopy (SLIM). The dispersion relation, i.e. decay rate vs. spatial mode, reveals that the mass transport is diffusive at short scales and deterministic at long scales.

DW2C.2 • 11:00

Invited

Digital Holography for the Life Sciences, Gert von Bally¹, Bjoern Kemper¹; ¹Center for BIOMEDICAL Optics and Photonics, Westfälische Wilhelms Univ. Münster, Germany. In the life sciences digital holographic microscopy provides high resolving, on-line, label-free, quantitative, multi-focus phase contrast imaging for the analysis of morphology dynamics and migration tracking in living cells.

Symphony I & II

BIOMED I

BW2A • Optical Coherence Tomography: Technology and Applications—Continue

BW2A.5 • 11:30

Quantitative Optical Imaging of Vascular Structure and Function in a Model of Peripheral Arterial Disease, Kristin M. Poole¹, Craig Duvall¹, Melissa C. Skala¹; ¹*BIOMEDical Engineering, Vanderbilt Univ., USA*. Optical coherence tomography and hyperspectral imaging were used to monitor the vascular response to hind limb ischemia. Measurements showed increases in collateral vessel formation and hemoglobin saturation consistent with existing techniques.

BW2A.6 • 11:45

Snapshot 3D Optical Coherence Tomography System using Image Mapping Spectrometer, Thuc-Uyen Nguyen¹, Nathan Hagen¹, Liang Gao¹, Tomasz Tkaczyk¹; ¹*Bioengineering, Rice Univ., USA*. A snapshot 3D Optical Coherence Tomography system was developed using Image Mapping Spectrometry. This proof-of-concept system can give depth profile at different spatial points in one snapshot to reduce motion artifact and enhance throughput.

BW2A.7 • 12:00

Assessing Nanoparticle Concentration Using MET-RiCS Optical Coherence Tomography, You Li¹, Francisco Robles^{1,2}, Kevin Seekell¹, Adam Wax¹; ¹*BIO-MEDical Engineering, Duke Univ., USA*; ²*Medical Physics Program, Duke Univ., USA*. We have recently developed METRiCS OCT to provide spatially resolved molecular information of chromosomes. Here we apply this method to measure the extinction spectra of nanoparticles at various concentrations for potential in vivo applications.

BW2A.8 • 12:15

Study on Non-invasive Micro-mechanical Biopsy using 3-Dimensional Optical Coherence Strainography, Yuki Ishii¹, Saeki Souichi¹; ¹*Yamaguchi Univ., Japan*. Authors have developed 3D-OCSA, which visualize tissue micromechanics using OCT. In this study, this was ex vivo applied to atherosclerotic plaque. Consequently, 3D-OCSA was clarified to be clinically effective as Micro-Mechanical Biopsy.

Symphony III

BIOMED 2

BW2B • Spectroscopy of Elastic Light Scattering - Continue

BW2B.4 • 11:30

Optical Spectral Imaging For Breast Margin Assessment: A Comprehensive Assessment of Sources of Contrast, Torre M. Bydlon¹, J. Quincy Brown¹, Stephanie Kennedy¹, Jennifer E. Gallagher¹, Matthew Caldwell¹, Marlee Junker¹, Lee G. Wilke², William T. Barry¹, Joseph Geradts¹, Nimmi Ramanujam¹; ¹*Duke Univ., USA*; ²*Univ. of Wisconsin School of Medicine and Public Health, USA*. Achieving tumor-free margins is desired to avoid recurrence. Diffuse reflectance imaging can assess margin status; however, understanding kinetics, cautery, and patient variability is needed to exploit optical contrast to detect positive margins.

BW2B.5 • 11:45

Measurements of tissue scattering properties using multi-diameter single fiber reflectance spectroscopy: experimental validation, Ute A. Gamm¹, Stephen C. Kanick¹, Dominic J. Robinson¹, Henricus J. Sterenborg¹, Arjen Amelink¹; ¹*Center for Optical Diagnostics and Therapy, Erasmus Medical Center, Netherlands*. MDSFR spectroscopy is a method that allows the quantification of μ_s 's and the phase function parameter γ . We are presenting an experimental validation of this method based on phantoms containing polystyrene spheres and show preliminary in vivo data.

BW2B.6 • 12:00

Label-Free Spectroscopic Identification of Fetal Nucleated Red Blood Cells from Maternal Blood, Vladimir Turzhitsky¹, Le Qiu¹, Lianyu Guo¹, Edward Vitkin¹, Eugene Hanlon¹, Irving Itzkan¹, Kee-Hak Lim¹, Lev T. Perelman¹; ¹*Center for Advanced BIOMEDical Imaging and Photonics, Harvard Univ., USA*. We present a spectroscopic microscopy system for measuring transmission and reflectance from erythrocytes. Spectroscopic markers are used to distinguish between fetal and adult cells for the application of genetic screening from maternal blood.

BW2B.7 • 12:15

Characterizing Intracellular Structural Dynamics with Optical Gabor Filtering, Heidi Sierra¹, Nada Boustany¹; ¹*BIOMEDical Engineering, Rutgers University, USA*. Optical Gabor filtering provides a linear measure of local object structure. We demonstrate the ability of this method to quantify directly object structure in a diatom, and present structural dynamics data in individual living cells.

Symphony IV

DH

DW2C • BIOMEDical Applications of Digital Holography II—Continue

DW2C.3 • 11:30

Dynamic of a vesicle suspension under shear flow by digital holographic microscopy, Minetti Christophe¹, Frank Dubois¹, Podgorski Thomas², Coupier Gwennou²; ¹*Ecole Polytechnique, Université libre de Bruxelles, Belgium*; ²*Laboratoire de Spectrométrie Physique, Université Joseph Fourier, France*. Vesicles are simplified models of living cells such as red blood cells. Hydrodynamical effects lead to a specific structure of the suspension that is analyzed by digital holographic microscopy on earth and in microgravity conditions.

DW2C.4 • 11:45

Digital Holographic Oscope for the study of biomechanical properties of eardrum, Mauricio Flores-Moreno¹, Fernando Mendoza Santoyo¹, Cosme Furlong^{2,3}, John Rosowski^{3,4}; ¹*Optics division, Centro de Investigaciones en Optica, Mexico*; ²*Mechanical department, Worcester Polytechnic Inst., USA*; ³*Eaton-Peabody Laboratory, Massachusetts Eye and Ear Infirmary, USA*; ⁴*MIT-Harvard division of Health Sciences and Technology, USA*. A Digital Holographic system is used at clinic to study biomechanics properties of tympanic membranes; differences between the DH techniques used for digital recording and numerical reconstruction are discussed.

DW2C.5 • 12:00

Field-Portable Pixel Super-Resolution Microscopy of Dense Samples using Lensfree Holograms Recorded at Multiple Heights, Alon Greenbaum¹, Uzair Sikora¹, Aydogan Ozcan^{1,2}; ¹*Electrical Engineering, Univ. of California, Los Angeles, USA*; ²*Bioengineering, Univ. of California, Los Angeles, USA*. By capturing lensfree in-line holograms of objects at multiple heights, phase and amplitude images of dense specimens (e.g. Papanicolaou smears) can be iteratively reconstructed over a large field-of-view (~30 mm²) with sub-micron resolution.

Symphony I & II

BIOMED I

Symphony III


BIOMED 2

Symphony IV


DH

12:15—13:30


LUNCH ON YOUR OWN

13:30 - 15:30 **BW3A • Breast Cancer Imaging**


Ilya Turchin; *Inst. of Applied Physics of the Russian Academy of Sciences, Russian Federation, President*

BW3A.1 • 13:30 **Invited** 

Near-infrared Imaging of Breast Cancer Using Intrinsic and Extrinsic Contrast Agents, Alexander Poellinger¹; ¹*Radiology, Charité, Germany*. Breast cancer is the most common malignancy among women in industrialized countries. Optical imaging using intrinsic and extrinsic contrasts is a promising technique for breast cancer detection and differentiation between benign and malignant breast lesions.

BW3A.2 • 14:00 

Joint image reconstruction for breast tumor diagnosis using both structural and functional information, Qianqian Fang¹, Stefan Carp¹, Mark Martino¹, Richard H. Moore², Daniel B. Kopans², David Boas¹; ¹*Athinoula A. Martinos Center for BIOMEDical Imaging, Massachusetts General Hospital, USA*; ²*Dept. of Radiology, Massachusetts General Hospital, USA*. We explore structural-prior-guided optical image reconstructions using a clinical population presenting breast lesions. We extend our algorithm with addition of tumor priors. This results in dramatic improvement in optical contrast of malignancy.

BW3A.3 • 14:15 

Nine-Wavelength Spectroscopy Guided by Magnetic Resonance Imaging Improves Breast Cancer Characterization, Michael A. Mastanduno¹, Shudong Jiang¹, Roberta diFlorio-Alexander², Brian Pogue¹, Keith D. Paulsen^{1,2}; ¹*Dartmouth College, USA*; ²*Department of Diagnostic Radiology, Dartmouth Hitchcock Medical Center, USA*. Combining nine discrete wavelengths for NIR Spectroscopy with MRI allows quantitative estimation of breast cancers in contrast scans. Combinations of PMT and spectrometers are used with validation in phantoms, normal subjects and pilot human cancers.

13:30 - 15:30

BW3B • Spectroscopy of Elastic Light Scattering II

Young Kim; *Purdue Univ., USA, President*

BW3B.1 • 13:30 **Invited**

Multi-spectral Morphology Scanning for Margin Detection in Breast Surgery, Brian Pogue¹, Ashley Laughney¹, Venkataramanan Krishnaswamy¹, Wendy Wells¹, Keith D. Paulsen¹; ¹*Engineering, Dartmouth College, USA*. A scanning full-spectrum imaging system was used to image and analyze the spectral morphology of resected breast cancer specimens, to evaluate the optimum parameters from which to diagnose involvement of cancer in the margins.

BW3B.2 • 14:00

Challenging the use of Intralipid as a scattering standard in tissue simulating phantoms measured by non-diffuse reflectance spectroscopy: the critical influence of scattering phase function, Stephen C. Kanick¹, Venkataramanan Krishnaswamy¹, Brian Pogue¹; ¹*Thayer School of Engineering, Dartmouth College, USA*. This study shows the influence that the scattering phase function of Intralipid has on reflectance spectra. Significant spectral remission changes result from simply changing the reflectance probe geometries utilized in tissue spectroscopy research.

BW3B.3 • 14:15

Scattering anisotropy as an imaging contrast for tissue organization in mesoscopic imaging, Zhengbin Xu¹, Ally-Khan Somani², Young Kim¹; ¹*Weldon School of BIOMEDical Engineering, Purdue Univ., USA*; ²*Department of Dermatology, Indiana Univ. School of Medicine, USA*. We report the utilization of tissue scattering anisotropy as an intrinsic imaging contrast. This could potentially be used to probe tissue architecture and organization for mesoscopic (between microscopic and macroscopic) imaging settings.

13:30 - 15:30

DW3C • Digital Holographic Microscopy III

Gert von Bally; *Westfaelische Wilhelms Univ. Munster, Germany, President*

DW3C.1 • 13:30 **Invited**

3D Tracking of the Brownian Motion of Polystyrene Beads with DHM, Dug Young Kim¹, Yoosung Bae²; ¹*Physics, Yonsei Univ., Republic of Korea*; ²*Information & Communications, GIST, Republic of Korea*. Three dimensional particle tracking is useful technology to characterize live cell or surrounding environment by tracing small particles. We present a novel technique to find the 3D position of a 2 micrometer bead by using DHM.

DW3C.2 • 14:00

Single-shot full field imaging in a dual-wavelength digital holographic microscope, Christophe Moser¹, Zahra Monemhaghdoost¹, Frederic Monfort³, Yves Emery³, Christian Depierreux²; ²*School of Engineering, LAPD, EPFL, Switzerland*; ³*School of Engineering, LOA, EPFL, Switzerland*; ³*LynceeTec, Switzerland*. We demonstrate volume diffractive structures to manipulate the coherence plane tilt at several two simultaneously to achieve full field 3D imaging in a low coherence digital off-axis holographic microscope (DHM) in a single shot.

DW3C.3 • 14:15

Studies on Digital Holographic Tomography, Anand Asundi¹, Wenjing Zhou², Wentao Hu²; ¹*School of Mechanical & Aerospace Engineering, Nanyang Technological Univ., Singapore*; ²*Precision Mechanical Engineering, Shanghai Univ., China*. In experiment, a section of optical fiber is used to be the tested object. It has parabola refraction index characteristic and symmetry 3D structure.

Symphony I & II

BIOMED I

BW3A • Breast Cancer Imaging—Continue

BW3A.4 • 14:30

Optical Assessment of Breast Density and its Dependence on Tissue Heterogeneity, Paola Taroni^{1,2}, Antonio Pifferi^{1,2}, Giovanna Quarto¹, Lorenzo Spinelli², Alessandro Torricelli¹, Francesca Abbate³, Nicola Balestreri⁴, Simona Menna³, Enrico Cassano³, Rinaldo Cubeddu^{1,2}, ¹Department of Physics, Politecnico di Milano, Italy; ²CNR-Istituto di Fotonica e Nanotecnologie, Italy; ³Breast Imaging Unit, European Inst. of Oncology, Italy; ⁴Department of Radiology, European Inst. of Oncology, Italy. The optical assessment of breast density was effectively performed using time domain 7-wavelength (635-1060 nm) optical mammography. Notwithstanding tissue heterogeneity, BI-RADS categories can be discriminated even with a single point measurement.

BW3A.5 • 14:45

Early Changes in Breast Cancer Blood Flow due to Chemotherapy: Potential Predictor for Therapeutic Efficacy, Regine Choe¹, Turgut Durduran^{2,4}, David R. Busch³, So Hyun Chung³, Saurav Pathak³, Han Y. Ban³, Ellen K. Foster³, Tiffany Aversa³, Erin M. Buckley³, Meeri N. Kim³, Carolyn Mies⁴, Mark A. Rosen⁴, Mitchell D. Schnall⁴, Angela DeMichele⁴, Arjun G. Yodh³, ¹BIOMEDical Engineering, Univ. of Rochester, USA; ²ICFO, Spain; ³Physics & Astronomy, Univ. of Pennsylvania, USA; ⁴Hospital of the Univ. of Pennsylvania, USA. Preliminary results on human subjects with breast cancer undergoing neoadjuvant chemotherapy suggest early changes in blood flow measured with diffuse correlation spectroscopy may serve as a potential predictor for therapeutic efficacy.

BW3A.6 • 15:00

Diffuse Optical Tomography Imaging System for Monitoring Breast Tumor Response to Neoadjuvant Chemotherapy, Jacqueline E. Gunther¹, Molly Flexman¹, Emerson Lim², Hyun K. Kim¹, Mindy Brown⁴, Dawn Hershman^{2,4}, Andreas H. Hielscher^{1,3}, ¹BIOMEDical Engineering, Columbia Univ., USA; ²Department of Internal Medicine, Columbia Univ., USA; ³Department of Radiology, Columbia Univ., USA; ⁴Herbert Irving Comprehensive Cancer Center, USA. We developed a diffuse optical tomography (DOT) system that can be used to perform longitudinal studies of breast tumors during neoadjuvant chemotherapy. Preliminary results demonstrate that DOT can image early tumor vascular response to treatment.

BW3A.7 • 15:15

Neoadjuvant Chemotherapy Monitoring using Dynamic Breast Compression Imaging, Stefan Carp¹, Christy M. Wanyo¹, Qianqian Fang¹, David Boas¹, Steven J. Isakoff², ¹Radiology / Martinos Center, Massachusetts General Hospital, USA; ²Gillette Breast Cancer Center, Massachusetts General Hospital, USA. We use diffuse optical breast tomography during fractional mammographic compression to monitor neoadjuvant chemotherapy response. Preliminary results show static and dynamic measurements are sensitive to therapy induced changes in breast cancer.

Symphony III

BIOMED 2

BW3B • Spectroscopy of Elastic Light Scattering II—Continue

BW3B.4 • 14:30

Rapid Determination of Tissue Hemoglobin Concentration and Oxygen Saturation of Head and Neck Cancers for Global Health Applications, Fangyao Hu¹, Karhik Vishwanath¹, Janelle E. Phelps¹, Justin Lo¹, Walter T. Lee^{2,3}, Nimmi Ramanujam¹, ¹BIOMEDical Engineering, Duke Univ., USA; ²Division of Otolaryngology-Head and Neck Surgery, Duke Univ. Medical Center, USA; ³Section of Otolaryngology-Head and Neck Surgery, Veterans Administration Medical Center, USA. A ratiometric method for quantitative estimation of tissue hemoglobin concentration and oxygen-saturation is presented. A 600X speed-up was achieved on clinical diffuse reflectance data relative to an inverse Monte Carlo with comparable accuracy.

BW3B.5 • 14:45

Within Vessel Multiple Sequential Scattering Sensitive Diffuse Correlation Spectroscopy Measurements to Erythrocyte Shear Induced Diffusion, Stefan Carp¹, Sava Sakadzic¹, Vivek J. Srinivasan¹, Nadege Roche-Labarbe², Maria Angela Franceschini¹, David Boas¹, ¹Radiology / Martinos Center, Massachusetts General Hospital, USA; ²Universite de Caen, France. We suggest that scatterer motion measured using diffuse correlation spectroscopy is substantially related to shear induced erythrocyte diffusion in the blood flow frame of reference, due to multiple sequential scattering events in most vessels.

BW3B.6 • 15:00

The Mapping of Tissues Scattering Properties on the Poincaré Sphere, Igor Meglinski¹, Callum Macdonald¹, Anthony Karl¹, Han-Seung Yoon², Michael Eccles², ¹Department of Physics, Univ. of Otago, New Zealand; ²Department of Pathology, Univ. of Otago, New Zealand. By tracking the state of polarization on the Poincaré sphere the scattering of circular polarized light has been exploited to point out properties of biological tissues, including cancerous tissues.

BW3B.7 • 15:15

The Correlation between Side Scattering and Internal Structures of Mammalian Cells with and without Acetic Acid Exposure, Judith R. Mourant¹, Oana C. Marina¹, Claire K. Sanders¹, ¹Bioscience, LANL, USA. The contribution of different cell constituents to side scatter is determined for mammalian cells with and without 0.6% acetic acid. Contributions depend on the polarization of the incident light and on exposure to acetic acid.

Symphony IV

DH

DW3C • Digital Holographic Microscopy III - Continue

DW3C.4 • 14:30

Short-Coherence Off-Axis Holographic Microscopy of Live Cell Dynamics, Stefan Witte^{1,2}, Andrius Plauska¹, Marloes L. Groot^{1,2}, ¹LaserLaB, VU Univ., Netherlands; ²Neuroscience Campus Amsterdam, VU Univ., Netherlands. We demonstrate single-shot holographic microscopy that combines ultrashort pulses with an off-axis geometry through a controlled pulse front tilt. Quantitative phase images of cells are obtained, and osmotic swelling of HEK293 cells is studied.

DW3C.5 • 14:45

High-speed 4-D biological microscope based on parallel phase-shifting digital holography, Tatsuki Tahara¹, Ryosuke Yonesaka¹, Seiji Yamamoto¹, Takashi Kakue¹, Peng Xia¹, Yasuhiro Awatsuji¹, Kenzo Nishio², Shogo Ura¹, Toshihiro Kubota³, Osamu Matoba⁴, ¹Graduate school of Science and Technology, Kyoto Inst. of Technology, Japan; ²Advanced Technology Center, Kyoto Inst. of Technology, Japan; ³Kubota Holography Laboratory Corporation, Japan; ⁴Graduate School of System Informatics, Kobe Univ., Japan. We constructed a high-speed four-dimensional (4-D) microscope for dynamically moving biological specimens. By use of parallel phase-shifting digital holography, 3-D behavior and phase distribution were captured at 150,000 frames-per-second.

DW3C.6 • 15:00

Heterodyne digital holography study of plasmonic nanoantennas, Sarah Y. Suck¹, Ariadna Martinez Marrades¹, Stéphane Collin², Nathalie Bardou², Yannick De Wilde¹, Gilles Tessier¹, ¹ESPCI - Institut Langevin, France; ²Laboratoire Photonique et Nanostructures, France. Optical nanoantennas convert near field to directional far-field radiation. Digital holography allows the characterization of the 3D directivity of scattering antennas, but also reveals heating induced by near field plasmonic confinement

Symphony I & II

Symphony III

Symphony IV

BIOMED I

BIOMED 2

DH

15:30—16:00

COFFEE BREAK, *Concerto Ballroom*

16:00 - 18:00

BW4A • TomographyHamid Dehghani; *Univ. of Birmingham, UK, Presider***BW4A.1 • 16:00**

Fast 3D Optical Mammography using ICG Dynamics for Reader Independent Lesion Differentiation, Sophie K. Piper¹, Paul Schneider², Nassia Volkwein², Nils Schreiter², Alexander Poellinger², Christoph H. Schmitz^{1,3}; ¹*Department of Neurology, Charité Berlin, Germany*; ²*Department of Radiology, Charité Berlin, Germany*; ³*NIRx Medizintechnik GmbH, Germany*. Based on ICG bolus kinetics of the absorption changes in the reconstructed DOT images in suspicious lesion bearing breasts, we derived a reader independent classification between malignant and benign lesions with high sensitivity and specificity.

BW4A.2 • 16:15 Invited

Wide-field Time Resolved Optical Tomography, Xavier Intes¹; ¹*RPI Rensselaer Polytechnic Inst., USA*. Abstract not available.

16:00 - 18:00

BW4B • New Spectroscopic Techniques and Applications**BW4B.1 • 16:00**

Noninvasive optical imaging and spectroscopy for quantitative monitoring of the progression of oral premalignant lesions, Sharon Mondrik¹, Richard A. Schwarz¹, Mark C. Pierce², Wen Gao¹, Mary K. Quinn¹, Vijayashree Bhattar³, Michelle D. Williams³, Nadarajah Vigneswaran⁴, Ann M. Gillenwater³, Rebecca Richards-Kortum¹; ¹*Bioengineering, Rice Univ., USA*; ²*BIOMEDICAL Engineering, Rutgers Univ., USA*; ³*Univ. of Texas M. D. Anderson Cancer Center, USA*; ⁴*Univ. of Texas Dental Branch at Houston, USA*. Interim results are presented from a longitudinal study in which optical imaging and spectroscopy are used to monitor progression of oral premalignant lesions. A total of 447 sites in 120 patients were tracked over time.

BW4B.2 • 16:15

Development of Spatial Frequency Domain Instrument for the Quantification of Layer Specific Optical Properties of Pigmented Lesions, Rolf B. Saege¹, Kendrew Au¹, Kristen M. Kelly², Anthony J. Durkin¹; ¹*Beckman Laser Inst., Univ. of California - Irvine, USA*; ²*Dermatology, Univ. of California - Irvine, USA*. A clinical, spatially modulated quantitative spectroscopy (SMoQS) instrument has been designed and deployed to evaluate its ability to quantitatively isolate layer-specific optical properties of pigmented lesions in skin in vivo.

BW4B.3 • 16:30

Validation of a Monte Carlo Model for Determination of Fluorophore Concentration on Scattering Media, Paulo R. Bargo¹, Steven L. Jacques², Scott A. Prah³; ¹*Johnson & Johnson Consumer Companies, USA*; ²*Oregon Health & Sciences Univ., USA*; ³*Oregon Medical Laser Center, USA*. Experimental validation of a Monte Carlo code for correcting the effect of optical properties on fluorescence measurements is presented. The error for predicting true concentration was 4% and 10% for absorbing-only and turbid samples, respectively.

16:00 - 18:00

DW4C • Special Techniques of Digital Holography IIIYi-Pai Huang; *National Chiao Tung Univ., Taiwan, Presider***DW4C.1 • 16:00 Invited**

Digital Holographic Interferometry and ESPI at Long Infrared Wavelengths with CO₂ Lasers, Marc Georges¹, Jean-François Vandenberg¹, Cedric Thizy¹, Frank Dubois², Patrick Queeckaert², Dominic Doyle³, Igor Alexeenko⁴, Giancarlo Pedrini⁴, Wolfgang Osten⁴; ¹*Centre Spatial de Liege, Universite de Liege, Belgium*; ²*Microgravity Research Center, Universite Libre de Bruxelles, Belgium*; ³*ESTEC, ESA, Netherlands*; ⁴*Institut für Technische Optik, Universität Stuttgart, Germany*. Holography and speckle techniques for various metrology and non destructive applications were developed in the 10 μm wavelength range allowing large displacements measurement. Other specific advantages are emphasized like combining temperature and displacement measurement.

DW4C.2 • 16:30

Combination of recording wavelengths for improvement of color reproduction of color digital holography using spectral estimation, Peng Xia¹, Yasunori Ito¹, Yuki Shimoza¹, Tatsuki Tahara¹, Takashi Kakue¹, Yasuhiro Awatsuji¹, Shogo Ura¹, Kenzo Nishio², Toshihiro Kubota³, Osamu Matoba⁴; ¹*Graduate School of Science and Technology, Kyoto Inst. of Technology, Japan*; ²*Advanced Technology Center, Kyoto Inst. of Technology, Japan*; ³*Kubota Holography Laboratory Corporation, Japan*; ⁴*Graduate School of System Informatics, Kobe Univ., Japan*. We propose a combination of recording wavelengths of color digital holography using spectral estimation for improvement of color reproduction, and numerically confirmed that the color differences were greatly reduced by the combination.

Symphony I & II

BIOMED I

BW4A • Tomography—Continue

BW4A.3 • 16:41

Tomographic Fluorescence Lifetime Imaging, Scott B. Raymond¹, Craig J. Goergen¹, Alexei Bogdanov², David J. Sosnovik¹, Anand T. Kumar¹; ¹*Radiology, Mass General Hospital, USA*; ²*Radiology, Univ. of Massachusetts Medical School, USA*. We present theory and methods for in vivo diffuse time domain fluorescence lifetime tomography. As examples, we will discuss in vivo lifetime imaging of both targeted and activatable probes in mouse models of cardiac disease and cancer.

BW4A.4 • 17:01

Virtual Source Patterns for Fluorescence Tomography, Gianluca Valentini¹, Nicolas Ducros¹, Andrea Bassi¹, Cosimo D'Andrea^{1,2}, Martin Schweiger³, Simon R. Arridge³; ¹*Department of Physics, Politecnico di Milano, Italy*; ²*Italian Inst. of Technology, Italy*; ³*Centre for Medical Image Computing, Univ. College London, Italy*. A novel method, named virtual source patterns method, is introduced to allow negative intensities in a pattern-based approach for fluorescence molecular tomography

BW4A.5 • 17:11

Fluorescence Optical Tomography of Preclinical Glioma Models Using Spatial Frequency Domain Imaging, Soren D. Konecky¹, Chris M. Owen², Tyler Rice¹, Pablo A. Valdes^{3,4}, Kolbein Kolste⁴, Brian C. Wilson⁵, Fredric Leblond⁴, David W. Roberts³, Keith D. Paulsen⁴, Bruce J. Tromberg¹; ¹*Beckman Laser Inst. and Medical Clinic, Univ. of California - Irvine, USA*; ²*Department of Neurological Surgery, Univ. of California - Irvine, USA*; ³*Section of Neurosurgery, Dartmouth-Hitchcock Medical Center, USA*; ⁴*Thayer School of Engineering, Dartmouth College, USA*; ⁵*Univ. of Toronto/Ontario Cancer Inst., Canada*. Spatial frequency domain imaging of 5-aminolevulinic acid induced protoporphyrin IX was used to recover absorption, scattering, and fluorescence properties of glioblastoma multiforme in tissue-simulating phantoms and in vivo in a mouse model.

Symphony III

BIOMED 2

BW4B • New Spectroscopic Techniques and Applications—Continue

BW4B.4 • 16:45

Diffuse Correlation Spectroscopy for Flow Assessment & Management of Acute Ischemic Stroke, Rickson C. Mesquita^{1,2}, Steven S. Schenkel², Turgut Durduran³, Christopher G. Favilla⁴, Meeri N. Kim², David L. Minkoff², Michael Mullen⁴, Joel H. Greenberg⁴, John A. Detre^{4,5}, Scott E. Kasner⁴, Arjun G. Yodh²; ¹*Inst. of Physics, Univ. of Campinas, Brazil*; ²*Department of Physics & Astronomy, Univ. of Pennsylvania, USA*; ³*ICFO - Institut de Ciències Fotòniques, Mediterranean Technology Park, Spain*; ⁴*Department of Neurology, Univ. of Pennsylvania, USA*; ⁵*Department of Radiology, Univ. of Pennsylvania, USA*. We used diffuse correlation spectroscopy to assess cerebral autoregulation in acute ischemic stroke patients. Larger perfusion changes were observed in the infarcted hemisphere, and a novel relationship between perfusion and NIHSS was discovered.

BW4B.5 • 17:00

Time-gated Cherenkov emission spectroscopy from linear accelerator irradiation of tissue phantoms, Rongxiao Zhang¹, Adam Glaser¹, Scott Davis¹, David Gladstone², Brian Pogue^{1,3}; ¹*Thayer School of Engineering, Dartmouth College, USA*; ²*Norris Cotton Cancer Center, Dartmouth-Hitchcock Medical Center, USA*; ³*Department of Physics and Astronomy, Dartmouth College, USA*. A time-gated-acquisition method is introduced to measure the Cherenkov emission from linear accelerator (LINAC) in tissue mimic phantom and shown to be an effective way to enhance the intensity of the Cherenkov emission over the ambient light.

BW4B.6 • 17:15

Effect of cerebral cortex sulci on near-infrared light propagation during monitoring and treatment, Ting Li^{1,2}, Qingming Luo³, Steven L. Jacques^{1,4}; ¹*Department of BIOMEDical Engineering, Oregon Health and Science Univ., USA*; ²*Center of Neuro-Inf., Univ. of Electron. Sci. & Technol. of China, China*; ³*Britton Chance Center for BIOMEDical Photonics, Wuhan National Laboratory for Optoelectronics, Huazhong Univ. of Science and Technology, China*; ⁴*Department of Dermatology, Oregon Health and Science Univ., USA*. Central sulcus substantially affects NIRS/NIRI spatial sensitivity and LLLT fluence rate in the study of light transport within a high-resolution 3D anatomical head structure, allowing deeper penetration of light than previous models predicted.

Symphony IV

DH

DW4C • Special Techniques of Digital Holography III—Continue

DW4C.3 • 16:45

Improved axial resolution of digital holography via compressive reconstruction, Lei Tian¹, Yi Liu¹, George Barbastathis^{1,2}; ¹*Massachusetts Inst. of Technology, USA*; ²*Singapore-MIT Alliance for Research and Technology (SMART) Centre, Singapore*. We experimentally show that compressed sensing can improve the axial resolution of digital holography when the resolution is limited by the finite pixel pitch.

DW4C.4 • 17:00

Two dimensional sub-pixel movement detection using spiral phase filtering and compressive holography, Yi Liu¹, Lei Tian¹, Yuanhao Huang², George Barbastathis^{1,2}; ¹*MIT, USA*; ²*Singapore-MIT Alliance for Research and Technology (SMART) Centre, Singapore*. We present experimental results of using spiral phase filtering and compressive holography to quantify two-dimensional (2D) sub-pixel movement

DW4C.5 • 17:15

Coherent Depth Fusing Method for Phase-only Hologram Generation, Jisoo Hong¹, Jiwoon Yeom¹, Byoung-ho Lee¹; ¹*School of Electrical Engineering, Seoul National Univ., Republic of Korea*. Phase-only hologram generation method, which can overcome the maximum longitudinal sampling rate of iterative Fourier transform algorithm, is proposed based on the depth fusing method developed considering coherent imaging system.

Symphony I & II

Symphony III

Symphony IV

BIOMED I

BIOMED 2

DH

BW4A • Tomography—Continue

BW4B • New Spectroscopic Techniques and Applications—Continue

DW4C • Special Techniques of Digital Holography III—Continue

BW4A.6 • 17:30

Whole Body Fluorescence Imaging in Humans, Jan Mehnert^{1,2}, Sophie K. Piper¹, Christina Habermehl¹, Christoph H. Schmitz^{1,3}, Hellmuth Obrig^{2,4}, Jens Steinbrink^{1,5}; ¹Department of Neurology, Charité Univ. Medicine Berlin, Germany; ²Department of Neurology, Max Planck Inst. for Human Cognitive and Brain Sciences, Germany; ³NIRx Medizintechnik GmbH, Germany; ⁴Clinic of Cognitive Neurology, Univ. of Leipzig, Germany; ⁵Center for Stroke Research, Charité Univ. Medicine Berlin, Germany. Whole body fluorescence imaging was performed in two adult subjects following injection of ICG. Results show that bolus tracking is very well feasible in humans and might be used for studying peripheral vascular diseases.

BW4A.7 • 17:45

Multi-View, Multi-Spectral Bioluminescence Tomography, James A. Guggenheim^{1,2}, Hector R. Basevi^{1,2}, Iain B. Styles², Jon Frampton³, Hamid Dehghani^{1,2}; ¹PSIBS Doctoral Training Centre, College of Engineering and Physical Sciences, Univ. of Birmingham, UK; ²School of Computer Science, College of Engineering and Physical Sciences, Univ. of Birmingham, UK; ³School of Immunity and Infection, College of Medical and Dental Sciences, Univ. of Birmingham, UK. An automated, multi-view, spectral bioluminescence tomography system that utilises structured-light-based surface capture techniques along with a model-based approach to image reconstruction is presented.

BW4B.7 • 17:30

Polarized Multispectral Imaging in a Rigid Endoscope Based on Polarized Light Scattering Spectroscopy, Ji Qi^{1,2}, Barriere, Clement^{1,2}, Daniel S. Elson^{1,2}; ¹Hamlyn Centre for Robotic Surgery, Imperial College London, UK; ²Department of Surgery and Cancer, Imperial College London, UK. We investigate polarized multispectral endoscopic imaging to detect the micron-sized scatterers, tested with microspheres and animal livers. It is feasible to endoscopically image scatterer size with potential for in vivo diagnosis of dysplasia.

DW4C.7 • 17:45

Compressive Fresnel holography for object reconstruction through an occluding plane, Yair Rivenson¹, Alon Rot¹, Sergey Balber¹, Adrian Stern¹, Joseph Rosen¹; ¹Ben-Gurion Univ. of the Negev, Israel. We report the ability to recover a partially occluded object from its recorded Fresnel hologram, by adopting the compressive Fresnel holography framework.

DW4C.6 • 17:30

Some Considerations About the Role of the Diaphragm in Digital Image-Plane Holography, Pascal Picart^{1,3}, Mayssa Karray¹, Pierre Slangen²; ¹LAUM CNRS, France; ²EMA, France; ³ENSIM, France. This paper presents a theoretical and experimental comparison between digital Fresnel holography and digital image-plane holography. The role of the aperture diaphragm in image-plane holography is highlighted and some figures of merit are discussed

DW4C.7 • 17:45

Compressive Fresnel holography for object reconstruction through an occluding plane, Yair Rivenson¹, Alon Rot¹, Sergey Balber¹, Adrian Stern¹, Joseph Rosen¹; ¹Ben-Gurion Univ. of the Negev, Israel. We report the ability to recover a partially occluded object from its recorded Fresnel hologram, by adopting the compressive Fresnel holography framework.

18:00—18:15

BIOMED CLOSING REMARKS, Symphony I & II

18:00—18:15

DH CLOSING REMARKS, Symphony IV

Key to Authors and Presiders

(Bold denotes Presider or Presenting Author)

A

Abbate, Francesca-BW3A.4
 Achilefu, Sam-BM2A.6, BTu3A.24, BW1B.2
 Adibi, Ali-BTu3A.46
 Adie, Steven-BW2A.1
 Adler, Desmond C-BTu2B.2
 Aguinaga, Maria del Pilar-BSu3A.38
 Ahmad, Adeel-BTu3A.85, BW2A.1
 Ahmed, El Mallahi-DSu4C.3, DTu3C.1
 Ai, Xun-BSu3A.39
 Ajeti, Visar-BSu4B.1
 Akens, Margarete K-BSu3A.83
 Akers, Walter-BM2A.6, BW1B.2
 Akin, Ata, Dr.-BSu3A.63
 Akin, Ata-BSu3A.95
 Akins, Meredith L.-BSu3A.35
 Al abdi, Rabah M-BSu3A.91, BSu3A.92, BSu3A.94
 Alcalá-Ochoa, Noe-BTu3A.97
 Aleman, Karen-BSu3A.58
 Alexandrov, Sergey-BSu3A.61, BTu3A.57
 Alexeenko, Igor-DW4C.1
 Alfano, Robert R-BW1B.6, JM3A.45
 Allen, Jont B-BTu3A.78
 Altman, Ron-BSu3A.78
 Alverna, Tiffany A-JM3A.13
 Amelink, Arjen-BW2B.5
 Amyot, Franck-BSu3A.75, BSu3A.85, JM3A.46
 Anastasio, Mark-BSu3A.43
 Andersen, Peter-BTu2B.5
 Anderson, Pamela G-BSu3A.66
 Andersson-Engels, Stefan-BSu4A
 Andronica, Randall-BSu3A.93
 André, Raphael-BTu3A.90
 Antal, Péter-BSu3A.28
 Applegate, Brian E-BTu2A.8, BW2A.3
 Arbeit, Jeffrey-BSu3A.43
 Arce-Diego, Jose Luis-BSu3A.6
 Ardeshirpour, Yasaman-BM2A.3,
 BSu3A.75, BTu3A.24
 Arridge, Simon R-BTu3A.41, BTu3A.5, BW4A.4
 Ashok, Praveen Cheriyan-BTu3A.80, JM3A.26,
 JM3A.35
 Aslan, Serdar-BSu3A.95
 Assayag, Osnath-BTu3A.95
 Asundi, Anand-DW3C.3
 Atchia, Yaaseen-BTu3A.49
 Atkinson, E. N-BTu3A.25
 Atlan, Michael-JM3A.66
 Au, Kendrew-BW4B.2
 Averna, Tiffany-BW3A.5, JM3A.41
 Awatsuji, Yasuhiro-DW3C.5, DW4C.2
 Axelsson, Johan-JM3A.15
 Ayata, Cenk-BTu3A.28

B

Babacan, S. Derin-BM4B.2
 Backman, Vadim-BM4B.6, BTu3A.88, BW2B,
 BW2B.2, JM3A.47
 Bae, Yoonsung-DW3C.1
 Bahgat Shehata, Andrea-JM3A.16
 Bahram, Javidi-DSu2C.1
 Baig, Sarfaraz-DSu2C.6
 Bainbridge, Alan-JM3A.27, JM3A.6
 Baker, Wesley B-BM4A.8, JM3A.13
 Bakhtiar, Atieh-BSu3A.72
 Balagopal, Bavishna-JM3A.35
 Balber, Sergey-DW4C.7
 Balestreri, Nicola-BW3A.4

Ban, Han Y-BW3A.5
 Banaji, Murad-JM3A.32
 Banaszak Holl, Mark M-DSu3C.2
 Bandara, Abey-BSu3A.13
 Banerjee, Partha-DTu2C.1, DTu3C.3
 Barada, Daisuke-DSu1C.3, DTu3C.4, DTu4C.5
 Baraghis, Edward-BTu2A.7
 Baran, Timothy M-BW2B.3, JM3A.17
 Barbastathis, George-BSu3A.69, DSu2C.2, DSu3C.3,
 DTu1C.1, DTu3C.6, DW4C.3, DW4C.4, JM1A
 Barbour, Randall Locke-BM4A, BSu2A.1,
 BSu3A.88, BSu3A.91, BSu3A.92, BSu3A.93,
 BSu3A.94, BSu4A.4, JM3A.69
 Barbour, San-Lian S-BSu3A.93
 Bardou, Nathalie-DW3C.6
 Bargigia, Ilaria-JM3A.16, JM3A.5, JM3A.7
 Bargo, Paulo R-BW4B.3
 Baribeau, François-BW1A.6
 Barone, Frank C-BSu4A.4
 Barriere, Clement-BW4B.7
 Barry, William T-BW2B.4
 Barsi, Christopher-DTu1C.3
 Baselli, Giuseppe-BM4A.1
 Basevi, Hector RA-BSu3A.64, BW4A.7
 Bassi, Andrea-BW4A.4, JM3A.16
 Bauer, Adam Q-BM4A.7, BW1B.2
 Beard, Paul-BM2B.3
 Bedard, Noah-BSu3A.76
 Bednarz, Michael-BM4B.2
 Beerl, Michal-BTu3A.61
 Behrooz, Ali-BTu3A.35, BTu3A.46
 Belenky, Gregory-BM4A.4
 Ben-Yakar, Adela-BSu2B.8, BSu4B
 Bénazech-Lavoué, Magali-BW1A.6
 Bentz, Brian-BSu3A.60
 Benveniste, Ana-BTu3A.19
 Berger, Andrew-BTu3A.36
 Bergethon, Peter-BM4A.5
 Bérubé-Lauzière, Yves-BSu3A.68, BW1A.6
 Berzina, Anna-JM3A.44
 Bezerra, Hiram-BTu4B.5
 Bhaduri, Basanta-BSu3A.37
 Bhatia, Sanjiv-BSu2A.7
 Bhattar, Vijayashree-BW4B.1
 Bi, Renzhe-BTu3A.15, BTu3A.81, JM3A.48
 Bi, Xiaohong-BW1B.7, JM3A.43
 Bianchi, Anna Maria-BM4A.1
 Biedermann, Benjamin-BTu2B.5
 Bigio, Irving J-BW2B.1
 Bilfinger, Thomas V-JM3A.37
 Binding, Jonas-BTu3A.83
 Binzoni, Tiziano-JM3A.40
 Bista, Rajan K-BSu3A.61, BTu3A.57
 Blatter, Cedric-BTu4B.2
 Boyler, Martha-BTu3A.60
 Bloas, David-BSu2A.5, BSu3A.31, BSu3A.78,
 BSu3A.80, BSu3A.97, BTu3A.17, BTu3A.28, BW3A.2,
 BW3A.7, BW3B.5
 Boccara, Albert-Claude-BTu1A, DSu4C.1, DW2C,
 BTu3A.75, BTu3A.83, BTu3A.95, BTu4B.4
 Bodnar, Olha-BW1A.6
 Bogdanov, Alexei, Jr-BM2A.4, BW4A.3
 Bogojevic, Andrej-BW2B.2
 Boireau-Adamezyk, Elise-JM3A.42
 Bolinsay, Linden-BTu4A.8
 Bolz, Mathias-BTu3A.71
 Bolz, Mathias-BTu3A.91
 Bonesi, Marco-BTu2B.5

Boppart, Stephen-BTu3A.78, BTu3A.85, BW2A.1
 Boretsky, Adam R-BSu3A.17, BTu3A.73
 Botwicz, Marcin-BSu3A.81, BW1A.6
 Bouchard, Jean-Pierre-BW1A.6
 Boucher, Richard C-BTu4B.6
 Bourdieu, Laurent-BTu3A.83
 Boustany, Nada-BW2B.7
 Bouza Dominguez, Jorge-BSu3A.68
 Boyd, Michael-BSu3A.73
 Bradu, Adrian-BTu3A.98
 Brewer, Molly A-BSu4B.1
 Briard, Paul-DSu2C.5
 Brooks, Dana H-BTu3A.62
 Brown, Christian T-BTu3A.80
 Brown, Christopher M-BSu2B.5,
 BSu3A.21, BSu3A.32, BTu3A.42
 Brown, J. Quincy-BW2B.4
 Brown, Mindy-BW3A.6
 Brown, Robert-BTu3A.93
 Buckley, Erin M-BW3A.5, JM3A.18, JM3A.20,
 JM3A.24
 Budansky, Yury-BW1B.6
 Bugeon, Laurence-BTu3A.23
 Bunting, Hectors F-BSu3A.44
 Burnett, Jennifer-BSu3A.26
 Busch, David Richard, Jr-BW3A.5, JM3A.13
 Bustamante, Theresa-BTu2B.3
 Button, Brian M-BTu4B.6
 Buys, Timon-BTu3A.25
 Bydlon, Torre M.-BW2B.4

C

Cabrera DeBuc, Delia-BTu3A.74
 Cadeddu, Jeffrey-JM3A.19
 Cady, Ernest-JM3A.27, JM3A.6
 Caffini, Matteo-BM4A.1
 Cahall, Joseph E-BM4A.4
 Cai, Xin-BM2B.4
 Caldwell, Matthew-BW2B.4
 Campagnola, Paul-BSu2B, BSu4B.1
 Canpolat, Murat-JM3A.33
 Cantor-Balan, Roni-BSu3A.66
 Cao, Liji-BTu3A.1
 Capala, Jacek-BM2A.3, BTu3A.24
 Cappon, Derek J-JM3A.2
 Carney, Paul-BTu3A.45, BTu3A.47, BW2A.1
 Carp, Stefan-BSu3A.78, BSu3A.97,
 BW3A.2, BW3A.7, BW3B.5
 Carrasco-Zevallos, Oscar-BW2A.3
 Carvalho, Luis Alberto-BTu3A.13
 Casale, Amanda E-BTu4A.3
 Casellas, Oscar-JM3A.36
 Cassano, Enrico-BW3A.4
 Castilla, Carlos, Dr.-BSu3A.41
 Castillo, Sara-BSu3A.19
 Catherine, Yourassowski-DTu3C.1
 Cazzell, Mary-BTu3A.34
 Ceron, Deanna-BTu3A.25
 Cerutti, Sergio-BM4A.1
 Chandra, Malavika-JM3A.14
 Chaney, Eric J-BTu3A.85
 Chang, Yia-Chung-JM3A.49
 Chang, Yu-Cheng-DM2C.1
 Charbon, Edoardo-BW1A.5
 Charchafieh, Jean-BSu4A.4

Key to Authors and Presiders

- Chatni, Muhammad-BSu3A.43
 Chaudhary, Ujwal-BTu3A.58, **BTu3A.60**
 Chelvam, Venkatesh-BSu3A.60
 Chen, Antony-BM2A.2
 Chen, Chao-Wei-**BTu4A.5**
 Chen, Chi-Wei-DM2C.1
 Chen, Chih-Hung-JM3A.53
 Chen, Howard H-BM2A.4
 chen, Jin-**BSu3A.77**
 Chen, Juan-BSu3A.12, BSu3A.3, BSu3A.83, BTu4A.2
 Chen, Lei-BTu3A.29
 Chen, Ling Hong-DSu2C.5
 Chen, Lingling-**BTu3A.23**
 Chen, Ruimin-BM2B.4, BSu3A.42, BSu3A.48
 Chen, Tsu-Han-DM2C.1
 Chen, Ye-BSu3A.4, BSu4B.5
 Chen, Yongping-**BSu3A.15**, **BTu3A.94**, BTu4B.7
 Chen, Yu-BTu4A.5, BTu4B.3
 Chen, Yun-Sheng-**BM2B.7**
 Chen, Yung Lin-**BSu3A.23**
 Chen, Zhan-DSu3C.2
 Chen, Zheng-Feng-JM3A.53
 Cheng, Chau-Jern-**DSu3C.5**, **DSu4C**
 Cheng, Ran-**BM4A.6**, BTu3A.30
 Cheng, Yih-Shyang-**DTu4C.1**, **JM3A.53**
 Cherkezyan, Lusik-**BM4B.6**
 Chernomordik, Victor-**BM2A.3**, **BSu3A.34**, BSu3A.75, BTu3A.24, JM3A.46
 Chhetri, Raghav K-BTu4B.6
 Chiccone, Chris-BTu3A.89
 Chitchian, Shahab-**BSu3A.17**, **BTu3A.73**
 Cho, Jaedu-**BW1A.3**
 Choe, Regine-**BW3A.5**, JM3A.13, JM3A.41
 Choi, Hee-Jin-**JM3A.64**
 Choi, Seung Ho-BSu3A.10
 Chowdhry, Fatima-BSu3A.85
 Chowdhury, Shwetadwip-**BSu4B.8**
 Christophe, Minetti-DSu4C.3, DTu3C.1, **DW2C.3**
 Chui, Po Ching-BTu3A.86
 Chung, So Hyun-BW3A.5
 Cifuentes, Jose C-JM3A.36
 Clancy, Neil T-**BSu3A.73**
 Clark, David C-DSu4C.6, **DW1C.5**
 Claus, Daniel-**DM4C.3**
 Clubb, Fred-BTu2A.8
 Coates, Emily E-BTu4A.5
 Coëtmellec, Sébastien-DSu2C.4
 Coleman, Andrew-BTu3A.87
 Colinet, Pierre-DTu2C.2
 Collin, Stéphane-DW3C.6
 Comstock, Christopher-BTu3A.31
 Conjusteau, Andre-BSu3A.57
 Contag, Christopher-BSu4B.5
 Contini, Davide-BM4A.1, BSu2A.4, BTu3A.50
 Cooper, Robert J-**BSu2A.5**
 Corless, David J-BSu3A.73
 Cosoroaba, Raluca Mioara-BTu3A.98
 Costa, Marco-BTu4B.5
 Cowling, Joshua-DSu3C.4, **DTu2C.5**
 Cox, Dennis D-BTu3A.25
 Crawford, Michael-BTu3A.89
 Creath, Katherine-**JM3A.72**
 Crofford, Leslie-BTu3A.27
 Cross, Michael-DSu4C.6
 Csáti, Dániel-BSu3A.28
 Cubeddu, Rinaldo-BM4A.1, BSu2A.4, BTu3A.50, BW1A.6, BW3A.4, JM3A.16, JM3A.5
 Cuccia, David John-**BW1A**
 Culver, Joseph P-BM2A.6, BM4A.7, BSu3A.71, BSu4A.2, BSu4A.7, BW1B.2, JM3A.68
- D**
 D'Andrea, Cosimo-BW4A.4
 D'Souza, Angela-JM3A.37
 D. Pham, Quang-DTu2C.4
 Da Silva, Anabela-**BTu3A.14**
 Dai, Guohao-BTu4A.6
 Dale, Anders M-BTu3A.28
 Dalimier, Eugénie-BTu3A.95
 Dalla Mora, Alberto-BTu3A.50, JM3A.16
 Dallas, William J.-DM4C.4, **DTu1C.2**, JM3A.63
 Dallman, Margaret J-BTu3A.23
 Dallo, Shatha-BSu3A.5
 Damania, Dhwanil-BM4B.6
 Daoudi, Khalid-BM2B.5, **BSu3A.47**
 Darne, Chinmay Dilip-**BTu3A.70**, BTu4A.4
 David, Franck-DSu2C.4
 Davidson, Sean-BTu2A.1
 Davis, Scott-BW1A.7, BW4B.5
 Dayal, Rajeev-BTu2A.4
 de Kock, Christiaan P-BSu4B.4
 de Poly, Bertrand-BTu3A.95
 De Wilde, Yannick-DW3C.6
 DeLuca, Jennifer-BM4B.3
 DeLuca, Keith-BM4B.3
 DeMichele, Angela-BW3A.5
 Debourdeau, Mathieu-BW1A.2
 Degan, Simone-BSu4B.2
 Dehaeck, Sam-**DTu2C.2**
 Dehaes, Mathieu-BSu4A.6
 Dehghani, Hamid-BM2A.6, **BSu3A.59**, BSu3A.64, BSu4A.2, BTu4A.7, BW1A.7, **BW4A**, BW4A.7, JM3A.68
 Delacruz, Mart-JM3A.47
 Delgado-Mederos, Raquel-JM3A.28
 Delikatny, Edward J-JM3A.41
 Della Frera, Adriano-JM3A.16
 Demidov, Valentin-**BW2A.4**
 Deng, Zixin-**BTu3A.6**
 Depeursinge, Christian-DW3C.2
 Derickson, Dennis-**BTu3A.89**
 Derouard, Jacques-BW1A.2
 Desbiolles, Pierre-BSu3A.62
 Desperito, Elise-JM3A.69
 Detre, John A-BW4B.4
 Deumié, Carole-BTu3A.14
 Devor, Anna-BSu3A.31, BTu3A.28
 Dewsnap, Robert-BSu3A.78
 Dhalla, Al-Hafeez-BSu4B.8, **BTu2B.3**
 Dholakia, Kishan-BTu3A.80, JM3A.26, JM3A.35
 Di Ninni, Paola-BSu2A.4, BW1A.6
 Diaz, David-JM3A.34
 Diaz, Laura K-JM3A.18
 diFlorio-Alexander, Roberta-BW3A.3
 Ding, Hao-BTu3A.19
 Ding, Yichen-BTu3A.48
 Dinia, Lavinia-JM3A.28
 Dinten, Jean-Marc-BTu3A.44, BW1A.2, JM3A.12
 Diop, Mamadou-**BTu3A.18**, BTu3A.53, JM3A.3
 Dixit, Sanhita S-**BSu3A.22**, BTu3A.31
 Do, Minh N-BM4B.2
 Dobbs, Jessica Lupinacci-**BTu3A.19**
 Dong, Jing-**BTu3A.15**, BTu3A.81, **JM3A.48**
 Dong, Lixin-**BTu3A.11**, **BTu3A.12**, BTu3A.30
 Dorey, Jean-Marc-DSu2C.4
 Doronin, Alexander-JM3A.10
 Douek, Michael-BTu3A.8
 Dowell, Alexander-BW1B.7
- Doyle, Dominic-DW4C.1
 Duan, Can-BTu3A.79
 Duan, Lian-BTu2B.4
 Dubeau, Simon-BM4A.2, BTu2A.7
 Dubois, Frank-DSu4C.3, **DTu3C.1**, DW2C.3, DW4C.1
 Ducros, Nicolas-BW4A.4
 Dufour, Suzie-BTu3A.49
 Durduran, Turgut-BSu3A.53, **BSu4A.1**, BTu3A.54, BW1A.6, BW3A.5, BW4B.4, JM3A.13, JM3A.28, JM3A.36, JM3A.40
 Durkin, Anthony J-BW4B.2
 Duvall, Craig-BW2A.5
 Dy, Mary-Clare Clarin-**BSu3A.1**
- E**
 Eccles, Michael-BW3B.6
 Edwards, W. Barry-BM2A.6
 Eftekhari, Ali A-BTu3A.46
 Eggebrecht, Adam Thomas-BSu3A.71, **BSu4A.2**, BSu4A.7, JM3A.68
 Ehlen, Thomas G-BTu3A.39
 Ehlen, Tom-BTu3A.25
 Eigenwillig, Christoph-BTu2B.2, BTu3A.90
 Ekermann-Haerter, Katharina-BTu3A.28
 Ekimov, Dmitry-**JM3A.65**
 El-Ghoussein, Fadi-**BTu3A.64**
 Elbaum, Leonard-BTu3A.60
 Eliceiri, Kevin-BSu4B.1
 Ellerbee, Audrey-BTu3A.84, BTu3A.92
 Elliott, Jonathan Thomas-**BTu3A.53**, BTu3A.63, JM3A.3
 Elliott, Martin J-JM3A.4
 Elson, Daniel S-BSu3A.73, BW4B.7
 Elster, Clemens-BW1A.6
 Elwell, Clare-JM3A.32, JM3A.4
 Emanuel, Asher-JM3A.37
 Emelianov, Stanislav-BM2B.7
 Emery, Yves-DW3C.2
 Enfield, Louise-**BTu3A.8**
 Engström, David-**DSu2C.3**, JM3A.59
 Ensher, Jason-BTu3A.89
 Erdmann, Rainer-**BTu3A.7**
 Erdogan, Sinem Burcu, Ms.-**BSu3A.63**
 Erenso, Daniel-**BSu3A.38**
 Erickson, Sarah J-BSu3A.74, **BTu3A.66**
 Ermilov, Sergey-BSu3A.57
 Esenaliev, Rinat-**BW1B**, **BW4B.8**
 Euhus, David-JM3A.21
 Evans, Dean-**DSu1C.1**
- F**
 Fales, Andrew-BM2A.8
 Fang, Qianqian-BSu3A.78, **BSu3A.96**, BSu3A.97, **BW3A.2**, BW3A.7
 Fang, Qiyin-JM3A.2
 Fanjul-Vélez, Félix-BSu3A.6
 Fantini, Sergio-BM4A.5, BSu3A.66, BTu3A.61
 Farina, Andrea-JM3A.16, JM3A.5, **JM3A.7**
 Faris, Gregory W-BSu3A.22, **BTu3A.31**
 Farone, Anthony-BSu3A.38
 Farone, Mary-BSu3A.38
 Farrell, Thomas J-JM3A.2
 Farzam, Parisa-**JM3A.40**
 Faulkner, Stuart-JM3A.27, JM3A.6
 Favazza, Christopher-BM2B.4
 Favilla, Christopher G-BW4B.4
 Fenoglio, Angela-BSu4A.6
 Ferhanoglu, Onur-BSu2B.8
 Ferland, Guylaine-BTu2A.

Key to Authors and Presiders

- Ferradal, Silvina L-BSu3A.71, BSu4A.2, **BSu4A.7**
 Feuer, Gavriel-BSu3A.92
 Fienup, James R-DM4C.5
 Figueroa, Daniel-BSu3A.2
 Fink, Hans-Werner-DW1C.3
 Fink, Mathias-**BSu1A.2**
 Fisher, John P-BTu4A.5
 Fleischer, Jason-BM4B.4, DM2C.3, **DSu3C**, DTu1C.3, DTu3C.5
 Flexman, Molly-BTu2A.4, BW3A.6, **JM3A.69**
 Flores-Moreno, Mauricio-**DW2C.4**
 Floyd, Thomas-JM3A.37
 Fluxa, Patricio Eliseo-**BSu3A.41**
 Fogel, Mark-JM3A.18
 Follen, Michele-**BTu3A.25**, BTu3A.39
 Forbess, Joseph M-BSu3A.70
 Foschum, Florian-**BTu3A.52**, BW1A.6
 Foster, Ellen K-BW3A.5, JM3A.13
 Foster, Thomas H-BW2B.3, JM3A.17
 Foust, Amanda J-**BTu4A.3**
 Frampton, Jon-BW4A.7
 Franceschetti, Silvana-BM4A.1
 Franceschini, Maria Angela-BSu3A.90, BSu4A.6, BW3B.5
 Frangos, Suzanne-JM3A.14
 Fratila, Raluca-BSu3A.52
 French, Paul-BTu3A.23
 Frey, Wolfgang-BM2B.7
 Friberg, Ari T-BTu3A.3
 Friedman, Daniel-JM3A.13
 Fujimoto, James-**BTu2B**
 Funk, Lutz-BSu3A.53
 Furlong, Cosme-DW2C.4
- G**
 Gagnon, Louis-BSu2A.5, **BSu3A.31**, BTu3A.17, BTu3A.28
 Gaiind, Vaibhav-BSu3A.60
 Gallagher, Jennifer E-BW2B.4
 Gallant, Pascal-BW1A.6
 Galler, Robert M-JM3A.37
 Gamba, Enrique-BTu2B.6
 Gamm, Ute Alice-**BW2B.5**
 Gandjbakhche, Amir-BM2A.3, BSu3A.34, BSu3A.58, BSu3A.72, BSu3A.75, BSu3A.85, BTu3A.24, JM3A.46
 Gao, Hanhong-**DTu3C.6**
 Gao, Hongyue-**DM2C.4**
 Gao, Liang-BSu3A.54, BW2A.6
 Gao, Peng-BSu3A.24
 Gao, Wei-BTu3A.74
 Gao, Wen-BW4B.1
 Gao, Xiaohu-BM2B.1
 Garavaglia, Mario-BSu3A.41
 Garcia-Sucerquia, Jorge-**DSu3C.6**, **DTu1C.4**
 Gaudet, Chantel R-BTu3A.36
 Gaudreau, Pierrette-BTu2A.7
 Gautam, Pritam-BTu3A.65
 Gautier, François-DW1C.2
 Georgakoudi, Irene-BSu2B.6, BSu3A.33
 Georges, Marc-**DW4C.1**
 Geradts, Joseph-BW2B.4
 Gerber, Ursina-JM3A.30
 Gerega, Anna-BSu3A.81, BTu3A.20, **JM3A.31**
 Gesualdi, Marcos-**DSu2C.7**
 Gevorgyan, Tigran-BSu3A.88, **BSu4A.4**
 Ghadyani, Hamid R-**BTu3A.9**, BW1A.7
 Ghaem-Maghani, Sadaf-BSu3A.73
 Ghijsen, Michael-BTu4A.8
- Giannoula, Alexia-**BSu3A.53**
 Giardini, Mario Ettore-**BTu3A.80**, JM3A.26
 Gibbs, Holly-BSu3A.29
 Gibson, Adam P-BTu3A.8
 Gigan, Sylvain-BTu3A.83
 Gilbert, David-BTu3A.89
 Gillioli, Isabella-BM4A.1
 Gillenwater, Ann M-BW4B.1
 Gillies, Alastair D-JM3A.35
 Girshovitz, Pinhas-**BSu3A.65**
 Gladstone, David-BW4B.5, JM3A.15
 Glaser, Adam-BW4B.5, **JM3A.15**
 Glickson, Jerry D-JM3A.41
 Glunde, Kristine-BSu2B.4
 Gmitro, Arthur F-BSu4B.6
 Godavarty, Anuradha-BSu3A.74, BSu3A.98, BTu3A.58, BTu3A.60, BTu3A.66
 Goddard, Jessica-BSu3A.2
 Goergen, Craig J.-**BM2A.4**, BW4A.3
 Goertz, David-BSu3A.55
 Goff, Donna A-JM3A.18, JM3A.20
 Goksör, Mattias-DSu2C.3, JM3A.59
 Golay, Xavier-JM3A.27, JM3A.6
 Golding, Ido-BM4B.2
 Goldstein, Goldie-JM3A.72
 Gomes, Andrew J-**JM3A.47**
 Gong, Hui-JM3A.25
 Gonzalez, Alberto A-JM3A.36
 Gonzalez, Jean-BSu3A.74, **BSu3A.98**, BTu3A.66
 Goodwin, James R-BTu3A.36
 Gorthi, Sai Siva-**DSu4C.4**
 Götzinger, Erich-BTu2B.5, BTu3A.71, BTu3A.76, **BTu3A.91**
 Graber, Harry L-BSu3A.91, BSu3A.92, BSu3A.93, BSu3A.94, BSu4A.4
 Grace, Michael, PhD-BTu3A.10
 Graf, Benedikt-BW2A.1
 Grajciar, Branislav-BTu4B.2
 Grant, Gerald-BM2A.8
 Grant, P. Ellen-BSu4A.6
 Greenbaum, Alon-**DW2C.5**
 Greenberg, Joel H-BM4A.8, BW4B.4
 Griffiths, Gary-BTu3A.24
 Grobmyer, Stephen-BSu3A.48
 Groot, Marloes L-BSu4B.4, DW3C.4
 Grootendorst, Diederik Johannes-**BSu3A.52**
 Gross, Michel-**BSu3A.62**
 Grover, Ginni-**BM4B.3**
 Gréhan, Gérard-DSu2C.5
 Guerrero-Baruah, Elizabeth-BTu3A.61
 Guerrero-Cazares, Hugo-BTu3A.77
 Guggenheim, James A-BSu3A.64, **BW4A.7**
 Guillaud, Martial-BTu3A.25
 Gulsen, Gultekin-BTu2A.3, BTu3A.43, BTu3A.6, BTu4A.8, BW1A.3
 Gulses, A. Alkan-**DM4C.2**
 Gunn, Jason R-BTu4A.1
 Gunther, Jacqueline Elizabeth-**BW3A.6**, JM3A.69
 Guo, Lianyu-BSu4B.3, BW1A.8, BW2B.6, **JM3A.9**
 Guo, Zijian-BSu3A.43
 Gupta, Satya Prakash-JM3A.67
 Gurley, Katelyn-BTu2A.5, BTu3A.27, **JM3A.8**
 Gutwein, Luke-BSu3A.48
 Guyot, Alexis-BTu3A.87
 Gwennou, Coupier-DW2C.3H
 Habermehl, Christina-BM4A.3, **BSu2A.2**, **BSu3A.84**, BW4A.6
 Haeberle, Henry-BSu4B.5
- Haertel, Romano-BTu3A.7
 Hagen, Nathan-BW2A.6
 Hajireza, Parsin-BSu3A.56
 Hakkarainen, Timo-**BTu3A.3**
 Hall, Michael-BSu3A.98, **BTu3A.58**, BTu3A.60
 Hallacoglu, Bertan-**BTu3A.61**
 Hanlon, Eugene-BSu4B.3, BW1A.8, BW2B.6, JM3A.9
 Hanna, Brian D-JM3A.24
 Harduar, Mark K-BW2A.4
 Harms, Fabrice-**BTu3A.95**
 Hartounian, Vahram-BTu3A.61
 Hasan, Tayyaba-**BM2A.1**, BTu4A.1
 Hasegawa, Satoshi-DTu2C.4, DTu3C.4
 Hassan, Moïnuddin-BM2A.3, BSu3A.34, BSu3A.58, BTu3A.24
 Hassanpour, Mahlega-**BSu3A.71**
 Hayasaki, Yoshio-**DTu2C.4**, DTu3C.4, DTu4C.5, **DW1C**
 Hayden, Rebecca S-BSu2B.6
 Haynie, Donald-DSu4C.6
 Hayward, Joseph E-JM3A.2
 He, Jie-**BTu2A.1**
 He, Lian-**BSu3A.79**, BW1A.4
 He, Zhenghong-DM2C.4
 Hebden, Jeremy-BSu2A.4, BTu3A.8
 Heflin, James R-**BSu3A.13**
 Helfield, Brandon-BSu3A.55
 Herrington, Simon-JM3A.35
 Hershman, Dawn-BW3A.6, JM3A.69
 Hervé, Lionel-**BTu3A.44**, BW1A.2
 Hettiarachchi, Kanaka-BSu3A.22
 Hielscher, Andreas H-BSu3A.89, BTu2A.4, BTu3A.38, BW3A.6, JM3A.69
 Higuchi, Takayuki-DTu2C.4
 Hill, David B-BTu4B.6
 Hiraki, Teruyuki-BM4A.8
 Hirose, Futoshi-BTu3A.71, BTu3A.76
 Hitzberger, Christoph K-**BTu2B**, BTu2B.5, BTu3A.71, BTu3A.76, BTu3A.91
 Ho, Hsin-Chia-BW1A.6
 Holmes, Jon-**BTu4B.1**
 Holt, Robert-BSu3A.59, BTu3A.63, **BTu4A.7**
 Holtom, Gary-BSu4B.7
 Homan, Kimberly-BM2B.7
 Hondebrink, Erwin-BM2B.5
 Hong, Jisoo-DM2C.6, DSu1C.4, **DW4C.5**
 Hong, Keehoon-**DM2C.6**, DSu1C.4
 Hong, Sung-In-JM3A.54, **JM3A.60**
 Hong, Youngjoo-BTu2B.4
 Horton, Nicholas Geoffrey-**BSu2B.2**
 Hoskote, Aparna-JM3A.4
 Howard, Scott-**BSu2B.3**
 Hoy, Christopher L-BSu2B.8
 Hsieh, Chia-Lung-DW1C.6
 Hsieh, Wang-Yu-**JM3A.56**
 Hsing, Mitchell-**BTu2A.3**
 Hu, Fangyao-**BW3B.4**, JM3A.22
 Hu, Song-**BM2B.8**, BSu3A.42
 Hu, Wentao-DW3C.3
 Hu, Xiaoge-BM2B.1
 Huang, Chih-Hsien-BSu3A.54
 Huang, Yi-Pai-**DM2C.1**, **DW4C**
 Huang, Yuanhao-**DSu2C.2**, DW4C.4
 Huber, Robert Alexander-BTu2B.2, BTu2B.5, BTu3A.90
 Hubler, Zita-BTu3A.85
 Huland, David-**BTu3A.42**
 Huppert, Theodore-BTu3A.17

Key to Authors and Presiders

- Hussain, Altaf-**BM2B.5**
Hussain, Syed-BSu3A.5
Huynh, Elizabeth-**BSu3A.55, BSu3A.8**
Hwu, Wen-Mei-BW2A.1
Hyman, Anne-BSu3A.13
- I**
Ichikawa, Tsubasa-**DTu4C.4**
Iliescu, Daciana-DM4C.3
Imi, Emiko-BTu3A.26
Inder, Terrie E-BSu4A.7
Intes, Xavier-BTu4A.6, **BW4A.2**
Inzana, Thomas-BSu3A.13
Isakoff, Steven J-BW3A.7
Ishii, Yuki-**BW2A.8**
Isnard, Vincent-DW1C.2
Ito, Hiroshi-BTu3A.51
Ito, Terumasa-**BSu4B.7**
Ito, Tomoyoshi-DTu2C.3, JM3A.50, JM3A.51
Ito, Yasunori-DW4C.2
Itzkan, Irving-BSu4B.3, BW1A.8, BW2B.6, JM3A.9
Ivey, Peter A-DSu3C.4, DTu2C.5
Izatt, Joseph-BSu4B.8, **BTu2B.1**, BTu2B.3, JM3A.65
- J**
Jacques, Steven L-BW4B.3, BW4B.6
Jaffer, Farouc A-BTu3A.62
Jakovels, Dainis-**JM3A.44**
Jang, Yun-Ho-**BSu2B.7**
Jasensky, Joshua-DSu3C.2
Jayakar, Prasanna-BSu2A.7
Jelfs, Beth-**JM3A.32**
Jelzow, Alexander-BSu2A.4
Jen, Tai-Hsien-DM2C.1
Jenkins, B. Keith-DM4C.2
Jenkins, Michael W.-**BTu4B**, BTu4B.5
Jeong, Kyeong-Min-**JM3A.54**, JM3A.60
Jeong, Myung Yung-BW1A.3
Jermyn, Michael-**BW1A.7**
Ji, Lijun-BTu3A.45, BTu3A.47
Ji, Minbiao-BSu4B.7
Jia, Jia-**JM3A.52**
Jia, Jingfei-BTu3A.38
Jiang, Huabei-BSu3A.48, BSu3A.50, **BTu2A**,
BTu3A.21, BTu3A.45, BTu3A.47
Jiang, Max-**BTu3A.45**, BTu3A.47
Jiang, Ruixin-BTu3A.21, BTu3A.45, **BTu3A.47**
Jiang, Shudong-BTu3A.64, BW3A.3
Jiang, Tony-**JM3A.22**
Jiang, Xiaoming-**BTu3A.1**
Jiao, Shuliang-**BM2B.6**
Jin, Cheng-**BM2A.5**, BSu3A.14, **BSu3A.9**
Jin, Dayong-BTu3A.48
Jin, Wanzhu-JM3A.9
Jo, Javier A-**BTu2A.8**
Joanne, Li-BTu3A.85
Jose, Jithin-BSu3A.52
Joshi, Pallavi-BSu3A.74
Jung, Jae-Hyun-DSu1C.5
Jung, Ki Won-**JM3A.41**
Jung, Moon-Youn-BTu2B.7
Jung, Woonggyu-BTu3A.78
Junker, Marlee-BW2B.4
- K**
Kacprzak, Michal-BSu2A.4, BTu3A.20, BW1A.6
Kainerstorfer, Jana M.-BSu3A.34, **BSu3A.58**,
BSu3A.72, BSu3A.75, BSu3A.85, JM3A.46
Kaipio, Jari P-BTu3A.41, BTu3A.5
Kakauridze, George-DM4C.1, **DSu3C**
Kakue, Takashi-DW3C.5, DW4C.2
Kanick, Stephen Chad-BTu3A.63, BW2B.5, **BW3B.2**
Kanno, Iwao-BTu3A.56
Kaplan, David L-BSu2B.6
Kapur, Payal-JM3A.19
Karl, Anthony-BW3B.6
Karpf, Sebastian-BTu2B.2
Karray, Mayssa-DW1C.2, DW1C.4, DW4C.6
Kasner, Scott E-BW4B.4
Kavuri, Venkaiah C-**BTu3A.22, BTu3A.37**
Kawabe, Yutaka-DM2C.2
Kawaguchi, Hiroshi-BTu3A.51
Kazmi, S. M. Shams-**BSu4A.3**
Keely, Patricia-BSu4B.1
Kelly, Damien P-DTu3C.2
Kelly, Dorothy-BSu3A.70
Kelly, Kristen M-BW4B.2
Kemper, Bjoern-DW2C.2
Kennedy, Stephanie-BW2B.4
Keskin-Ergen, Yasemin, Dr.-BSu3A.63, BSu3A.95
Keurer, Henry-BTu3A.19
Keyser, Kent-BSu3A.39
Khadka, Sabin-BTu3A.65
Khalil, Michael-**BTu2A.4**
Khmaldze, Alexander-**DSu3C.2**
Khoury, Christopher-BM2A.8
Kienle, Alwin-BTu3A.52, **BTu3A.99**, BW1A.6
Kiire, Akihiro-DTu3C.4
Kiire, Tomohiro-**DTu4C.5**
Kikuchi, Takahiro-**BTu3A.56**
Kilosandze, Barbara-**DM4C.1**
Kim, Arnold-BTu3A.4, BTu3A.40
Kim, Chang-Seok-BW1A.3
Kim, Chulhong-BSu3A.55
Kim, Dae-Chan-BSu3A.25
Kim, Daekeun-BSu2B.7
Kim, Dug Young-**BW3C.1**
Kim, Hanyoung-BSu3A.22, BTu3A.31
Kim, Hee-Seung-JM3A.54, JM3A.60
Kim, Heeseok-BW2A.1
Kim, Hyun K-**BSu3A.89**, BTu2A.4, BTu3A.38, BW3A.6,
JM3A.69
Kim, Hyun-Eui-JM3A.54
Kim, In-Kyong-BTu2A.4
Kim, Jong S-BTu3A.85
Kim, Meeri N-BW3A.5, BW4B.4
Kim, Myung K-DSu4C.6, DW1C.5, **DW1C.7**, JM3A.61
Kim, Seunghwan-BTu2B.7
Kim, Taewoo-**BSu3A.30**
Kim, Young-**BSu3A.10, BW3B**, BW3B.3
Kim, Young Min-**DSu1C.2**
Kim, Youngmin-**DSu1C.4**, DSu1C.5
Kinashi, Kenji-DM2C.2, **JM3A.58**
Kinsky, Michael-BW4B.8
Kiszonas, Richard-BTu3A.66
Klaunberg, Katy-BW1A.6
Klein, Sabine-JM3A.30
Klein, Thomas-BTu2B.2, BTu2B.5, **BTu3A.90**
Klemme, Dietmar-BTu3A.7
Knutson, Jay-BTu3A.24
Kobat, Demirhan-BSu2B.2
Koch, Joshua-BSu3A.70
Koch, Stefan P-BM4A.3, BSu2A.2, BSu3A.84
Koenig, Anne-BTu3A.44, BW1A.2, **JM3A.12**
Kofke, W. Andrew-JM3A.14
Kolehmainen, Ville-BTu3A.41, **BTu3A.5**
Kolios, Michael C-BTu3A.72
Kolonics, Attila-**BSu3A.28**
Kolste, Kolbein-BW4A.5
Konecky, Soren D.-**BW4A.5**
Kopans, Daniel B-BW3A.2
Kosty, Jennifer A-JM3A.14
Krasinski, Jerzy-BSu3A.2
Krishnamurthy, Savitri-BTu3A.19
Krishnaswamy, Venkataramanan-BTu3A.59, BW3B.1,
BW3B.2
Kristoffersen, Anna-BTu3A.54
Krstajić, Nikola-BTu3A.80, JM3A.26
Krüger, Arne-BM4A.3
Kubota, Toshihiro-DW3C.5, DW4C.2
Kukhtarev, Nikolai-**DTu3C.3**
Kukhtareva, Tatiana-DTu3C.3
Kumar, Anand T.N.-BM2A.4, **BW4A.3**
Kuo, A.-JM3A.65
Kuo, Anthony-BTu2B.3
Kuo, Chaincy-BTu3A.35
Kurihara, Kazuki-**BTu3A.51**
Kurita, Taiichiro-DTu4C.3
Kurokawa, Kazuhiro-BTu3A.82
Kusano, Masashi-BTu3A.56
Kut, Carmen-**BTu3A.77**
Kuzmin, Nikolay V-BSu4B.4
Kuzmina, Ilona-JM3A.44
Kwon, Hyunkyung-JM3A.64
Kwong, Tiffany C-BTu4A.8
- L**
Lai, Puxiang-BW1A.1
Lam, Edmund Y-BW2A.2
Lam, Sylvia F-BTu3A.25, BTu3A.39
Lamb, Jonathan R-BTu3A.23
Lane, Pierre-BTu3A.25, **BTu3A.39**
LaRocca F.-JM3A.65
Larsson, Fridrik-**BSu3A.66**
Latrive, Anne-**BTu4B.4**
Latychevskaia, Tatiana-**DW1C.3**
Laughney, Ashley-BW3B.1
Laurik, Lenke-BTu3A.74
Lauritsen, Kristian-BTu3A.7
Le, Kelvin-BSu3A.2
Leblond, Fredric-BSu3A.59, BTu3A.63, BTu4A.7,
BW4A.5
Lebrun, Denis-DSu2C.4
Leclair, Sébastien-BW1A.6
Leclercq, Mathieu-DW1C.2
Lee, Byounggho-DM2C.6, DSu1C.4, DSu1C.5,
DW4C.5, **JM1A.2**
Lee, Chieh-Cheng-**DM4C.7**
Lee, Daniel C-BSu3A.88, BSu3A.93, BSu4A.4
Lee, Jin-Moo-BM2B.8, BM4A.7
Lee, Jonah-BTu3A.27
Lee, Kijoon-BTu3A.15, BTu3A.81, JM3A.48
Lee, Sang-Won-BTu2B.7
Lee, Seung Gol-BSu3A.25
Lee, Seung-Cheol-JM3A.41
Lee, Ting-Yim-BTu3A.53, JM3A.3
Lee, Vivian-BTu4A.6
Lee, Walter T-BW3B.4
Lee, Wonjun-**BSu3A.25**
Léger, Jean-François-BTu3A.83
Lehtikangas, Ossi-**BTu3A.4**
Lei, Ming-BSu3A.24
Leigh, Steven Y-BSu3A.4, BSu4B.5
Leitgeb, Rainer A-BTu4B.2
Lesaffre, Max-JM3A.66
Lesage, Frédéric-BM4A.2, **BTu2A.7**, BW1A.6
Levi, Ofer-BTu3A.49

Key to Authors and Presiders

- Levy, Hart-BTu3A.49
 Li, Dong-BSu3A.20, BW1B.3
 Li, Li-BSu3A.20
 Li, Lin-BTu3A.32, **BTu3A.34**
 Li, Lujie-DTu2C.6
 Li, Ming-Jun-BSu2B.4, BSu3A.35
 Li, Shuxia-BW1B.3
 Li, Ting-**BW4B.6**, **JM3A.25**
 Li, Xiao-DM2C.4
 Li, Xiaoqi-**BSu3A.50**, **BTu3A.21**
 Li, Xin-JM3A.52
 Li, Xingde-**BSu1A**, BSu2B.4, BSu3A.15, BSu3A.35, BSu3A.36, BTu3A.77, BTu3A.93, BTu3A.94, BTu4B.7
 Li, You-**BW2A.7**
 Li, Zhiming-BTu3A.48
 Liang, Chia-Pin-**BTu4B.3**
 Liang, Kexian-BM2A.6, BW1B.2
 Liang, Wenxuan-BSu2B.4, **BSu3A.36**
 Liao, Lin-Yao-DM2C.1
 Liao, Steve M-BSu4A.7
 Liao, Wenjun-BSu3A.48
 Libien, Jenny-BSu4A.4
 Licht, Daniel J-JM3A.18, JM3A.20, JM3A.24
 Liebert, Adam-BSu2A.4, BSu3A.81, BSu3A.82, **BTu3A.20**, BW1A.6, JM3A.31
 Lim, Emerson-BW3A.6, JM3A.69
 Lim, Kee-Hak-BW2B.6
 Lim, Liang-BW1B.4
 Lim, Yiheng-BTu2B.4
 Lin, Charles P-BTu2A.2
 Lin, Haibo-BTu3A.96
 Lin, Pei-Yi-**BSu4A.6**
 Lin, Qiaoya-**BSu3A.12**, **BSu3A.3**
 Lin, Rebecca-BW1B.5
 Lin, Wei-Chiang-BSu2A.7
 Lin, Yu-BSu3A.79, **BW1A.4**
 Lin, Yuting-BTu2A.3, **BTu3A.43**, BTu3A.6, **BTu4A.8**, BW1A.3
 Lin, Zi-Jing-BTu3A.22, **BTu3A.32**, BTu3A.34, BTu3A.37
 Ling, William-**BTu3A.92**
 Liopo, Anton-BSu3A.57
 Liu, Changgeng-DSu4C.6, **JM3A.61**
 Liu, Chengbo-JM3A.22
 Liu, Hanli-BSu3A.70, BSu4A.5, BTu3A.22, BTu3A.32, BTu3A.33, BTu3A.34, BTu3A.37, BTu3A.65, JM3A.19, JM3A.21
 Liu, Honglin-BW1A.1
 Liu, Jonathan T.C.-**BSu3A.4**, **BSu4B.5**
 Liu, Juan-JM3A.52
 Liu, Jung-Ping-DM4C.7, JM3A.56
 Liu, Tracy W-**BSu3A.14**, **BSu3A.83**, **BTu4A.2**
 Liu, Yang-BSu3A.61, BTu3A.57, **BW1B.2**
 Liu, Yi-DSu2C.2, DW4C.3, **DW4C.4**
 Lo, Eng-BSu3A.31, BTu3A.28
 Lo, Justin-BW3B.4
 Lochocki, Benjamin-BSu3A.18
 Lodder, Johannes C-BSu4B.4
 Long, Douglas-BTu3A.27
 Longchamp, Jean-Nicolas-DW1C.3
 Lopez-Penalver, Cristina-BTu3A.66
 Lopez-Rios, Jorge A-BTu3A.97
 Lovell, Jonathan F-BM2A.5, BSu3A.55, BSu3A.8, BSu3A.9
 Low, Philip-BSu3A.60
 Lu, Chien-Hung-**DTu1C.3**
 Lu, Yujie-BTu3A.70, **BTu4A.4**
 Luby-Phelps, Katherine-BSu3A.35
 Luk, Alex T-BTu3A.43
 Luo, Dao-Zheng-DM4C.7
 Luo, Qingming-BW4B.6, JM3A.25
 Lurie, Kristen-**BTu3A.84**
 Lynch, Jennifer M-JM3A.18, JM3A.20, **JM3A.24**
 Lyons, Michelle R-BM4B.5
- M**
 Ma, Shih-Hsin-JM3A.56
 MacAulay, Calum E-BTu3A.25, BTu3A.39
 MacDonald, Thomas D-BSu3A.14
 Macdonald, Callum-BW3B.6
 Macdonald, Rainer-BSu2A.4, BTu3A.50
 Madaan, Tushaar-JM3A.6
 Magazov, Salavat-BSu2A.4
 Mahadevan-Jansen, Anita-BW1B.7, JM3A.43
 Mahendroo, Mala-BSu3A.35
 Makita, Shuichi-BTu3A.82
 Mäkynen, Anssi-JM3A.65
 Mallas, Georgios-**BTu3A.62**
 Mallipeddi, Raj-BTu3A.87
 Mandella, Michael J-BSu4B.5
 Mandeville, Emiri T-BSu3A.31, BTu3A.28
 Mangla, Sundeep-BSu4A.4
 Maniewski, Roman-BSu3A.82, BTu3A.20, JM3A.31
 Manohar, Srirang-BSu3A.45, BSu3A.52
 Mansvelter, Huibert D-BSu4B.4
 Mao, Xiang-JM3A.34
 Marchington, Robert F-JM3A.35
 Marcos, Susana-BTu2B.6
 Mariampillai, Adrian-BTu3A.72
 Marina, Oana C-**BW3B.7**, JM3A.23
 Marjanovic, Marina-BTu3A.85
 Marple, Eric-BW1B.4
 Marschall, Sebastian-BTu2B.5
 Martelli, Fabrizio-BSu2A.4, BW1A.6
 Marti Fabregas, Joan-JM3A.28
 Martinez Marrades, Ariadna-DW3C.6
 Martino, Mark-BSu3A.80, **BSu3A.97**, BW3A.2
 Masamoto, Kazuto-BTu3A.56
 Maslov, Konstantin-BM2B.4, BM2B.8, BSu3A.42, BSu3A.43, BSu3A.49, BSu3A.54
 Mastanduno, Michael A-BW1A.7, **BW3A.3**
 Masuda, Nobuyuki-DTu2C.3, JM3A.50, JM3A.51
 Mata Pavia, Juan-**BW1A.5**
 Mateos, Nicolas-BTu3A.54
 Matoba, Osamu-DW3C.5, DW4C.2
 Matsubara, Isao-DM4C.4, DTu1C.2, **JM3A.63**
 Matsuda, Kiyofumi-DSu3C.3
 Matz, Rebecca-DSu3C.2
 Mavadia, Jessica-BTu3A.77, **BTu4B.7**
 Mayer, Markus A-BTu3A.73
 Mayzner-Zawadzka, Ewa-BTu3A.20
 Mazilu, Michael-JM3A.35
 Mazurenka, Mikhail-BSu2A.4, **BTu3A.50**, BW1A.6
 McAlpine, Jessica N-BTu3A.25, BTu3A.39
 McCormick, David A-BTu4A.3
 McGinty, James-BTu3A.23
 McNabb, Ryan P.-JM3A.65
 McLaughlin-Drubin, Margaret-BSu3A.33
 McVeigh, Elliot-BTu3A.77
 McWilliam, Richard-DSu3C.4, DTu2C.5
 Medvedev, Andrei-BSu3A.72
 Meglinski, Igor-**BW3B.6**, **JM3A.10**
 Mehnert, Jan-BM4A.3, BSu2A.2, BSu3A.84, **BW4A.6**
 Mendoza Santoyo, Fernando-DW2C.4
 Menna, Simona-BW3A.4
 Merkel, Alyssa-JM3A.43
 Mermut, Ozzy-BW1A.6
 Mesquita, Rickson C-**BW4B.4**, JM3A.14, **JM3A.37**
- Meunier-Guttin-Cluzel, Siegfried-DSu2C.5
 Michaelsen, Kelly-**BTu3A.59**
 Mies, Carolyn-BW3A.5
 Milej, Daniel-BSu2A.4, **BSu3A.81**, BTu3A.20, BW1A.6, JM3A.31
 Miller, Dianne-BTu3A.25
 Miller, Eric-BSu3A.66
 Min, Sung-Wook-DSu1C.2
 Minagawa, Taisuke-**BTu3A.54**
 Minato, Kotaro-BSu3A.1
 Minkoff, David L-BW4B.4, JM3A.14
 Minneman, Michael-BTu3A.89
 Mir, Mustafa-**BM4B.2**
 Mitzner, Wayne-BTu3A.93
 Mitra, Kunal, PhD-BTu3A.10
 Mitrani, Daniel-JM3A.36
 Mitropoulos, Tanya-**BSu4B.2**
 Miwa, Mitsuharu-JM3A.11
 Mizuno, Toshihiko-JM3A.11
 Mohammed, Omar-BSu3A.38
 Mohan, Karan-**DSu4C.5**
 Molteni, Erika-BM4A.1
 Mondrik, Sharon-**BW4B.1**
 Monemhaghdoost, Zahra-DW3C.2
 Monfort, Frederic-DW3C.2
 Montejo, Ludguier D.-**BTu3A.38**
 Montenegro, Lisa-JM3A.18, JM3A.20
 Moore, Richard H-BW3A.2
 Moreira, Thais-BTu4B.3
 Moriyama, Eduardo H-BTu4A.2
 Morrissey, Colm-BW1B.7
 Moser, Christophe-**DW3C.2**
 Motamedi, Massoud-BSu3A.17, BTu3A.73
 Mounier, Denis-DW1C.4
 Mourant, Judith R-BW3B.7, **JM3A.23**
 Muenzel, Stefan-**DM2C.3**
 Mukherjee, Sovanlal-**BSu3A.44**
 Mullen, Michael-BW4B.4
 Mulvey, Christine-BW2B.1
 Münger, Karl-BSu3A.33
 Muramatsu, Mikiya-DSu3C.3
 Murari, Kartikeya-BSu2B.4, BSu3A.35, BSu3A.36
 Musacchia, Joe-BTu3A.28
 Mutyal, Nikhil N-BW2B.2
- N**
 Nahas, Amir-**BTu3A.75**, JM3A.12
 Naim, Maryam Y-JM3A.18, JM3A.20
 Najafizadeh, Laleh-BSu3A.34, BSu3A.58, BSu3A.72, BSu3A.75, **BSu3A.85**, JM3A.46
 Nakamura, Junya-DM2C.5
 Nalcioglu, Orhan-BW1A.3
 Nankivil, Derek-BTu2B.3
 Naser, Mohamed Abdelaziz-**BTu3A.2**
 Nasu, Hatsuko-BTu3A.26
 Navas-Moreno, Maria-**JM3A.1**
 Nazareth, Daryl P-JM3A.17
 Negrean, Adrian-BSu4B.4
 Negrutiu, Meda Lavinia-BTu3A.98
 Nehmetallah, Georges-**DM4C.6**, DTu3C.3
 Neidrauer, Michael-JM3A.34
 Nevsehirl, Turan D, Mr.-BSu3A.63
 Nguyen, Cac Thi-**BTu3A.78**
 Nguyen, Dang Khoa-BM4A.2
 Nguyen, Thuc-Uyen-**BW2A.6**
 Nichols, John D-BSu3A.93
 Nicolson, Susan-JM3A.18, JM3A.20

Key to Authors and Presiders

Nie, Zhaojun-JM3A.2
 Niedre, Mark-**BSu3A.67**, **BTu2A.2**
 Nigam, Abhishek-**JM3A.55**, JM3A.67
 Ninou, Jordi-JM3A.36
 Nishide, Junichi-DM2C.2
 Nishio, Kenzo-DW3C.5, DW4C.2
 Nissilä, Ilkka-BTu3A.5
 Noakes, David-BSu3A.73
 Noiseux, Isabelle-BW1A.6
 Nolte, David-**DSu2C**, **DSu4C.2**
 Nordstrom, Robert J.-**BTu4A**
 Nothdurft, Ralph-BM2A.6
 Notingher, Ioan-BSu3A.40
 Ntziachristos, Vasilis-BTu3A.62
 Nyman, Jeffry-BW1B.7, JM3A.43

O

O'Donnell, Matthew-**BM2B.1**
 Obata, Takayuki-BTu3A.51
 Obrig, Hellmuth-BM4A.3, BW4A.6
 Oda, Motoki-BTu3A.26
 Ogawa-Ochiai, Keiko-JM3A.39
 Ogura, Hiroyuki-BTu3A.26
 Okada, Eiji-BTu3A.51, BTu3A.56
 Oldenburg, Amy-**BTu4B.6**, DSu4C.5
 Oliverio, Nestor H-JM3A.36
 Olvedy, Vera-BTu3A.74
 Olweny, Ephrem-JM3A.19
 Oraevsky, Alexander-**BSu3A.57**
 Oraintara, Soontorn-BTu3A.33
 Ortega-Quijano, Noé-BSu3A.6
 Ortiz, Sergio-**BTu2B.6**
 Osten, Wolfgang-DW4C.1
 Ouzounov, Dimitre G-BSu2B.5, **BSu3A.21**, BSu3A.32, BTu3A.42
 Owen, Chris M-BW4A.5
 Ozcan, Aydogan-DW2C.5

P

Pande, Paritosh-BTu2A.8
 Panigrahi, Pradeepta K-**JM3A.67**
 Panovska-Griffiths, Jasmina-JM3A.32
 Panzica, Ferruccio-BM4A.1
 Papademetriou, Maria-**JM3A.4**
 Papazoglou, Elisabeth S-JM3A.34
 Park, Jae-Hyeung-JM3A.54, JM3A.60
 Park, Jesung-BTu2A.8
 Park, Minyoung-JM3A.64
 Park, Soojin-JM3A.14
 Park, Soon-gi-**DSu1C.5**
 Patankar, Manish-BSu4B.1
 Pathak, Saurav-BW3A.5, JM3A.41
 Pattani, Varun-**BM2A.7**
 Patterson, Michael S-BTu3A.2
 Paulsen, Keith D-BTu3A.59, BTu3A.64, BTu3A.9, BW3A.3, BW3B.1, BW4A.5
 Pavlova, Ina-**BSu2B.1**, BSu3A.32, BTu3A.42
 Pedrini, Giancarlo-DW4C.1
 Pégard, Nicolas Christian-**BM4B.4**
 Pei, Yaling-BSu3A.93
 Pelivanov, Ivan-BM2B.1
 Pellizzaro, Aline-BSu3A.38
 Peng, Leilei-**JM3A.71**
 Peng, Tong-BTu3A.48
 Peng, Yan-JM3A.21
 Penney, Graeme-BTu3A.87
 Perelman, Lev T.-BSu4B.3, **BW1A.8**, BW2B.6, **JM1A**, JM3A.9
 Perez-Merino, Pablo-BTu2B.6

Perrien, Daniel-JM3A.43
 Persson, Martin-DSu2C.3, **JM3A.59**
 Peter, Jörg-BTu3A.1
 Peterson, Charlotte-BTu3A.27
 Peterson, Ralph-BSu3A.5
 Petrov, Georgi I-JM3A.10
 Petrov, Irene-BW4B.8
 Petrov, Yuriy-BW4B.8
 Petruccelli, Jonathan-**BSu3A.69**
 Pfeil, Douglas-BSu3A.88, BSu3A.93, BSu4A.4
 Pflieger, Mark E-**BSu2A.1**, BSu3A.93
 Pham, Hoa-**BM4B.7**
 Pham, Quang Duc-**DTu3C.4**
 Phelps, Janelle E-BW3B.4
 Piao, Daqing-**BSu3A.2**, BSu3A.44, BTu2A.6, **BTu3A.67**, BTu3A.69
 Picart, Pascal-**DTu2C**, **DW1C.2**, **DW1C.4**, **DW4C.6**
 Pichardo-Molina, Juan L-BTu3A.97
 Pierce, Mark C-BTu3A.68, BW4B.1
 Pierro, Michele Luigi-**BM4A.5**
 Piestun, Rafael-BM4B.3
 Pifferi, Antonio-BSu2A.4, BTu3A.50, BW1A.6, BW3A.4, JM3A.16, JM3A.15, JM3A.5
 Piper, Sophie-BM4A.3
 Piper, Sophie Käthe-**BW4A.1**, BW4A.6
 Piras, Daniele-BSu3A.45
 Pircher, Michael-BTu2B.5, **BTu3A.71**, BTu3A.76, BTu3A.91, **BW2A**
 Piyawattanametha, Wibool-BSu2B.8
 Planat-Chrétien, Anne-BTu3A.44, BW1A.2, JM3A.12
 Plauska, Andrius-DW3C.4
 Podoleanu, Adrian G-BTu3A.98
 Poellinger, Alexander-**BW3A.1**, BW4A.1
 Pogue, Brian-**BSu2A**, BSu3A.59, BTu3A.59, BTu3A.63, BTu3A.64, BTu3A.9, BTu4A.1, BTu4A.7, BW1A.7, BW3A.3, **BW3B.1**, BW3B.2, BW4B.5, JM3A.15
 Poh, Catherine-BTu3A.39
 Poher, Vincent-JM3A.12
 Pohida, Tom-BSu3A.75
 Poilane, Christophe-DW1C.4
 Polizzotto, Mark N-BSu3A.58
 Polydorides, Alexandros-BTu3A.68
 Ponce de Leon, Yenisey-**BTu3A.97**
 Poole, Kristin M-**BW2A.5**
 Poon, Ting-Chung-DM2C.4, DM4C.7, **DSu3C**
 Popescu, Gabriel-BM4B.2, BM4B.7, BSu3A.30, BSu3A.37, **DTu1C**, **DW2C.1**
 Pouliot, Philippe-**BM4A.2**, BTu2A.7
 Powell, Elizabeth-JM3A.27
 Pozzo-Miller, Lucas-BSu3A.39
 Prael, Scott A-BW4B.3
 Prchal, Josef T-JM3A.1
 Price, David-JM3A.27, JM3A.6
 Price, Roderick-BTu3A.25
 Prins, Christian-BSu3A.45
 Protano, Marion-Anna-BTu3A.68
 Prough, Donald-BW4B.8
 Psaltis, Demetri-DW1C.6
 Pu, Yang-**BW1B.6**, **JM3A.45**
 Pu, Ye-DW1C.6
 Pursley, Randall-BSu3A.75
 Purvis, Alan-DSu3C.4, DTu2C.5
 Puszka, Agathe-BTu3A.44, **BW1A.2**
 Putt, Mary-BM4A.8

Q

Qi, Ji-**BW4B.7**
 Qiu, Le-**BSu4B.3**, BW1A.8, BW2B.6, JM3A.9
 Qu, Jianan Y.-BSu3A.20, **BW1B.1**, BW1B.3

Quarto, Giovanna-BW3A.4, **JM3A.5**
 Queeckers, Patrick-DW4C.1
 Quinn, Kyle P.-**BSu2B.6**
 Quinn, Mary K-BW4B.1
 Quinones-Hinojosa, Alfredo-BTu3A.77
 Quirin, Sean-BM4B.3

R

Ra, Hyejun-BSu2B.8
 Radosevich, Andrew J-BTu3A.88, **BW2B.2**
 Ragheb, John-BSu2A.7
 Rahman, Rafn-BSu3A.58
 Rajaram, Narasimhan-JM3A.22
 Ramachandran, Siddharth-BSu3A.13
 Ramanujam, Nimmi-BW2B.4, BW3B.4, JM3A.22
 Ramella-Roman, Jessica C-BTu3A.94, **JM3A.38**
 Rasio, Jonathan-BTu3A.85
 Rasmussen, John-BTu4A.4
 Rativa, Diego-BSu3A.18
 Raymond, Scott B-BW4A.3
 Raza, Shaan-BTu3A.77
 Razani, Marjan-**BTu3A.72**
 Rector, David M-BM4A.4
 Rehman, Shakil-**DSu3C.3**
 Reinsberger, Claus-BSu2A.5
 Reivich, Martin-BM4A.8
 Remacha, Clément-**DSu2C.4**
 Ren, Ming-BTu3A.32
 Ren, Qiushi-BTu3A.48
 Restrepo, Jhon F.-DSu3C.6
 Revilla, Ruben-JM3A.36
 Rey, Gustavo-BTu3A.58
 Rice, Brad-BTu3A.35
 Rice, Tyler-BW4A.5
 Richards-Kortum, Rebecca-BSu3A.26, BTu3A.19, BTu3A.68, BW4B.1
 Richardson, Thomas-**BTu3A.87**
 Riches, Andrew-JM3A.35
 Riggs, William-BW1B.4
 Riley, Jason David Richard-**BSu3A.75**, BSu3A.85, JM3A.46
 Rivenson, Yair-DSu2C.1, **DW4C.7**
 Rivera, David R-**BSu2B.5**, BSu3A.21, BSu3A.32, BTu3A.42
 Rix, Herve-BSu3A.82
 Roberts, David W-BW4A.5
 Roberts, Philipp-BTu3A.71, BTu3A.76, BTu3A.91
 Robertson, Nicola-JM3A.27, JM3A.6
 Robinson, Dominic J-BW2B.5
 Robinson, Holly-BTu4A.4
 Robinson, Sarah-BTu3A.78
 Robles, Francisco-BW2A.7
 Roche-Labarbe, Nadege-BSu4A.6, BW3B.5
 Rodenburg, John-DM4C.3
 Roehrborn, Claus G-JM3A.19
 Rogers, Jeremy D-BTu3A.88, BW2B.2
 Rohde, Shelley B.-**BTu3A.40**
 Rolland, Jannick-BSu3A.41
 Rollins, Andrew-BTu4B.5
 Roman, Manuela-**BSu3A.74**, BSu3A.98, BTu3A.66
 Rominu, Mihai-BTu3A.98
 Rosen, Joseph-DSu2C.1, DW4C.7
 Rosen, Mark A-BW3A.5, JM3A.13
 Rosenberg, Irwin-BTu3A.61
 Rosowski, John-DW2C.4
 Rossi Sebastiano, Davide-BM4A.1
 Rot, Alon-DW4C.7
 Roudier, Martine-BW1B.7
 Rouse, Andrew R-BSu4B.6

Key to Authors and Presiders

Roussakis, Emmanuel-BSu3A.31, BTu3A.28
 Rowland, Barbara-JM3A.43
 Rowlands, Christopher-**BSu3A.40**
 Roy, Hemant K-BW2B.2, JM3A.47
 Ruderman, Sarah-JM3A.47
 Ruers, Theo J-BSu3A.52
 Runnels, Judith-BTu3A.2
 Ruvinskaya, Lana-BSu3A.90
 Ryan, Stephen J-BTu3A.30

S

Saager, Rolf B-**BW4B.2**
 Saengkaew, Sawatree-DSu2C.5
 Saha, Siby P-BTu3A.30
 Saha, Subrata-BSu3A.92
 Saiz, Ricardo-JM3A.36
 Sajjadi, Amir Yousef-**BTu3A.10**
 Sakadzic, Sava-BSu3A.31, **BTu3A.28**, BW3B.5
 Sakahara, Harumi-BTu3A.26
 Sakai, Wataru-DM2C.2, JM3A.58
 Sakamoto, Yuji-DTu4C.4
 Sakatani, Kaoru-BTu3A.51
 Salas-Garcia, Irene-BSu3A.6
 Samir Jafri, Samir-BTu4B.3
 Samkoe, Kimberley S-BTu4A.1
 Samson, Benjamin-JM3A.66
 Samuels, Joshua-**JM3A.34**
 Samuelson, Sean-BTu3A.79
 Sanders, Claire K-BW3B.7
 Sanders, William-DSu4C.5
 Sando, Yusuke-**DSu1C.3**
 Sasabe, Hiroyuki-DM2C.2
 Sasaki, Kazuhiro-BTu3A.82
 Saso, Srdjan-BSu3A.73
 Sassaroli, Angelo-BM4A.5, BSu3A.66, **BTu3A.16**,
 BTu3A.61
 Sato, Akira-DTu2C.4
 Satterwhite, Lisa L-BM4B.5
 Saunders, Debra-BSu3A.2
 Sauvage, Vincent-BSu3A.73
 Savage, H. E-JM3A.45
 Sawosz, Piotr-BSu3A.82, JM3A.31
 Schantz, S. P-JM3A.45
 Schei, Jennifer Lynn-**BM4A.4**
 Schenkel, Steven S-BW4B.4, JM3A.14, JM3A.37
 Schiaffi, Elena-BM4A.1
 Schlaggar, Bradley L-BM4A.7
 Schlanitz, Ferdinand-BTu3A.91
 Schmidt-Erfurth, Ursula-BTu3A.71, BTu3A.76,
 BTu3A.91
 Schmitt, Joseph M-BTu2B.2
 Schmitz, Christoph H-**BM4A.3**, BSu2A.2, BSu3A.84,
 BSu3A.93, BW4A.1, BW4A.6
 Schnall, Michael D-JM3A.13
 Schnall, Mitchell D-BW3A.5
 Schneider, Paul-BW4A.1
 Schoenau, Thomas-BTu3A.7
 Scholkmann, Felix-JM3A.30
 Schonbrun, Ethan-DSu4C.4
 Schreiter, Nils-BW4A.1
 Schwab, Peter-JM3A.24
 Schwartzbauer, Gary-BTu4B.3
 Schwarz, Richard A-BW4B.1
 Schweiger, Martin-BTu3A.5, BW4A.4
 Schäfer, Jan-BTu3A.99
 Seed, N. Luke-DSu3C.4, DTu2C.5
 Seekell, Kevin-BW2A.7
 Seeley, Emily-DSu3C.2

Selb, Juliette-BSu3A.78, **BSu3A.80**
 Selim, M. Angelica-BSu4B.2
 Semmler, Wolfhard-BTu3A.1
 Setälä, Tero-BTu3A.3
 Sevick-Muraca, Eva M-BTu3A.70, BTu4A.4
 Sexton, Kristian J-BTu4A.1
 Shahni Karamzadeh, Nader-**BSu3A.72**
 Shahni karamzadeh, Nader-BSu3A.85
 Shaked, Natan-BSu3A.65
 Shang, Yu-BM4A.6, BSu3A.79,
 BTu2A.5, **BTu3A.27**, **BTu3A.29**, **BTu3A.30**, BW1A.4,
 JM3A.8
 Shao, Peng-BSu3A.46, BSu3A.56
 Sharma, Manu-**BW1B.4**
 Sharma, Vikrant-**JM3A.19**, **JM3A.21**
 Shaul, Merav-BTu3A.61
 Shelton, Ryan L-BW2A.3
 Shemonski, Nathan-BW2A.1
 Sheppard, Colin-DSu3C.3
 Sheridan, John-**DM4C**, **DTu3C.2**
 Sheth, Nisith-BTu3A.87
 Shi, Wei-BSu3A.56
 Shieh, Po-Tuan-DM2C.1
 Shih, Meng-Mu-**BSu3A.16**, **BSu3A.51**, **JM3A.29**
 Shikayama, Takahiro-JM3A.11
 Shimobaba, Tomoyoshi-
DTu2C.3, **JM3A.50**, **JM3A.51**
 Shimozato, Yuki-DW4C.2
 Shin, Dongsuk-**BTu3A.68**
 Shiraki, Atsushi-JM3A.50
 Shivalingaiah, Shivanjani-JM3A.21
 Shrestha, Sebina-BTu2A.8
 Shung, Kirk-BM2B.4, BSu3A.42
 Sibbett, Wilson-BTu3A.80, JM3A.26
 Siebert, Thorsten-BTu3A.7
 Sierra, Heidy-**BW2B.7**
 Sikora, Uzair-DW2C.5
 Silva, Guilherme T-BSu4B.4
 Simniotopoulos, James-BSu3A.75
 Sinescu, Cosmin-**BTu3A.98**
 Singh, Dhananjay Kumar-**JM3A.62**, JM3A.67
 Sircan-Kucuksayan, Aslinur-JM3A.33
 Situ, Guohai-**DTu3C.5**
 Skala, Melissa C-BW2A.5
 Slangen, Pierre-DW4C.6
 Smiddy, William-BTu3A.74
 Smirnov, Aleksandr-BTu3A.24
 Smith, Anne M-BTu4A.4
 Smith, George-**JM1A.1**
 Smith, Harriet O-JM3A.23
 Smith, J. R-BSu3A.73
 Smith, Nataliya-BSu3A.2
 Smith, Paul D-BSu3A.34, BSu3A.58, BSu3A.75
 Smith-Osborne, Alexa-BSu4A.5
 Snyder, Abraham Z-BM4A.7, BSu4A.2
 So, Peter-**BM4B**, BSu2B.7, BW1B.5
 Sohn, Rebecca-BSu3A.43
 Solgaard, Olav-BSu2B.8, BSu4B.5
 Soller, Eric-BW1B.5
 Solomon, Metasebya-**BM2A.6**
 Soman, Ally-Khan-BW3B.3
 Somfai, Gabor-BTu3A.74
 Somogyi, Aniko-BTu3A.74
 Song, Byoung-Sub-DSu1C.2
 Song, Hyun-Woo-**BTu2B.7**
 Song, Qinghai-BSu3A.10
 Song, Yinchen-**BSu2A.7**
 Sordillo, Laura-BW1B.6

Sosnovik, David E-BM2A.4
 Sosnovik, David J-BW4A.3
 Souichi, Saeki-BW2A.8
 Soulard, Florian Bryce-**DSu3C.4**, DTu2C.5
 Spigulis, Janis-JM3A.44
 Spinelli, Lorenzo-**BM4A.1**, BSu2A.4, **BW1A.6**,
 BW3A.4
 Srikuea, Ratchakrit-BTu3A.27
 Srinivasan, Vivek J-BSu3A.31, BTu3A.28, BW3B.5
 Srivastava, Anushree-BSu3A.4
 St Lawrence, Keith-BTu3A.18, BTu3A.53, BTu3A.63,
 JM3A.3
 Stadtmiller, Joe-BSu3A.78
 Stamatas, Georgios N-**JM3A.42**
 Steenberg, Wiendelt-**BM2B**, BM2B.5, BSu3A.45,
 BSu3A.47, BSu3A.52
 Steinbrink, Jens-BM4A.3, BSu2A.2, BSu3A.84,
 BW4A.6
 Steinkellner, Oliver-BSu2A.4
 Sterenborg, Henricus J-BW2B.5
 Sterling, Julie-JM3A.43
 Stern, Adrian-**DSu2C.1**, **DTu3C**, DW4C.7
 Stoyanov, Danail-BSu3A.73
 Stratul, Stefan Ioan-BTu3A.98
 Straub, Adam-BSu2B.3
 Stufflebeam, Steve-BSu2A.5
 Styles, Iain B-BSu3A.64, BW4A.7
 Su, Yikai-DM2C.4
 Subramanian, Hariharan-BM4B.6
 Suck, Sarah Y-DW3C.6
 Sudlow, Gail-BW1B.2
 Sugisaka, Jun-ichiro-DTu4C.5
 Sugiura, Tadao-BSu3A.1
 Sun, Cuiru-BTu3A.72
 Sun, Jingjing-BSu3A.48, **BTu3A.79**
 Sun, Qunhui-DSu2C.6
 Sun, Zhenghui-BM4A.8
 Suslick, Kenneth-BTu3A.85
 Sutin, Jason-**BSu3A.90**
 Suzuki, Nao-BSu2A.5
 Suzuki, Toshihiko-BTu3A.26
 Sviridov, Alexander-BSu3A.34
 Symons, Brock-BTu3A.27
 Szipöcs, Róbert-BSu3A.28

T

Tachtsidis, Ilias-**JM3A.27**, JM3A.32, JM3A.4, JM3A.6
 Tahara, Tatsuki-**DW3C.5**, DW4C.2
 Tai, Yuan-Chuan-BM2A.6
 Takahashi, Yosuke-BTu3A.51
 Takaki, Yasuhiro-**DM2C.5**, **DSu1C**
 Takawa, Hiroyuki-BTu3A.56
 Tan, I-Chih-BTu3A.70, BTu4A.4
 Tanaka, Naoaki-BSu2A.5
 Tang, Cha-Min-BTu4B.3
 Tang, Guichen-JM3A.45
 Tang, Li-Chuan-JM3A.49
 Tang, Yuanhe-BTu3A.48
 Taniguchi, Yusuke-JM3A.50
 Tao, Shaohua-**JM3A.57**
 Taromi, Paola-**BW3A.4**, JM3A.16, JM3A.5, JM3A.7
 Tarvainen, Tanja-BTu3A.4, **BTu3A.41**, BTu3A.5
 Tatrai, Erika-BTu3A.74
 Tavakoli, Behnoosh-**BSu3A.86**

Key to Authors and Presiders

- Taylor, Harriet B-BTu3A.23
Tchintga, Robert-BTu3A.74
Teh, Seng Khoon-**BW1B.3**
Ten Haken, Bennie-BSu3A.52
Tessier, Gilles-**DW3C.6**
Thayer, David A-BTu3A.43
Thizy, Cedric-DW4C.1
Thomas, David-JM3A.27, JM3A.6
Thomas, Podgorski-DW2C.3
Tian, Fenghua-**BSu3A.70, BSu4A.5**, BTu3A.33, BTu3A.65
Tian, Lei-BSu3A.69, DSu2C.2, **DW4C.3**, DW4C.4
Tichauer, Kenneth M.-BSu3A.59, **BTu3A.63, BTu4A.1**, BTu4A.7
Tilbury, Karissa-BSu4B.1
Tippie, Abbie E-**DM4C.5**
Tkaczyk, Tomasz-BSu3A.76, BW2A.6
Toborek, Michal-BTu3A.29
Topala, Florin Ionel-BTu3A.98
Toriz-Garcia, Jose J-DSu3C.4, DTu2C.5
Toronov, Vladislav-BW2A.4, JM3A.3
Torrucelli, Alessandro-BM4A.1, BSu2A.4, BW1A.6, BW3A.4
Torzicky, Teresa-**BTu2B.5**, BTu3A.71, BTu3A.76, BTu3A.91
Tosi, Alberto-BTu3A.50, JM3A.16
Towner, Rheel A-BSu3A.2
Trachtenberg, John-BTu2A.1
Troen, Aron M-BTu3A.61
Tromberg, Bruce J-**BTu1A.1**, BW4A.5
Truong Van, Tri-BM4A.2
Trépanier, Francois-BTu2B.2
Tsai, Hsiao-rho-BSu3A.60
Tsourkas, Andrew-**BM2A.2**
Tsumijima, Sho-JM3A.58
Tsumura, Norimichi-JM3A.39
Tsutsumi, Naoto-**DM2C.2**, JM3A.58
Tunnell, James-BM2A.7, BW1B.4
Turchin, Ilya-**BW3A**
Turon, Pau-BSu3A.53
Turzhitsky, Vladimir-BSu4B.3, BW1A.8, **BW2B.6**, JM3A.9
Tyagi, Anandita-BSu3A.93
Tzeranis, Dimitrios Spyridon-**BW1B.5**
- U**
Ueda, Yukio-**BTu3A.26**
Uldrick, Thomas S-BSu3A.58
Upadhye, Sudeep-BW2B.2
Ura, Shogo-DW3C.5, DW4C.2
Uttam, Shikhar-**BSu3A.61**, BTu3A.57
- V**
Valdes, Pablo A-BW4A.5
Valencia, Alejandra-BTu3A.54
Valentini, Gianluca-**BW4A.4**
Valim, Niksa-BSu3A.67
van Kuijk, Frederik J-BSu3A.17, BTu3A.73
van Leeuwen, Ton G-BSu3A.45, BSu3A.52
van Niekerk, Dirk-BTu3A.25
van Veldhoven, Spiridon-BSu3A.45
van der Steen, Ton-**BM2B.2**
Vandebrounhorst, Katrina-BSu3A.70
Vandenrijt, Jean-François-DW4C.1
Vanzetta, Ivo-BTu3A.14
Vardeny, Valy-JM3A.1
Varga, Boglarka-BTu3A.74
Vasalatiy, Olga-BTu3A.24
Vass, Clemens-BTu3A.76
- Veilleux, Israël-BTu2A.1
Vela-Garcia, Carmen-BSu3A.18
Velasquez, Daniel-DTu1C.4
Velders, Aldrik-BSu3A.52
Verdecchia, Kyle-**BSu2A.3**
Verpillat, Frédéric-BSu3A.62
Verrier, Nicolas-JM3A.66
Vigneswaran, Nadarajah-BW4B.1
Vinogradov, Sergei A-BSu3A.31, BTu3A.28
Visani, Elisa-BM4A.1
Vishwanath, Karhik-BW3B.4
Visscher, Martijn-BSu3A.52
Vitkin, Edward-BSu4B.3, BW1A.8, BW2B.6, JM3A.9
Vo-Dinh, Tuan-BM2A.8
Vohnsen, Brian-**BSu3A.18**, BSu3A.19
Volkwein, Nassia-BW4A.1
von Bally, Gert-**DW2C.2, DW3C**
Vuong, Barry-BW2A.4
- W**
Wabnitz, Heidrun-**BSu2A.4**, BTu3A.50, BW1A.6
Wali, Ramesh-JM3A.47
Waller, Laura A-DM2C.3, DTu3C.5
Wang, Danni-BSu3A.4, BSu4B.5
Wang, Jinyu-**BTu3A.83**
Wang, Ke-BSu2B.2
Wang, Lidai-BSu3A.54
Wang, Lihong V.-BM2B.4, BM2B.8, **BSu1A.1**, BSu3A.42, BSu3A.43, BSu3A.49, BSu3A.54, BW1A.1
Wang, Michael R-DSu2C.6
Wang, Weichao-BTu3A.48
Wang, Wubao-BW1B.6, JM3A.45
Wang, Xiaolei-DTu2C.6
Wang, Yongtian-JM3A.52
Wang, Yu-**BSu3A.49**, JM3A.58
Wang, Zhao-**BTu4B.5**
Wanyo, Christy M-BW3A.7
Warren, Warren S-BSu4B.2
Wassermann, Eric-BSu3A.75, JM3A.46
Watanabe, Takashi-**JM3A.11**
Watson, John-DM4C.3
Wawrzyn, Krzysztof-BW2A.4
Wax, Adam-BM4B.5, BW2A.7
Webb, Kevin J-**BSu3A.60**
Webb, Watt W.-BSu2B.1, BSu2B.5, BSu3A.21, BSu3A.32, BTu3A.42
Weersink, Robert-BTu2A.1
Wei, Chen-wei-BM2B.1
Weigel, Udo Michael-BTu3A.54
Weigel, Udo-BW1A.6
Weigel, Udo Michael-**JM3A.36**
Weigl, Wojciech-BTu3A.20, JM3A.31
Weingarten, Michael S-JM3A.34
Weingast, Jessica-BTu4B.2
Weis, Christine-BSu3A.53
Weitao, Tao-BSu3A.5
Weliwitigoda, Geethika-BSu3A.66
Welker, Gabriel-BSu3A.38
Wells, Wendy-BW3B.1
Wen, Zilong-BSu3A.20
West, Anne E-BM4B.5
Whelan, Harry T-JM3A.10
White, Brain R-BSu4A.2, BM4A.7, BSu3A.71
Wierwille, Jeremiah-BTu4B.3
Wieser, Wolfgang-**BTu2B.2**, BTu2B.5, BTu3A.90
Wilganowski, Nathaniel-BTu4A.4
Wilke, Lee G-BW2B.4
- Williams, Gavin-DSu3C.4, DTu2C.5
Williams, Logan-DM4C.6
Williams, Michelle D-BW4B.1
Wilson, Brian C-BSu3A.14, BSu3A.83, BTu2A.1, BTu4A.2, BW4A.5
Wilson, Christy-BM2A.8
Wilson, David-BTu4B.5
Wilson, Jesse W-BSu4B.2
Winarni, Maria-BTu3A.81
Wise-Milestone, Lisa-BSu3A.83
Witte, Stefan-**BSu4B.4, DW3C.4**
Wojtkiewicz, Stanislaw-**BSu3A.82**
Wolf, Martin-BW1A.5, JM3A.30
Wolf, Ursula-**JM3A.30**
Wolter, Nicolas E-BTu4A.2
Wong, Kenneth K-BTu3A.86, BW2A.2
Wu, Lei-BSu3A.48
Wu, Pengfei-DSu2C.6
Wu, Tzu-Yu-**BSu4B.6**
Wu, Weicheng-BSu3A.90
Wu, Xue Cheng-DSu2C.5
Wysocki, Michael-BTu3A.61
Wyvill, Kathleen M-BSu3A.58
- X**
Xi, Jiefeng-BSu3A.36, BTu3A.77, **BTu3A.93**, BTu3A.94, BTu4B.7
Xi, Lei-**BSu3A.48**, BTu3A.21
Xi, Peng-**BTu3A.48**
Xia, Jinjun-BM2B.1
Xia, Jun-**BSu3A.43**
Xia, Peng-DW3C.5, **DW4C.2**
Xia, Wenfeng-**BSu3A.45**
Xie, Hao-BTu3A.48
Xie, Huikai-BSu3A.48, BTu3A.79
Xie, Jinghui-JM3A.52
Xie, X. Sunney-BSu4B.7
Xu, Baogang-BM2A.6
Xu, Chris-BSu2B.2, BSu2B.3, BSu2B.5, BSu3A.21, BSu3A.32, BTu3A.42
Xu, David-BM2B.7
Xu, Guan-**BTu2A.6**
Xu, Heng-BTu3A.35
Xu, Jianbing-**BTu3A.86**, BW2A.2
Xu, Jin-BSu3A.20
Xu, Xiao-**BW1A.1**
Xu, Yan-**BSu3A.87**
Xu, Yong-**BSu3A.88**, BSu3A.91, BSu3A.93, BSu4A.4
Xu, Yuan-BW2A.4
Xu, Zhengbin-BSu3A.10, **BW3B.3**
Xylas, Joanna-**BSu3A.33**
- Y**
Yakovlev, Vladislav V-JM3A.10
Yamaguchi, Takeshi-DTu4C.3
Yamaki, Etsuko-BTu3A.26
Yamamoto, Kenji-**DM2C, DTu4C.2**, DTu4C.3
Yamamoto, Satoshi-JM3A.39
Yamamoto, Seiji-DW3C.5
Yamanaka, Takeshi-BTu3A.26
Yamashita, Daisuke-BTu3A.26
Yamashita, Yutaka-BTu3A.26
Yamauchi, Makoto-DSu3C.3
Yamauchi, Midori-**JM3A.39**
Yan, Ping-BM2B.8
Yan, Shikui-BTu4A.4

Key to Authors and Presiders

Yang, Changhui-**BM4B.1**
 Yang, Guang-Zhong-BSu3A.73
 Yang, Joon-Mo-**BM2B.4**
 Yang, Seungmoo-BM4B.6
 Yang, Shaohua-BTu3A.32
 Yang, Victor .X.D-BTu3A.72
 Yang, Victor X. D.-BW2A.4
 Yang, Wei-BTu3A.19
 Yang, Xin-**DW1C.6**
 Yang, Yanlong-BSu3A.24
 Yang, Yanqi-BW1B.3
 Yang, Yuanlong-BW1B.6
 Yannas, Ioannis V-BW1B.5
 Yao, Baoli-BSu3A.24
 Yao, Jixing-**BTu3A.33**
 Yao, Junjie-BM2B.4, **BSu3A.54**
 Yao, Lei-BTu3A.21
 Yarchoan, Robert-BSu3A.58
 Yaseen, Mohammad A-BSu3A.31, BTu3A.28
 Yasuno, Yoshiaki-**BTu2B.4, BTu3A.82**
 Yatagai, Toyohiko-DSu1C.3, DTu3C.4, DTu4C.5
 Ye, Jing Yong-**BSu3A.5**
 Ye, Tong-BSu3A.24, **BSu3A.39**
 Yeatts, Andrew B-BTu4A.5
 Yegappan, Chidambaram-JM3A.48
 Yeh, Alvin-BSu3A.29
 Yennu, Amarnath-BSu4A.5
 Yennu, Amarnath S. S.-**BTu3A.65**
 Yeom, Jiwoon-DM2C.6, DSu1C.4, DW4C.5
 Yi, Ji-**BTu3A.88**
 Yildirim, Murat-BSu2B.8
 Yin, Chun-Yi-JM3A.49
 Yodh, Arjun G-BM4A.8, BW3A.5, BW4B.4, JM3A.13, JM3A.14, JM3A.18, JM3A.20, JM3A.24, JM3A.37
 Yonesaka, Ryosuke-DW3C.5
 Yoon, Han-Seung-BW3B.6
 Yoshida, Hirofumi-BTu3A.71, BTu3A.76
 Yoshikawa, Hiroshi-**DTu4C, DTu4C.3**
 Yoshimori, Kyu-**DW1C.1**
 Yoshimoto, Kenji-BTu3A.26
 Yu, Chung-Chieh-**DM4C.4**, DTu1C.2, JM3A.63
 Yu, Guoqiang-BM4A.6, BSu3A.79, **BTu2A.5**, BTu3A.27, BTu3A.29, BTu3A.30, BW1A.4, JM3A.8
 Yu, Ping-**BTu3A.96**
 Yu, Xiao-**DSu4C.6**
 Yuan, Hsiangkuo-**BM2A.8**
 Yuan, Zhen-BTu3A.47
 Yucel, Meryem Ayse-BSu2A.5, **BTu3A.17**
 Yung, Rex-BTu3A.93

Z

Zabih Yeganeh, Hadi-**JM3A.3**
 Zaccanti, Giovanni-BSu2A.4, BW1A.6
 Zappa, Franco-BTu3A.50, JM3A.16
 Zecevic, Dejan-BTu4A.3
 Zemp, Roger J-**BSu3A.46, BSu3A.56**
 Zeng, Yan-**BSu3A.20**, BW1B.3
 Zettergren, Eric-BTu2A.2
 Zhai, Hongchen-**DTu2C.6**
 Zhan, Yuxuan-BSu4A.2, **JM3A.68**
 Zhang, Anqi-**BTu3A.69**
 Zhang, Bailin-BSu3A.5
 Zhang, Chi-**BSu3A.42**
 Zhang, Cong-BM4A.2, BTu2A.7
 Zhang, Fan-BTu3A.68
 Zhang, Hao F-BM2B.6
 Zhang, Jennifer Y-BSu4B.2
 Zhang, Qizhi-BTu3A.47
 Zhang, Rongxiao-**BW4B.5**, JM3A.15
 Zhang, Tao-**BSu2A.6, BTu3A.55**
 Zhang, Xuemei-BM2A.2
 Zhang, Yuhua-BSu3A.39
 Zhang, Yuying-**BSu2B.4**, BSu3A.15, **BSu3A.35**, BSu3A.36
 Zhang, Z.-DSu2C.2
 Zhang, Zhihong-BSu3A.12, BSu3A.3
 Zhao, Jianlin-**DSu3C.1**
 Zhao, Lingling-**BTu4A.6**
 Zhao, Ming-JM3A.71
 Zheng, Gang-**BM2A**, BM2A.5, BSu3A.12, BSu3A.14, BSu3A.3, BSu3A.55, BSu3A.8, BSu3A.83, BSu3A.9, BTu4A.2
 Zheng, Juanjuan-**BSu3A.24**
 Zheng, Wei-BW1B.3
 Zhi, Miaochan-**BSu3A.29**
 Zhou, Guangyin-BSu3A.48
 Zhou, Jack-BSu3A.4
 Zhou, Junli-BTu3A.45, BTu3A.47
 Zhou, Qifa-BM2B.4, BSu3A.42, BSu3A.48
 Zhou, Weibin-JM3A.71
 Zhou, Wenjing-DW3C.3
 Zhu, Qing-BSu3A.43, BSu3A.86, BSu3A.87, **JM3A.70**
 Zhu, Qun-BSu3A.59, BTu4A.7
 Zhu, Rui-BTu3A.86, **BW2A.2**
 Zhu, Tingting-**JM3A.6**
 Zhu, Yizheng-**BM4B.5**
 Zhuang, Xiaowei-**BTu1A.2**
 Zielinski, Rafal-BM2A.3, BTu3A.24
 Zimmermann, Bernhard-**BSu3A.78**, BSu3A.80
 Zimmermann, Judith-BTu3A.6
 Zimmermann, Trelawny-JM3A.46
 Zirak, Peyman-BTu3A.54, **JM3A.28**, JM3A.36, JM3A.40
 Zolek, Norbert-BSu2A.4, BSu3A.81, BW1A.6, JM3A.31
 Zotter, Stefan-BTu2B.5, BTu3A.71, **BTu3A.76**, BTu3A.91
 Zou, Jun-BSu3A.54
 Zubkov, Leonid-JM3A.34
 Zucchelli, Lucia-BM4A.1, BSu2A.4
 Zuo, Ziwei-BSu3A.13

Biomedical Optics and 3D Imaging Congress

- Biomedical Optics (Biomed)
- Digital Holography and 3D Imaging (DH)

Exhibit: 29 April – 2 May ♦ Miami Hilton Downtown, Miami, Florida, USA

Allied Laser Solutions

61 Union Street
Westfield, MA 01085
P: +1 413.562.4006
F: +1 413.562.6167
arb@alliedlasersolutions.com
www.alliedlasersolutions.com

Allied Laser Solutions (ALS) is the exclusive North American distributor for Innolas Laser Munich, a German leading manufacturer of Pulsed Nd: Yag. Models ranging from mJ to 2J @ 1064nm @ 20Hz for scientific and 200uJ @ 500KHz for industrial. Many options like 532, 355, 266, 213, seeding, tunable dye lasers & OPOs available.

Becker & Hickl GmbH

Nahmitzer Damm 30
Berlin 12277 Germany
91 Boylston Street
Brookline, MA 02445
P: +49 30. 787. 5632
F: +49 30. 787. 5734
info@becker-hickl.com
www.becker-hickl.com

World Leader in Time Correlated Single Photon Counting (TCSPC) for picosecond time resolved measurements of repetitive optical waveforms. Applications include diffuse optical tomography, fluorescence lifetime measurement, fluorescence lifetime imaging, and single molecule detection. Products include data recording and analysis electronics and software, photon counting detector modules, picosecond diode lasers and confocal scanners to convert any research grade microscope into a confocal laser scanning microscope. New compact lower cost OEM modules now available.

Boston Electronics Corporation

91 Boylston Street
Brookline, MA 02445 USA
P: +1 617.566.3821
F: +1 617.731.0935
boselec@boslec.com
www.boselec.com

Photon Counting specialists. US Agents for Becker & Hickl GmbH of Berlin Germany and for id Quantique SA of Carouge (Geneva) Switzerland. Time Correlated Single Photon Counting (TCSPC) for Diffuse Optical Tomography and for Fluorescence Lifetime measurement applications including FLIM/FRET. Picosecond time resolved measurements of repetitive optical waveforms in convenient modular hardware for science.

Boulder Nonlinear Systems, Inc.

450 Courtney Way, #107
Lafayette, CO 80026 USA
P: +1 303.604.0077
kelly@bnonlinear.com
www.bnonlinear.com

Boulder Nonlinear Systems, Inc. (BNS) designs, manufactures, and sells standard and custom light control solutions. Spatial Light Modulators, Polarization Rotators, and Optical Shutters are offered for beam forming, beam steering, biotechnology, microscopy, military/civil defense, phase/polarization control, pulse shaping, wavefront analysis/testing, and other applications.

Genia Photonics, Inc.

500 Cartier Blvd. W Suite 131
Laval, QC H7V 5B7 Canada
P: +1 450.680.3401
F: +1 450.680.3391
info@geniaphotonics.com
www.geniaphotonics.com

Genia Photonics Inc. is an innovative company specializing in high-speed picosecond fiber-based lasers and spectroscopic measurement systems. Centered around our patented fiber laser technology, Genia's compact, easy to use and controlled via software systems will change the methodology for various applications in biomedical, industrial as well as defense and security.

Hamamatsu Corporation

360 Foothill Road
Bridgewater, NJ 08807 USA
P: +1 908.231.0960
F: +1 908.231.1539
hbylicki@hamamatsu.com
www.hamamatsu.com/

Hamamatsu Corporation is the North American subsidiary of Hamamatsu Photonics K.K. (Japan), a leading manufacturer of devices for the generation and measurement of infrared, visible, UV light and x-rays. These devices include photomultiplier tubes, photodiodes, image sensors, cameras, and light sources. Hamamatsu Photonics also offers specialized systems for select applications.

2012 Biomedical Optics and Three-Dimensional Imaging Technical Program Update Sheet

ID Quantique

Chemin de la Marbrerie 3
Carouge, Geneva CH-1227 Switzerland
P: +41.22.301.83.71
F: +41.22.301.83.79

michael.desert@idquantique.com
www.idquantique.com

IDQ offers photon-counters based on avalanche photodiodes in Geiger mode for the visible and infrared regions. It also includes Telecom short-pulse laser sources (id300). id100 is a photon counter based on silicon APD for VIS wavelength. id210 and id220 are based on InGaAs/InP APD (900-1700nm). The id210 has a 100MHz max. trigger rate and can operate in free running. The id220 offers the lowest dark count rate in free-running. The id400 is optimized for 1064nm.

Innolas Laser GmbH

Justus-von-Liebig-Ring 8
Krailling 82152 Germany
P: +1 413.562.4040
F: +1 413.562.6167

info@innolas-laser.com
www.innolas.com

Innolas is a leading German manufacturer of pulsed Nd:YAG lasers. Innolas offers models from 200-2000mJ, available in flash lamp or diode pumped lasers in order to go up to 200Hz. SHG, THG, FSG, seeding, and double pulse options are available.

ISS, Inc.

1602 Newton Drive
Champaign, IL 61822 USA
P: +1 217. 359. 8681
F: +1 271. 359. 7879

samantha.redes@iss.com
www.iss.com

ISS will be exhibiting the OxiplexTS – the first non-invasive monitoring device capable of determining the absolute concentration of the oxygenated and deoxygenated hemoglobin in tissues. ISS also provides a confocal microscope for FLIM, FRET, FFS applications; lifetime fluorimeters working in either frequency-domain or TCSPC mode and modular components for building your own fluorometer or confocal microscope. Please visit us at www.ISS.com.

Lucid, Inc.

95 Methodist Hill Drive Suite 500
Rochester, NY 14623 USA
P: +1 585.239.9800
F: +1 585.239.9806

lucid@lucid-tech.com
www.lucid-tech.com

Lucid is the word leader in noninvasive confocal cellular imaging of skin in vivo. The company's innovative technologies are applied in a wide variety of application in basic research, cosmetics, aesthetics, pharmaceuticals and medical imaging and diagnostics. Lucid has built a secure networking platform that allows images to be captured and shared with a diverse team, enhancing the ability of the user to collaborate with others.

Navitar, Inc.

200 Commerce Drive
Rochester, NY 14623
P: +1 585.359.4000
F: +1 585.359.4999

info@navitar.com
www.navitar.com

Navitar is a leading manufacturer of precision optics for biotechnology and medical applications. Our high performance modular components - from Bio Kohler illumination to fluorescence to HMC[®] objectives - integrate into OEM and biotech research imaging systems. We help you create a solution as unique as your application.

NKT Photonics

1400 Campus Drive West
Morganville, NJ 07751 USA
P: +1 732.972.9937
F: +1 732.414.4094

laser_sales@nktphotonics.com
www.nktphotonics.com

NKT Photonics provides supercontinuum solutions, from nonlinear fibers to complete SuperK laser systems with plug and play accessories.

Supercontinuum laser sources provide a white light output with the brightness of a laser and the spectral width of a lamp, replacing lasers and other sources used today for fluorescence imaging, OCT, FLIM, FRET and other applications in the 400-2400nm wavelength range. Use all the light, or tune, shape and manipulate it with our SuperK accessories.

Photonics Media

2 South Street
Pittsfield, MA 01201 USA
P: +1 413.499.0514
F: +1 413.442.3180

www.photonics.com

Photonics Media – the Pulse of the Industry – invites you to explore the information leader and all that we have to offer. As the publisher of Photonics Spectra, BioPhotonics and EuroPhotonics magazines, Photonics Buyers' Guide, Photonics.com, and more, we bring you the news, research and applications articles you need to succeed. Visit www.Photonics.com for your FREE subscriptions and much more.

PicoQuant Photonics North America, Inc.

8A Pumpkin Lane
Westfield, MA 01085 USA
P: +1 413.562.6161
F: +1 413.562.6167

info@picoquant-usa.com
www.picoquant-usa.com

Product lines include Pulsed Diode Lasers, Time-Correlated Single Photon Counting (TCSPC) electronics and detectors, fluorescence lifetime spectrometers, time-resolved fluorescence microscopes and upgrade kits for Laser Scanning Microscopes. Applications include Single Molecule Spectroscopy, Fluorescence Lifetime Imaging (FLIM), Fluorescence Resonance Energy Transfer (FRET), Fluorescence Correlation Spectroscopy (FCS), Optical tomography and Quantum Key Distribution.

2012 Biomedical Optics and Three-Dimensional Imaging Technical Program Update Sheet

PolarOnyx, Inc.

2526 Qume Drive, Suites 17&18

San Jose, CA 95131 USA

P: +1 408.573.0930

F: +1 408.573.0932

sales@polaronyx.com

www.polaronyx.com

World leading company in high energy/power ultrashort (fs,ps,ns) fiber lasers. Excellent for material processing, micromachining, spectroscopy, microscopy, biomedical instrumentation & optical sensing applications. OEM and instrument version are available. Wavelength ranges from UV to Mid-IR. Contact: Lihmei Yang, Director Sales & Product, lihmeiyang@polaronyx.com.

New products: Compact high energy/power ultrafast fiber lasers (UV to Mid-IR), GHz ultrafast fiber laser.

Santec USA Corporation

433 Hackensack Ave

Hackensack, NJ 07601 USA

P: +1 201. 488. 5505

F: +1 201. 488. 7702

info@santec.com

www.santec.com

Established in 1979, Santec is a global photonics engineering company and a leading manufacturer of Tunable Lasers, Optical Test and Measurement Products and Optical Components. Santec's high speed scanning levels were developed specifically for OCT applications, and feature high power, wide tuning, and fast scan to achieve high resolution real time 2-D imaging. Santec also offers a complete OCT system, IVS-200, which utilizes the HSL-200.

Time-Bandwidth Products, Inc.

8A Pumpkin Lane

Westfield, MA 01085 USA

P: +1 413. 564. 0610

F: +1 413. 562. 6167

sales-usa@tbwp.com

www.tbwp.com

Time-Bandwidth Products manufactures passively mode-locked tunable and fixed pico and femtosecond DPSS lasers using our patented SESAM® technology. Wavelengths from 262nm to 1550nm are available at different rep rates and power levels reaching up to 50W to match your application in research or for industrial applications.



No photography is permitted in the exhibit hall.

Thank you!

Toptica

1286 Blossom Drive Suite 1

Victor, NY 14564 USA

P: +1 585.657.6663

F: +1 877.277.9897

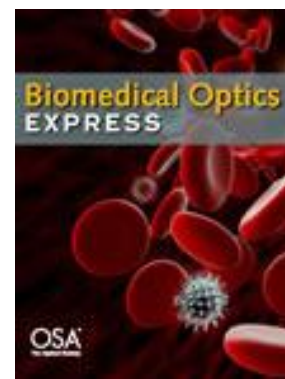
lisa.riggs@toptica-usa.com

<http://www.toptica.com/>

TOPTICA is a recognized global leader in diode laser and ultrafast technology for industrial and scientific markets. We offer the widest range of single mode tunable light in the 190 to 2900nm and 0.5-2.5THz spectral region with various accessories to measure, characterize, stabilize and analyze light. Our robust and most compact ultrafast fiber lasers are opening new avenues for spectroscopy, microscopy and life sciences, even for clinical integration. With our Passion for Precision, TOPTICA delivers!

Biomed and DH THANK OUR CORPORATE SPONSORS!

THORLABS



2012 Biomedical Optics and Three-Dimensional Imaging Technical Program Update Sheet

Withdrawn Presentations

BSu3A.53 (BIOMED Poster Session I), **In-vivo Imaging of Embedded Surgical Sutures and the Surrounding Physiology with Photoacoustic Microscopy**, A. Giannoula¹, L. Funk², C. Weis², P. Turon², T. Durduran¹; ¹ *Institute of Photonic Sciences, Castelldefels, Spain*; ² *Braun Surgical SA, Barcelona, Spain*.

DSu2C.7 (Special Techniques of Digital Holography) **Photorefractive Digital Holographic Microscopy**, Marcos Gesualdi¹; ¹ *Universidade Federal do ABC (UFABC), Santo Andre, Brazil*.

JM3A.22 (Joint BIOMED/DH Poster Session), **In vivo quantification of tumor metabolic demand in pre-clinical models using optical spectroscopy**, Tony Jiang¹, Narasimhan Rajaram¹, Chengbo Liu^{1,2}, Fangyao Hu¹, Nimmi Ramanujam¹; ¹ *Biomedical Engineering, Duke University, USA*; ² *School of Life Science and Technology, Xi'an Jiatong University, Xi'an, China*.

Changes in Presenters

BM2B.5, **Quantitative Photoacoustic Imaging by Acousto-Optically Measured Light Fluence**, will be presented by Khalid Daoudi, *University of Twente, MIRA Institute for Biomedical Technology and Technical Medicine - Biomedical Photonic Imaging group, Netherlands*

BW2A.2, **Dual-Band FDML Laser for Swept Source Spectroscopic OCT**, will be presented by Jianbing Xu, *the Univ. of Hong Kong, China*.

JM3A.4, **Wavelet synchronization index to assess variations in regional cerebral oxygenation in infants on life support**, will be presented by Ilias Tachtsidis, *Univ. College London, UK*.

JM3A.32, **Individualised Optimisation of Modelling Cerebral Oxgenation Near-Infrared Spectroscopy Signals** will be presented by Ilias Tachtsidis, *Univ. College London, UK*.

JM3A.38, **Correction of Shape-induced artifacts in spectroscopic imaging of biological media**, will be presented by Thu Nguyen, *Catholic Univ., USA*

JM3A.46, **Normative database of judgment of complexity task with functional near infrared Spectroscopy Application for TBI** will be presented by Laleh Najafizadeh, *HJF/CNRM/NIH, USA*

JM3A.55, **Superposition Procedure for Improvement of Digital Holographic Particle Field Reconstruction** will be presented by Dhananjay Kumar Singh, *I.I.T. Kanpur, India*

JM3A.62, **Geometrical Characterization of Micro-fiber in 3D Volume using Digital In-line Holography**, will be presented by Dhananjay Kumar Singh, *I.I.T. Kanpur, India*

JM3A.67, **Intensity Based Holographic Reconstruction of Symmetric and Asymmetric Object Field**, will be presented by Dhananjay Kumar Singh, *I.I.T. Kanpur, India*

JM3A.69, **Diffuse Optical Tomography Imaging of the Hemodynamic Response to a Breath Hold for Use in Breast Cancer Detection** will be presented by Jacqueline Gunther, *Columbia Univ., USA*.

Presider Changes

Session BW3A, **Breast Cancer Imaging (13:30-15:30 Wednesday 2 May)** will be presided by Stefan Andersson-Engels, *Lund Univ., Sweden*.

Session BW4B, **New Spectroscopic Techniques and Applications (16:00 - 18:00, Wednesday 2 May)** will be presided by Martin Wolf, *Univ. Hospital of Zurich, Switzerland*.

Change in Author

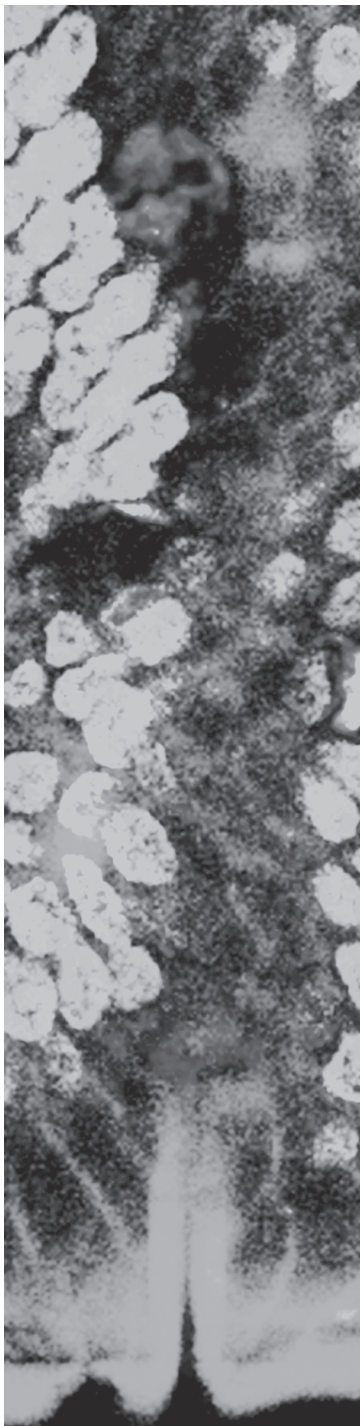
BW1B.6, **Stokes Shift Spectroscopy and imaging for highlighting the difference of breast cancerous and normal tissues**, added author Tang Guichen, *City College of City Univ of New York - Physics, Institute for Ultrafast Spectroscopy and Lasers, USA*.

Program Changes

Myung "Paul" Kim will now be giving a tutorial presentation in place of George Barbastathis. The presentation will be titled: **Special Techniques in Digital Holography** and will be presented on Tuesday, 1 May from 8:00-8:40 am during the Digital Holographic Microscopy II session.

The OIDA Session will be held 18:00-20:00 Tuesday, 1 May in Symphony IV.

2012 OSA
OPTICS &
PHOTONICS
CONGRESS



POSTDEADLINE PAPERS

Biomedical Optics and Three-Dimensional Imaging

Biomedical Optics (BIOMED)

Digital Holography & 3-D Imaging (DH)

ISBN 978-1-55752-945-9

28 April – 2 May 2012

Miami Hilton Downtown
Miami, Florida, USA

www.osa.org/congresses

Photo credit: Diaspro, Alberto; et al. Multi-Photon excitation
microscopy. Biomedical Engineering Online, 2006, 5:36.

OSA[®]
The Optical Society

Biomedical Optics Postdeadline Session

Sunday, 29 April 2012, *Symphony I & II*

16:30 – 20:40

16:30 – 19:30

BSu5A • BIOMED Postdeadline Session

Xingde Li; *Johns Hopkins University, USA, Presider*

BSu5A.1 • 18:30

Branched gold nanoparticles for a combined photoacoustic imaging and photothermal therapy, A. D'Hollander^{1,2}, D. Fuchs³, B. Vanspauwen², H. Jans², G. Vandeveld¹, L. Lagae^{2,4}, U. Himmelreich¹; ¹*Radiology / BioNMR Unit, K.U.Leuven, Belgium*; ²*imec, Belgium*; ³*Visualsonics, Canada*; ⁴*Solid State Physics and Magnetism, K.U.Leuven, Belgium*. In this work, both *in vitro* and *in vivo* studies will show that branched AuNPs are ideally suited for a combined photoacoustic imaging and photothermal therapy of cancer.

BSu5A.2 • 18:40

Upconverting nanoparticles as contrast agents for *in vivo* luminescence imaging and tomography

Stefan Andersson-Engels¹, Haichun Liu¹, Can T. Xu¹, Pontus Svenmarker¹, Anna Gisselsson², Pontus Kjellman², Linda Andersson², Rene in't Zandt², Fredrik Olsson², and Sarah Fredriksson²; ¹*Department of Physics, Lund University, Sweden*; ²*Genovis AB, Sweden*. Upconverting nanoparticles have recently drawn increasingly attention as contrast agents for optical bioimaging. They enable autofluorescence-free imaging within the tissue optical window, and improved spatial resolution as compared to conventional fluorescence-based contrast agents.

BSu5A.3 • 18:50

On the Validity of Assumptions to Incorporate Absorption in Monte Carlo Simulations, Katherine W. Calabro and Irving J. Bigio; *Dept. of Biomedical Engineering, Boston University, USA*; *Dept. of Electrical and Computer Engineering, Boston University, USA*. Incorporation of absorption in Monte Carlo simulations of light transport in tissue is widely achieved by assuming photon packets and equal fractional loss per step. We report differences between this method and more rigorous algorithms under conditions common in biomedical optics research.

BSu5A.4 • 19:00

Numerical nonlinear microscopy of collagen fibres, Daaf Sandkuijl^{1,2,3}, Adam Tuer^{1,2,3}, Danielle Tokarz^{1,3,4}, and Virginijus Barzda^{1,2,3}; ¹*Department of Chemical and Physical Sciences, University of Toronto Mississauga, Canada*; ²*Department of Physics, University of Toronto, Canada*; ³*Institute for Optical Sciences, University of Toronto, Canada*; ⁴*Department of Chemistry, University of Toronto, Canada*. Numerical results of a new method of collagen fibril nonlinear microscopy are presented. Focalspot shaping and polarization control of the excitation beam is used, which generates unique collagen fibril signatures in the far field pattern.

BSu5A.5 • 19:10

Bacteria Classification by Means of the Statistical Analysis of Fresnel Diffraction Patterns of Bacteria Colonies,

Halina Podbielska¹, Igor Buzalewicz¹, Agnieszka Suchwałko^{1,3}, Alina Wieliczko²; ¹*Bio-Optics Group, Institute of Biomedical Engineering and Instrumentation, Wrocław University of Technology, Poland*; ²*Department of Epizootiology and Veterinary Administration with Clinic of Infectious Diseases, Wrocław University of Environmental and Life Science, Poland*; ³*Medicwave AB, Strandgatan, Sweden*. The novel optical system for analysis of Fresnel diffraction patterns of bacterial colonies is proposed. Obtained results have shown that features extraction and statistical of Fresnel patterns enables bacteria species classification with high accuracy.

BSu5A.6 • 19:20

Scattered Light Fluorescence Microscopy in Three Dimensions,

C. Aegerter¹, G. Ghielmetti¹; ¹*Physik-Institut, University of Zurich, Switzerland*. Here we show that imaging behind strongly turbid layers is possible using wave-front shaping of the illuminating light and the optical memory effect. The imaging method is shown to be applicable in three dimensions.

BSu5A.7 • 19:30

Computer Aided Monitoring of Neoadjuvant

Chemotherapy for Breast Cancer, David R. Busch¹, Wensheng Guo², Regine Choe³, Turgut Durduran⁴, Michael D. Feldman⁵, Carolyn Mies⁵, Brian J. Czerniecki⁶, Julia Tchouf⁶, Angela DeMicheleg⁷, Mark A. Rosenh⁸, Michael D. Schnall⁸, and Arjun G. Yodh¹; ¹*Dept. Physics and Astronomy, Univ. of Pennsylvania, USA*; ²*Department Biostatistics, Univ. of Pennsylvania, USA*; ³*Dept. Biomedical Engineering, University of Rochester, USA*; ⁴*ICFO-Institut de Ciencies Fotoniques Castelldefels, Spain*; ⁵*Dept. Pathology and Laboratory Medicine, Univ. of Pennsylvania, USA*; ⁶*Dept. Surgery, Univ. of Pennsylvania, USA*; ⁷*Dept. Medicine (Hematology/Oncology) and Epidemiology*; ⁸*Dept. of Radiology, Univ. of Pennsylvania, USA*. Diffuse Optical Tomography creates 3D maps of physiological properties. We previously reported a statistical analysis of these maps to automatically localize cancer. We now utilize this technique to monitor locally advanced cancers during neoadjuvant chemotherapy.

Biomedical Optics Postdeadline Session

Sunday, 29 April 2012, *Symphony I & II*

16:30 – 20:40

BSu5A.8 • 19:40

Measurement of Raman Spectra for Tomographic Reconstruction, Jennifer-Lynn Demers¹, Scott Davis¹, Brian W. Pogue¹, Michael D. Morris²; ¹*Thayer School of Engineering, Dartmouth College, USA*; ²*Department of Chemistry, Univ. of Michigan, USA*. Raman signal is measured through a tomography set-up with 8 distinct spectrometers allowing for increased spectral resolution. Reconstructed images show good localization and contrast of Raman signal to background for Teflon inclusions within gelatin-based phantoms.

BSu5A.9 • 19:50

PDT induced changes assessed by time-gated fluorescence tomography ¹Ulas Sunar, ¹Weirong Mo, ¹Daniel Rohrbach; *Dept of Cell Stress Biology & PDT Center, Roswell Park Cancer Institute, USA*. We report 3D reconstruction of fluorescence yield and lifetime of a photosensitizer before and after PDT. The results demonstrate both yield and lifetime contrasts may be useful for PDT monitoring.

BSu5A.10 • 20:00

In-vivo risk stratification of pancreatic cancer by evaluating optical properties in duodenal mucosa, ¹Nikhil N. Mutyal, ¹Andrew Radosevich, ²Shailesh Bajaj, ²Sudeep Upadhye, ¹Jeremy D. Rogers, ²Hemant K. Roy, ¹Vadim Backman. ¹*Department of Biomedical Engineering, Northwestern Univ., USA*; ²*Department of Gastroenterology, Northshore Univ. Healthsystems, USA*. We present a novel approach of measuring optical properties with fiber optic probe from endoscopically accessible Peri-Ampullary duodenum as way to detect pancreatic cancer at early stages.

BSu5A.11 • 20:10

Breast Cancer Detection in the Spectral Subspace of Biomarkers, Yi Sun¹, Yang Pu², Laura A. Sordillo², Yuanlong Yang², R. R. Alfano²; ¹*Electrical Engineering Department, Institue for Ultrafast Spectroscopy and Lasers and Physics Department of The City College of City University of New York, USA*. A novel approach of fluorescent spectral subspace of four key biomarkers with 340 nm excitation is proposed to detect breast cancer and determine efficacy of collagen, NADH, flavin, and elastin.

BSu5A.12 • 20:20

Single gradient-index-multimode-fiber Enabled Fourier-domain Low Coherence Interferometry and Reflectance Spectroscopy Towards Fine-needle-probing of Steatosis, Anqi Zhang¹, Daqing Piao¹, Kenneth E. Bartels², G. Reed Holyoak², Jerry W. Ritchey³; ¹*School of Electrical and Computer Engineering, Oklahoma State University, USA*; ²*Department of Veterinary Clinical Sciences, Center for Veterinary Health Sciences, Oklahoma State University, USA*; ³*Department of Veterinary Pathobiology, Center for Veterinary Health Sciences, Oklahoma State University, USA*. We present dual-modality Fourier-domain common-pass low coherence interferometry and reflectance spectroscopy based on single gradient-index multimode fiber fitting a 24 gauge needle. The objective is to assess the condition of donor liver steatosis.

BSu5A.13 • 20:30

Preliminary Intravital Microscopic Analysis Reveals Specific Monocyte Uptake of Circulating Nanotubes and Peptide-Dependent Delivery into Tumor, ¹Bryan R. Smith, ¹Eliver Ghosn, ¹Harikrishna Rallapalli, ¹Jarrett Rosenberg, ¹Jennifer Prescher, ¹Lee Herzenberg, ¹Sanjiv S. Gambhir; *Stanford University Departments of Radiology, Immunology, Bioengineering, and Chemistry, USA*. Nanoparticle targeting efficiency to tumor is poor and not well-understood. Applying intravital microscopy in a mouse-model to interrogate vasculature-targeted nanotubes, we found that monocytes specifically take up nanotubes and are programmed to enter tumor.

Digital Holography and Three-Dimensional Imaging Postdeadline Session

Sunday, 29 April 2012, *Symphony IV*

16:30 – 19:30

16:30 – 19:30

DSu5B • DH Postdeadline Session

Myung K. "Paul" Kim; *Univ. of South Florida, USA, Presider*

DSu5B.1 • 18:30

Dry Decoupling Of Index Of Refraction And Topography Through Digital Holographic Microscopy, Freddy Alberto Monroy Ramírez¹, Jorge Garcia-Sucerquia²; ¹*Physics Department, Universidad Nacional de Colombia, Colombia;* ²*School of Physics, Universidad Nacional de Colombia, Colombia.* In interferometric essays the measured phase merges the topography and index of refraction. Multiple wavelength illumination, variation of the index of refraction of the surrounding medium in containing cambers are common methods to separate those two features of the samples. In this work we present the use of the change of the air pressure on a perfusion camber to decouple the topography and index of refraction. The method is applied to fully characterize a partially stripped optical fibre.

DSu5B.2 • 18:45

Measurement of Asymmetric Temperature Field by Using Digital Holographic Multidirectional Interferometry, Doleček Roman^{1,2}, Psota Pavel^{1,2}, Lédl Vít^{1,2}, Vít Tomáš^{1,2}, Václavík Jan^{1,2}, Kopecký Václav²; ¹*Research Centre TOPTEC, Institute of plasma physics ASCR, Czech Republic;* ²*Technical University of Liberec Studentská Czech Republic.* This paper presents a digital holographic method for measurement of periodic asymmetric temperature fields. The method is based on modified Twyman-Green setup, in which only one precisely synchronized and triggered CCD allows for the 3D measurement and reconstruction.

DSu5B.3 • 19:00

Comparison of Digital Holographic Method for Very Small Amplitudes Measurement with Single Point Laser Interferometer and Laser Doppler Vibrometer, Psota Pavel¹, Lédl Vít¹, Doleček Roman¹, Václavík Jan¹, Šulc Miroslav¹; ¹*Institute of Plasma Physics, Czech Republic.* This paper describes a measurement setup and measurement results of simultaneous measurement of small vibration by a recently developed digitally holographic method, single point laser interferometry and laser Doppler vibrometer.

DSu5B.4 • 19:15

New Calculation Method for Quadrature Phase-shifting Interferometer and Its Application to Digital Holography, Suezou Nakadate¹, Tomohiro Kiire¹, Shinya Sawada², Masato Shibuya¹; ¹*Dep. of Media and Image Tech., Faculty of Engineering, Tokyo Polytechnic University, Japan;* ²*Center for Optical Research and Education, Utsunomiya University, Japan.* A new calculation method for a quadrature phase-shifting interferometer is presented and its application to digital holography is also described. Two sets of quadrature phase-shifted interferograms or holograms are acquired and the new calculation method proposed gives the phase distribution of the wavefront measured. The principle of the calculation method with computer simulations and its application to digital holography with experimental results are given.

DSu5B.5 • 19:30

High fidelity reconstruction of three-dimensional objects by FINCH fluorescence microscopy, Nisan Siegel^{1,2}, Joseph Rosen^{1,2,3}, Gary Brooker^{1,2}; ¹*Department of Biomedical Engineering, Johns Hopkins University, USA;* ²*Microscopy Center, Johns Hopkins University Montgomery County Campus, USA;* ³*Department of Electrical and Computer Engineering, Ben-Gurion University of the Negev, Israel.* FINCH holography produces super-resolved images above and below the focal plane of the microscope objective but with different magnifications. A method is presented to faithfully reconstruct 3D objects with dimensional fidelity.

**BSu5A: Biomedical Optics (BIOMED)
Postdeadline Papers**

Sunday 29 April, 2012

Symphony I & II

16:30 – 20:40

Antoine D'Hollander
imec, Kapeldreef 75
3001 Leuven
Belgium
+3216228952

Branched gold nanoparticles for a combined photoacoustic imaging and photothermal therapy

A. D'Hollander^{1,2}, D. Fuchs³, B. Vanspauwen², H. Jans², G. Vandeveldel¹, L. Lagae^{2,4}, U. Himmelreich¹

¹Radiology / BioNMR unit, K.U.Leuven, Leuven, Belgium ²imec, Leuven, Belgium ³Visualsonics, Toronto, Canada ⁴Solid State Physics and Magnetism, K.U.Leuven, Leuven, Belgium

Abstract

In this work, both *in vitro* and *in vivo* studies will show that branched AuNPs are ideally suited for a combined photoacoustic imaging and photothermal therapy of cancer.

Introduction

Cancer is a complex disease. Still today, the detection and monitoring is time-consuming, costly and complex. Therefore, there remains a need for more efficient detection, imaging and treatment techniques. Decreasing the therapy complexity by combining the detection and treatment using only one optical technique would be a big advantage in this field. In this work we will show that gold nanoparticles (AuNPs) have such a huge potential as an optical agent for the combined photoacoustic (PA) imaging and photothermal therapy (PTT) of cancer¹⁻³. Branched AuNPs were chosen in this work because of their high absorption coefficient in the NIR-region which is essential for the proposed optical techniques⁴.

Material and methods.

Synthesis: The branched AuNPs were synthesized by a procedure based on Hao et al. and characterized with UV-Vis absorption spectroscopy and TEM⁵. In addition, they were coated with a self-assembled monolayer (SAM) to retain stability in physiological conditions.

In vitro: AuNPs were exposed to ovarian cancer cells (SKOV3) for different times (1, 3, 6, 12, 24h). The AuNPs uptake by the cancer cells was evaluated by ICP-OES and dark-field microscopy. Next, PTT was induced after laser irradiation and evaluated by fluorescence microscopy (living cell/nucleus staining). In addition, PA signals of the cells with and without branched AuNPs were measured by suspending the cells (100k cells/ μ L) in an agar (1.5%) phantom.

In vivo: Ten million SKOV3 cells were injected in both lower limbs of mice. After three weeks, 50 μ L of branched AuNPs (9.2×10^{11} NPs/mL) were injected in the left tumor. The right tumor served as a control and was injected with 50 μ L DPBS. PA signals were measured at the tumor site. Finally PTT was induced and the tumor reduction (or growth) was evaluated by bioluminescent imaging (BLI), magnetic resonance imaging (MRI) and histology.

Results.

Branched AuNPs were successfully synthesized with an absorption wavelength in the NIR-region (~ 680 nm) (Figure 1). After functionalizing the AuNPs with a SAM the wavelength shifted by 10 nm indicating the presence of the coating layer. This chemical coating preserved the stability of the AuNPs in physiological condition, which was confirmed by a salt aging procedure.

Next, SKOV3 tumor cells were incubated with branched AuNPs. After twelve hours of incubation, a significant amount of AuNPs was detected within the cells (~ 20 pg Au/cell). Longer incubation times did not lead to any significant increase in intracellular uptake of AuNPs. Dark-field microscopy (Figure 1), TEM and PA imaging were used to visualize the intracellular uptake of AuNPs. Already after three hours of incubation, a significant PA signal could be detected. Intenser PA signals could be detected by increasing the incubation time. An incubation time of 24 hours was used prior to PTT. Laser irradiation was applied for 5 min (690 nm, 35 W/cm²) at the tumor spot. The

AuNPs efficiently absorbed the light and converted it in to heat. This heat caused necrosis of the cells as indicated by a live cell/nucleus staining where a decrease of the fluorescence live cell signal was detected (Figure 1).

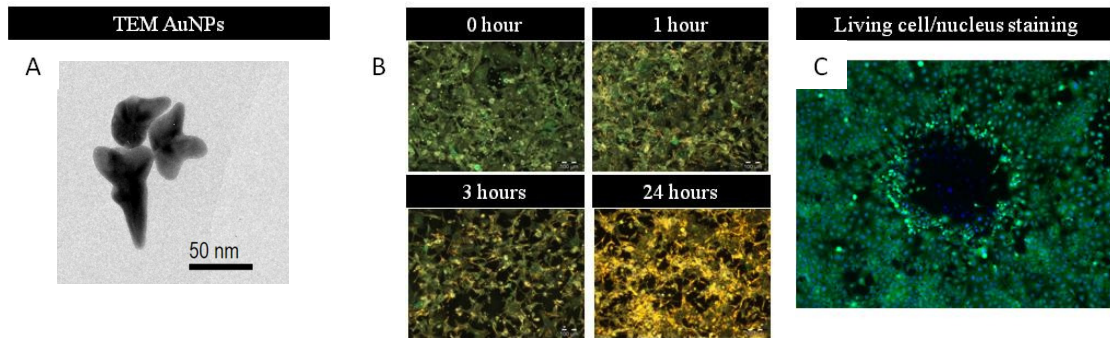


Figure 1. (A) TEM image of branched AuNPs (B) Dark-field images of cells incubated with AuNPs with different incubation times. (C) Fluorescence image of cells after *in vitro* PTT. Caelein AM corresponds to the living cells (green) and Hoechst to the cell nucleus (blue)

In a next step, the branched AuNPs were used for the combined PA imaging and PTT of cancer *in vivo*. After AuNP injection in the tumor located at the lower limb of a mouse, PA signals could be detected with a high signal to noise ratio (Figure 2). The ultrasound/PA overlay images showed that most AuNPs were located between the tumor and the skin after injection, which is probable due to a high tumoral fluid pressure. PTT was induced by irradiating the tumors with the laser for 5 min. Directly after therapy a decrease in tumor volume was clearly observed by BLI & MRI. The tumors were monitored over time and in the first three days after therapy a decreased BLI signal was observed. Using MRI, a gap in the tumor was detected at the irradiation spot (Figure 2). Histology data confirmed a loss of cell integrity, indicating necrosis. However, after four days the tumor size increased, indicating tumor regrowth. Presumably the laser spot was too small to irradiate the full tumor or an inhomogenous AuNP distribution within the tumor didn't allow to fully destroy the tumoral tissue. Future experiments will be conducted to optimize the PTT.

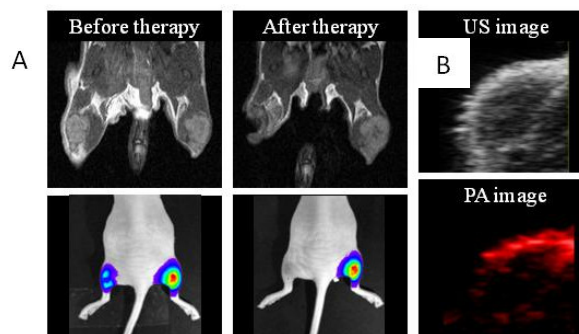


Figure 2. (B) MRI (top) and BLI (bottom) before and after PTT. (C) *In vivo* ultrasound (US; top) and PA (bottom) image of AuNPs injected in tumor

Conclusion.

Both *in vitro* and *in vivo* studies proved that branched AuNPs were ideally suited for a combined PA imaging and PTT. AuNPs coated with a SAM, were able to accumulate in significant amounts in the tumor cells. Because of their high absorption cross section in the NIR, the AuNPs were clearly detectable in PA imaging and could destroy tumor cells in PTT. In conclusion branched AuNPs show great promise within 'nano'-medicine and can help decrease the complexity of cancer monitoring and therapy.

References.

- 1 Huang X. & El-Sayed M.A. Gold nanoparticles: optical properties and implementations in cancer diagnosis and photothermal therapy. *Journal of advanced research*.2010, 1, 13-28
- 2 Yang X., Stein E.W., Ashkenazi S. & Wang L.V. Nanoparticles for photoacoustic imaging. *Wiley interdisciplinary reviews: nanomedicine and nanobiotechnology*. 2009, 1 (4): 360-368
- 3 Luke G.P., Yeager D. & Emelianov S.Y. Biomedical applications of photoacoustic imaging with exogenous contrast agents. *Annals of biomedical engineering*. 2011, 40 (2), 422-437
- 4 Van de Broek B., Devoogdt N., D'Hollander A., Gijs H.-L., Jans K., Lagae L., Muyltermans S., Maes G. & Borghs G. Specific cell targeting with nanobody conjugated branched gold nanoparticles for photothermal therapy. *ACS Nano*. 2011, 5 (6), 4319-4328
- 5 Hao, E.; Bailey, R. C., Schatz, G. C., Hupp, J. T., Li & S. Y. Synthesis and Optical Properties of "Branched" Gold Nanocrystals. *Nano Lett*. 2004, 4, 327–330.

Upconverting nanoparticles as contrast agents for *in vivo* luminescence imaging and tomography

Stefan Andersson-Engels¹, Haichun Liu¹, Can T. Xu¹, Pontus Svenmarker¹, Anna Gisselsson², Pontus Kjellman², Linda Andersson², Rene in't Zandt², Fredrik Olsson², and Sarah Fredriksson²

¹Department of Physics, Lund University, Lund, Sweden

²Genovis AB, Lund, Sweden

stefan.andersson-engels@fysik.lth.se

Abstract: Upconverting nanoparticles have recently drawn increasingly attention as contrast agents for optical bioimaging. They enable autofluorescence-free imaging within the tissue optical window, and improved spatial resolution as compared to conventional fluorescence-based contrast agents.

© 2012 Optical Society of America

OCIS codes: 110.0113, 170.0170, 190.3970, 190.7220, 350.5730

1. Background

Imaging has become an increasingly important tool in drug discovery and development, as it provides a tool for minimally invasive monitoring [1]. *In vivo* alterations at the organ, tissue, cell or even molecular level can be closely monitored in animal studies to improve the understanding of basic pathological physiology. Studies over days, weeks and months on each individual are possible with repeated imaging. With improved imaging capabilities it is possible to further increase the reliability and accuracy and thereby further facilitate translational research. All imaging modalities used clinically today are also available for preclinical imaging; while optical imaging is the most common modality used in small animal *in vivo* imaging due to its simplicity and cost-effectiveness [2].

The main limitations of fluorescence small animal molecular imaging are tissue autofluorescence, poor resolution and poor light penetration, making it difficult to image deeply located regions with high sensitivity [3]. Furthermore, photobleaching of the traditionally used fluorescence probes sets a limit for repeated imaging required in longitudinal studies [4]. Upconverting nanoparticles (UCNPs) have a potential to overcome these limitations by their unique properties. UCNPs are synthesized as small crystals doped with certain trivalent lanthanide ions or transition metals [5, 6]. Common materials are ytterbium and yttrium in combination with small amounts of other ions, like for instance erbium (Er) or thulium (Tm). Such Yb/Tm-codoped UCNPs are excited at a wavelength of around 980 nm and emit light at 800 nm. Both the excitation and emission wavelengths are close to optimal for *in vivo* imaging in tissue [7]. Due to the anti-Stokes shift of the upconverting signal, the signal can be truly background-free without influence from any tissue autofluorescence [8, 9]. This increases drastically the signal-to-background ratio, making it possible to measure very weak signals from tissue. Another benefit of UCNP imaging is the possibility to obtain an improved spatial resolution in the recorded images [10]. This is due to the non-linear relation between the emitted signal and the excitation power. This non-linear dependence alters the sensitivity map for the nanoparticles within the tissue [11]. Based on these unique properties, this study was designed to investigate the potential of upconverting nanostructures as probes in optical imaging - through phantom studies as well as *in vivo* imaging. The goal of this research is to find probes that can facilitate improved optical imaging characteristics in terms of sensitivity and resolution.

2. Upconverting nanoparticle synthesis and first toxicology tests

Efficient NaYF₄:Yb³⁺,Tm³⁺@NaYF₄ upconverting nanoparticles were synthesized through an efficient stoichiometric method [12,13]. Briefly, the NaYF₄:Yb³⁺,Tm³⁺ particles were first grown in a mixture of oleic acid and octadecene at 300 °C, after the nucleation from rare earth, sodium and fluoride ions. A coating layer of NaYF₄ was subsequently grown without dopants. The crystals were washed and precipitated before further coating with a combination of poly(maleic anhydride-alt-1-octadecene) (PMAO) and polyoxyalkyleneamine (MW2000). The final nanostructures had a diameter of approximately 20-30 nm (hydrodynamic diameter) and were stored in 150 mM NaCl until use. Initial

toxicology and proliferation test were performed on hepatocellular carcinoma Hep G2 cells. The proliferation profile and toxicity profile did not indicate any adverse effects within the concentration range tested (up to 170 pg/cell).

3. Phantom experiments

The resolution of diffuse transmission tomography was evaluated for two capillaries filled with either a suspension of UCNP or the dye DY-781. The capillary tubes were located at a depth of 7 mm into a diffusely scattering tissue phantom from the source side and 10 mm from the detector side. The phantom was made from water, intralipid and ink. It had approximately the same optical properties at all three wavelengths of interest in this study (785 nm for exciting the DY-781, 800 nm for detection of the light emitted from both probes, and 975 nm for exciting the UCNP): $\mu_a = 0.5 \text{ cm}^{-1}$ and $\mu'_s = 10.1 \text{ cm}^{-1}$ (measured by time-of-flight spectroscopy [14]). The resulting maps of the capillaries are presented in Fig. 1, comparable resolved at 9 and 6 mm for the dye and UCNP, respectively.

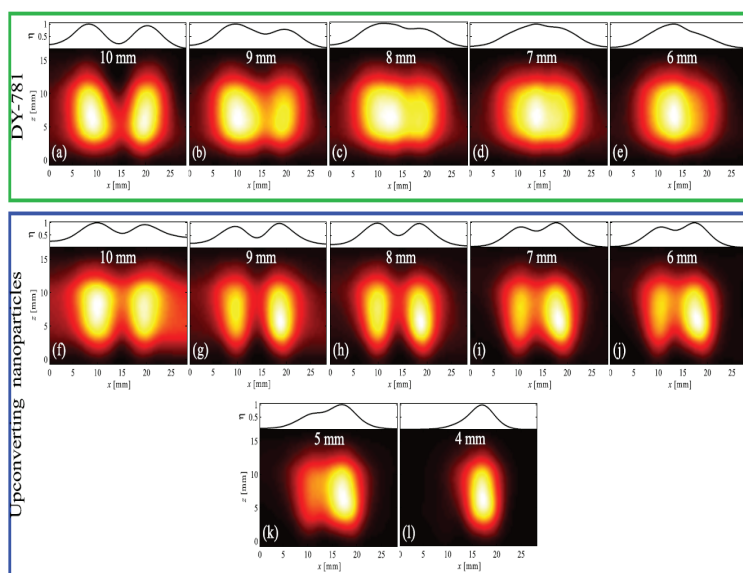


Fig. 1. Cross-sectional images of luminescence tomography reconstructions of two capillary tubes filled with the conventional DY-781 dye or with UCNP. The corresponding intensity profiles are also shown as line plots. The capillary tubes were placed at a depth of $z = 7 \text{ mm}$. The separation distance between the tubes was varied from 10 mm to 4 mm (only to 6 mm for Dy-781, stepsizes of 1 mm). The use of UCNP clearly leads to reconstructions with higher spatial resolution.

4. *In vivo* experiments

The retention of the particles in the lymphatic system was visualized *in vivo*, 24 hours post injection, for the popliteal (SLN) and the iliac lymph node. The presence of UCNP in the lymph nodes were evaluated *in vivo* following subcutaneous injection in the right hind paws of male Wistar rats (weight 200-250 gram, concentration UCNP 0.26 mg Y^{3+}/ml , injection volume 100 μl). The lymph nodes were visualized by an Andor iXon CCD camera following excitation at 975 nm with a power density of 200 mW/cm^2 and a spot size of $\phi = 3 \text{ mm}$. A resulting epi-luminescence image is illustrated in figure 2. The results from optical imaging shows that the nanostructures have been retained in the inguinal node 24 hours following the injection. The localization of the lymph nodes was verified by subsequent resection.

5. Conclusion

We illustrate first a significant improvement in spatial resolution for UCNP as compared to conventional dye fluorophores, due to the non-linear dependence on the excitation light fluence distribution within a tissue phantom for the UCNP. Then we also show the use of highly efficient UCNP for *in vivo* sentinel lymph node imaging in a rat. The results suggest that UCNP can be very powerful as contrast agents for small animal optical imaging.

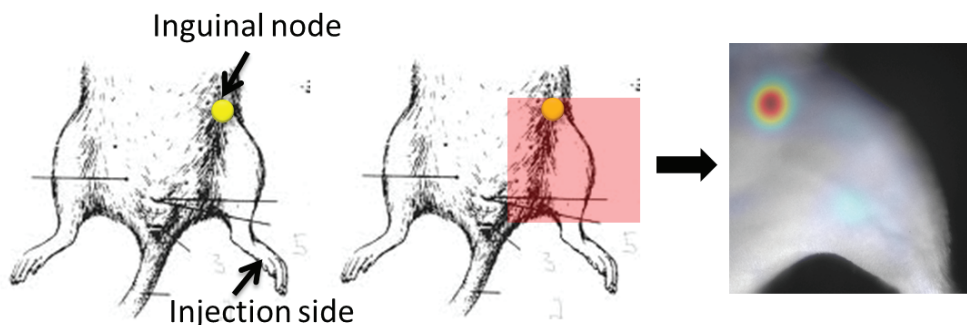


Fig. 2. Optical image acquired 24 hours post injection of UCNPs. The particles were injected in the right hind paw and are clearly detectable in the inguinal node.

References

1. Ralph Weissleder and Mikael J. Pittet. Imaging in the era of molecular oncology. *Nature*, 452(7187):580–589, April 2008.
2. Vasilis Ntziachristos, Jorge Ripoll, Lihong V Wang, and Ralph Weissleder. Looking and listening to light: the evolution of whole-body photonic imaging. *Nat Biotechnol.*, 23(3):313–320, Mar 2005.
3. Scott C Davis, Brian W Pogue, Hamid Dehghani, and Keith D Paulsen. Contrast-detail analysis characterizing diffuse optical fluorescence tomography image reconstruction. *J Biomed Opt.*, 10(5):050501, 2005.
4. Shiwei Wu, Gang Han, Delia J. Milliron, Shaul Aloni, Virginia Altoe, Dmitri V. Talapin, Bruce E. Cohen, and P. James Schuck. Non-blinking and photostable upconverted luminescence from single lanthanide-doped nanocrystals. *Proceedings of the National Academy of Sciences*, 106(27):10917–10921, 2009.
5. François Auzel. Upconversion and anti-stokes processes with f and d ions in solids. *Chem Rev.*, 104(1):139–173, Jan 2004.
6. Guanying Chen, Gabriel Somesfalean, Yan Liu, Zhiguo Zhang, Qiu Sun, and Fuping Wang. Upconversion mechanism for two-color emission in rare-earth-ion-doped ZrO_2 nanocrystals. *Phys. Rev. B.*, 75(19):195204, May 2007.
7. Qiuqiang Zhan, Jun Qian, Huijuan Liang, Gabriel Somesfalean, Dan Wang, Sailing He, Zhiguo Zhang, and Stefan Andersson-Engels. Using 915 nm laser excited $Tm^{3+}/Er^{3+}/Ho^{3+}$ -doped $NaYbF_4$ upconversion nanoparticles for *in vitro* and deeper *in vivo* bioimaging without overheating irradiation. *ACS Nano*, 5(5):3744–3757, May 2011.
8. Dev K Chatterjee, Abdul J Rufaihah, and Yong Zhang. Upconversion fluorescence imaging of cells and small animals using lanthanide doped nanocrystals. *Biomaterials*, 29(7):937–943, Mar 2008.
9. Can T. Xu, Niclas Svensson, Johan Axelsson, Pontus Svenmarker, Gabriel Somesfalean, Guanying Chen, Huijuan Liang, Haichun Liu, Zhiguo Zhang, and Stefan Andersson-Engels. Autofluorescence insensitive imaging using upconverting nanocrystals in scattering media. *Applied Physics Letters*, 93(17), OCT 27 2008.
10. P. Svenmarker, C. T. Xu, and S. Andersson-Engels. Use of nonlinear upconverting nanoparticles provides increased spatial resolution in fluorescence diffuse imaging. *Optics Letters*, 35(16):2789–2791, 2010.
11. Can T. Xu, Johan Axelsson, and Stefan Andersson-Engels. Fluorescence diffuse optical tomography using upconverting nanoparticles. *Applied physics letters*, 94(25):251107–251107–3, 2009.
12. Zhengquan Li and Yong Zhang. An efficient and user-friendly method for the synthesis of hexagonal-phase $NaYF_4 :Yb, Er/Tm$ nanocrystals with controllable shape and upconversion fluorescence. *Nanotechnology*, 19(34):345606, 2008.
13. Feng Wang, Renren Deng, Juan Wang, Qingxiao Wang, Yu Han, Haomiao Zhu, Xueyuan Chen, and Xiaogang Liu. Tuning upconversion through energy migration in core-shell nanoparticles. *Nat Mater.*, 10:968–973, 2011.
14. T. Svensson, E. Alerstam, D. Khoptyar, J. Johansson, S. Folestad, and S. Andersson-Engels. Near-infrared photon time-of-flight spectroscopy of turbid materials up to 1400 nm. *Review of Scientific Instruments*, 80(6):063105, 2009.

On the Validity of Assumptions to Incorporate Absorption in Monte Carlo Simulations

Katherine W. Calabro and Irving J. Bigio

*Dept. of Biomedical Engineering, Boston University, 44 Cummington St. Boston MA USA 02215;
Dept. of Electrical and Computer Engineering, Boston University, 8 St. Mary's St. Boston MA USA -2215
kcalabro@bu.edu; bigio@bu.edu*

Abstract: Incorporation of absorption in Monte Carlo simulations of light transport in tissue is widely achieved by assuming photon packets and equal fractional loss per step. We report differences between this method and more rigorous algorithms under conditions common in biomedical optics research.

OCIS codes: (170.0170) Medical optics and biotechnology; (170.3660) Light propagation in tissues

1. Introduction

Monte Carlo (MC) stochastic simulations are widely used for the purpose of simulating the propagation of photons in turbid media, such as tissue. Not only are MC simulations considered to be more accurate than analytical models, such as diffusion theory, but MC methods can be adapted to represent a wide range of geometrical configurations and tissue characteristics, especially for conditions under which other models are not valid. The primary limitation of the MC method is its computational expense; due to this challenge, algorithms to enhance computation efficiency are commonly employed.

One such approach, for the incorporation of absorption, was implemented by Wang, Jacques and Zheng in the code commonly referred to as MCML (Monte Carlo for Multi-Layered tissues)[1]. Within the biomedical optics community, the core of this code has been widely used and adapted for a range of applications, and has provided great value to the field as a whole. To model photon absorption, the MCML method implements an algorithm that treats light as packets of photons, starting with a weight of unity. During a packet's propagation, a constant fraction of its weight is reduced whenever a scattering event occurs, with the loss determined by the albedo of the medium, which combines the scattering and absorption coefficients. This approach improves efficiency because, by letting each packet run to completion (albeit with reduced weight contribution), computational 'effort' is not expended to track photons that are completely absorbed and therefore do not contribute to the final results. Fewer photons thus need to be simulated, reducing computational time.

However, from a physics perspective, scattering and absorption are independent phenomena, and photons are quanta that are absorbed, or not, based on probabilistic events; thus this treatment of absorption is an approximation that may not be accurately representative for a range of simulation conditions where the diffusion approximation is not valid. Furthermore, the packet approach allows for more signal to be recorded for a smaller number of simulated photons, but at the expense of fewer variations in pathways among the collected photons. Consequently, especially for short source-detector separations, the visitation histories may not be stochastically representative.

A more intuitive approach is to consider photons as discrete, quantized entities, and to allow scattering and absorption events to be independently determined statistically. With a much larger number of photons to track, this will increase computational expense significantly, but with technical advancements, such as parallel computing on Graphical Processing Units (GPUs), which can decrease simulation time by a factor of 300-1000x, the use of more rigorous representations is now reasonable [2,3].

In this work, we present the implementation of three alternative representations of absorption for MC simulations, and compare the results for a range of absorption coefficients, scattering coefficients, phase functions, and collection geometries.

2. Methods

A Monte Carlo code, based on traditional MCML, and adapted for use on a (GPU) by Alertram et al., was used as a template for our simulations [2]. This code was modified to launch and collect photons from within the areas and numerical apertures of user-defined fibers at the surface of a turbid medium. The code was further modified to provide a choice of phase function, allowing the user to select among Henyey-Greenstein, modified Henyey-Greenstein, or Mie-theory based phase functions. The choice of absorption method is indicated by a command argument at run time, allowing the same input file to be used, independent of method chosen. Four absorption algorithms were implemented for comparison: 1) the standard MCML method, 2) a quantized photon method, 3) a

packet method similar to MCML, but using Beer's law for weight reduction, and 4) a post-processing method based on scaling of a zero-absorption simulation.

1) Standard MCML: During a photon propagation step, a random scattering distance (s) is sampled based on the expected step size defined by the inverse of the total attenuation coefficient ($\mu_t = \mu_s + \mu_a$), where μ_s and μ_a are the scattering and absorption coefficients, respectively. Absorption is then accounted for by reducing the weight of the photon packet by an amount equal to the product of the albedo ($\alpha = \mu_a/\mu_t$) and the previous weight ($W_{i,j-1}$), where i refers to the current photon, and j to the current propagation step. Reflectance (R) is calculated as the sum of the weights of the collected photons divided by the number of launched photons (NLP), as detailed in equation (1), where ξ is a uniformly distributed number between 0 and 1, and NCP is the total number of collected photons.

$$s = -\ln(\xi)/\mu_t; \quad W_{i,j} = W_{i,j-1} - \alpha * W_{i,j-1}; \quad R = (\sum_{i=1}^{NCP} W_i)/NLP. \quad (1)$$

2) Quantized photons: For this method, scattering and absorption interactions are considered separately. Therefore, the scattering distance, s , is calculated from the scattering coefficient only (μ_s), not the total scattering coefficient (μ_t) as in method 1). More importantly, absorption occurs independently. At the beginning of a propagation step, not only is a scattering distance, s , sampled, but an absorption distance, a , is also sampled based on the inverse of the absorption coefficient (μ_a). If a is larger than s , scattering is the next event to occur, and the remainder of the propagation step is performed; but if a is smaller than s , an absorption event is the next event to occur, at which point the photon is terminated, and a new one is launched. Collected photons are those that never experience an absorption event. Equation (1) provides details of this method.

$$s = -\ln(\xi)/\mu_s; \quad a = -\ln(\xi)/\mu_a; \quad R = NCP/NLP. \quad (2)$$

3) Beer's law weight reduction: This method is very similar to the standard MCML algorithm, but as in the quantized photon method, the effects of scattering and absorption are separated. Therefore, the scattering distance is sampled based only on the scattering coefficient. The photon packet method is still applied, but the weight loss at each step is variable, and is based on the pathlength of the current step according to Beer's law, without a dependence on scattering. Reflectance is again calculated as the sum of the weights of the collected photons divided by the number of launched photons. Equation (3) provides details of this method.

$$s = -\ln(\xi)/\mu_s; \quad W_{i,j} = W_{i,j-1} - \exp(-\mu_a s) * W_{i,j-1}; \quad R = (\sum_{i=1}^{NCP} W_i)/NLP. \quad (3)$$

4) Post-processing scaling: With this method, propagation of the packet proceeds as in the standard MCML, but without packet loss until the collection point, at which time the weight is reduced by the application of Beer's law for absorption based on the total path length. This offers the advantage of generating results for multiple absorption coefficient values from a single simulation, significantly reducing the number of simulations to be run. While methods 2) and 3), to the best of our knowledge, have not been reported in the literature, this post-processing method has been used by a handful of authors[4–6].

$$s = -\ln(\xi)/\mu_s; \quad R = (\sum_{i=1}^{NCP} e^{-\mu_a L_i})/NLP. \quad (4)$$

Simulations for a range of absorption coefficients ([0-20] cm^{-1}), scattering coefficients (5, 30 cm^{-1}), and anisotropy factors, g ([0.5-0.95]), were generated using a two fiber illumination/collection geometry. The effect of source-detector separation was also considered, with fiber separation values ranging from 150 μm to 2mm. For each combination of variables, results were calculated as the average from four identical simulations, each terminating upon the collection of 2,500 photons.

3. Results

Differences in calculated reflectance among methods follow several general trends.

- As compared to the MCML method, the quantized method estimates lower reflectance, the Beer's law packet method estimates higher reflectance, and the post-processing method results in nearly identical reflectance values.
- Differences increase as the absorption coefficient, μ_a , increases.
- Absolute differences are greater for large scattering coefficient (μ_s) values, but are greater on a percentage basis for smaller scattering coefficients apparently due to lower overall reflectance.
- Differences are greater when the anisotropy factor, g , is lower.

- Absolute differences are greater when the source-detector separation distance is small, but the percentage difference is often greater for large separation distances at large absorption coefficient values, apparently due to small absolute reflectance.

The MC simulation results illustrated in Figure 1 represent conditions for which differences in reflectance of different absorption methods are large (a: 150- μm fiber separation with $g=0.5$), and small (b: 2-mm fiber separation with $g=0.95$). Error bars represent standard deviations for multiple simulation runs, but in many cases are too small to distinguish. For the data represented in Figure 1a, the difference among methods, as compared to MCML, can be as high as 65%. Whereas for the data represented in Figure 1b, differences are less than 2.5%

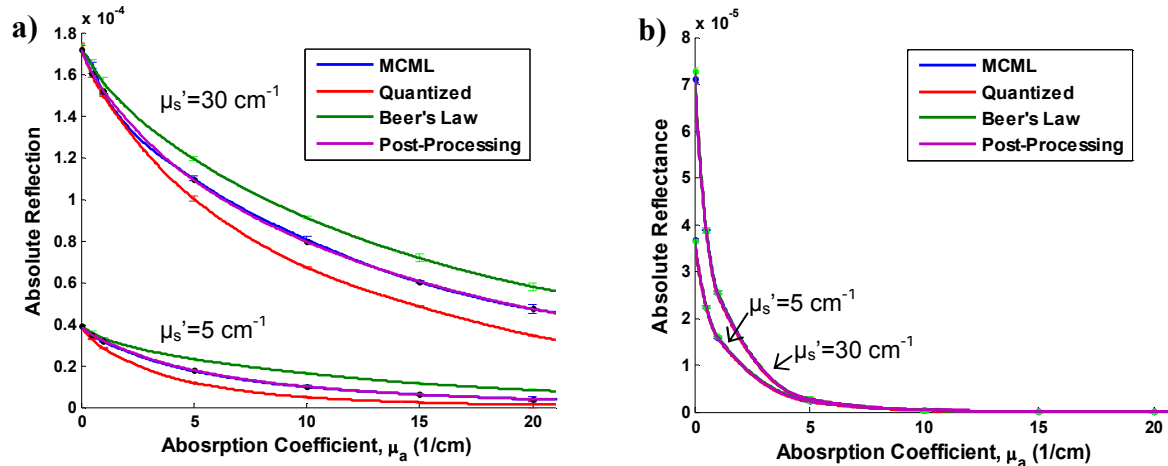


Figure 1: Absolute reflectance values simulated for all four absorption methods, under a range of input parameters: a) 150 μm fiber separation with $g=0.5$ (differences between MCML and post-processing methods are indistinguishable); and b) 2mm fiber separation with $g=0.95$

4. Conclusion

The results presented here demonstrate that the widely used method for incorporating absorption, as implemented in MCML, is not equivalent to methods that provide a more physically intuitive approach for absorption. It is currently unclear why these differences occur, and which method is most representative of reality, but we submit that a method that accounts for the quantum-mechanical nature of photon interaction is, to us, more compelling; nonetheless, as a first step, this work highlights the need for more thorough investigation of the assumptions currently being used to model absorption.

It is encouraging that these results verify that method 4), being used by some, is indeed equivalent to the MCML method, thus placing this method on firmer footing as a valid approach for the parameter space in which MCML is accurate, thus enabling significant computational time savings by implementing this method.

We would like to point out that for tissue properties and geometry conditions originally applied to MC, i.e., conditions for which the diffusion theory is valid, the absorption methods behave nearly identically, and thus the MCML absorption method is certainly valid in this regime. Like many other photon transport details, such as the influence of phase function [7], the effects of absorption are sensitive to variations under non-diffuse conditions, when source-detector separation distances are small and/or scattering does not dominate absorption, and for that parameter range, the specific method to incorporate absorption becomes important.

4. References

- [1] L. Wang, S. L. Jacques, and L. Zheng, "MCML - Monte Carlo modeling of light transport in multi-layered tissues," *Computer methods and programs in biomedicine* **47**, 131–146 (1995).
- [2] E. Alerstam, T. Svensson, and S. Andersson-Engels, "Parallel computing with graphics processing units for high-speed Monte Carlo simulation of photon migration," *Journal of biomedical optics* **13**, 060504 (2008).
- [3] Q. Fang and D. A. Boas, "Monte Carlo simulation of photon migration in 3D turbid media accelerated by graphics processing units," *Optics Express* **17**, 20178–20190 (2009).
- [4] R. Reif, O. A' Amar, and I. J. Bigio, "Analytical model of light reflectance for extraction of the optical properties in small volumes of turbid media," *Applied optics* **46**, 7317–7328 (2007).
- [5] S. C. Kanick, D. J. Robinson, H. J. C. M. Sterenborg, and A. Amelink, "Monte Carlo analysis of single fiber reflectance spectroscopy: photon path length and sampling depth," *Physics in Medicine and Biology* **54**, 6991–7008 (2009).
- [6] I. Meglinski and S. Matcher, "Quantitative assessment of skin layers absorption and skin reflectance spectra simulation in the visible and near-infrared spectral regions," *Physiological Measurement* **23**, 741–753 (2002).
- [7] J. R. Mourant, J. Boyer, A. H. Hielscher, and I. J. Bigio, "Influence of the scattering phase function on light transport measurements in turbid media performed with small source – detector separations," *Optics Letters* **21**, 546–548 (1996).

Numerical nonlinear microscopy of collagen fibres

Daaf Sandkuijl,^{1,2,3} Adam Tuer,^{1,2,3} Danielle Tokarz,^{1,3,4} and Virginijus Barzda^{1,2,3*}

¹Department of Chemical and Physical Sciences, University of Toronto Mississauga, 3359 Mississauga Road North, Mississauga, ON, Canada L5L 1C6

²Department of Physics, University of Toronto, 60 St. George Street, Toronto, ON, Canada M5S 1A7

³Institute for Optical Sciences, University of Toronto, 60 St. George Street, Suite 331, Toronto, ON, Canada M5S 1A7

⁴Department of Chemistry, University of Toronto, 80 St. George Street, Toronto, ON, Canada M5S 3H6

Author e-mail address: d.sandkuijl@utoronto.ca

Abstract: Numerical results of a new method of collagen fibril nonlinear microscopy are presented. Focalspot shaping and polarization control of the excitation beam is used, which generates unique collagen fibril signatures in the far field pattern.

OCIS codes: (180.4315) Nonlinear microscopy; (170.3880) Medical and biological imaging

1. Introduction

Nonlinear microscopy of collagen fibres provides unprecedented information regarding the structure of the extracellular matrix in tissue samples. Furthermore, the signal strength is excellent, which means the technique can be noninvasive when using proper excitation sources, well-designed optics, and sensitive detection equipment.

Using advanced focal spot shaping techniques and polarization-selective second harmonic imaging, more information can be extracted from tissue samples regarding the collagen fibre orientation. This paper presents a new technique for imaging collagen fibrils using a CCD camera, in which each orientation and position of the fibril has a unique far field intensity and phase distribution signature.

2. Numerical implementation

Calculations were performed in Matlab, using a focal spot calculation program based on the angular spectrum representation [1-3]. The program can calculate nonlinear signal generation from arbitrary input beams and arbitrary nonlinear susceptibility distributions at the focus [3].

3. Results

3.1 Focal field

Second harmonic generation from collagen fibrils at the focus was calculated for several fibril orientations. The excitation beam was assumed to be a fundamental Hermite-Gaussian beam and was modified using a phase-only spatial light modulator. The phase profile was a pi-phase shift through the centre of the beam, at an angle which was varied during imaging. The resulting beam resembles a first-order Hermite-Gaussian beam, but has the benefit that the out-of-phase lobes can be rotated at will, and that it can be generated using a normal laser output mode. Figure 1 shows the focal field of such a mode, where the phase discontinuity is oriented at 30 degrees with respect to the laboratory y-axis. Note that the focal plane is the XY-plane, and Z is the optical axis.

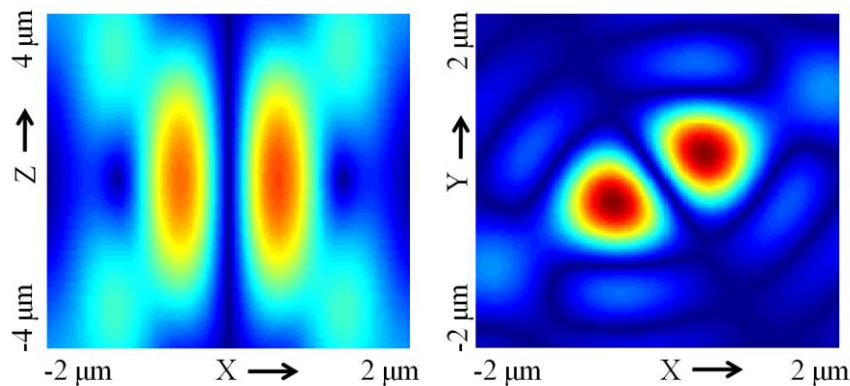


Figure 1: Focal field in a 0.75 NA objective for the modified fundamental Hermite-Gaussian beam. A spatial light modulator is used to introduce a pi-phase shift through the centre of the beam, which generates a focal spot similar to a first-order Hermite-Gaussian beam. The phase in this example was oriented at 30 degrees with respect to the y-axis.

As can be seen from Figure 1, the collagen fibrils will experience maximum signal generation when they are aligned parallel to the two intense lobes of the radiation. In addition, the input polarization can be varied without affecting the phase distribution. Therefore, a two-dimensional analysis can be done by rotating the lobes of the focal distribution using the spatial light modulator, and by varying the input polarization using a polarizer and/or half-wave plate.

3.2 Far field radiation from collagen fibrils

By varying the input polarization and the orientation of the focal field lobes and recording CCD images at the back aperture of the collection objective, the orientation of collagen fibrils at the focus can be determined. In the following figures, the CCD image at the back aperture of the collection objective is recorded for several input polarizations and phase cut orientations. The vertical axis indicates the angle of the linear input polarization, running from x-polarized (origin) to y-polarized (top). The horizontal axis indicates the orientation of the out-of-phase lobes. At the origin the lobes are both along the x-axis and at 90 degrees the lobes lie long the y-axis. The focal field depicted in Figure 1 would occur at 30° along the x-axis the following figures.

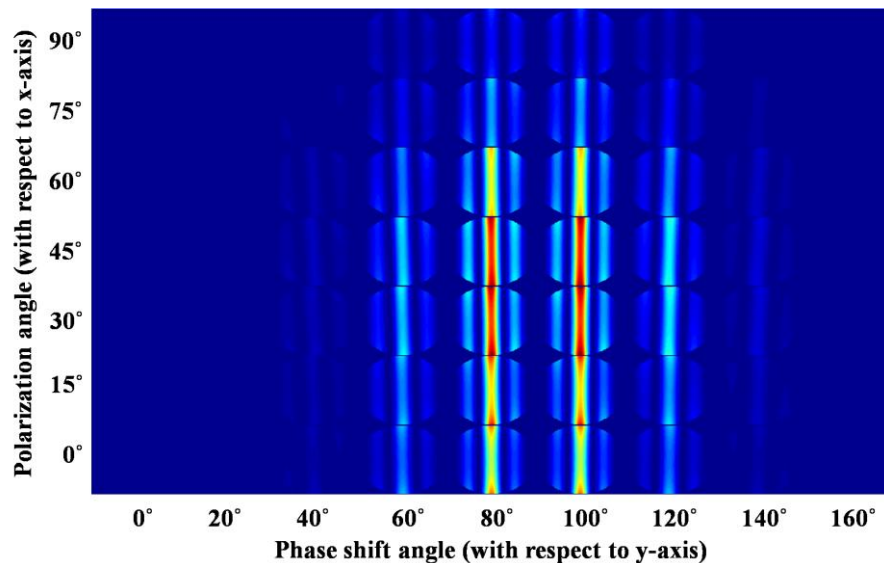


Figure 2: The far field radiation pattern at the back aperture of the collection objective for a collagen strand located in the focal plane parallel to the y-axis. The signal is maximal when both lobes of the focal field distribution interact with the fibril.

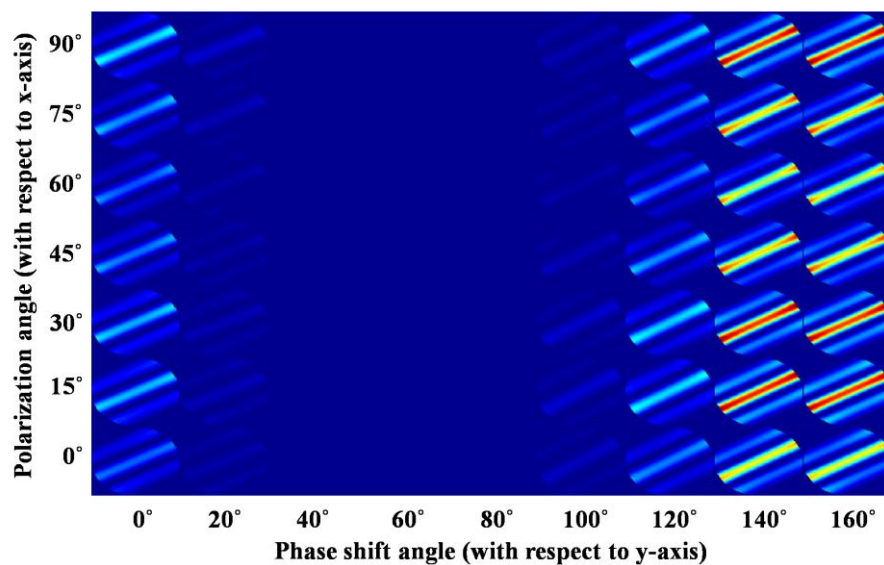


Figure 3: The far field radiation pattern at the back aperture of the collection objective for a collagen strand located in the focal plane, at an angle of 60 degrees with the y-axis. The signal distribution has shifted on both axes.

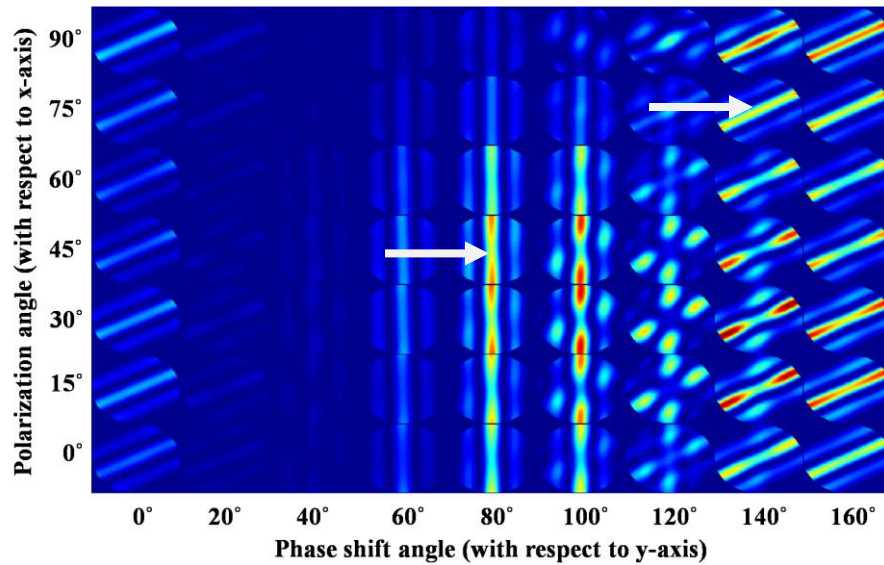


Figure 3: The far field radiation pattern at the back aperture of the collection objective for two stacked collagen strands located in the focal plane, one parallel to the y-axis and one at an angle of 60 degrees with the y-axis. Both fibrils are individually distinguishable (arrows), and their orientations can be determined unambiguously. Interference is also observed.

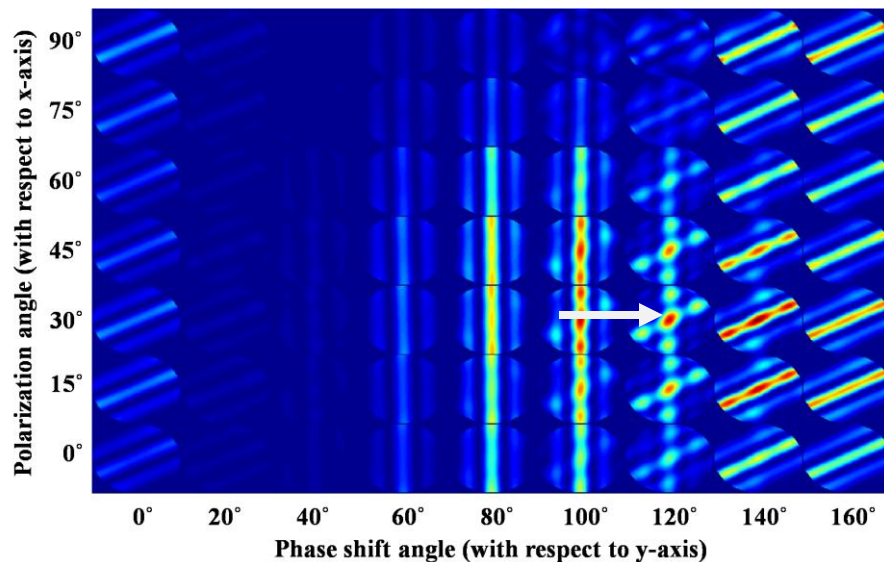


Figure 3: The far field radiation pattern at the back aperture of the collection objective for two collagen strands spaced 1.8 μm apart, one parallel to the y-axis and one at an angle of 60 degrees with the y-axis. The interference has noticeably changed from the stacked case (arrow), which can be used to determine the distance between the fibrils.

4. Conclusions

We present a new imaging technique that can be used to separately image collagen fibrils in a nonlinear microscope. The orientation and position of each fibril leaves a unique signature on the far field intensity and phase pattern. This technique is highly beneficial for imaging the orientation of the extracellular matrix, since it highlights the orientation of the fibrils at the focus unambiguously.

5. References

- [1] B. Richards, E. Wolf, "Electromagnetic diffraction in optical systems II. Structure of the image field in an aplanatic system," Proc. R. Soc. Lond. A Math. Phys. Sci. **253**(1274), 358–379 (1959).
- [2] L. Novotny and B. Hecht, "Principles of nano-optics," Cambridge U. Press (2006)
- [3] D. Sandkuijl, A. Tuer, D. Tokarz, J. E. Sipe and V. Barzda, "Numerical nonlinear microscopy of second and third harmonic generation," manuscript in preparation

Bacteria Classification by Means of the Statistical Analysis of Fresnel Diffraction Patterns of Bacteria Colonies

Halina Podbielska^{*1}, Igor Buzalewicz¹, Agnieszka Suchwałko^{1,3}, Alina Wieliczko²

¹Bio-Optics Group, Institute of Biomedical Engineering and Instrumentation, Wrocław University of Technology, Wybrzeże Wyspińskiego 27, 50-370 Wrocław, Poland

²Department of Epizootiology and Veterinary Administration with Clinic of Infectious Diseases, Wrocław University of Environmental and Life Science, Plac Grunwaldzki 45, 50-366, Wrocław, Poland

³Medicwave AB, Strandgatan 1, 302 50 Halmstad, Sweden

*Corresponding author: halina.podbielska@pwr.wroc.pl

Abstract: The novel optical system for analysis of Fresnel diffraction patterns of bacterial colonies is proposed. Obtained results have shown that features extraction and statistical analysis of Fresnel patterns enables bacteria species classification with high accuracy.

OCIS codes: (170.0170) Medical optics and biotechnology, (170.0110) Imaging systems, (280.4788) Optical sensing and sensors, (290.2558) Forward scattering, (100.2960) Image analysis.

1. Introduction

The presence of pathogenic bacteria in the environment may cause the risk of e.g. food contamination or severe problems for hospitalized patients. Therefore, rapid and effective methods of bacteria classification are in focus of interest in many fields of life science, health safety and food production. The additional risk factor is the increase of bacteria resistance to the commonly used antibiotics and sterilization techniques, as well. For these reasons, many efforts are taken to elaborate novel techniques for bacteria classification. Particularly, many researches are interested in optical methods, since they offer many advantages. e.g. the possibility of nondestructive and noncontact measurements. Moreover, these methods enable the further verification of obtained results by other techniques conventionally used in microbiological laboratories. The optical methods of bacteria classification are based on different detection principles; as fluorescence and infrared spectroscopy, flow cytometry, surface plasmon resonance, light scattering etc. [1-4]. However, in most cases, they analyze single bacterial cells. In recent years, the novel approach analyzing the forward light scattering on bacterial colonies, was proposed [5-9]. Previously performed by our group experiments have shown that analysis of bacteria colonies Fourier spectra, considered in general as diffraction patterns, can be used to estimate the bacteria colonies number and in consequence, to assess antimicrobial properties of various antimicrobial agents [10-12]. Recently, we have proposed new optical system with converging spherical wave illumination for examination of the light diffraction on bacterial colonies. According to our knowledge, it is the first attempt to use such optical system in microbiological examination. Proposed system exhibits unique properties: it allows for compression of the observation plane to the finite region in the space, observation of Fresnel or Fraunhofer patterns in the same setup and diffraction patterns scaling. These advantages are not offered by optical configurations [13]. Obtained results have shown that Fresnel diffraction pattern of bacterial colonies possesses unique features, which can be used in the process of classification of bacteria species. In the presented paper, the computer-aided extraction of Fresnel patterns features, is proposed. Statistical methods as linear discriminant analysis (LDA), cross-validation technique (CV) and analysis of variance (ANOVA) will be used to optimize the bacteria species classification based on certain features of Fresnel diffraction patterns of bacterial colonies. Obtained results for seven bacteria species: *Citrobacter freundii* (PCM 531), *Escherichia coli* (PCM O119), *Proteus mirabilis* (PCM 547), *Pseudomonas aeruginosa* (ATCC 27853), *Salmonella enteritidis* (ATCC 13076), *Staphylococcus aureus* (PCM 2267) and *Staphylococcus intermedius* (PCM 2405), have shown that basing on Fresnel patterns of bacterial colonies it is possible to distinguish the bacteria species with 92% accuracy. Calculation were conducted by using the free accessible software R for statistical analysis [14].

2. Proposed optical system configuration

In the optical system with converging spherical wave illumination, a converging spherical wave illuminates the analyzed sample and the diffraction pattern is recorded. The optical system includes the laser diode module (635 nm, 1 mW), neutral density filter, linear polarizer, beam expander, iris diaphragm, transforming lens, XYZ sample positioning stage, CCD camera and computer.

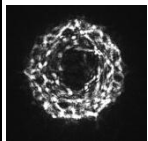
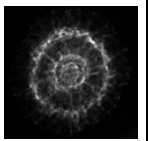
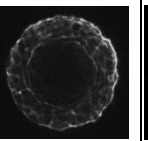
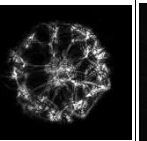
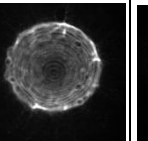
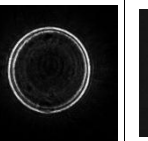
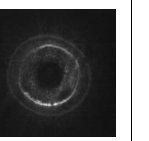
3. Features extraction of Fresnel patterns of bacterial colonies

Fresnel diffraction patterns of bacterial colonies exhibit unique spatial structures. They contain set of the diffraction rings, but the number and sizes of these rings depend on the bacteria species. This is correlated with the morphology of colony, as well as amplitude and phase properties that are unique for each species. To extract these features of diffraction patterns of different bacteria species colony expressed by discrete pixel intensities, their properties will be analyzed in the concentric annulus-shaped zones of the patterns, further called *rings*. Each Fresnel pattern was limited by the circle covering entire pattern, which center and radius were manually marked. Radius of this circle was then divided into 3, 5 and 10 equal pieces, from which rings were created. The Fresnel patterns partitioning was performed in ImageJ software [15], by the dedicated macro. As a classification features the mean value and standard deviation of the pixels intensities of the given rings, were used. 8 bits gray-scale images in TIFF format, were analyzed. This gives us 256 intensity levels per each pixel. Each image has width of 1280 pixels and height of 1024 pixels. The Fresnel pattern covers at least 40% of the image space.

4. Statistical analysis of Fresnel patterns and bacteria species classification

Bacteria species names were used as grouping variable for classification analysis. Number of representative images of diffraction patterns that were included into analysis for each group, is shown in Table 1 along with the exemplary Fresnel patterns.

Table 1: Number of images that were included into analysis for each of the bacteria species an exemplary Fresnel patterns of bacterial colonies

Bacteria species	<i>Citrobacter freundii</i>	<i>Escherichia coli</i>	<i>Proteus mirabilis</i>	<i>Pseudomonas aeruginosa</i>	<i>Salmonella enteritidis</i>	<i>Staphylococcus aureus</i>	<i>Staphylococcus intermedius</i>
Number of analyzed Fresnel patterns	49	53	47	50	55	50	29
Exemplary Fresnel patterns of bacterial colonies							

The LDA (Linear Discriminant Analysis) was exploited to classify bacteria species basing on their diffraction pattern rings features. Next, the analysis of variance (ANOVA) was used to choose the features of Fresnel patterns, which in the best way classify the bacteria species. ANOVA in its simplest version is a method to compare mean values of numerical variables in several groups determined by a factor variable. We took classification features as numerical variables and bacteria species as factor variable. For each continuous feature we tested hypothesis that mean values of this feature are equal for all seven analyzed groups of bacteria. For each feature the p -value from ANOVA was used as a measure of group separation: the lower is p -value, the better is the separation. Features were sorted using this separation measure. Several best features were used to build LDA classification models. In the next step, models with the best features are built. Their accuracy is estimated using cross validation method (CV). Obtained results are depicted in Table 2.

Table 2: V error for the best fitted LDA models after ANOVA for 3, 5 and 10 rings partitioning

ring number partitioning	3	5	10
LDA model features	mean.2, sd.1, mean.1, mean.3, sd.3	mean.3, sd.1, sd.2, mean.2, mean.1, mean.4, mean.5, sd.5, sd.4	sd.1, mean.4, mean.5, sd.3, sd.4, sd.2, mean.1, mean.10, mean.7, mean.2, mean.6, sd.5, mean.3, mean.9, mean.8.
CV terror	9,01 %	9,91 %	8,11 %

5. Summary

The novel configuration of the optical system with converging spherical wave illumination for examination of diffraction patterns of bacteria colonies, is presented. It enables the compression of the observation plane to the finite region in the space, diffraction pattern scaling and lower level of aberrations. Fresnel diffraction patterns of

bacterial colonies recorded in the proposed optical system are unique signature of each bacteria species. Therefore, they can be used for bacteria species classification. Performed computer-aided features extraction of Fresnel patterns and statistical analysis based on LDA, CV and ANOVA methods, have shown that independently of number of rings partitioning obtained, classification error is smaller than 10%. Feature selection methods like ANOVA allowed to reduce this error rate even more: less than 8% for 10 rings partitioning. Performed experiments and data analysis demonstrated that Fresnel diffraction patterns recorded in the proposed optical system can be used for bacteria species classification with high accuracy (nearly 92%) and can be applied in microbiological laboratories for diagnosis and control.

6. Acknowledgments

We would like to thank Dr. Artur Suchwafko for helpful comments and support. This work was partially supported by the Research Grant from the Polish Ministry of Science and Higher Education (No N N505 557739). The support of the European Union under the European Social Fund (No DG-G/2733/11) is gratefully acknowledged, as well.

7. References

- [1] R. T. Noble, S. B. Weisbeg; “ A review of technologies for rapid detection of bacteria in recreational waters”, *Journal Of Water and Health*, 3(4), 381 – 391 (2005).
- [2] D. L. Rosen, “Airborne bacterial endospores detected by use of impinge containing aqueous terbium chloride”, *Applied Optics*, 45(13), 3152 – 3157 (2006).
- [3] G. E. Fernandes, Y. L. Pan et al.,” Simultaneous forward- and backward- hemisphere elastic- light- scattering patterns of respirable- size aerosols”, *Optics Letters*, 31(20), 3034 – 3036 (2006).
- [4] J. C. Auger, K. B. Aptowicz et al., “Angularly resolved light scattering from aerosolized spores: Observations and calculations”, *Optics Letters*, 32(22), 3358 – 3360 (2007).
- [5] P.P. Banada, S. Guo, B.Bayraktar, E. Bae, B. Rajwa, J.P. Robinson, E.D. Hirleman, and A.K Bhunia, “Optical forward-scattering for detection of *Listeria monocytogenes* and other *Listeria* species”, *Biosensors and Bioelectronics* **22**, 1664-1671 (2007).
- [6] E. Bae, P.P. Banada, K. Huff, A.K. Bhunia, J.P. Robinson, and E.D. Hirleman, “Analysis of time-resolved scattering from macroscale bacterial colonies”, *Journal of Biomedical Optics* **13**(1), 014010 (2008).
- [7] P.P. Banada, K. Huff, Amornrat Aroonual, E. Bae, B. Rajwa, B. Bayraktar, A. Adil, J.P. Robinson, E.D. Hirleman, and A.K. Bhunia, “Label-free detection of multiple bacterial pathogens using light scattering sensor”, *Biosensors and Bioelectronics* **24**,.1685-1692 (2009).
- [8] E. Bae, N. Bai, A. Aroonual, J. P. Robinson, A. K. Bhunia, E. D. Hirleman, “Modeling light propagation through bacterial colonies and its correlation with forward scattering”, *J. Biomed. Opt.* **15**(4), 045001-1–10 (2010).
- [9] E. Bae, A. Aroonual, A.K. Bhunia, and E.D. Hirleman, “On the sensitivity of forward scattering patterns from bacterial colonies to media composition”, *Journal of Biophotonics* **4**(4), 236-243 (2011).
- [10] I. Buzalewicz, K. Wysocka-Król, H. Podbielska, “Exploiting of optical transforms for bacteria evaluation in vitro,” *Proc. SPIE* **7371**, 73711H-73711H-6 (2009).
- [11] I. Buzalewicz, K. Wysocka-Król, H. Podbielska, “Image processing guided analysis for estimation of bacteria colonies number by means of optical transforms”, *Optics Express* **18**(12), 12992-13005 (2010).
- [12] I. Buzalewicz, K. Wysocka-Król, K. Kowal, H. Podbielska, “Evaluation of antibacterial agents efficiency” in *Information Technologies in Biomedicine 2*, E. Pietka, J. Kawa ed. (Springer-Verlag, Berlin, 2010).
- [13] I. Buzalewicz, A. Wieliczko, H. Podbielska, “Influence of various growth conditions on Fresnel diffraction patterns of bacteria colonies examined in the optical system with converging spherical wave illumination “, *Optics Express* **19**(22), .21768-21785, (2011).
- [14] <http://www.r-project.org/>
- [15] Abramoff, M., Magalhães, P., and Ram, S., “Image processing with ImageJ,” *Biophotonics international* **11**(7), 36–42 (2004).

Scattered light fluorescence microscopy in three dimensions

Giulia Ghielmetti and Christof M. Aegerter*

Physik-Institut, University of Zurich, Winterthurerstrasse 190, 8057 Zurich, Switzerland

* aegerter@physik.uzh.ch

Abstract: Recently, we have proposed a method to image fluorescent structures behind turbid layers at diffraction limited resolution using wave-front shaping and the memory effect. However, this was limited to a raster scanning of the wave-front shaped focus to a two dimensional plane. In applications, it can however be of great importance to be able to scan a three dimensional volume. Here we show that this can be implemented in the same setup. This is achieved by the addition of a parabolic phase shift to the shaped wave-front. Via the memory effect, this phase shift leads to a shift of the interference based focus in the z-direction, thus opening the possibility of three dimensional imaging using scattered light fluorescence microscopy. Here, we show an example of such a three dimensional image of fluorescent nano-beads taken behind a turbid layer more than 10 mean free paths thick. Finally, we discuss the differences of the scanning in the z-direction with that in the x-y plane and the corresponding possibilities and limitations of the technique.

OCIS codes: (290.4210) Multiple Scattering; (110.0180) Microscopy; (110.7050) Turbid Media; (030.6140) Speckle.

1. Introduction

Turbid media are highly limiting to the imaging of biomedical processes in that depth of penetration into tissues of interest is strongly limited by multiple scattering of light [1-5]. Building on previous work in the area of wave-front shaping of visible light [6-9], we have recently presented a method with which to image fluorescent structures behind turbid layers at diffraction limited resolution [10]. This method has been taken up in the mean time by other groups using different avenues for creating a time-reversal based focus [11-13]. Here, we show that this method can be extended to provide a three dimensional imaging of these structures akin to a scanning confocal microscope [14]. The scanning in all dimensions relies on the presence of a correlation of the light after the turbid layer, known as the memory effect [15-17], which can be used to change the position of the interference based focus formed due to wave-front shaping of time-reversal of the incoming light. The geometry of the setting to be imaged, in particular the distance of the turbid layer to the structure of interest determines the scanning range of the microscope. For the artificial sample used here, the scanning range in the third dimension exceeds that in plane and volumes of $10 \times 10 \times 100 \mu\text{m}^3$ can be studied.

As a means to create samples illustrating the technique of fluorescent imaging behind a turbid layer, we created mock samples by covering one side of a glass microscope slide (thickness: $a = 1 \text{ mm}$) with Zinc Oxide pigment. The thickness of this layer was approximately $15 \mu\text{m}$ corresponding to more than 15 mean free paths. Thus, the light behind this layer is highly disordered and has undergone at least 200 scattering events. Thus, the layer is completely intransparent. On the other side of the microscope slide, we have attached a number of fluorescent nano-beads (Poybeads 450 nm), which can act as a marker. The absorption spectrum of the beads has a maximum around 480 nm, which corresponds to our illuminating light and emission maximally at 530 nm. The beads have a diameter of 450 nm comparable to the resolution we have previously determined in the x-y directions [10].

The optical setup consists of an illuminating blue laser (Spectra- Physics Cyan 40 mW, 488 nm), which is expanded and passed through a galvo-scanner (General Scanning LDS-07-OH) before being reflected off a spatial light modulator (Holoeye HEO 1080 P), which is computer controlled. The optimization of the incoming wave-front will be carried out by this SLM. The scanning in the x-y plane is carried out by the galvo scanner tilting the incoming wave front, whereas the z-direction will be scanned by the SLM by the addition of a parabolic phase pattern to the optimized one. The surface of the SLM is then imaged onto the surface of the scattering layer with a 40x microscope objective (Zeiss A-Plan 40x/0.25). This yields a illuminated spot on the turbid layer with a diameter of $r = 80 \mu\text{m}$. Behind the sample, a Semrock GFP-3035B filter is used to discard the illuminating light, such that only the fluorescent signal is detected by a Photomultiplier (Hamamatsu). The signal in the photomultiplier is the scanned signal illustrated in the figures below after having passed through a low pass filter to increase the signal to noise ratio.

2. Results

In Fig. 1, we show the fluorescence image of a 450 nm diameter bead hidden behind a turbid layer. The in-plane image has a resolution of 300 nm, as we have shown before [10], thus showing the size of the beads (see part (e)) of

the figure, where the bead is fully in focus). The subsequent part of the figure show successive scan images of the same particle using a wave-front shaped focus, i.e. behind the turbid layer. The images are made at different nominal positions of the focal point, where the imaging plane is shifted in the z direction by $2\ \mu\text{m}$ in every step, except between part (d) and (e) as well as (e) and (f), where the step size is one micron [14]. The scanning through the bead can be clearly seen and a cut through the z-direction at the bead position yields the resolution that is obtained in this way. As discussed above, the scan range of the image is limited by the correlation length implied by the memory effect. The size of the image in the plane reflects the maximum scanning range, where the intensity in the focus has decreased by a factor of 2. This implies that a fluorescent bead at the edge of the image would be less intense by roughly a factor of 2 than one in the centre. In the z-direction, the scan range shown in Fig.1 is much smaller than the theoretical limit, such that effectively the intensity in the focus is constant for all images.

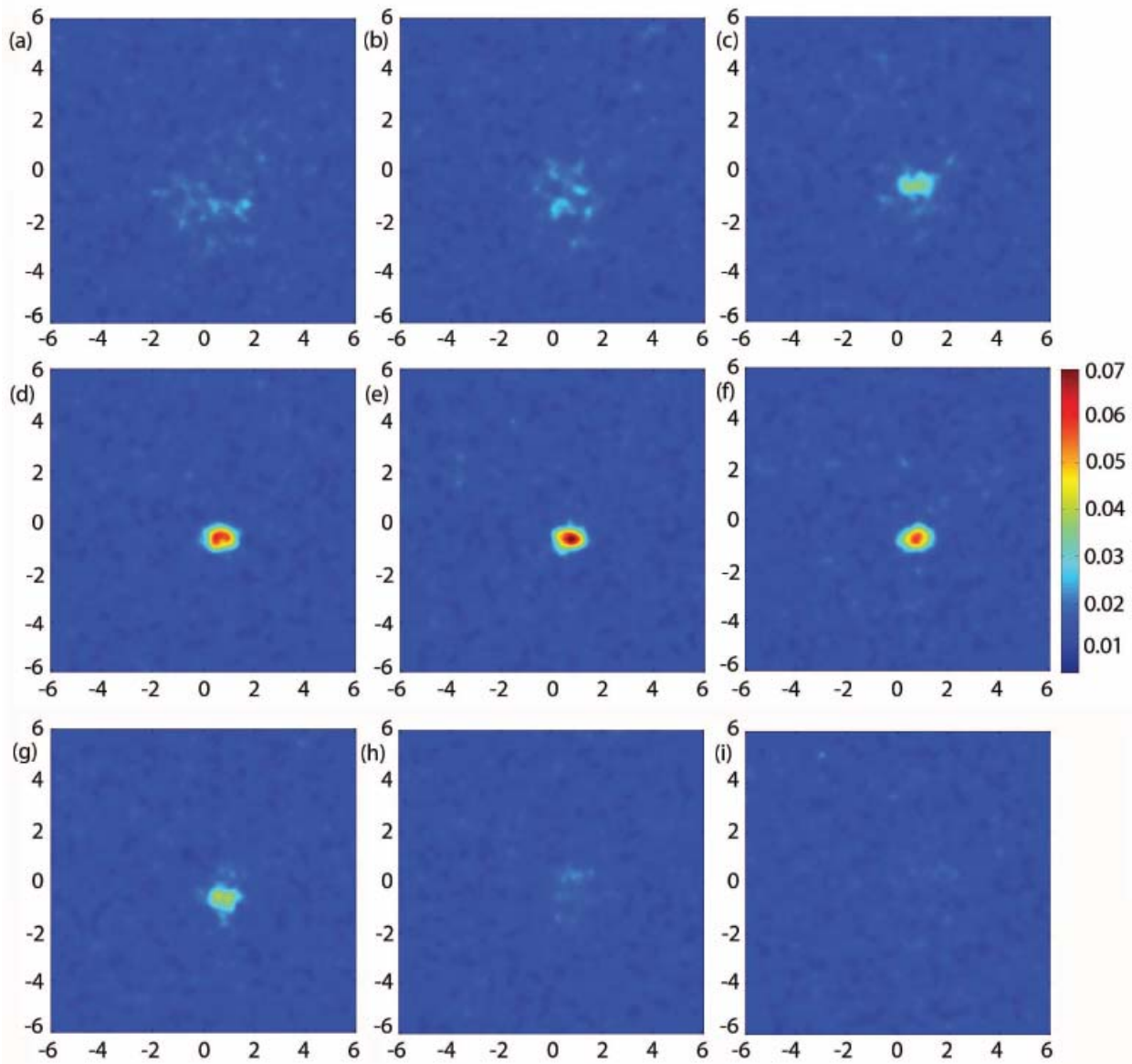


Fig. 1: (a)-(i) The fluorescence signal of a $450\ \text{nm}$ diameter fluorescent bead hidden behind a turbid layer. The images show the scattered light fluorescence image of the same bead and on the same intensity scale, while the position of the focal plane differs for the images. In (a), the position is at $-7\ \mu\text{m}$ behind the bead and consecutively moves forward in steps of $2\ \mu\text{m}$, until it lies $7\ \mu\text{m}$ in front of the bead position in image (i). The center of the bead, which would therefore lie between image (d) and its neighbor has been added as well in part (e). Thus, the difference in z position between parts (d) and (e) as well as (e) and (f) corresponds to only 1 micron. The scan range in this case is a window in the x-y plane of $12 \times 12\ \mu\text{m}^2$. The three dimensional structure of the bead can be clearly seen [14].

3. Conclusions

In conclusion, we have shown that scattered light fluorescence microscopy can be used for a three dimensional imaging of fluorescent structures hidden behind extremely turbid layers [13]. The resolution of the images is limited by the size of the interference based focus, which in turn is limited by the wavelength of the light used. However, it is neither determined by the optical elements used in the setup nor the scattering properties of the layer in front of the structure of interest. The field of view available to the microscope is dependent on the distance to the turbid layer, as well as the thickness of the layer. We have previously shown that in an egg geometry, similar to our artificial samples, a plane of $12 \times 12 \mu\text{m}^2$ can be imaged [10]. In the z-direction, we have shown here that similar fields of view can be achieved. In fact, due to the way in which the distance between the layer and the structure of interest enters in the memory effect, the theoretically achievable field of view in the z-direction is actually bigger, in the case here up to $60 \mu\text{m}$. Therefore, even structures close to the scattering layer could be studied in this way.

With this possibility of three dimensional scanning of the focus, applications of scattered light fluorescence microscopy become possible. This can work in the absence of any direct optical access, as long as there is e.g. a fluorescent structure on which the optimization can be carried out [7]. The main drawback of the technique remains in the temporal resolution, which is driven by the rate of change possible in the SLM used for the optimization. Currently this leads to long exposure times of the order of 30 minutes needed for creating three dimensional images. However, recent progress in the development of piezo-element based SLMs [18] make it possible to increase the speed of the SLM by at least three orders of magnitude [19], which makes applications possible. This can be seen by the time scale of the dynamics of fluctuations in e.g. *Drosophila* pupae, which is of the order of a minute [20]. Alternatively, phase conjugation may also allow an increase in temporal resolution [21].

4. References

- [1] J.B. Pawley (ed.) *Handbook of Biological Confocal Microscopy (3rd ed.)*, Springer, Berlin (2006).
- [2] F. Helmchen and W. Denk, "Deep tissue two-photon microscopy", *Nat. Methods* **2**, 932-940 (2005).
- [3] A. Diaspro, ed., *Confocal and Two-Photon Microscopy: Foundations, Applications and Advances*, Wiley-Liss, New York, (2002).
- [4] C. Vinegoni, C. Pitsouli, D. Razansky, N. Perrimon, and V. Ntziachristos, "In vivo imaging of *Drosophila melanogaster* pupae with mesoscopic fluorescence tomography" *Nat. Methods* **5**, 45-47 (2008).
- [5] M. Wolf, M. Ferrari, and V. Quaresima, "Progress of near-infrared spectroscopy and topography for brain and muscle clinical applications", *J. Biomed. Opt.* **12**, 062104 (2007).
- [6] I. M. Vellekoop and A. P. Mosk, "Focusing coherent light through opaque strongly scattering media", *Opt. Lett.* **32**, 2309-2311 (2007).
- [7] I.M. Vellekoop, E.G. van Putten, A. Lagendijk, and A.P. Mosk, "Demixing light paths inside disordered metamaterials", *Opt. Express* **16**, 67-80 (2008).
- [8] G. Lerosey, J. de Rosny, A. Tourin, and M. Fink, "Focusing beyond the diffraction limit with far-field time reversal", *Science* **315**, 1120-1122 (2007).
- [9] Z. Yaqoob, D. Psaltis, M.S. Feld, and C. Yang, "Optical phase conjugation for turbidity suppression in biological samples", *Nat. Photonics* **2**, 110-115 (2008).
- [10] I. M. Vellekoop and C.M. Aegerter, "Scattered light fluorescence microscopy: imaging through turbid media", *Opt. Lett.* **35**, 1245-1247 (2010).
- [11] C. L. Hsieh, Y. Pu, R. Grange, G. Laporte, and D. Psaltis, "Imaging through turbid layers by scanning the phase conjugated second harmonic radiation from a nanoparticle", *Opt. Express* **18**, 20723-20731 (2010).
- [12] M. Cui, E.J. McDowell, and C. Yang, "An in vivo study of turbidity suppression by optical phase conjugation (TSOPC) on rabbit ear," *Opt. Express* **18**, 25-30 (2010).
- [13] M. Cui and C. Yang, "Implementation of a digital optical phase conjugation system and its application to study the robustness of turbidity suppression by phase conjugation," *Opt. Express* **18**, 3444-3455 (2010).
- [14] G. Ghilmetti and C.M. Aegerter "Scattered light fluorescence microscopy in three dimensions" *Opt. Express* **20**, 3744 (2012).
- [15] D.L. Fried, "Anisoplanatism in Adaptive Optics" *J. Opt. Soc. Am.* **72**, 52-61 (1982).
- [16] S. Feng, C. Kane, P.A. Lee, and A.D. Stone, "Correlations and Fluctuations of Coherent Wave Transmission through Disordered Media", *Phys. Rev. Lett.* **61**, 834-837 (1988).
- [17] I. Freund, M. Rosenbluh, and S. Feng, "Memory effects in propagation of optical waves through disordered media", *Phys. Rev. Lett.* **61**, 2328-2331 (1988).
- [18] D. Akbulut, T.J. Huisman, E.G. van Putten, W.L. Vos, and A.P. Mosk, "Focusing light through random photonic media by binary amplitude modulation," *Opt. Express* **19**, 4017-4029 (2011).
- [19] D.B. Conkey, A.M. Caravaca-Aguirre, and Rafael Piestun, "High-speed scattering medium characterization with application to focusing light through turbid media", *Opt. Express* **20**, 1733-1740 (2012).
- [20] I.M. Vellekoop and C.M. Aegerter, "Focusing light through living tissue", *Proc. SPIE* **7554**, 755430 (2010).
- [21] M. Cui, "A high speed wavefront determination method based on spatial frequency modulations for focusing light through random scattering media," *Opt. Express* **19**, 2989-2995 (2011).

Computer Aided Monitoring of Neoadjuvant Chemotherapy for Breast Cancer

David R. Busch^a, Wensheng Guo^b, Regine Choe^c, Turgut Durduran^d, Michael D. Feldman^e, Carolyn Mies^e, Brian J. Czerniecki^f, Julia Tchou^f, Angela DeMichele^g, Mark A. Rosen^h, Michael D. Schnall^h, and Arjun G. Yodh^a

*Dept. Physics and Astronomy^a, University of Pennsylvania,
209 S. 33rd St., Philadelphia, PA 19104*

*Department Biostatistics^b, Dept. Pathology and Laboratory Medicine^c, Dept. Surgery^f, Dept. Medicine
(Hematology/Oncology) and Epidemiology^g, Dept. of Radiology^h University of Pennsylvania; Dept. Biomedical
Engineering, University of Rochester^e; ICFO-Institut de Ciències Fòniques Castelldefels, Spain^d;*

drbusch@physics.upenn.edu

Abstract: Diffuse Optical Tomography creates 3D maps of physiological properties. We previously reported a statistical analysis of these maps to automatically localize cancer. We now utilize this technique to monitor locally advanced cancers during neoadjuvant chemotherapy.

© 2012 Optical Society of America

OCIS codes: (170.3830) Mammography; (170.1610) Clinical applications; (170.6510) Spectroscopy, Tissue Diagnostics

Roughly 288 thousand new cases of and 40 thousand deaths from breast cancer are predicted in 2011 [1]. An increasingly popular treatment protocol is neoadjuvant chemotherapy which involves administering chemotherapy prior to surgical removal of the tumor [2]. During this time, it is sometimes possible to observe the effects of a particular drug regimen on the physiology of a specific tumor. This capability permits early determination of the effectiveness of a particular chemotherapy regimen, which can be critical for both efficacy of treatment and patient quality of life. Indeed neoadjuvant chemotherapy monitoring is an active area of research in clinical medicine [3–5], including optical imaging and monitoring [6–8].

Diffuse Optical Tomography (DOT) provides 3D maps of hemoglobin concentration, blood oxygen saturation, and optical scattering coefficients in deep tissues. DOT data sets are rich in information and provide functional information about tissue. Very recently, we developed and applied a statistical image analysis technique for DOT to a breast cancer data set [9]; the statistical approach derived a signature for normal and cancerous tissues based on a collection of optical parameters measured within each subject and across the full subject population [10]. Specifically, the approach converts 3D DOT reconstructions of total hemoglobin concentration, blood oxygen saturation, and tissue scattering coefficient into a single 3D DOT-based *probability of malignancy* image, which, in turn, enables volumetric tissue segmentation into ‘normal’ and ‘cancerous’ regions.

In the present contribution we have applied this statistical technique to create probability of malignancy images from serial DOT measurements of patients during the course of their neoadjuvant chemotherapy. We thus measure the changes in tumor region probability of malignancy longitudinally and compare these variations to clinical radiology observations. Preliminary results suggest that the statistical analysis of DOT data provides useful quantitative information about therapeutic effects during neoadjuvant chemotherapy.

A population of 35 biopsy-confirmed lesions and logistic regression were used to generate an optimized weighting vector for to compute tissue probability of malignance based on optically measured total hemoglobin, blood oxygen saturation, and reduced scattering. We then applied this probability of malignancy weighting to three new subjects who were imaged by DOT during neoadjuvant chemotherapy. The subjects received 4 cycles of Adriamycin and then 4 cycles Taxotere every two weeks; DOT measurements were first made prior to or within the first two cycles and at various time-points thereafter. We observe qualitative differences in the probability of malignancy parameter time course between subjects with complete versus incomplete responses to chemotherapy.

Since chemotherapy affects both normal and tumor tissue, i.e., it produces changes in optically measured physiological properties of both tissue types [11], we normalized the tissue optical properties in each subject to corresponding data taken from the patient’s healthy tissue at a pre-chemotherapy time point. For example, a so-called Z-score for

total hemoglobin concentration (Hb_t) in a tissue volume element of a single patient is defined as:

$$zHb_{td}^{(t)} = \frac{\ln [Hb_{td}^{(t)}] - \langle \ln [Hb_{td}^{(t=0)}] \rangle_H}{\sigma [\ln [Hb_{td}^{(t=0)}]]_H}. \quad (1)$$

Here, the subscript index $d = H, M$ specifies healthy (H) and malignant (M) tissue region, and the superscript index t denotes time with $t = 0$ as the pre-chemotherapy time point. Note, we log-transform (\ln) the data and the denominator is the standard deviation (σ) of the log-transformed voxel data in the patient's healthy tissue region. The statistical approach employs these normalized Z-scores for total hemoglobin, scattering and blood oxygen saturation in an otherwise identical procedure that is previously described [10] to calculate probability of malignancy for each tissue voxel.

Results of our analysis are shown in Fig. 1. Intriguingly, the subject (3) with partial response to chemotherapy showed much less initial change in the probability of malignancy than those with complete response; unfortunately, she left the study prior to acquisition of additional time points. Subject 1 had a complete response to chemotherapy by radiology (MRI), but pathology found scattered point foci of a few cancerous cells each. Subject 2 was a complete responder by both radiology (MRI) and pathology. Subject 3 was a partial responder by both radiology (mammography and ultrasound) and pathology. These data suggest that partial responders to chemotherapy may have significantly different optical signatures, in agreement with previous suggestions (e.g., Roblyer *et al* [7]). However, the results of our current study can only be considered preliminary as the population is small and the number of time points few.

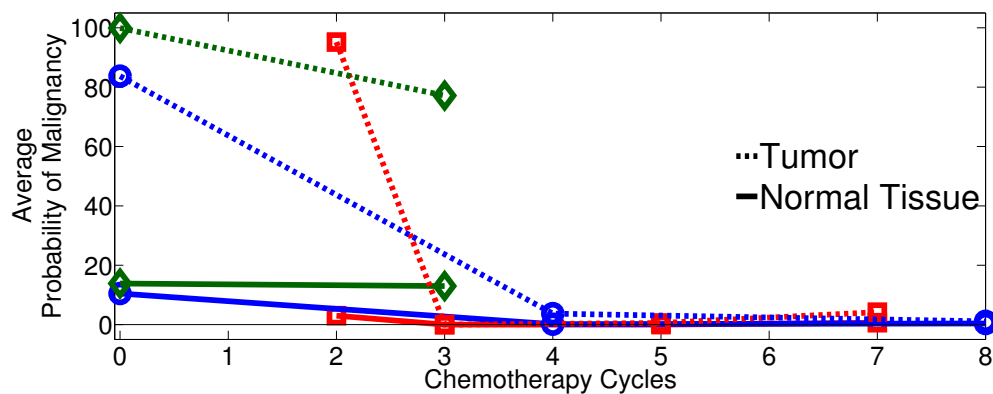


Fig. 1. Average probability of malignancy versus chemotherapy cycle for normal and tumor tissue in three subjects, normalized to first optical measurement. Subjects 1 and 2 (red squares and blue circles, respectively) were complete responders by MRI. Subject 3 (green diamonds) was a partial responder by MRI and pathology. Note that Subject 1 did not have an optical measurement prior to beginning chemotherapy.

We introduce and demonstrate a statistical technique for automated analysis of the response to neoadjuvant chemotherapy. The method utilizes a *probability of malignancy* derived from a population of known cancers and applied to serial imaging during chemotherapy. The pilot study shows significant changes in calculated probability of malignancy, suggesting that changes in the signature of cancer as measured by diffuse optical tomography may be an effective technique for monitoring the efficacy of neoadjuvant chemotherapy and that further study of this approach is worthwhile.

References

1. Carol DeSantis, Rebecca Siegel, Priti Bandi, and Ahmedin Jemal. Breast cancer statistics, 2011. *CA: A Cancer Journal for Clinicians*, 61(6):408–418, 2011.
2. M. Kaufmann, G. von Minckwitz, H. D. Bear, A. Buzdar, P. McGale, H. Bonnefoi, M. Colleoni, C. Denkert, W. Eiermann, R. Jackesz, A. Makris, W. Miller, J.-Y. Pierga, V. Semiglazov, A. Schneeweiss, R. Souchon, V. Stearns, M. Untch, and S. Loibi. Recommendations from an international expert panel on the use of neoadjuvant (primary) systemic treatment of operable breast cancer: new perspectives 2006. *Annals of Oncology*, 2007.

3. Lori R. Arlinghaus, Xia Li, Mia Levy, David Smith, E. Brian Welch, John C. Gore, and Thomas E. Yankeelov. Current and future trends in magnetic resonance imaging assessments of the response of breast tumors to neoadjuvant chemotherapy. *Journal of Oncology*, 2010. cited By (since 1996) 4.
4. L.J. Esserman, D.A. Berry, M.C.U. Cheang, C. Yau, C.M. Perou, L. Carey, A. DeMichele, J.W. Gray, K. Conway-Dorsey, M.E. Lenburg, et al. Chemotherapy response and recurrence-free survival in neoadjuvant breast cancer depends on biomarker profiles: results from the i-spy 1 trial (calgb 150007/150012; acrin 6657). *Breast Cancer Research and Treatment*, pages 1–14, 2011.
5. K.P. McGuire, J. Toro-Burguete, H. Dang, J. Young, A. Soran, M. Zuley, R. Bhargava, M. Bonaventura, R. Johnson, and G. Ahrendt. Mri staging after neoadjuvant chemotherapy for breast cancer: Does tumor biology affect accuracy? *Annals of surgical oncology*, 18(11):3149–3154, 2011.
6. H. Soliman, A. Gunasekara, M. Rycroft, J. Zubovits, R. Dent, J. Spayne, M.J. Yaffe, and G.J. Czarnota. Functional imaging using diffuse optical spectroscopy of neoadjuvant chemotherapy response in women with locally advanced breast cancer. *Clinical Cancer Research*, 16(9):2605, 2010.
7. D. Roblyer, S. Ueda, A. Cerussi, W. Tanamai, A. Durkin, R. Mehta, D. Hsiang, J.A. Butler, C. McLaren, W.P. Chen, and Bruce Tromberg. Optical imaging of breast cancer oxyhemoglobin flare correlates with neoadjuvant chemotherapy response one day after starting treatment. *Proceedings of the National Academy of Sciences*, 108(35):14626–14631, 2011.
8. R. Choe and T. Durduran. Diffuse optical monitoring of the neoadjuvant breast cancer therapy. *Selected Topics in Quantum Electronics, IEEE Journal of*, PP(99):1, 2011.
9. Regine Choe, Soren D. Konecky, Alper Corlu, Kijoon Lee, Turgut Durduran, David R. Busch, Brian J Czerniecki, Julia Tchou, Douglas L. Fraker, A DeMichele, B. Chance, S. R. Arridge, M. Schweiger, Joseph P. Culver, Mitchell D. Schnall, Mary E. Putt, Mark A Rosen, and Arjun G. Yodh. Differentiation of benign and malignant breast tumors by in-vivo three-dimensional parallel-plate diffuse optical tomography. *Journal of Biomedical Optics*, 14(2):024020 (18pp), 2009.
10. David R. Busch, Wensheng Guo, Regine Choe, Turgut Durduran, Michael D. Feldman, Carolyn Mies, Mark A. Rosen, Mitchell D. Schnall, Brian J. Czerniecki, Julia Tchou, Angela DeMichele, Mary E. Putt, and Arjun G. Yodh. Computer aided automatic detection of malignant lesions in diffuse optical mammography. *Medical Physics*, 37(4), April 2010.
11. D. B. Jakubowski, A. E. Cerussi, F. Bevilacqua, N. Shah, D. Hsiang, J. Butler, and B. J. Tromberg. Monitoring neoadjuvant chemotherapy in breast cancer using quantitative diffuse optical spectroscopy: a case study. *Journal of Biomedical Optics*, 9(1):230–238, 2004.

Measurement of Raman Spectra for Tomographic Reconstruction

Jennifer-Lynn Demers¹, Scott Davis¹, Brian W. Pogue¹, Michael D. Morris²

1: Thayer School of Engineering, Dartmouth College, Hanover, NH 03755

2: Department of Chemistry, University of Michigan, Ann Arbor, MI 48109

jldh@dartmouth.edu

Abstract: Raman signal is measured through a tomography set-up with 8 distinct spectrometers allowing for increased spectral resolution. Reconstructed images show good localization and contrast of Raman signal to background for Teflon inclusions within gelatin-based phantoms.

OCIS codes: (140.3550) Lasers, Raman; (170.5660) Raman Spectroscopy; (110.6960) Tomography

1. Introduction

By combining Raman spectroscopy with optical tomography it is possible to obtain better spatial resolution when constructing for the region of the Raman emitted photons. With an accurate model for light scattering and absorption in thin tissues, it would be possible to increase the spatial resolution while decreasing the signal distortion of the Raman signal.

Past research using Raman spectroscopy for bone imaging has focused on obtaining results for one emission wavelength, rather than the entire spectrum [1,2]. It is possible to use a similar model and technique to obtain data over the entire Raman emission spectrum in order to ultimately reconstruct the spectra values. The reconstructed Raman signal of bone would be useful when attempting to characterize and study bone health in an in-vivo setting.

Raman spectra of bone have been acquired for different disease states [3], as well as different levels of maturation, and initial experiments have been completed to acquire Raman spectra through the skin and muscle. The peaks of interest are assigned to phosphate, carbonate and amide components, which are connected to the carbonated apatite and octacalcium phosphate portions of the bone matrix. Through shifts in the peak location and changes in relative intensity, changes in the chemical structure of the bone can be tracked.

2. Data Acquisition

An integrated optical and MR imaging platform was developed allowing for the possibility of image-guided reconstructions [4]. The eight optical fiber bundles connect to eight spectrometers with cooled CCD detection. Each fiber is simultaneously connected to the spectrometer and the 830nm laser source, allowing for the use of each fiber as both a source and detector. A delrin fiber holder allows for repeatable placement of the fiber bundles on the surface of the phantom or leg. Both the Raman spectra and the excitation spectra are recorded for each source detector pair, for a total of 56 channels collected for each sample.

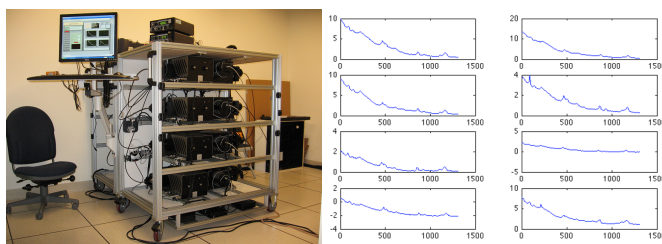


Figure 1: (A) Eight spectrometer set-up with fiber bundles that can extend into the MR room for image-guided reconstructions, (B) Example of 8 acquired spectra

An 850 long pass filter is included in the optical pathway for Raman collection and a 4OD filter is included for excitation collection. The entrance slit width is set to 75 microns. Each Raman spectra is acquired 3 times for each source detector pair in order to reduce the effects of cosmic ray spikes on the data through median filtering. A 16-point Hamming window is convolved with the data to decrease the pixel-to-pixel variation in the data followed by a wavelength shift correction, calculated from neon spectra, to account for spectrometer-to-spectrometer variation.

The Raman spectra features are extracted from the acquired spectra using a baselining method, where a polynomial is fit to each spectrum's background features. The order of the polynomial is chosen by the smallest cumulative error between the background and the polynomial for 3rd to 5th degree fittings. Background features can come from fibers, filters and non-Raman regions of the sample. After subtraction of the polynomial from the data, the Raman signal is more easily viewed. A single value for the excitation value and the Raman value is obtained for each source detector pair by integration over the wavelengths of interest. The Raman value can be representative of one main peak, the ratio of peaks, or the sum of multiple peaks.

Gelatin phantoms were constructed using agar, 1% intralipid and water and had an outer diameter of 27mm to mimic the size of rat legs. Teflon rods were Raman generating inclusions within the gelatin based phantoms and had a diameter of 5mm or 12.7mm. For gelatin phantoms, the location and diameter of the Teflon inclusion is noted for generation of a 2D mesh. MRI dicom images could provide the basis for more complex meshes based on the segmentation of the biological components within the leg.

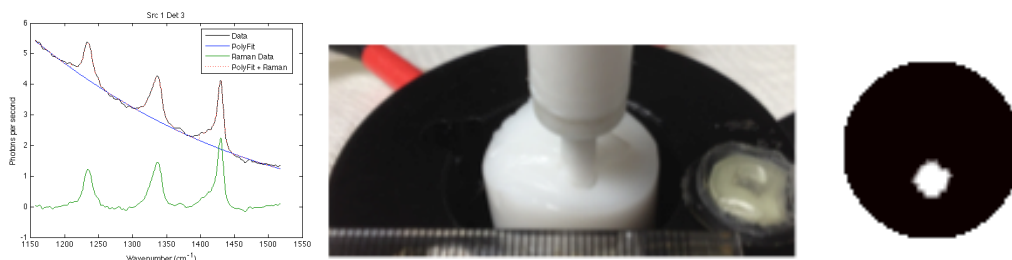


Figure 2: (A) Plot of the measured spectra, the polynomial fit to the background and the remaining baselined Raman signals, (B) Gelatin-based phantom with 5mm inclusion, (C) binary image showing the location of the Teflon inclusion

3. Image Reconstruction

The source detector specific values are used as inputs into the NIRFAST reconstruction algorithm [5], which involves fitting the measured and integrated data to data from a light propagation model. Reconstruction of Raman signal is comparable to reconstruction of fluorescence yield, which is the combination of the quantum yield of the fluorophore and the absorption coefficient of the fluorescent compound at the excitation wavelength.

The initial guess for the optical properties of the sample is unique to the different tissue or material types within the sample. The optical properties are updated at each step of the iterative reconstruction algorithm. The stopping criterion for the algorithm is when the projected error change is less than 0.5%.

The contrast to background ratio was calculated by finding the mean value of the reconstruction results for each node within the region of expected Teflon signal and dividing by the mean value of the reconstruction for all other nodes within the mesh.

4. Results

For gelatin-based phantoms the algorithm was able to reconstruct the Raman signal in the correct orientation, and with a contrast to background ration ranging from 7.0 to 9.7 for both the 5mm and 12.7mm sized Teflon inclusions. Figure 3 shows the reconstructed images in the second row, below binary images showing the two regions within the mesh.

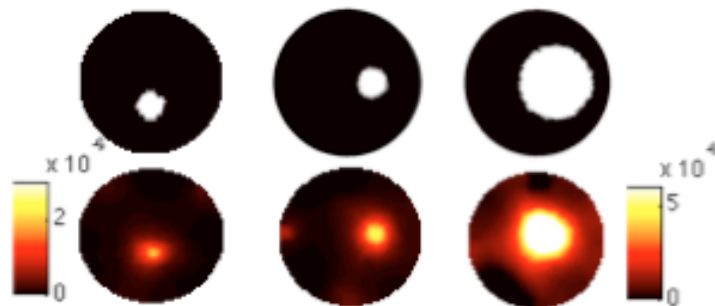


Figure 3: Experimental reconstructed Raman spectra for gelatin-based phantoms with Teflon inclusions. The first two reconstructions are on the same scale, and the third has a maximum value twice as large.

If the changing the scale of the color bar on the reconstructed images it is possible that the visual contrast can better match the calculated values for contrast to background ratio. The 12.7mm Teflon inclusion has the greatest Raman signal, but also the highest background value. In the 5mm Teflon inclusion phantoms the background is very low except for some cases where edge artifacts occur in line with the source and detector placement.

5. Discussion

By altering the criteria for the amount of error allowed in a fitting for a source-detector pair to be included in the reconstruction it is possible to decrease the effect of edge artifacts on the reconstructed result. By increasing the cut off for the projection error change, we can increase the region of the Raman signal to better match the regions of the mesh, but we see a decrease in the contrast to background ratio. It appears that by using Teflon inclusions in a gelatin-based phantom, we are able to create a simplified Raman system, and that the signal can be reconstructed to the correct spatial region.

More complex systems, such as bone within tissue, would likely suffer from similar issues when reconstructing the signal, but the ability to use segmented images from an MRI to constrain the reconstruction regions would likely lead to increased signal, as seen in fluorescence models [4]. Simple bone and gelatin-based phantoms are currently being investigated for data acquisition and the ability to reconstruct Raman signal.

6. Conclusion

We have successfully created Raman phantoms with Teflon inclusions and gelatin and intralipid based backgrounds. The next step in the study is successfully reconstructing the Raman signal from bone in gelatin-based phantoms before moving into the in-vivo measurements.

Future work will look at the effect of the slit width on the spectral resolution of the measured Raman signal and the trade off between the spectral resolution and the signal to noise ratio based on the amount of light measured per source detector pair.

7. References

1. Schulmerich, M.V., et al., *Noninvasive Raman tomographic imaging of canine bone tissue*. J Biomed Opt, 2008. **13**(2): p. 020506.
2. Srinivasan, S., et al., *Image-guided Raman spectroscopic recovery of canine cortical bone contrast in situ*. Opt Express, 2008. **16**(16): p. 12190-200.
3. Crane, N.J., et al., Raman spectroscopic evidence for octacalcium phosphate and other transient mineral species deposited during intramembranous mineralization. Bone, 2006. **39**(3): p. 434-442.
4. Scott C. Davis, K.S.S., Julia A. O'Hara, Summer L. Gibbs-Strauss, Keith D. Paulsen, Comparing implementations of magnetic-resonance guided fluorescence molecular tomography for diagnostic classification of brain tumors. Journal of Biomedical Optics, 2010. **15**(5).
5. Dehghani, H., et al., Near infrared optical tomography using NIRFAST: Algorithm for numerical model and image reconstruction. Communications in Numerical Methods in Engineering, 2009. **25**(6): p. 711-732.

PDT induced changes assessed by time-gated fluorescence tomography in a head and neck tumor model

Ulas Sunar, Weirong Mo, Daniel Rohrbach

Dept of Cell Stress Biology & PDT Center, Roswell Park Cancer Institute, Buffalo, NY

Abstract: We report the simultaneous 3D reconstruction of fluorescence yield and lifetime of a photosensitizer (HPPH) before and after PDT. HPPH-mediated PDT induced significant changes in fluorescence yield and lifetime. This pilot study demonstrates that time-domain fluorescence tomography may be useful for assessing photosensitizer distributions in deep tissue during PDT monitoring.

OCIS codes: General (170.0170) Medical optics and biotechnology; (170.3660) Light propagation in tissues; (170.3880) Medical and biological imaging.

1. Introduction

Photodynamic therapy (PDT) is an emerging treatment option for head and neck cancer. It is based on drug (photosensitizer) activation by light, resulting in generation of singlet oxygen which initiates cell kill and vascular destruction. It has advantageous over established treatment modalities such as radiation and chemo due to its much less side effects and higher organ preservation rates with increased quality of life.

So far PDT is mainly applied for superficial applications such as skin and oral cancer [1]. Recently there is an increasing interest for interstitial treatment of larger and deeper tumors such as those in the base of tongue or large neck nodes [1]. For effective PDT dosimetry, one needs to know the drug dose in tissue; thus it is desirable to know volumetric drug distribution [2]. It has been also shown that changes in drug distribution (photobleaching) during PDT are related to singlet oxygen generation and thus PDT efficacy [3]. Drug photobleaching can be monitored by changes in drug fluorescence yield. Lifetime can also be indicator of PDT response since changes in the microenvironment such as pH and oxygen induce changes in lifetime [4,5].

In this work we quantified PDT-induced depth-dependent photobleaching and lifetime changes using custom time-domain fluorescence diffuse optical tomography (TD-FDOT) system. Our results show that PDT induced significant changes in fluorescence yield and lifetime. This study demonstrates the utility of the TD-FDOT system for monitoring PDT with fluorescence yield and lifetime contrasts.

2. Methods

We constructed a TD-FDOT system based on time-gated image intensifier and CCD system (PicoStar HR-12, LaVision), a galvo scanner (Cambridge) and a picosecond pulsed laser diode (Becker-Hickl) [6]. Both laser excitation (660 nm, HPPH photosensitizer peak, OD2 filter) and fluorescence “emission” data (720nm bandpass filter) were acquired. In order to acquire the time-resolved signals, the “comb” mode of the image intensifier was utilized. The gate width was 0.8 ns. The delay of the temporal acquisition was set to be [0-12] ns, with the incremental step 0.8 ns. For image reconstruction, normalized Born approximation was used after transforming time-domain data set into frequency-domain data set [7,8]. For the results shown here, only the base frequency, 78MHz was used. The *in vivo* mouse imaging and PDT treatments were performed in compliance with Roswell Park Cancer Institute Animal Study Committees’ requirements. A male SCID mouse was inoculated subcutaneously with human head and neck tumor tissue obtained from a patient during an ongoing clinical trial. The tumor was implanted on the right lateral flank of the mouse and grew up to a diameter of approximately 10 mm. The photosensitizer HPPH (3 $\mu\text{mol/kg}$) was injected iv 24-hour before imaging. Fluorescence and excitation scans were performed at pre-PDT. Then PDT treatment was done (75 mW/cm^2 , 10 minutes, 45 Joules/cm^2). After the PDT treatment finished, fluorescence and excitation scans were performed again for post-PDT quantification. Differences in pre-PDT and post-PDT were assumed to be due to therapy induced changes.

3. Results

Fig.1. shows the difference images of fluorescence yield and lifetime by subtracting the pre-PDT images from the post-PDT images. Images at different depths ($Z = [1, 5, 9, 13, 17]$ mm) are shown from left to right with $Z=1$ mm is close to source plane and $Z=17$ mm is close to the detector plane of the imaging slab.

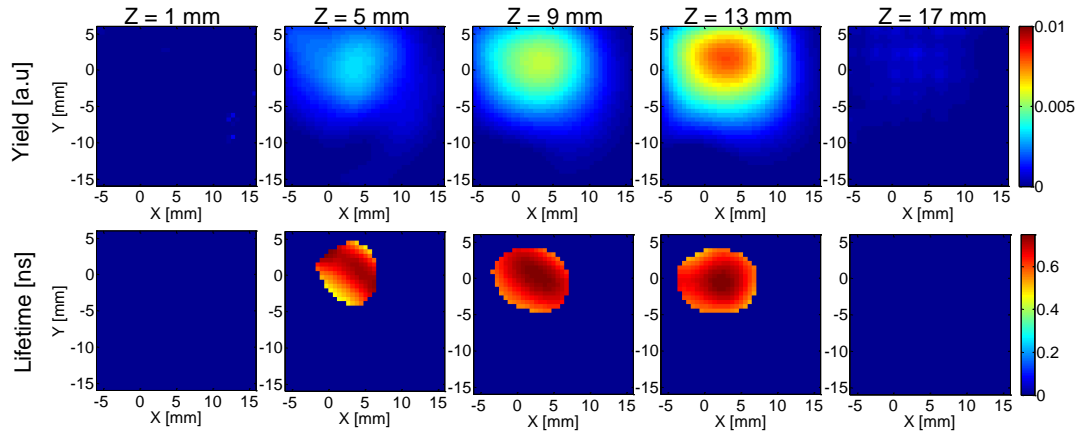


Fig. 1. Image reconstruction results of yield and lifetime images of a mouse tumor and surrounding normal areas, showing the PDT induced differences in yield and lifetime by subtracting ‘after-PDT’ from ‘pre-PDT’ at different depths $z=1,5,9,13, 17$ mm.

It is clear from the yield images that HPPH-mediated induced significant photobleaching and the photobleaching was depth-dependent, possibly due to the propagation of the PDT irradiation photons. Photobleaching was higher (~20%) close to the detector plane ($Z = 13$ mm) where PDT treatment light was administered. These results verify that our TD-FDOT system can quantify changes in photosensitizer distributions at different depths. The difference images of HPPH lifetime showed that lifetime increased after PDT. The mean lifetime increased from $\sim 4.3 \pm 0.2$ ns to $\sim 5.0 \pm 0.2$ ns, resulting in a ~16% of increase at the middle slice ($Z = 9$ mm). As much as ~700 ps change in lifetime is expected to be due to PDT-induced physiological changes such as changes in oxygenation and pH [4,5].

In this work, we report the application of time-domain fluorescence diffuse optical tomography for quantifying the PDT induced changes in fluorescence yield and lifetime in a clinically relevant head and neck tumor model. Our results showed the fluorescence yield of HPPH decreased and lifetime increased as a result of PDT. Our results highlight the potential that TD-FDOT can provide both fluorescence yield and lifetime parameters for monitoring and potentially assessing the PDT response in preclinical and clinical settings.

Acknowledgements. We thank Dr. Ravindra K. Pandey for providing the drug. We acknowledge Dr. Elizabeth Repasky lab for providing head and neck tumor model. We also thank Scott Galas for useful discussions regarding image reconstructions. This research is partially supported by RPCI Startup Grant (U. Sunar) and PO1 PDT Grant (NCI CA55791 (B. W. Henderson)).

4. References

- [1] Quon, H. *et al.* Photodynamic therapy in the management of pre-malignant head and neck mucosal dysplasia and microinvasive carcinoma. *Photodiagnosis and photodynamic therapy* **8**, 75-85 (2011)
- [2] Axelsson, J., Swartling, J. & Andersson-Engels, S. In vivo photosensitizer tomography inside the human prostate. *Optics letters* **34**, 232-234,(2009).
- [3] B. C. Wilson, M. S. Patterson, and L. Lilge, "Implicit and explicit dosimetry in photodynamic therapy:a new paradigm.," *Lasers Med. Sci.* **12**, 182-199 (1997).

[4] A. D. Scully, R. B. Ostler, D. Phillips, P. O'Neill, K. M. S. Townsend, A. W. Parker, and A. J. MacRobert, "Application of fluorescence lifetime imaging microscopy to the investigation of intracellular PDT mechanisms," *Bioimaging*, **5**, 9-18 (1997).

[5] D. Sud, W. Zhong, D. G. Beer, and M. A. Mycek, "Time-resolved optical imaging provides a molecular snapshot of altered metabolic function in living human cancer cell models," *Opt. Express* **14**, 4412-4426 (2006).

[6] Mo W., Rohrbach D., Sunar U. "Imaging a PDT photosensitizer in vivo with a time gated fluorescence tomography system," *J. Biomed. Opt.* **17**: 7 11602SSR (2012).

[7] R. E. Nothdurft, S. V. Patwardhan, W. Akers, Y. Ye, S. Achilefu, and J. P. Culver, "In vivo fluorescence lifetime tomography," *J. Biomed. Opt.* **14**, 024004 (2009).

In-vivo risk stratification of pancreatic cancer by evaluating optical properties in duodenal mucosa

¹Nikhil N. Mutyal, ¹Andrew Radosevich, ²Shailesh Bajaj, ²Sudeep Upadhye, ¹Jeremy D. Rogers, ²Hemant K. Roy, ¹Vadim Backman

¹Department of Biomedical Engineering, Northwestern University, Evanston, IL 60208

²Department of Gastroenterology, Northshore University Healthsystems, Evanston IL 60201
nikhil@northwestern.edu

Abstract: We present a novel approach of measuring optical properties with fiber optic probe from endoscopically accessible Peri-Ampullary duodenum as way to detect pancreatic cancer at early stages.

©2010 Optical Society of America

OCIS codes: (170.6510) Spectroscopy, tissue diagnostics; (290.1350) Backscattering, (060.2310) Fiber optics

Introduction:

Pancreatic cancer is one of the deadliest cancers with a 5 year survival rate of less than 5% and is the 4th largest cause of cancer-related deaths in the United States [1]. The dismal survival rate is due in a large part to our inability to detect a pancreatic cancer at an early stage when cure is still possible. Detecting curable pancreatic cancer is therefore paramount to decreasing its mortality. EUS and ERCP are accurate but too invasive/expensive for population screening. This underscores the need for minimally intrusive pre-screen although current approaches including blood biomarkers have been disappointing. Optical spectroscopy is a promising technique for minimally invasive detection of cancers and precancers [2]. Our group has recently developed Low-Coherence Enhanced Backscattering Spectroscopy (LEBS) to measure optical properties of tissue with depth limited capability. Moreover, we have shown that optical properties change in field of carcinogenesis as results of micro-architectural change, measurement of which can lead to cancer detection far earlier than possible by conventional techniques. For pancreatic cancer, there is emerging genetic/epigenetic and epidemiological evidence that the duodenum may be a surrogate site (potentially related to pancreatic ductal juices). Using benchtop LEBS system; we have shown that duodenal biopsies were able to discriminate between pancreatic cancer cases and controls [3]. However, to implement this clinically, this needs to be done *in situ* with an endoscopically compatible probe. In this abstract we present initial results with 34 patients taken *in vivo*.

1. LEBS fiber optic probe: Principles

The design and construction of LEBS fiber optic probe is described elsewhere[4]. The LEBS intensity peak, as shown in Fig.1a, is the Fourier transform of spatial backscattering impulse- response function ($P(r)$) multiplied by spatial coherence function ($C(r)$). Thus, measurement of LEBS peak as a function of scattering angle can be used to infer information about $P(r)$ and, from it, the optical and physical properties of tissue. The principle of this probe was to acquire LEBS signals for 3 backscattering angles within the LEBS intensity cone with each collection fiber. This is achieved by collinear alignment of four fibers as shown in Fig.1b. Channel Z is connected to the source. Channels A & A' sample 0.6 ± 0.24 degrees on either side of the peak. Channel B samples 1.18 ± 0.24 degrees which approximated the incoherent baseline (the width of a backscattering intensity cone is governed by L_{SC} , since LEBS width in spatial domain and spatial coherence function are related by Fourier transform). Finally, when this geometry is superimposed over the LEBS collection from the 2D peak, the angular intensity distribution profile, as shown in Fig. 1c, is obtained. While Fig.1c shows each collection fiber in 2D, the actual intensity obtained through

the probe is an average of all pixels. Also the actual probe does not collect the channel Z, since it is connected to the light source.

To confirm that the probe is measuring optical scattering properties, we performed an experiment with a phantom of varying l_s^* with constant g which mimics the optical properties of tissues. The phantom was prepared by mixing polystyrene beads (Thermo Fisher, CT) in water according to concentration governed by Mie theory to attain certain l_s^* & g . The parameter calculated was Pseudo Enhancement (PE), which is defined as the (LEBS signal of channel A) - (LEBS signal of channel B) (obtained after background subtraction and normalization by a spectralon reflectance standard with >98% reflectance). In order to match this result with theory, we used the Monte Carlo (MC) simulation method based on Mie theory for LEBS discussed in other publications [5]. To calculate PE from MC we superimposed the collection geometry on 2D LEBS peak to measure angles corresponding to collection fibers for varying l_s^* & g . From this MC result we calculated PE and matched with experimental data. As shown in Fig. 1d, there is a good match between MC and experimental data after applying a constant multiplicative scaling factor as described in our previous publications [5]. Additionally, by using MC data we constructed a calibration curve and validated the measured optical properties with actual optical properties. As shown in Fig. e, there is a good match between actual l_s^* and measured l_s^* (average error <3%).

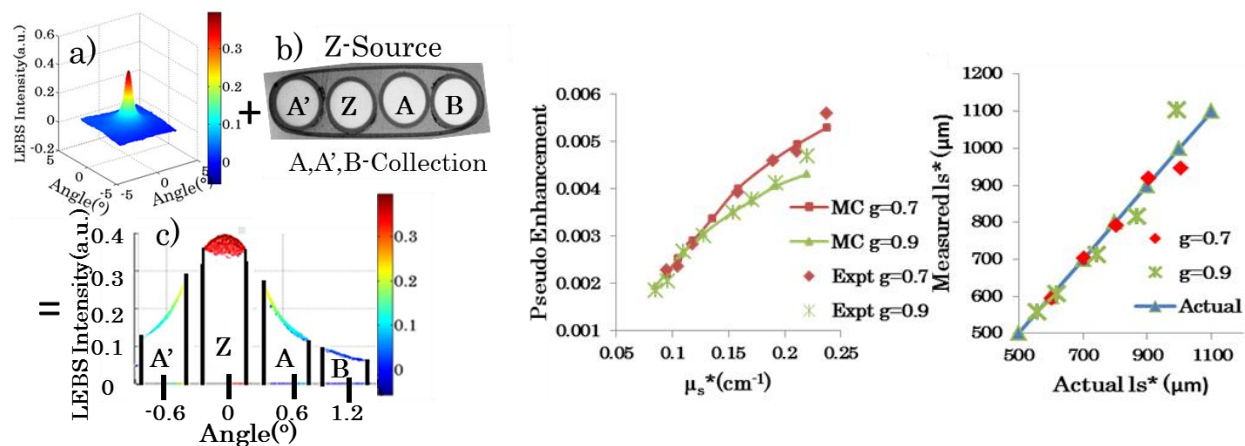


Fig.1. a) 2D LEBS peak is shown for white reflectance standard with LSC $27\mu\text{m}$ at 680nm which is obtained from LEBS ex-vivo system. b) The front end of the probe is shown, with fiber Z used as illumination and other three (A', A & B) used as collection. c) Once the fiber geometry is superimposed on the LEBS 2D peak the shown profile is obtained (the black lines indicate boundaries of collection fibers and intensities collected are on top with color representing corresponding intensities captured from 2D peak in Fig. a) d) Pseudo Enhancement as a function of μ_s^* with L_{sc} constant (27 microns) e) Calibration curve for probe measured from phantom with varying optical properties mimicking tissue

2. In-vivo detection of pancreatic cancer:

In order to validate clinically, we evaluated a 34 patients (23 controls and 11 with pancreatic adenocarcinoma) undergoing upper endoscopy (EGD, EUS or ERCP). Probe readings were taken from the endoscopically normal Peri-Ampullary mucosa (within 2 cm of the papilla). It was seen that transport mean free path (l_s^*) which is represented by Pseudo Enhancement reduces in case of cancer patients. Also, spectral slope characterizing distribution of length scales and index of correlation function (m) goes down in field carcinogenesis indicating increase 'm' and fractal dimension. The AUROC (for combined logistic regression model of PE & SS) for pancreatic cancer was 81 % which is classified as excellent performance with 75% sensitivity and 87% specificity. We demonstrate, for the first time, that interrogation of the endoscopically normal duodenum with our novel LEBS fiber optic probe can discriminate patients with and without pancreatic cancer. This could potentially be done through standard EGD in high risk cohorts (family history, smokers, new diabetics etc.).

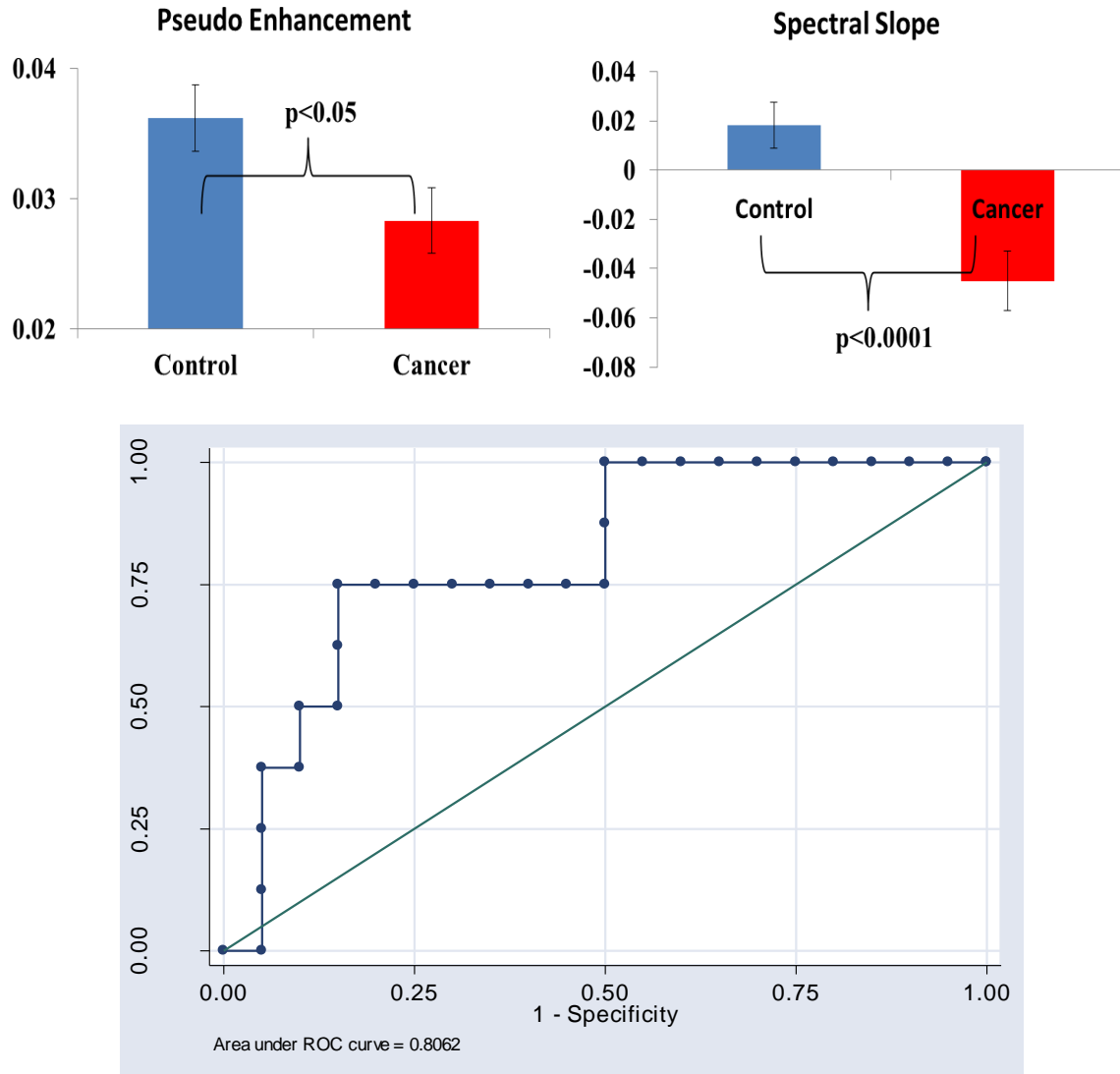


Fig.2. Pseudo Enhancement and spectral slope are significantly reduced with pancreatic cancer. The AUROC curve shows >80 % accuracy which is classified as excellent performance with 75% sensitivity and 87% specificity.

4. References

- [1] R.E. Brand, M.M. Lerch, W.S. Rubinstein, J.P. Neoptolemos, D.C. Whitcomb, R.H. Hruban, T.A. Brentnall, H.T. Lynch, M.I. Canto and P.t. ISIDP, "Advances in counseling and surveillance patients at risk for pancreatic cancer", *Gut* 56 (2007), 1460–1469.
- [2] G. A. Wagnieres, W. M. Star, and B. C. Wilson, "In Vivo Fluorescence Spectroscopy and Imaging for Oncological Applications", *Photochem. Photobiol.* 68, 603 (1998).
- [3] V. Turzhitsky, Y. Liu, N. Hasabou, M. Goldberg, H. K. Roy, **V. Backman**, R. Brand, Investigating Population Risk Factors of Pancreatic Cancer by Evaluation of Optical Markers in the Duodenal Mucosa, *Disease Markers*, 25, 313-321 (2009) (invited paper) PMC2730822.
- [4] Nikhil N. Mutyal, Vladimir Turzhitsky, Jeremy D. Rogers, Andrew Radosevich, Hemant K. Roy, Michael J. Goldberg, Mohammed Jameel, Andrej Bogojevich, Vadim Backman, "Design and Implementation of Fiber Optic Probe for measuring Field Effect of Carcinogenesis with Low-Coherence Enhanced Backscattering Spectroscopy (LEBS)", *Biomedical Optics (BIOMED) 2010 paper: BTuD90*
- [5] V. Turzhitsky, A. J. Radosevich, N. N. Mutyal, J. D. Rogers, **V. Backman**, Measurement of Optical Scattering Properties with Low-Coherence Enhanced Backscattering Spectroscopy, *JBO*, 16(6), 067007, 1-14 (2011).

Breast Cancer Detection in the Spectral Subspace of Biomarkers

Yi Sun¹, Yang Pu², Laura A. Sordillo², Yuanlong Yang² and R. R. Alfano^{2*}

¹Electrical Engineering Department, ²Institute for Ultrafast Spectroscopy and Lasers and Physics Department of The City College of City University of New York, Convent Avenue at 138th Street, New York, NY 10031

*Corresponding author: R. R. Alfano: ralfano@sci.cuny.cuny.edu

Abstract: A novel approach of fluorescent spectral subspace of four key biomarkers with 340 nm excitation is proposed to detect breast cancer and determine efficacy of collagen, NADH, flavin, and elastin.

OCIS codes: 300.300, 170.170, 300.6170

1. Introduction

Since the first report on the laser-induced fluorescence from biological tissues in 1980s [1], fluorescence spectroscopy has been widely used for diagnoses cancer, to develop into a field called optical biopsy [2]. Fluorescent spectra of biochemicals play an important role in discrimination of cancer tissue from normal tissue [3] [4]. It is observed that cancer tissue contains more NADH and less collagen than normal tissue [3] [5] [6]. Quantification of the key biochemical components or biomarkers in a tissue provides a means of cancer detection. Multiple curve resolution (MCR) [7] can be employed to quantify the biochemical components by analyzing fluorescence spectrum. However, the fluorescent spectrum of a tissue is a superposition of spectra of various biochemicals and molecules. Thus, component quantification is essentially an ill-posed problem. MCR, which is a model-free data fitting method, might result in invalid solutions. Moreover, component quantification cannot guarantee to obtain sufficient statistics of the biomarkers and useful information for cancer detection is inevitably reduced in terms of information theory. In the cancer detection point of view, a classifier can be trained directly using training samples of normal and cancerous fluorescent spectra. However, a fluorescent spectrum is sampled to have a high dimension space. To obviate the effect of curse of dimensionality, principal component analysis (PCA) can be applied to reduce the dimension by projecting fluorescent spectra of tissue samples onto a few of principal components and then a tissue is classified in the spectral subspace spanned by the PCs [8]. However, contribution of important biomarkers to the principal components is usually unknown while many unknown biochemicals may contribute to the principal components.

In this study, for the first time to our knowledge, a new theoretical approach is used for cancer detection in the subspace of biomarkers' fluorescence spectra. Specifically, the basis of spectral subspace of biomarkers are obtained by the Gram-Schmidt method using the spectra of biomarkers. The spectra of tissue samples are projected onto the subspace. The support vector machine (SVM) [9] in the subspace is trained by using training samples. The receiver operation characteristic (ROC) in terms of separability and specificity is obtained. The approach is applied to breast cancer detection using fluorescent spectra with excitation of 340 nm and using four biomarkers, collagen, NADH, flavin, and elastin.

2. Method

Given K biomarkers that have fluorescent spectra $c_k(\lambda)$, $k = 1, \dots, K$ where λ is wavelength. Since the biomarkers are components of a tissue, the fluorescent spectrum of the tissue can be considered to be composed of $s(\lambda) = \sum_{k=1}^K a_k c_k(\lambda) + z(\lambda)$. Here, a_k are positive constants each proportional to the quantity of a biomarker. $z(\lambda)$ is the spectrum due to other biochemicals and noise. In the approach of MCR, a_k of a tissue are estimated and then used to classify the tissue as cancerous or normal. However, quantification of a_k is an ill-posed problem, and the estimated a_k may be significantly biased from the true value and even be invalid, making the classification unreliable.

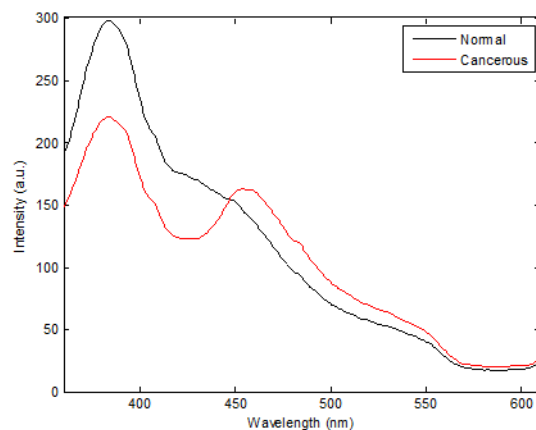


Fig. 1. Average spectra of normal and cancerous samples.

Since cancerous and normal tissues shall be discriminated by the biomarkers, all information useful in cancer detection is embedded in the subspace spanned by the fluorescent spectra $c_k(\lambda)$. The basis spectra of the subspace can be obtained by singular value decomposition (SVD) in the descent order of powers of singular vectors. However, to clearly see how each biomarker contributes to the subspace and affects classification, the basis spectra are obtained by the Gram-Schmidt method as $b_k(\lambda)$, $k = 1, \dots, K$. The spectrum of a tissue $s(\lambda)$ is projected onto the subspace and forms a K -dimensional vector \mathbf{s} where the k th component is the inner product of $s(\lambda)$ and $b_k(\lambda)$. By the projection, \mathbf{s} retains the component in the spectral subspace of biomarkers but gets rid of all other components orthogonal to the subspace. Statistically speaking, \mathbf{s} is a sufficient statistic and contains all information useful in cancer detection when the biomarkers are used. In practice, $s(\lambda)$ is sampled at discrete wavelength, producing, say N samples. In general, K is much smaller than N . Hence, the projection onto the subspace also significantly reduces the dimension and effectively obviates the curse of dimensionality when training a classifier.

By using training samples of cancerous and normal tissues, a classifier, a hyperplane $\mathbf{w}^T \mathbf{s} = b$, in the subspace is obtained by SVM with which the sensitivity and specificity can be calculated accordingly. Changing the distance b of the hyperplane to the origin but retaining the normal angle determined by \mathbf{w} , ROC can be obtained in term of sensitivity versus $1 - \text{specificity}$.

3. Experimental results

The proposed approach is applied to breast cancer detection using four biomarkers, collagen, NADH, flavin, and elastin with 340 nm wavelength excitation. Fluorescent spectra of 37 normal tissues and 37 breast cancerous tissues are measured. Their average spectra are shown in Fig. 1.

The fluorescent spectra of the four biomarkers are shown in Fig. 2 and their crosscorrelation matrix is given in Table 1. Flavin has low crosscorrelation with other biomarkers in the fluorescent spectrum, which implies that it can provide a significant component additional to the subspace spanned by {collagen, NADH, elastin}.

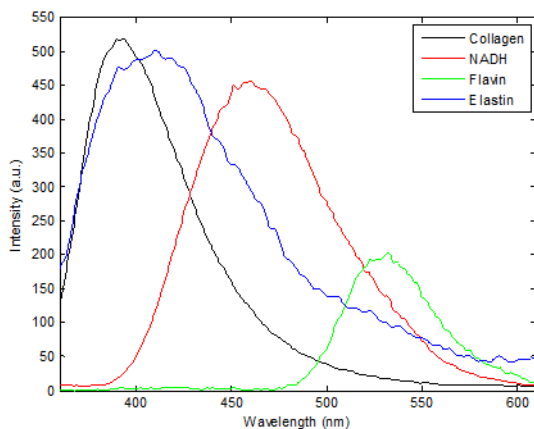


Fig. 2. Fluorescent spectral of four biomarkers.

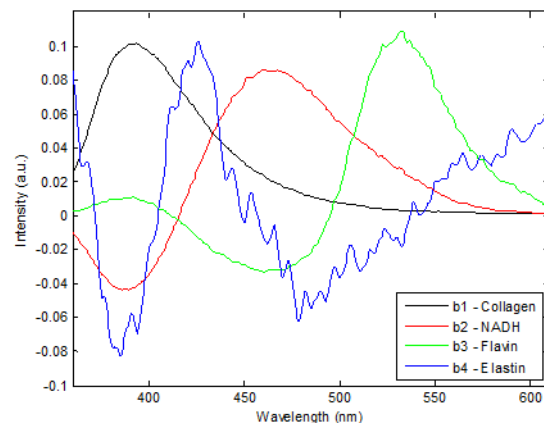


Fig. 3. Basis spectra of four biomarkers.

Fig. 3 illustrates the basis spectra of the subspace spanned by the spectra of all four biomarkers, which are obtained by the Gram-Schmidt method in the order of collagen, NADH, flavin, and elastin. That is, $b_1(\lambda)$ is obtained by normalizing spectrum of collagen to unit length, $b_2(\lambda)$ is obtained by taking the component of NADH spectrum that is orthogonal to $b_1(\lambda)$ and then normalized to unit length, etc. If all the four biomarkers are used to classify the 74 samples using the SVM, the sensitivity is 0.919, specificity is 0.973, the area under curve (AUC) of ROC is 0.992, and the number of support vectors (SV #) is 18 as listed in the last row of Table 2. The closer to one the AUC is, the better the performance is.

To investigate the efficacy of a biomarker in cancer detection, the performance of all possible combinations of four biomarkers is calculated and the results are presented in Table 2. For example, Fig. 4 illustrates the data samples, support vectors, SVM classifier and NADH in the subspace spanned by the spectra of {collagen, NADH}. It is clear that collagen alone is incapable of properly classifying the normal and cancerous samples, as shown in

Table 1. Crosscorrelations

	1	2	3	4
1	1	0.423	0.065	0.940
2	0.423	1	0.342	0.691
3	0.065	0.342	1	0.218
4	0.940	0.691	0.218	1

1 - collagen, 2 - NADH, 3 - flavin, 4 - elastin

Fig. 4 and the first row of Table 2. However, collagen and NADH jointly can classify very well the samples with sensitivity of 0.919 and specificity of 0.973 as shown in Table 2. The best performance is obtained by the combination of {collagen, NADH, elastin} with sensitivity of 0.946, specificity of 0.973, AUC of 0.993, and 18 support vectors. Table 2 also indicates that if collagen is not used, performance becomes worse; and this is similarly true for NADH. Hence, the order of efficacy of the biomarkers in breast cancer detection in this experiment is collagen, NADH, elastin, flavin. In fact, the performance of {collagen, NADH, elastin} is better than that of {collagen, NADH, elastin, flavin}. This implies that though Table 1 indicates that flavin provides a significant component in another dimension orthogonal to the subspace spanned by {collagen, NADH, elastin}, the additional component that {collagen, NADH, elastin} cannot provide does not increase the discriminability of cancer. Table 2 also implies that when a combination of biomarkers makes samples easier to be classified in a subspace, the support vectors are fewer.

Table 2. Performance versus biomarkers

Biomarkers	Sensitivity	Specificity	AUC	SV #
1	0.649	0.514	0.582	74
2	0.486	0.541	0.524	74
3	0.459	0.568	0.571	74
4	0.595	0.514	0.554	74
1, 2	0.919	0.973	0.962	30
1, 3	0.919	0.919	0.964	28
1, 4	0.919	0.973	0.992	18
2, 3	0.486	0.730	0.671	73
2, 4	0.919	0.946	0.969	29
3, 4	0.784	0.838	0.877	54
1, 2, 3	0.919	0.919	0.964	28
1, 2, 4	0.946	0.973	0.993	18
1, 3, 4	0.838	0.919	0.948	35
2, 3, 4	0.919	0.946	0.969	29
1, 2, 3, 4	0.919	0.973	0.992	18

1 - collagen, 2 - NADH, 3 - flavin, 4 - elastin.

3. Conclusion

For the first time, we proposed a novel theoretical approach to experimental data to cancer detection from the fluorescence spectral subspace of biomarkers. Projection of sample spectra onto the subspace of biomarkers' spectra

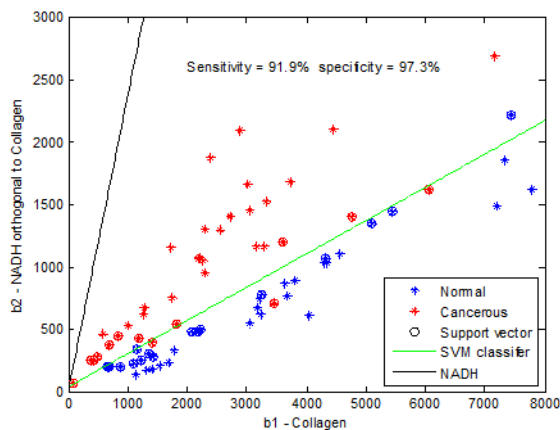


Fig. 4. Samples, support vectors, SVM classifier and NADH component in the subspace spanned by collagen and NADH.

retains all useful information for cancer detection while significantly reducing sample dimension. The efficacy of biomarkers in cancer detection can be determined in the subspace by SVM. The proposed approach applied for breast cancer detection with fluorescent spectrum of 340 nm wavelength excitation achieves high performance with sensitivity of 94.6% and specificity of 97.3%. The efficacy of biomarkers is in the order of collagen, NADH, and elastin while flavin does not provide additional discriminability. The approach may be useful in detection of other cancers.

4. Acknowledgement

This research is supported in part by the U. S. Army Medical Research and Materiel Command grants of W81XWH-08-1-0717 (CUNY RF 47170-00-01) and W81XWH-11-1-0335 (CUNY RF # 47204-00-01).

5. References

- [1] R. R. Alfano, D. Tata, J. Cordero, P. Tomashefsky, F. Longo, and M. Alfano, "Laser induced fluorescence spectroscopy from native cancerous and normal tissue", *IEEE J. Quantum Electron*, **20**, 1507-1511 (1984).
- [2] R. R. Alfano, G. C. Tang, Asima Pradhan, W. Lam, Daniel S. J. Choy, Elana Opher, "Fluorescence spectra from cancerous and normal human breast and lung tissues", *IEEE J. of Quant. Electron QE*, **23**, 1806 (1987).
- [3] Y. Pu, W.B. Wang, G. C. Tang, R. R. Alfano, "Changes of collagen and NADH in human cancerous and normal prostate tissues studied using fluorescence spectroscopy with selective excitation wavelength", *J. Biomed. Opt.*, **15**, 047008-1-5 (2010).
- [4] Y. Pu, G. C. Tang, W. B. Wang, H. E. Savage, S. P. Schantz, and R. R. Alfano, "Native fluorescence spectroscopic evaluation of chemotherapeutic effects on malignant cells using nonnegative matrix factorization analysis", *Technol. Cancer Res. Treat.*, (TCRT), **10**, Issue 2, 113-120 (2011).
- [5] Irene Georgakoudi, Brian C. Jacobson, et al., "NAD(P)H and collagen as *in vivo* quantitative fluorescent biomarkers of epithelial precancerous changes", *Cancer Research* **62**, 682-687, (2002).
- [6] Rebekah Drezek, Konstantin Sokolov, et al., "Understanding the contributions of NADH and collagen to cervical tissue fluorescence spectra: modeling, measurements, and implications", *Journal of Biomedical Optics*, **6(4)**, 385-396 (2001).
- [7] A. Kandelbauer, W. Kessler, and R. W. Kessler, "Online UV-visible spectroscopy and multivariate curve resolution as powerful tool for model-free investigation of laccase-catalysed oxidation", *Ana. Bioanal. Chem.* **390**:1303-1315 (2008).
- [8] J. Mo, W. Zheng, J. J. H. Low, J. Ng, A. Ilancheran, and Z. Huang, "High wavenumber raman spectroscopy for *in vivo* detection of cervical dysplasia", *Anal. Chem.* **81**: 8908-8915 (2009).
- [9] C. Cortes and V. N. Vapnik, "Support-Vector Networks," *Machine Learning*, **20**: 273-297 (1995).

Single gradient-index-multimode-fiber enabled Fourier-domain low coherence interferometry and reflectance spectroscopy towards fine-needle-probing of steatosis

Anqi Zhang,¹ Daqing Piao,^{1*} Kenneth E. Bartels,² G. Reed Holyoak,² Jerry W. Ritchey³

¹School of Electrical and Computer Engineering, Oklahoma State University, Stillwater, OK 74078, USA

²Department of Veterinary Clinical Sciences, Center for Veterinary Health Sciences, Oklahoma State University, Stillwater, OK 74078, USA

³Department of Veterinary Pathobiology, Center for Veterinary Health Sciences, Oklahoma State University, Stillwater, OK 74078, USA

*daqing.piao@okstate.edu

Abstract: We present dual-modality Fourier-domain common-pass low coherence interferometry and reflectance spectroscopy based on single gradient-index multimode fiber fitting a 24 gauge needle. The objective is to assess the condition of donor liver steatosis.

OCIS codes: 170.4500 Optical coherence tomography; 170.6510 Spectroscopy, tissue diagnostics; 170.3890 Medical optics instrumentation.

1. Introduction

Each year more than 6000 liver transplants are performed in USA, and approximately 17,000 patients in US are waiting for donated livers to become available [1]. The concomitant lack of suitable donors has pressed hepatic surgeons across the US to use livers of “marginal” quality such as fatty livers from living or deceased donors. Steatosis in the donor livers is the main risk factor for initial poor-function or non-function of the graft after transplant, as the fatty livers are particularly susceptible to ischemia reperfusion injury (IRI) [2].

The size of the fat vacuolae determines the two microscopic categories of steatosis [3]: (1) micro-vesicular steatosis, when more than 90% of the lipid vacuolae are smaller than the hepatocyte nucleus, as illustrated by the dotted arrows in Fig. 1; (2) macro-vesicular steatosis, when a single large droplet occupies most of the cell, displacing the cytoplasm and nucleus to a ring around the droplet, as pointed by the solid arrows in Fig. 1. Macro-steatosis in the donor organ represents a major risk to organ recipients [4]. Micro-steatosis, on the other hand, is not associated with an increased risk of dysfunction [5]. A quantitative and instantaneous instrument for screening the intensity of steatosis, and further discriminating macro-steatosis from micro-steatosis, does not exist clinically.

Increased lipid content in liver tissue, regardless of the sizes of the droplets, has shown to increase the reflectance scattering in surface-measurement near-infrared (NIR) reflectance spectroscopy (RS) [7]. Since macro-steatosis differs from micro-steatosis in the scatter-size, it may be feasible to base upon the scattering spectral profile to discriminate between the two types of steatosis. On the other hand, lipid-rich tissue generally appears to have a signal-poor interior when imaged by low coherence interferometry (LCI) [8], due to the diminished back-scattering. When imaged by LCI, the macro-steatosis may present interior signal-poorness, however the micro-steatosis could reveal interior signal-enhancement as a result of the aggregation of small lipid droplets. Hence we propose that combining the complimentary information of RS and LCI, ideally in a single-fiber probing scheme for minimally invasive multi-site sampling, could help to better assess lipid content and potentially differentiate macro-steatosis from micro-steatosis in donor liver. In this study we demonstrate using scattering particle that a single gradient index (GRIN) multimode (MM) fiber accommodates the LCI coherent gating and RS broad-spectral measurement.

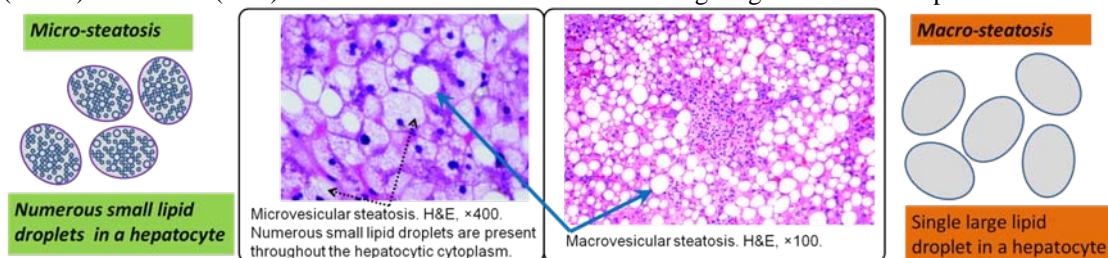


Figure 1. Micro-vesicular (dotted smaller arrow) and macro-vesicular (solid larger arrow) steatosis [6]

2. Development of single GRIN MM fiber based Fourier-domain LCI and RS system

The use of GRIN MM fiber in LCI was demonstrated in a Mach-Zehnder time-domain configuration, using a single-mode (SM) fiber as the source of illumination and a GRIN MM fiber as the light collector [9]. We present in this study a Fourier-domain common-pass LCI based on GRIN MM fiber that integrates RS sampling through the same

fiber probe. The schematic of this single GRIN MM fiber based dual-modality LCI and RS system is illustrated in Fig. 2. The SM fiber-coupled light of 840nm center wavelength and 50nm FWHM bandwidth, giving 6.23 μ m theoretical coherence length in air, from a super-luminescent diode (SLD) (Superlumdiode Inc.) is coupled to the rest of the system comprised of the GRIN MM fiber, which has 50 μ m core diameter, 125 μ m cladding diameter, 245 μ m coating diameter (fitting a 24 gauge needle), and 0.2 numerical aperture. The GRIN MM fiber coupler C1 with 50/50 coupling ratio directs the SLD light to sample the tissue. The light reflected at the facet of the probing fiber serves as the reference signal for coherent gating in LCI. This common-path LCI configuration is appealing as disposable fiber-probes of inconsistent lengths may be connected to C1 without the need of adjusting the reference pathlength. A Deuterium/Halogen light source (DH2000, OceanOptics Inc.) is also coupled to the probing fiber through C1 and another 50/50 GRIN MM coupler C2 for RS. The sample-reflected light collected by the probing fiber is guided to the detection units through C1, C2, and another 50/50 GRIN MM coupler C3, which connects a Fourier-domain LCI detector and a compact RS spectrometer (NT58-303, Edmund Optics Inc.). The Fourier-domain LCI detection unit consists of an achromatic lens L1 ($f=5$ mm), a transmission diffraction grating (1200lines/mm, Wasatch Photonics), an achromatic lens L2 ($f=200$ mm) and a 10bit line-scan camera (L104k-2k, Basler AG).

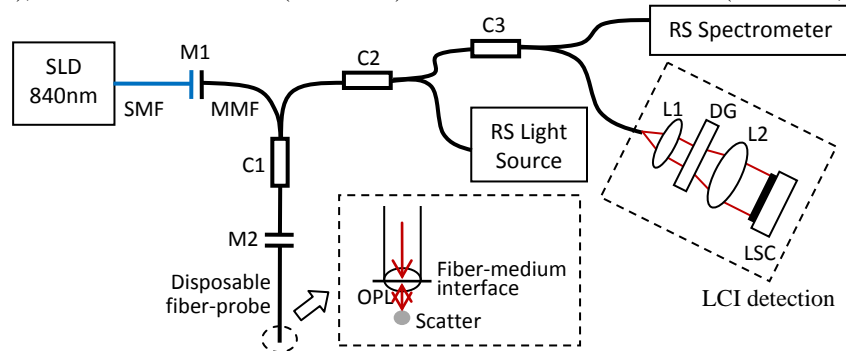


Fig. 2. Schematic of the dual-modality system. Fourier-domain LCI and RS share the same probing fiber but different sources and detection units. SMF: single mode fiber; MMF: multimode fiber; M1-M2: FC/PC to FC/PC mating sleeve; C1-C3: 50/50 fiber coupler; OPL: optical path length; L1-L2: achromatic lens; DG: diffraction grating, LSC: line scan camera.

In the Fourier-domain LCI measurement, each A-line is obtained and then processed through Labview platform as: 1) subtracting the fiber-facet originated reference spectrum from the interferometric signal of object, 2) re-sampling the signal into linear wave number vector, $k = 2\pi/\lambda$, 3) applying group velocity dispersion (GVD) compensation following the method described by Wojtkowski et al. [10], 4) performing Fourier transformation. The parameters for dispersion compensation are determined at one depth, which are then applied at all depths throughout the measurement. The A-line shown in the following section is obtained in less than 125ms.

3. Performance of dual-modality measurements

3.1 Point-spread function of Fourier-domain LCI with group-velocity-dispersion compensation

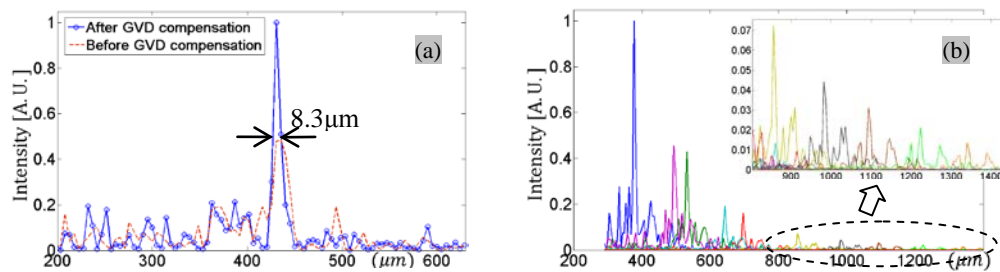


Fig. 3. (a) One A-line of mirror object at 431 μ m depth shows the resolution as 8.3 μ m. (b) The overlapped A-lines of mirror object located at different depths.

The mirror as the object is used to measure the point spread function (PSF) of the Fourier-domain LCI system. Figure 3 (a) illustrates one single A-line for mirror located at 431 μ m away from the fiber tip, before and after the GVD is compensated. After the GVD compensation the side-peaks remain relatively unchanged in intensity, however the main peak is substantially enhanced, reaching a 8.3 μ m resolution in air (6.24 μ m in tissue). As no optical lens is used at the tip of the probe to focus light onto the scattering object, LCI signal drops dramatically along the depth. Figure 3 (b) illustrates the situation of overlapping A-lines measured for mirror located at a set of randomly selected depths of 377 μ m, 494 μ m, 532 μ m, 644 μ m, 697 μ m, 857 μ m, 982 μ m, 1094 μ m, 1224 μ m and

1340 μm . As this situation mimics LCI measurements of multiple scatterers along the axial direction, it appears that the side peak at each mirror position add constructively to the depth-resolved back-scattering profile.

3.2 Dual-modality non-simultaneous measurement of LCI and RS from Titanium(IV) oxide

Titanium(IV) oxide (TiO_2) nanoparticle is used to test the dual-modality LCI and RS through the single probing fiber. Since the LCI source overwhelms the LCI source in the LCI spectrum, the two measurements were performed not simultaneously. As the average particle size of TiO_2 (<100nm) is less than the LCI resolution, it is expected that the LCI reveals a clear back-scattering profile over depth. The measurement results in Figure 4 (a) show about 50dB signal reduction over a 1mm depth range of TiO_2 .

The RS spectral profile measured from TiO_2 is illustrated in Figure 4(b) in comparison to the spectra profiles obtained from water and bare fiber in air. We have demonstrated previously that the reflectance spectral profile of scatterer can be normalized against that of water and air to obtain a wavelength-dependent scattering intensity profile that represents the reduced scattering coefficient of the scatterer [11].

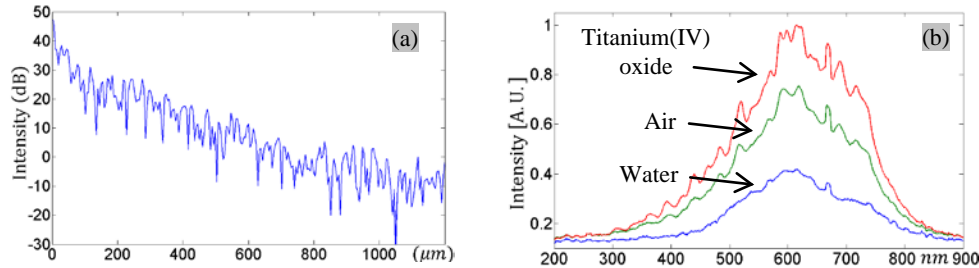


Fig. 4. (a) The A-line measured in Fourier-domain LCI from TiO_2 nanoparticle, which shows a clear back-scattering profile. (b). The spectrum measured in RS from water, air and TiO_2 nanoparticle. The spectrum of TiO_2 nanoparticle is higher in intensity than that of air and water.

4. Discussion

The tissue penetrating depth of LCI in liver may be at the order of hundreds of microns to no more than 1mm, due to high absorption. This shallow sampling depth could be comparable to the average sampling depth of single-fiber reflectance spectroscopy. Within this sampling depth, the main peaks of LCI signal originating from individual clustered small scatterers of sizes smaller than the axial resolution could be constructively augmented by the numerous side peaks to reveal a scattering-rich interior; whereas, the LCI signal originating from individual single large scatterer of sizes several times greater than the axial resolution could appear to have a scattering-poor interior. By adding the scattering intensity and scattering power information extractible from normalized RS measurements, it may be possible to distinguish large scatterers from the cluster of small scatterers with the size of single large scatterer.

Acknowledgement

This research is funded by Oklahoma Center for the Advancement of Science and Technology (grant HR11—0043).

References

- [1] T. M. Fishbein, M. I. Fiel, S. Emre, O. Cubukcu, S. R. Guy, M. E. Schwartz, C. M. Miller, and P. A. Sheiner, "Use of livers with microvesicular fat safely expands the donor pool," *Transplantation*; **64**, 248-251 (1997).
- [2] A. K. Chui, K. Haghighi, D. Painter, M. Jayasundera, G. Hall, A. R. Rao, D. J. Verran, G. W. McCaughan, and A. G. Sheil, "Donor fatty (steatotic) liver allografts in orthotopic liver transplantation," *Transplant Proc.*; **30**, 3286-3287 (1998).
- [3] R. S. Markin, J. L. Wisecarver, S. J. Radio, R. J. Stratta, A. N. Langnas, K. Hirst, and B.W. Jr. Shaw, "Frozen section evaluation of donor livers before transplantation," *Transplantation*; **56**(6), 1403-1409 (1993).
- [4] A. Halon, D. Patrzalek, and J. Rabczyn'ski, "Hepatic steatosis in liver transplant donors: rare phenomenon or common feature of donor population?" *Transplant. Proc.*; **38**, 193-195 (2006).
- [5] C. J. Imber, S. D. St Peter, A. Handa, and P. J. Friend, "Hepatic steatosis and its relationship to transplantation Liver," *Transplant.*; **8**, 415-423 (2002).
- [6] R. Ramachandran, and S. Kakar (2009), "Histological patterns in drug-induced liver disease," *Clin Pathol.*; **62**, 481-492 (2009).
- [7] B. L. McLaughlin, A. C. Wells, S. Virtue, A. Vidal-Puig, T. D. Wilkinson, C. J. Watson, and P. A. Robertson, "Electrical and optical spectroscopy for quantitative screening of hepatic steatosis in donor livers," *Phys Med Biol.*; **55**(22), 6867-6879 (2010).
- [8] H. Yabushita, B. E. Bouma, S. L. Houser, H. T. Aretz, I. K. Jang, K. H. Schlendorf, C. R. Kauffman, M. Shishkov, D. H. Kang, E. F. Halpern, and G. J. Tearney, "Characterization of human atherosclerosis by optical coherence tomography," *Circulation*; **106**(13), 1640-1645 (2002).
- [9] B. Varghese, V. Rajan, T. G. Van Leeuwen, and W. Steenbergen, "Evaluation of a multimode fiber optic low coherence interferometer for path length resolved Doppler measurements of diffuse light," *Rev Sci Instrum.*; **78**(12), 126103 (2007).
- [10] M. Wojtkowski, V. J. Srinivasan, T. H. Ko, J. G. Fujimoto, A. Kowalczyk, and J. S. Duker, "Ultrahigh-resolution, high-speed, Fourier domain optical coherence tomography and methods for dispersion compensation," *Opt. Express* **12**(11), 2404-2422 (2004).
- [11] D. Piao, K. McKeirnan, Y. Jiang, M.A. Breshears, and K.E. Bartels, "A low-cost needle-based single-fiber reflectance spectroscopy method to probe scattering changes associated with mineralization in intervertebral discs in chondrodystrophoid canine species – A pilot study," *Photonics and Lasers in Medicine*, accepted.

Preliminary Intravital Microscopic Analysis Reveals Specific Monocyte Uptake of Circulating Nanotubes and Peptide-Dependent Delivery into Tumor

Bryan R. Smith, Eliver Ghosn, Harikrishna Rallapalli, Jarrett Rosenberg, Jennifer Prescher, Lee Herzenberg, Sanjiv S. Gambhir

Stanford University
Departments of Radiology, Immunology, Bioengineering, and Chemistry
318 Campus Drive East
Clark Center, E-150
Stanford, CA 94305

Bryan R. Smith
brsmith@stanford.edu

Abstract: Nanoparticle targeting efficiency to tumor is poor and not well-understood. Applying intravital microscopy in a mouse-model to interrogate vasculature-targeted nanotubes, we found that monocytes specifically take up nanotubes and are programmed to enter tumor.

Molecular targeting of nanoparticles (nps) is known to increase tumor uptake, but is believed to do so via a direct np ligand-receptor binding mechanism. It is also well-known that monocytes tend to accumulate in tumor. The present work unexpectedly suggests that 1. An important monocyte subset implicated in cancer takes up our injected nanotubes and 2. Circulating monocytes can be programmed by molecularly-targeted nps to increase preferential deposition into tumor.

We used intravital microscopy (IVM) to visualize U87MG tumor, transfected with Enhanced Green Fluorescent Protein (EGFP), in a surgically-implanted dorsal window chamber mouse model (n=25 mice). We employed 488 nm, 633 nm, and 748 nm lasers to excite tumor cells, cy5.5 conjugated to SWNTs, and long circulating dye that was injected to visualize the tumor blood vessels, respectively. While focusing on the vasculature of the tumor and its surrounding tissue, we tail-vein injected single-walled carbon nanotubes (SWNTs) conjugated to cy5.5 dye. In real time, we visualized uptake of SWNTs into circulating cells within the blood vessels and their subsequent behavior once they entered the tumor interstitium. Three different SWNT conditions were employed: SWNTs were conjugated to RGD (arginine-glycine-aspartic acid) peptide which binds integrin $\alpha_v\beta_3$ (overexpressed on the surface of tumor blood vessels), while RAD peptide (similar to RGD, yet non-specific to the integrin) and unconjugated SWNTs (plain) were controls. We observed that circulating cells took up SWNTs within seconds of injection (see Figure 1) and no cells were labeled in controls. We verified the identity of the cells by extracting blood and using 12-color fluorescence activated cell sorting (FACS) with an antibody panel. We also used the intrinsic Raman

signature of SWNTs to verify their presence and quantify their overall tumor uptake by using Raman imaging in living subjects.

Shockingly, SWNTs were taken up into a specific subset of blood monocytes with exquisite specificity. Nearly 100% of Ly-6C^{hi} monocytes took up SWNTs (see Figure 1) in blood, while only ~2% or less Ly-6C^{int} and Ly-6C^{lo} monocytes and neutrophils displayed SWNT signal. Furthermore, interestingly SWNTs induced transient activation of the Ly-6C^{hi} monocytes (increase in cd11b expression at 2 hours, return to baseline by 6 hours even though SWNTs remained in monocytes). We observed a sharp decrease of SWNT-laden monocytes in blood at 2 and 6 hours p.i. At the same time, in the spleen (measured at 6 hours post-injection) Ly-6C^{hi} monocytes also comprised the vast majority of cells taking up SWNTs. We observed an ~3-fold increase of Ly-6C^{hi} monocytes in spleen compared to controls. This suggests that SWNTs may induce transient monocyte activation leading to deposition of some fraction of blood monocytes into the spleen.

We observed rapid uptake, within a minute of injection, of SWNTs into circulating monocytes when injecting plain SWNTs, compared with several hours when peptide-conjugated SWNTs were injected. Monocytes were observed within the vasculature after SWNT uptake and were categorized as either 1) non-interacting (free-flowing) monocytes or 2) interacting monocytes (crawling along the luminal vessel surface). At one day post-injection, we observed more non-interacting monocytes containing plain SWNTs than those with RAD, and more RAD than RGD ($p=0.0001$). However, interacting monocytes displayed the reverse trend ($p=0.0057$), suggesting that the presence of peptides linked to SWNTs encouraged interaction of the monocytes with the endothelium. In the first week post-injection, we found significantly more monocytes interacting with vessels in the plain condition than in the RGD-SWNT condition ($p<0.0001$), with no difference between RAD and plain SWNTs. No non-interacting monocytes were found remaining in the circulation by one week post-injection.

We also observed SWNT-laden monocytes within the tumor interstitium, and by Day 7 post-injection significantly more monocytes in the RGD-SWNT condition were present than in control conditions ($p<0.0001$). We furthermore noticed that total SWNTs in tumor increased over the first week post-injection for RGD/RAD, but only for the first 3 days post-injection for plain SWNTs. Together with the above results, the data imply that targeted SWNTs are programming monocytes to deliver SWNTs into tumor via the monocytes as a “Trojan Horse.” These data thus indicate that in living subjects RGD may encourage not only typical np ligand-receptor binding routes and tumor uptake, but also indirect uptake into monocytes and subsequent trafficking into tumor, which increases

uptake. The RGD-SWNT laden monocytes appear to be preferentially taken up into tumor compared with SWNTs lacking RGD.

In conclusion, these results could (1) lead to improved np design to increase monocyte delivery, (2) transform non-specific tumor monocytes into specific delivery vehicles, and (3) may explain the high tumor uptake displayed by injected SWNTs compared with other nanoparticle types (~10-15% with SWNTs compared with typically 8% or less with other nanoparticle varieties).

Figure 1.

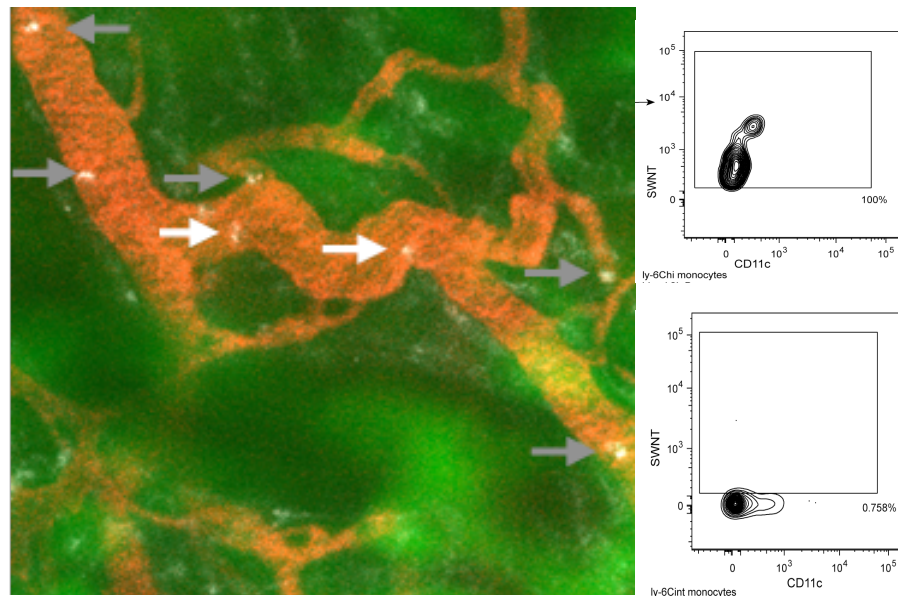


Figure 1. SWNTs are taken up in the circulation into circulating Ly-6C^{hi} monocytes. At left tumor is green, blood vessels are red, and SWNTs are in grayscale. In this image, SWNTs had been injected into the tail vein of a SCID mouse fitted with a window chamber. The arrows in the image point to flowing monocytes that have taken up cy5.5-SWNTs. On the right are FACS plots demonstrating that ~100% of the monocytes in blood take up SWNTs, while other circulating cells (such as the Ly-6C^{intermediate} monocytes shown on the right bottom) do not take them up in general in blood.

**DSu5B: Digital Holography and
Three-Dimensional Imaging (DH)
Postdeadline Papers**

Sunday 29 April, 2012

Symphony IV

16:30 – 19:30

Dry Decoupling Of Index Of Refraction And Topography Through Digital Holographic Microscopy

Freddy Alberto Monroy Ramírez^{1*} and Jorge Garcia-Sucerquia²

¹ Physics Department, Universidad Nacional de Colombia, Sede Bogotá, Colombia

² School of Physics, Universidad Nacional de Colombia, Sede Medellín, Colombia, 050034

*famonrovr@unal.edu.co

Abstract: In interferometric essays the measured phase merges the topography and index of refraction. Multiple wavelength illumination, variation of the index of refraction of the surrounding medium in containing chambers are common methods to separate those two features of the samples. In this work we present the use of the change of the air pressure on a perfusion chamber to decouple the topography and index of refraction. The method is applied to fully characterize a partially stripped optical fibre.

OCIS codes: (090.1995) Digital Holography, (090.2880) Holographic Interferometry, (110.0180) Microscopy.

1. Introduction

The phase difference recorded in interferometry merges the index of refraction and the topography of the object through which the light travels. Only under very restrictive conditions one can consider that the phase difference of the interferometric essay is merely due to the change of the index of refraction [1]. In general, such phase difference $\Delta\phi$ is given by $\Delta\phi = 2\pi/\lambda_0 n\Delta r$, with λ_0 the wavelength of the illuminating wave, n the index of refraction of sample which has a topography Δr . To separate the information of the index of refraction from the topography different methods have been presented in the literature [2,3]. One of the most celebrated methods uses the change of index of refraction of the medium that surrounds the sample under study. The sample is enclosed in a glass chamber with an inlet and outlet; the chamber is sequentially filled with known media of indexes of refraction n_m and $n_m + \delta n_m$ to produce two phase differences from which the topography and the index of refraction can be extracted. This conceptually simple approach has a fairly complicated implementation; to migrate from the medium with index of refraction n_m to a medium with index of refraction $n_m + \delta n_m$ the chamber has to be emptied totally from the medium n_m and refilled with the medium $n_m + \delta n_m$; those media are generally liquids, some could be oily, which dirty and contaminates the chamber and the sample. As a viable alternative, in this work we present a method that by changing the internal pressure of the chamber the index of refraction around the sample is changed and therefore the index of refraction and topography of the sample can be separate. The proposed method is applied to determine the index of refraction and topography of a partially stripped optical fiber.

2. Experimental setup calibration of the glass chamber.

Figure 1 shows the digital holographic microscope used to show the index of refraction and topography separation via air pressure changes of the glass chamber. The optical setup is based on a Mach-Zehnder-type interferometer. A He-Ne laser is split into a reference and object beam. The object beam illuminates the glass chamber which is connected to a vacuum pump. On the top wall of the chamber an air sealed hole is made such that the object, in this case a partially stripped optical fiber, is introduced. The superposition of the object and reference beams is recorded on a CMOS with 1024x1280 square pixels of 4.65 μm side. From the intensity recorded by the CMOS camera, a regular angular spectrum approach [4] has been implemented to compute the phase difference $\Delta\phi_{s,0}(x, y)$. Figure 2 illustrates the glass chamber with the partially stripped optical fiber introduced and the corresponding coordinates system; panel A shows a side view and panel B presents a down-top view of the system. As a plane wave illuminates perpendicularly the side of the glass chamber, the recorded phase difference is given by:

$$\Delta\phi_{s,0}(x, y) = 4\pi/\lambda_0 \left[\left(r_d^2 - y^2 \right)^{\frac{1}{2}} (n_m - n_d) \right]. \quad (1)$$

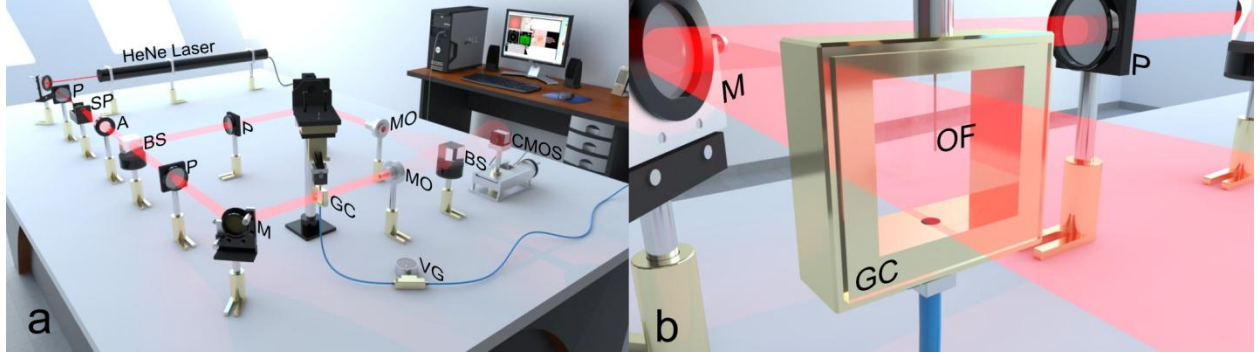


Figure 1. Experimental setup of the implemented DHM. Panel a illustrates the complete setup, panel b shows a zoomed in view of the glass chamber. **SF**: spatial filter **P**: linear polarizers. **A**: collimating lens. **M**: mirrors. **BS**: beam splitters. **MO**: microscope objectives, **OF** optical fiber, **VG**: vacuum gauge, CMOS camera (1280x1024) square pixels of 4.65 μm side, **GC**: glass chamber.

This phase difference carries on the information of the $r_d(x, y)$ topography and the index of refraction index $n_d(x, y)$ of the optical fiber. As expected the measured phase difference depends on the index of refraction of the surrounding medium n_m . This dependency means that a new phase difference $\Delta\phi_{s1}(x, y)$ can be computed if the surrounding medium is changed to a index of refraction $n_m + \delta n_m$, namely:

$$\Delta\phi_{s1}(x, y) = 4\pi/\lambda_0 \left[(r_d^2 - y^2)^{\frac{1}{2}} (n_m + \delta n_m - n_d) \right] \quad (2)$$

From equation (1) and (2) one can calculate the topography:

$$r_d(x, y) = \left\{ \left[\frac{\lambda_0}{4\pi\delta n_m} (\Delta\phi_{s1}(x, y) - \Delta\phi_{s0}(x, y)) \right]^2 + y^2 \right\}^{\frac{1}{2}} \quad (3)$$

and the index of refraction of the optical fiber:

$$n_d(x, y) = n_m - \frac{\Delta\phi_{s0}(x, y) \delta n_m}{(\Delta\phi_{s1}(x, y) - \Delta\phi_{s0}(x, y))}, \quad (4)$$

for the stripped section of the fiber. For the non-stripped portion one can calculate similarly for $r_c(x, y)$ and $n_c(x, y)$, respectively.

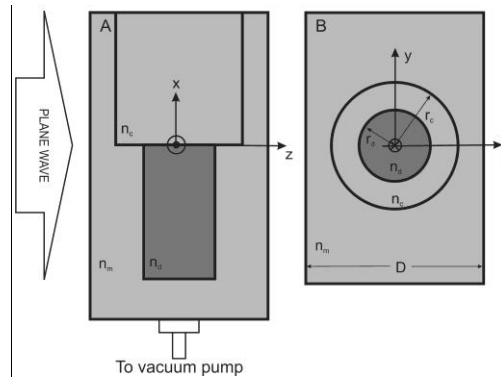


Figure 2. Schematic representation of the partially stripped optical fiber introduced in the glass chamber and the coordinate system. Side view of the system in panel A and panel B shows a down-top view. n_m : index of refraction of the medium, n_c , r_c index of refraction and radius of the non-stripped portion of the optical fiber, n_d , r_d = index of refraction and radius of the stripped portion of the optical fiber, D = length of the glass chamber.

To avoid the process of emptiness and refill of the glass chamber with liquids of different index of refraction, we propose to change the air pressure of the chamber to obtain the required δn_m . The introduced change of the index of refraction has been calibrated by using a conventional approach based on the fringe migration on a Michelson type

interferometer [5]. From that calibration the change of the index of refraction in the chamber as a function of the air pressure P (in cm Hg) is given by:

$$\delta n_m = 4 \times 10^{-6} P. \quad (5)$$

3. Results

To produce the two phase difference maps, the pressure P in the chamber has been changed from 0 to 15000cmHg. According with the calibration equation (5) this pressure change introduces a variation on the index of refraction of medium $\delta n_m = 0.06$. With this change the two phase differences were introduced in equations (3) and (4) to obtain the values for the index of refraction and topography for the optical fiber.

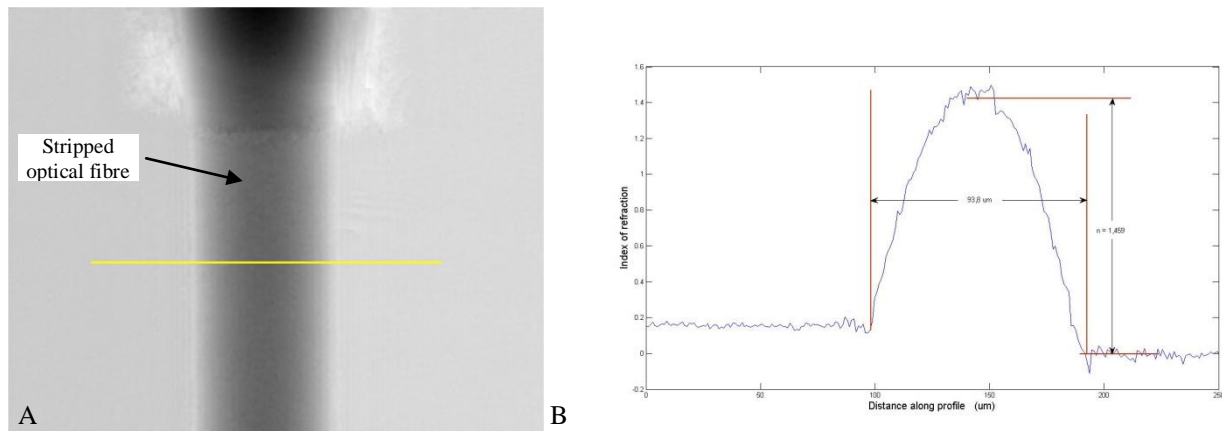


Figure 3. In panel A index of refraction map of the optical fiber for $P = 50$ cm Hg and in panel B profile of the index of refraction calculated along the yellow line of the panel A.

From equations 3 and 4, maps for the radius and index of refraction of the stripped portion of the optical fiber are computed. Regions of interest are therefore chosen on the maps and averages of the values are considered as the measured parameters. On the stripped region a radius of $r_d = 46.9 \pm 0.3$ and an index of refraction $n_d = 1.459 \pm 0.013$ were the measured parameters. These two values are in good agreement with those provided by the manufacture of the optical fiber $r_d = 50 \mu\text{m}$ and $n_d = 1.455$. For the non-stripped region the method here proposed provides a $r_c = 84.1 \pm 0.3 \mu\text{m}$ and $n_c = 1.423 \pm 0.013$ for this region the manufacturer does not provide information.

In summary, we have presented a method to unscramble the topography and the index of refraction in interferometry essays. The method changes the index of refraction of the surrounding medium by modifying the pressure of the glass chamber. This dry method avoids the sometimes fairly complicate change of oily liquids in the chambers. The method has been applied for measuring the index of refraction and topography of an optical fiber.

4. References

- [1] Charrière F., A. Marian, F. Montfort, J. Kühn, T. Colomb, E. Cucho, P. Marquet, Ch. Depeursinge, "Cell refractive index tomography by digital holographic microscopy," *Opt. Lett.* 31, 178-180 (2006).
- [2] Benjamin Rappaz, Pierre Marquet, Etienne Cucho, Yves Emery, Christian Depeursinge, and Pierre Magistretti, "Measurement of the integral refractive index and dynamic cell morphometry of living cells with digital holographic microscopy," *Opt. Express* 13, 9361-9373 (2005).
- [3] F. A. Monroy-Ramírez and J. Garcia-Sucerquia, "Optical Fibre Characterization through Digital Holographic Microscopy", in *Digital Holography and Three-Dimensional Imaging*, Optical Society of America, paper JMA18. OSA/BIO MED/DH (2010).
- [4] Ch. J. Mann, L. Yu and M. K. Kim, "Movies of cellular and sub-cellular motion by digital holographic microscopy", *BioMedical Engineering OnLine* 2006, 5:21.
- [5] Volokhova, S. Ya., Kolesova, É. B., "Interferometer for evaluating the refractive index of air in: Measurement techniques", ISSN 1573-8906, Vol. 11 (8. 1968).

Measurement of Asymmetric Temperature Field by Using Digital Holographic Multidirectional Interferometry

Doleček Roman^{1,2}, Psota Pavel^{1,2}, Lédl Vít^{1,2}, Vít Tomáš^{1,2}, Václavík Jan^{1,2}, Kopecný Václav²

*1 research Centre TOPTEC
Institute of plasma physics ASCR
Sobotecká 1660
Turnov, Czech Republic*

*2 Technical University of Liberec
Studentská 2
Liberec, Czech Republic
pavel.psota@tul.cz*

Abstract: This paper presents a digital holographic method for measurement of periodic asymmetric temperature fields. The method is based on modified Twyman-Green setup, in which only one precisely synchronized and triggered CCD allows for the 3D measurement and reconstruction.

OCIS codes: (090.1995) Digital holography; (090.2880) Holographic interferometry; (100.6780) Temperature

1. Introduction

For the measurement of temperature field parameters it is essential to use contactless, non-invasive and very precise method. Digital holographic interferometry (DHI) matches the above mentioned criteria. It is whole-field, non-invasive and differential technique well established in industry and research. In DHI at least two holograms h_1 , h_2 of two wavefronts (the first one in an initial condition and the second one after the change of a temperature field) have to be recorded by a digital sensor. Digital holograms are interference patterns formed by a reference wave and the wave transmitting through the area of interest (measured temperature field). Let's assume that the temperature field is located at a distance d far from CCD. The numerical reconstruction is calculated by multiplication of digital holograms h_i with the complex amplitude of the reference wave r . Optical fields in the image plane U_i are calculated by the Sommerfeld formula which describes the diffraction of a light wave at the hologram in distance d far from the hologram. The Sommerfeld integral can be solved by Fresnel approximation which in discrete finite form can be written as:

$$U_i(n, m) = \exp\left(j\pi\lambda d \left[\left(\frac{n}{N\Delta\varepsilon}\right)^2 + \left(\frac{m}{M\Delta\eta}\right)^2 \right]\right) \times \sum_{k=1}^N \sum_{l=1}^M h_i(k\Delta\varepsilon, l\Delta\eta) r(\Delta\varepsilon, l\Delta\eta) \exp\left(\frac{j\pi}{\lambda d} \left((k\Delta\varepsilon)^2 + (l\Delta\eta)^2 \right)\right) \exp\left(-j2\pi \left(\frac{kn}{N} + \frac{lm}{M}\right)\right), \quad (1)$$

where $j = \sqrt{-1}$ and λ is the wavelength of the used light. The stored hologram consists of $N \times M$ discrete values. Physical pixels size of used CCD is $\Delta\varepsilon \times \Delta\eta$. The equation (1) can be solved effectively by the FFT-algorithm. Intensity I and phase φ distributions are determined by

$$I_i(n, m) = |U_i(n, m)|^2, \quad (2)$$

$$\varphi_i(n, m) = \arctan(\text{Im}(U_i(n, m)) / \text{Re}(U_i(n, m))).$$

If those two digital holograms are individually reconstructed (1) and their phase distributions are calculated (2), then the interference phase can be determined in a pointwise manner by a modulo 2π subtraction [1]. The interference phase and a refractive index change are linearly dependent. Combining the Gladstone-Dale relation, which relates the index of refraction to the density of a gas, with the ideal gas equation one could get the dependence of the refractive index on the temperature [1, 2]. Examination of asymmetric temperature fields could not be done generally without the use of tomographic approach which requires large number of different projections of measured field. Holographic setup, having several different observing directions, could be constructed [3], but the benefits of such complicated method are questionable. It would be necessary to use many digital sensors in the DHI measurement setup to obtain digital holograms for different viewing directions. However, for periodical coherent phenomena the problem can be solved in much smarter way - having only one digital sensor. The key point for such approach is in precisely synchronized and triggered capture time in relation to the proper phase of the measured

phenomenon. It allows either the measurement of very fast phenomena or to capture the area of interest from different directions.

2. Experimental setup and data processing

Fig. 1 shows the setup, which is based on the Twyman-Green type of holographic interferometer [4, 5]. This setup offers two-times higher sensitivity compared to Mach-Zehnder interferometer. Laser beam has wavelength 532 nm, power 150 mW. The beam is split by the polarizing beam splitter BS1 equipped with half wavelength retardation plates into two beams after the mechanical shutter. Beam 1 acts as a reference wave and the beam 2 acts as an object wave. The beams are spatially filtered and collimated. The object beam passes through the measured area twice, see Fig. 1. The reference wave and the object wave are recombined by another beam splitter BS2 and resulting interference pattern is captured by a digital camera. Used camera is AVT Stingray - F 504 with resolution of 2045×2056 pixels, each pixel having the size $3.45 \times 3.45 \mu\text{m}$. Images are transferred to the computer via Fire Wire B interface enabling the frame rate of 6.5 FPS. The image from camera – digital hologram – is cropped to 2048×2048 pixels.

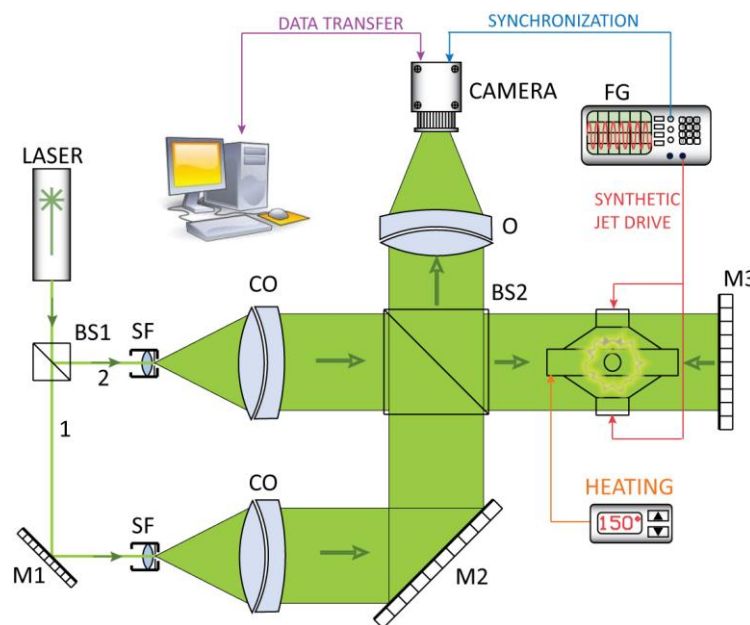


Fig. 1: Holographic setup for asymmetric temperature field measurement. (BS-beam splitter, M-mirror, SF spatial filter, CO-collimating objective, O-focusing objective, FG-function generator).

The object under investigation is synthetic jets (SJ) [6]. There are jets of fluid generated by pushing/pulling fluid through an orifice by the interactions within the train of counter-rotating vortex. SJ are generated by two actuators – blowers. The fluid is heated in space between blowers to increase refractive index difference in surrounding air and generated mass flux. The heating cartridge is heated on 150°C and the frequency of the synthetic jets is 15 Hz. To get the tomographic data it is necessary to obtain holograms from different viewing directions. Therefore the SJ is fixed on a rotation platform stage. The camera capture time is synchronized with the SJ puff driven by function generator with the help of an external trigger, which enables to capture the hologram with precisely defined delay. The coherence of the SJ phenomenon (self-similarity of repeated phenomena) allows to use the trigger to capture holograms in the same relative phase of the phenomenon in every cycle, see Fig. 2. Since the synchronization frequency is higher than the camera frame rate, the hologram is not captured after each synchronization signal but some cycles of the phenomenon are skipped. Therefore it is possible to measure very high frequency phenomenon with use of lower frame rate camera. During the measurement, firstly, the reference hologram of switched off steady state SJ was recorded. Subsequently, the sequence of digital holograms for relative delays starting at 0 ms with step 2 ms to 16 ms was captured. The whole measuring process was repeated for different viewing directions by platform stage rotation from 0° with step of 10° to 170° . The semi-automatic software application was developed for the reconstruction of the digital holograms. This way, all necessary data for 3D reconstruction were obtained.

3. Results

The consequence of triggering process of coherent SJ phenomenon is shown in Fig. 2. The showed pictures were captured for the angle of view 40° with 20 ms delay. The reconstructed 2D temperature fields correspond to the same time as well as for the same direction but in different periods of the repeated phenomenon. It can be easily seen that the temperature fields are nearly identical and the differences among them can be neglected for the tomographic reconstruction.

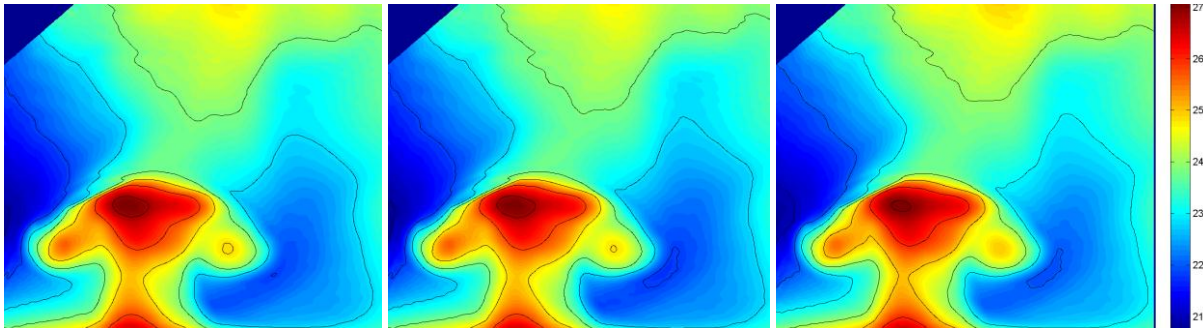


Fig. 2: The consequence of a precise camera and SJ synchronization: the temperature field distributions with angle of view 40° and the same relative time delay 8ms in different cycles of the periodical phenomenon.

The dynamic evolution of temperature field in time is shown in Fig. 3. The holograms were captured for angle 0° with time delays 0ms (left), 8ms and 16ms (right).

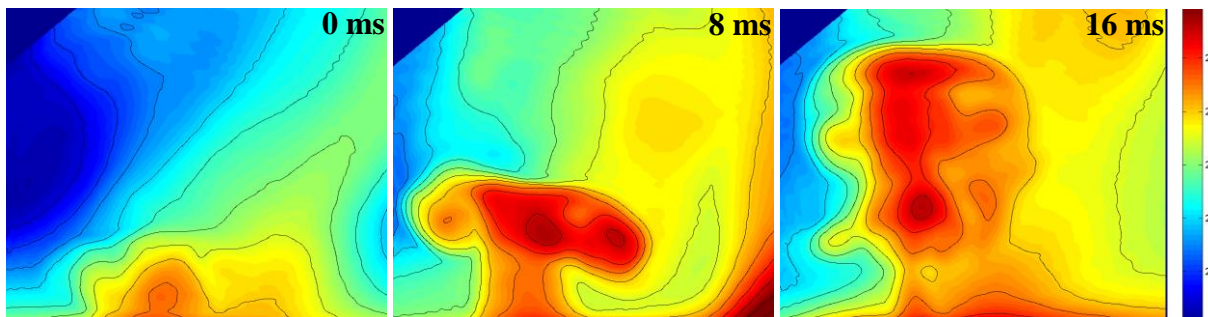


Fig. 3: The dynamic evaluation of temperature field: angle of view 0° in different relative delays.

The paper presents the simple way for asymmetric temperature field measurement with the use of tomography employing only one digital camera. Another paper dealing with data processing with the aim of getting the 3D volume data from the measurement is in preparation.

4. References

- [1] T. Kreis, *Handbook of Holographic Interferometry :Optical and Digital Method* (Berlin: Wiley , 2004).
- [2] U. Schnars and E. Jueptner, *Digital Holography* (Berlin: Springer , 2005).
- [3] M.Antoš, New three-dimensional configuration of multidirectional phase tomograph, *Proceedings of the SPIE*, pp.66090R-66095, (2007)
- [4] V. Lédl and T. Vít, "Identification of the temperature field in pulsatile impinging flow ," in *AIP Conference Proceedings*. (Italy, 2010), pp 135-138.
- [5] R. Doleček, V. Lédl, V. Kopecký, P. Psota, J. Václavík and T. Vít, "Prospects of digital holographic interferometry in heat transfer measurement," in *Experimental Fluid Mechanics*. (Liberec, 2009).
- [6] Z. Trávníček. and V. Tesař, 2003, "Annular synthetic jet used for impinging flow mass-transfer", *Int. J. Heat Mass Transfer*, 46, 3291–3297

Comparison of Digital Holographic Method for Very Small Amplitudes Measurement with Single Point Laser Interferometer and Laser Doppler Vibrometer

Psota Pavel, Lédl Vít, Doleček Roman, Václavík Jan, Šulc Miroslav

*Institute of Plasma Physics
Prague, Czech Republic
pavel.psota@tul.cz*

Abstract: This paper describes a measurement setup and measurement results of simultaneous measurement of small vibration by a recently developed digitally holographic method, single point laser interferometry and laser Doppler vibrometer.

OCIS codes: (090.1995) Digital holography; (120.7280) Vibration analysis; (120.3180) Interferometry

1. Introduction

Vibration analysis is very required tool in modern research and industry. In the market, there is a broad portfolio of measurement devices, which are usually based on Doppler phenomenon, correlation analysis, speckle ESPI and others. Another physical principle suited for vibration analysis is digital holography (DH). The DH based methods are non-invasive, very precise and in addition DH enables to measure displacement over the whole-field.

The experimentally easiest and the most often applied holographic method for vibration analysis is the time average holographic interferometry which was introduced by Powell and Stetson [1]. Unfortunately, for amplitudes smaller than approximately one tenth of the wavelength of used laser light, the time-average method reaches its limit of minimum measurable amplitude. This problem was solved by frequency shifted holographic interferometry introduced by Aleksoff [2]. In the frequency shifted holography the frequency of the reference wave is modulated by an integer multiple $n\omega$ of the object vibration frequency ω : $f_{ref}(t) = e^{jn\omega t}$. If the object wave U_p is not modulated and the reference wave U_R is modulated by f_{ref} , the resulting intensity in the hologram plane at time t is proportional to: $I(t) = |U_p + f_{ref}(t)U_R|^2$. Using solution of interference holographic equation and properties of Bessel functions we obtain: $I(p) = |U_{jn}|^2 = J_n^2(d(p)e(p))$. Frequency shifted holography is used to increase the sensitivity for vibrations with small as well as with large amplitudes. $J_0^2(0)$ is unity in time average holography with no modulation, and has zero slope (the derivative is constant). For the small amplitudes, it is difficult to determine significant intensity variation in the bright field. On the other hand $J_1^2(0)$ has a positive slope in the dark field yielding visible intensity variations even for small amplitudes. This is the key of the method. The smallest detectable amplitude was estimated by Ueda, Miida and Sato[3] as $d(p) \approx \lambda/3500$.

Typical analogue recording media being used in past in holography did not have uniform and repeatable response. Therefore it was impossible to determine quantitative values of amplitude precisely. The measurement usually served for estimation of both vibration amplitudes and for mode structure determination.

In recent years, the resolution of CCD or CMOS have reached such a resolution. It is possible to capture micro-interference pattern with high spatial resolution, which led to rising of digital holography. Moreover, modern digital cameras bring the advantage of very uniform and repeatable response and they can be considered as a radiometric detector. This fact led to development of digital holography method for measurement of very small amplitude which enables to determine quantitative values of amplitude precisely [4]. The method is based on the application of frequency shifted digital holography with the employment of phase shifting principles. Phase shifting reduces the noise rapidly. Low overall noise is a key factor to get a very high resolution of the method. The frequency shift as well as the phase shift is realized by proper setting of Bragg cells in the holographic setup.

The method was successfully used for measurement of ring and disc piezoelectric transformers [5]. However, it is necessary to verify the reliability of the method and determine the measurement error. The reliability of the method was tested by simultaneous measurement of unimorph membrane for different excitation voltages by

holographic method, commercial vibrometer based on Doppler principle and single-point laser Michelson interferometer [6].

2. Experimental setup and data processing

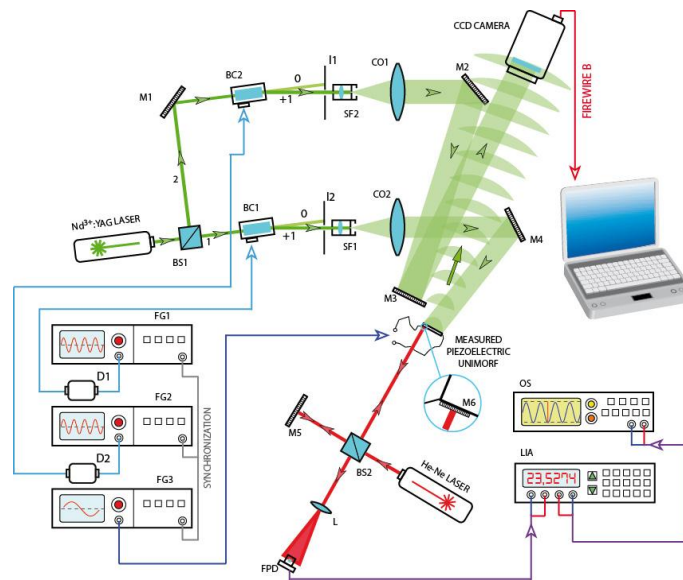


Fig. 1: Holographic and interferometric setup for small amplitude vibration measurement. (BS – beam splitter, M – mirror, SF – spatial filter, CO – collimating objective, O – focusing objective, FG – function generator, OS – oscillator, LIA – lock-in amplifier, L – lens, FPD – fast photodiode).

Fig. 1 shows the measurement setup which includes two of three mentioned measurement methods. Considering the readability of the scheme, the vibrometer measurement is not depicted there. Digital holographic measurement is based on the Mach-Zehnder type of holographic interferometer. The laser beam has wavelength 532 nm and power 100 mW. The beam is split by the polarizing beamsplitter equipped with half wavelength retardation plates into two beams after the mechanical shutter. The first beam acts as a reference wave. Each beam is frequency shifted by an acousto-optic frequency modulator (Bragg cell) with a fundamental frequency of 40 MHz. The beams are spatially filtered and collimated. The reference beam hits CCD after two reflections on mirrors M2 and M3. The object beam illuminates the sample and the light scattered from its surface is impinging the CCD sensor. The setup is designed as an off-axis Leith-Upatnieks scheme. The angle between the beams is set to be approximately 3° . The camera is AVT Stingray - F 504 with resolution of 2452 x 2056 pixels, each pixel having the size 3.45 x 3.45 μm . The image from camera – digital hologram – is cropped to 2048 x 2048 pixels. The sequence of 16 frames was captured.

For the Michelson interferometric measurement a stabilized He-Ne laser with a wavelength of 632.8 nm is used as a light source. The beam is divided by a beamsplitter BS2 to two interferometer arms. The sample with the mirror M6 is placed at the first arm. The sample can vibrate with the frequency of the applied electric field from AC source. An active element, holding a constant phase difference $\pi/2$ between waves from both arms, is situated in the second reference arm. Beams are joined after reflection, and the interference pattern is projected to the photodiode by the lens. The lock-in amplifier LIA and, simultaneously, the scope OS are used for signal detection. A computer is used for experiment control and data acquisition. With use of lock-in amplifier technique the Michelson interferometer enables to measure amplitudes in the order of 10^{-12}m .

The vibrometer was precisely set to measure in the same point as the interferometric method. Since the holographic method measures in a whole-field, after the data evaluation, it was necessary to consider just the values, which correspond to single-point methods.

The object under investigation is piezoelectric unimorph membrane. The measurement was realized for three different driven frequencies: 2 kHz, 9 kHz and 13 kHz. The set of measurement for different excitation voltages amplitudes (10V, 20V, 30V, 50V, 100V, 200V) was performed on the unimorph at every frequency. Due to thermal properties and relevance of measurements, the different method measurements were done in the same time.

3. Results

The measured data for 13 kHz drive frequency obtained by simultaneous measurement are plotted at Fig. 2. From the physical point of view, the linear behavior was predicted. Therefore, deviation from linearity as a reliability factor was also calculated and visualized at Fig. 2. The relative deviations between methods are plotted at Fig. 3. On the basis of obtained data, one may claim that all methods fulfill linearity requirements. The deviation between methods (especially for amplitude bigger than 1 nm) is in tolerance range of the methods. The interferometric lock-in method and the vibrometer based method are considered as a reliable and precise method and it was shown, that the holographic method has comparable parameters in the measurement range.

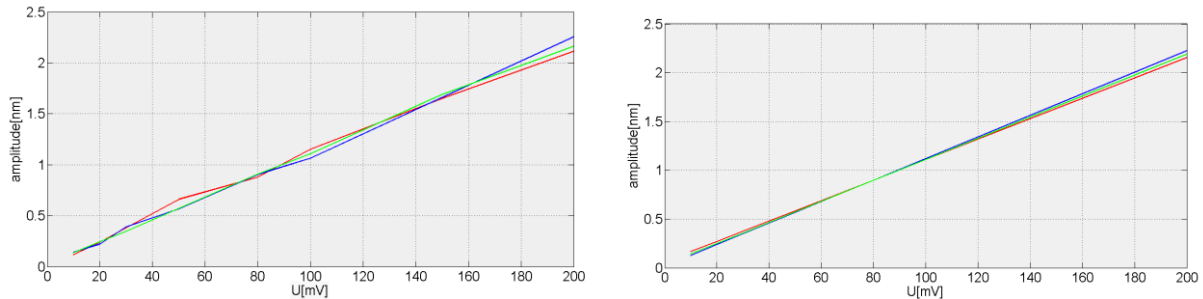


Fig. 2: Left: the measured data (holographic method – blue line, vibrometerbased method – green line, interferometric lock-in method – red line); Right: linear regression of measured data. The linearity of holographic method, vibrometer based method and interferometric lock-in method are 99.72%, 99.85% and 99.55%.

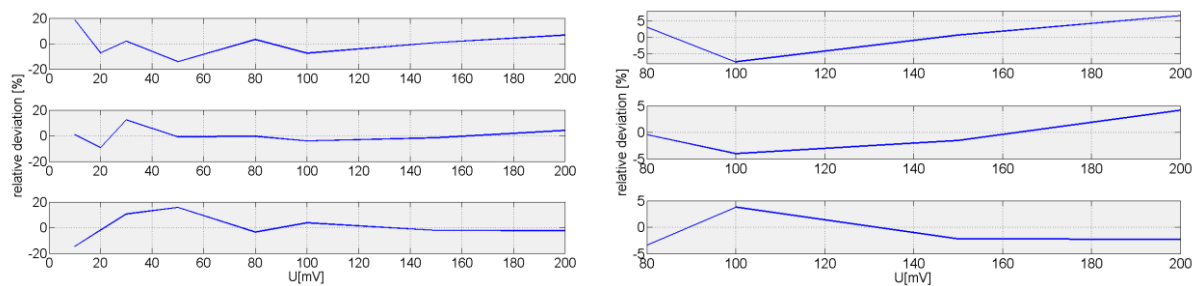


Fig. 3: Left: a) relative deviations between holographic and interferometric method (the average deviation is 7,513%), b) relative deviations between holographic and vibrometer method (the average deviation is 4,25%) and c) relative deviations between vibrometer and interferometric method (the average deviation is 6,85%); Right: relative deviations between methods for amplitudes greater than approximately 1nm with average deviation 4.47%, 2.54% and 2.93% .

4. References

- [1] R.L. Powell and K.A. Stetson, "Interferometric vibration analysis by wavefront reconstruction," J. Opt. Soc. Am. **55** (12), 1593–1598, 1965.
- [2] C. C. Aleksoff, "Temporally Modulated Holography," Appl. Opt. **10**, 1329-1341, 1971.
- [3] M. Ueda, S. Miida, and T. Sato, "Signal-to-noise ratio and smallest detectable vibration amplitude in frequency-translated holography: an analysis," Appl. Opt. **15**, 2690-2694, 1976.
- [4] V. Lédl, J. Václavík, R. Doleček and V. Kopecký, "Frequency Shifted Digital Holography for the Measurement of Vibration with Very Small Amplitudes," AIP Conf. Proc. 1253, **415**, 2010.
- [5] V. Lédl, P. Psota, R. Doleček, J. Erhart, V. Kopecký, "A digital holographic method for the measurement of piezoelectric transformers vibrations," The 20th IEEE International Symposium on Applications of Ferroelectrics International Symposium on Piezoelectric Force Microscopy & Nanoscale Phenomena in Polar Materials, 2011.
- [6] M. Sulc, in *Interferometry Principles and Applications*, edited by M E Russo, Nova Science Publishers, ISBN: 978-1-61209-347-5, 2011, pp. 55-94.

New Calculation Method for Quadrature Phase-shifting Interferometer and Its Application to Digital Holography

* Suezou Nakadate,¹ Tomohiro Kiire,² Shinya Sawada¹ and Masato Shibuya¹

¹Dep. of Media and Image Tech., Faculty of Engineering, Tokyo Polytechnic University, 1583 Iiyama, Atsugi, Kanagawa 243-0297, Japan

²Center for Optical Research and Education, Utsunomiya University, 7-1-2 Yoto, Utsunomiya, Tochigi 321-8585, Japan

*e-mail: nakadate@mega.t-kougei.ac.jp

Abstract: A new calculation method for a quadrature phase-shifting interferometer is presented and its application to digital holography is also described. Two sets of quadrature phase-shifted interferograms or holograms are acquired and the new calculation method proposed gives the phase distribution of the wavefront measured. The principle of the calculation method with computer simulations and its application to digital holography with experimental results are given.

OCIS codes: (120. 3180) Interferometry; (090. 1995) Digital Holography

1. Introduction

Quadrature phase-shifting interferometer(QPI) has been proposed for fast acquisition of phase information of a target object, and it has been applied to digital holography to obtain the entire information in a wavefront. The digital interferometer including holography has recently been enhanced by improvement in throughputs of computers and by advancing high resolution and sensitivity in imaging devices. This phase-shifting digital interferometer (PSDI) also has the advantage of providing high quality wavefront measurements, and phase-shifting digital holography(PSDH) and phase-shifting speckle interferometry(PSSI) which are regarded as interferometry for diffuse object. Fresnel transformation of digital hologram provides a method of three dimensional image reconstruction using low-resolution imaging device. High-speed phase measurement however is required for the PSDI, PSDH and PSSI when an object is in motion. Ordinary phase-shifting interferometry for high-speed measurements needs three or more imaging sensors that detect simultaneously the irradiance of each phase-shifted fringe pattern located spatially. It is somewhat troublesome to use multiple cameras to the PSDIs because the position of each image sensor must be adjusted precisely pixel by pixel in order to obtain the phase information accurately. As an alternative method, there is also a high-speed method adopting a pixelated mask in which each pixel of an image sensor has a particular amount of phase-shift with a micro-optic array and in which the phase at the pixel is calculated as the representative of a group of pixels. However, phase shift error among adjacent pixels may cause phase errors of the measurement especially in PSDH and PSSI because the size of speckle on the image sensor by a scattered object is extremely small. To solve the above problems simultaneously, it is necessary either to decrease the pitch of the pixels in the imaging sensor or to reduce the number of phase-shifting fringes extracted from the image acquired at the instant state in the temporally changed interferometer.

We have previously proposed a quadrature phase-shifting interferometer (QPI) in which the phase sum and the difference between the two states in the interferometer changed temporally can be obtained [1]. In this paper, we propose a new calculation method to obtain the phase distribution of an interferogram in the QPI. Its verification with computer simulations and its application to digital holography with experimental results are also presented.

2. Principle

In this section, we describe the principle of the phase calculation method in PSDI with computer simulations.

The Phase Calculation Method for QPI

An example of ideal setup for QPI(PSDH) is shown in Fig.1, which records simultaneously two fringe patterns(holograms) in quadrature. Suppose that two sets of two fringe patterns in quadrature are acquired before and after the change in the interferometer varying temporally. The quadrature phase-shifted fringe patterns before the change in the interferometer can be expressed by

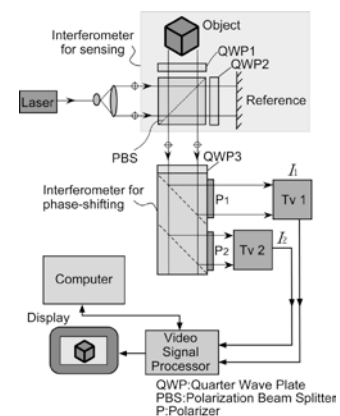


Fig.1. Setup for ideal quadrature phase-shifting digital Interferometer.

$I_1 = A + B \cos \theta$, $I_2 = A - B \sin \theta$, and after the change in the interferometer, the intensities of fringe patterns in quadrature are also written as $I_3 = A + B \cos(\theta + \varphi)$, $I_4 = A - B \sin(\theta + \varphi)$, where the original phase of the interferometer is expressed as θ and the phase difference between the change in the interferometer is written as φ , which can be known or unknown values due to such environmental disturbances, object or reference displacement. The bias and modulation factor of the interferogram are expressed by A and B respectively. Then the square of modulation term B can be expressed with $I_1 - A$, $I_2 - A$, $I_3 - A$, and $I_4 - A$ using the equation of $\cos^2 \theta + \sin^2 \theta = 1$ as follows,

$$B^2 = (I_1 - A)^2 + (I_2 - A)^2 = (I_3 - A)^2 + (I_4 - A)^2. \quad (1)$$

This equation is solved for the bias term A to yield the following equation,

$$A = \frac{I_3^2 + I_4^2 - I_1^2 - I_2^2}{2(I_3 + I_4 - I_1 - I_2)}. \quad (2)$$

Substitute his term A to the intensities of the interferograms, the phase θ in the interferograms is calculated as follows,

$$\theta = \tan^{-1} \left(\frac{-(I_1 - I_2)^2 - (I_2 - I_3)^2 + (I_2 - I_4)^2}{(I_1 - I_2)^2 - (I_1 - I_3)^2 - (I_1 - I_4)^2} \right). \quad (3)$$

Here, in order to obtain a phase over the whole range of 2π radians, set both of the denominator and numerator's sign a plus if $I_3 + I_4 - I_1 - I_2 > 0$, whereas set both of them a minus if $I_3 + I_4 - I_1 - I_2 < 0$. Thus the phase θ of the interferogram can be obtained excepting for $I_3 + I_4 - I_1 - I_2 = 0$, and this ill condition is caused by both of the denominator and numerator in Eq.3 approaching zero simultaneously. In practice the equation of $I_3 + I_4 - I_1 - I_2$ is equal to $2\sqrt{2}B \cos(\theta + \varphi/2 + 3\pi/4) \sin(\varphi/2)$ and the zeros of this equation are same as them of both the denominator and numerator in Eq.3. One of the ill conditions, $\sin(\varphi/2) = 0$, implies that the phase difference φ must not become zero, namely either the object or the interferometer must change in this techniques. The other one is occurred when the phase $\theta + \varphi/2$ is equal to $3\pi/4$ or $-\pi/4$ radians. This fact shows that the resultant phase has two noisy points over the whole range of 2π radians, which is half the number of this type of ill condition compared to the method proposed before[1]. The phase noise caused by the ill condition can be avoided by using spatially smoothed data of the denominator and numerator in Eq.3.

By the similar calculations described above, the phase $\theta + \varphi$ of the interferograms after the changing in the interferometer is also obtained by the following equation,

$$\theta + \varphi = \tan^{-1} \left(\frac{-(I_1 - I_4)^2 - (I_2 - I_4)^2 + (I_3 - I_4)^2}{(I_1 - I_3)^2 + (I_2 - I_3)^2 - (I_3 - I_4)^2} \right). \quad (4)$$

The phase difference φ can be also calculated using two resultant phases $\theta + \varphi$ and θ .

Computer Simulations

To verify the phase calculation method mentioned above a simple computer simulation is performed. Phase-shifted fringes in lens testing for the wavefront measurement are generated with 512×512 pixels and 256 gray levels for contrast of unity. The original phase θ is assumed that the amounts of all aberration of spherical, comma, astigmatism are the same of λ which is the wavelength of light and the tilting of the reference wave is 2λ . The fringe patterns in quadrature are shown in Fig.2(a) and (b). As the phase change φ the defocus of testing lens is caused by 2λ and its fringe patterns in quadrature are shown in Fig.2(c) and (d). The phases calculated by using Eqs.(3), (4) and the phase difference are shown in Fig.3(a) –(c), respectively. The resultant phases show that the phase can be calculated over whole range of 2π radians. However some noises are occurred especially in the central part of the phase images, and these will be singular points caused by the ill condition described above.

3. Experimental Results for Digital Holography

The experimental setup is shown in Fig.4, in which we utilized the Twyman-Green polarization interferometer and a single image sensor is adopted for the experimental verification of this QPI method avoiding phase calculation errors caused by position mismatching with each image sensor. A He-Ne laser is used as the light source for wavelength of 632.8nm and an output power is 15mW. No imaging lens is used in the setup so that we could detect signals from objects directly using a charge-coupled device (CCD)

with a resolution of 640×480 pixels. A glass slide base plate with a 15mm step is used as the scattering object. Its surface has been sprayed with eggshell white paint upon which the letters “t” and “p” are printed in black on the base plate and the step of the object, respectively. Phase shifting at the hologram plane is induced by displacement of a mirror mounted on a piezoelectric transducer (PZT) in the reference beam. Four holograms are recorded with shifting phases equally in a step of 90 degrees. These holograms are used to calculate the phase of them by the QPI method. Phase image made of 640×480 pixels are cut out and copied the data at the bottom of the image to yield 512×512 pixels for the Fourier transform which is shown in Fig.5(a) by using this QPI method. The object images reconstructed from the phase holograms shown in Fig.5(b) and (c) by the convolution method. The distances z in the reconstruction images shown in Fig.5(b), (c) are 2.3 and 2.5, respectively, where z means the distance from the CCD to the object planes with respect to an arbitrary unit distance which is not to be a physical distance in this interferometer. The phase hologram calculated by the QPI method is noisy compared to that by the four-bucket method because of the singular point in the phase calculation for the QPI method. However both images of the letters reconstructed at each distance can be observed clearly. This result shows that this QPI method will be useful for 3D image reconstruction using digital holograms.

4. Conclusion

We have demonstrated the new calculation method for quadrature phase-shifting interferometer. The method described is applicable to fields such as digital holography and provides us with 3D image reconstruction of a moving object that is feasible with the hologram obtained in this high-speed QPI.

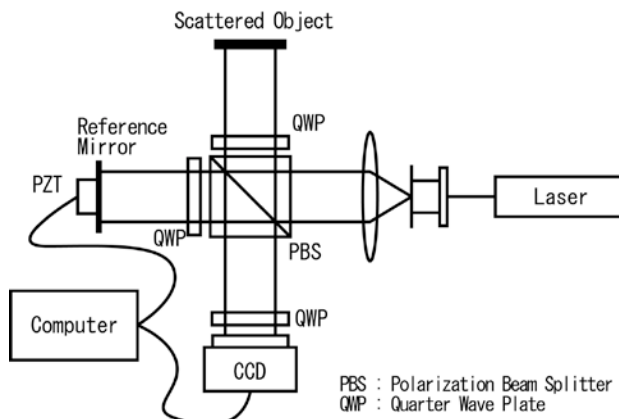


Fig4. Experimental setup of quadrature phase-shifting digital holography for feasibility study of ideal setup shown in Fig.1.

5. References

- [1] T. Kiire, S. Nakadate, M. Shibuya “Digital holography with a quadrature phase-shifting interferometer,” *Appl. Opt.* **48**, 1308-1315 (2009).

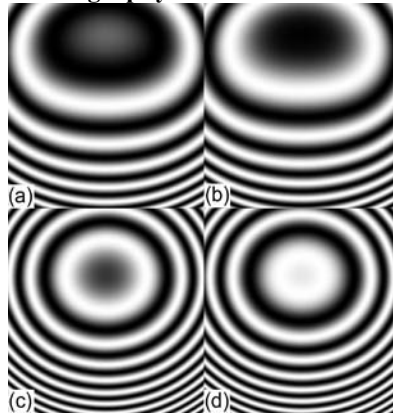


Fig.2. Fringes in quadrature (a), (b) before defocusing of lens, (c), (d) after the defocusing.

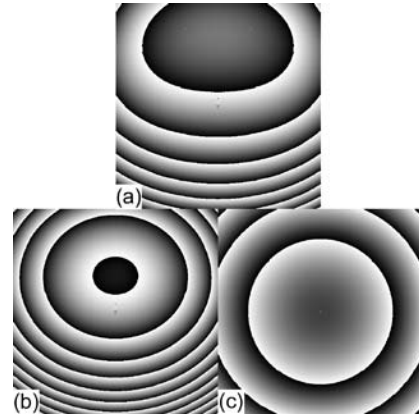


Fig.3. Resultant phases (a), (b) using Eqs.(3) and (4), respectively, (c) the phase difference between (a) and (b), which is proportional to the defocusing of lens.

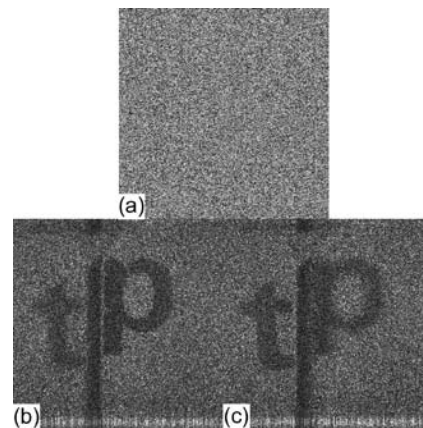


Fig5. (a) Phase distribution calculated by this method, and (b), (c) reconstructed images focused on the respective letters “p” and “t”.

High fidelity reconstruction of three-dimensional objects by FINCH fluorescence microscopy

Nisan Siegel^{1,2}, Joseph Rosen^{1,2,3}, and Gary Brooker^{1,2*}

¹*Department of Biomedical Engineering, Johns Hopkins University, 9605 Medical Center Drive,
Rockville, Maryland 20850 USA*

²*Microscopy Center, Johns Hopkins University Montgomery County Campus,
Rockville, Maryland 20850 USA*

³*Department of Electrical and Computer Engineering, Ben-Gurion University of the Negev, P.O. Box 653, Beer-Sheva 84105, Israel
*gbrooker@jhu.edu*

Abstract: FINCH holography produces super-resolved images above and below the focal plane of the microscope objective but with different magnifications. A method is presented to faithfully reconstruct 3D objects with dimensional fidelity.

© 2012 Optical Society of America

OCIS codes: (090.1760) Computer holography; (100.6890) Three-dimensional image processing; (110.0180) Microscopy;; (180.2520) Fluorescence microscopy; (180.6900) Three-dimensional microscopy. (090.1995) Digital holography.

1. Introduction

An important property of holographic microscopy is the collection of all of the three-dimensional (3D) optical data from objects in a 3D field with few or a single exposure, as opposed to the laborious standard optical methods of collecting stacks of 2D images as the sample or objective is moved to each plane of focus in the 3D volume. Fresnel Incoherent Correlation Holography (FINCH) [1-3] is a hybrid technique that has recently been introduced and which offers significant promise for recording three-dimensional information from incoherent sources such as fluorescent objects. In FINCH, the hologram is created from a complex Fresnel hologram from each point source in an incoherently emitting object, using a single beam geometry. FINCH faithfully reproduces objects above and below the optical plane of focus. However, as in optical imaging, the transverse magnification changes based on the longitudinal distance of objects from the focal plane of the input lens with the exception that objects above and below the focal plane are in focus with FINCH and out of focus by standard optical imaging (see Fig. 1). To date, the analysis of FINCH has been done most thoroughly for objects at the focus of the microscope objective [1-5].

Recently we have shown that FINCH microscopy is inherently super-resolving in the lateral dimensions at the focal plane in comparison to conventional microscope imaging using the same optics [6]. This sets the stage for gathering the full 3D field of an object in a few exposures, but also in capturing the field at higher resolution than is possible by standard optical methods. However, in order to fully exploit the superior resolution properties of FINCH microscopy, it is necessary to understand what the optical effects are of placement of the object at positions other than at the focal plane of the objective. We have analyzed these effects both theoretically and experimentally for a FINCH fluorescence microscopy system. This information has allowed us to reconstruct objects with high dimensional and image fidelity throughout the volume captured by FINCH holograms. The displacement Δz_s of the object away from the focal plane of the objective, or an object with significant depth, will result in the alteration of the light cones used to create the FINCH hologram, as shown in Fig. 1, which will in turn affect the final reconstructed images. The curve of the reconstruction depth z_r as a function of Δz_s reaches a minimum or maximum near $\Delta z_s = 0$, so that 3D images are best taken above or below this object plane for simplicity of reconstruction. Equation (1) shows the dependence of transverse magnification (M_T) on Δz_s , where f_0 is the focal length of the objective, z_s is the distance of the object from the objective, d is the distance from the objective to the SLM, and z_h is the distance from the SLM to the CCD:

$$M_T = \frac{z_h}{f_0} \quad \text{for } z_s = f_0 \quad \text{and} \quad \frac{z_h f_0}{z_s(f_0 - d) + f_0 d} \quad \text{for } z_s \neq f_0 \quad (1)$$

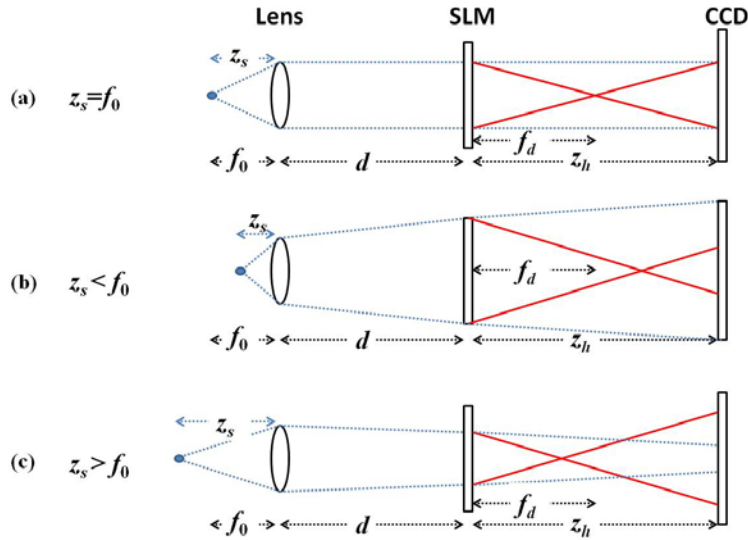


Fig. 1: FINCH with the object (a) at the focus of the collimating lens, (b) above the focus of the collimating lens and (c) below the focus of the collimating lens. f_d refers to the focal length of the diffractive lens pattern displayed on the SLM; all other variables are defined in the text. The diagram describes a static FINCH system operating on an object with significant depth above and below the focus of the collimating lens, thus f_0 , d , f_d and z_h remain constant over the three subdiagrams.

2. Methods

The fluorescence microscope apparatus and FINCH holography setup used in these experiments was configured exactly as previously described [6]. Holograms were captured at various distances Δz_s above and below the objective plane of focus of a single plane fluorescent USAF slide. The best-focused reconstructed image was calculated for every position of Δz_s .

3. Results and Discussion

As can be seen in Fig. 2, good super resolution images could be obtained above and below the plane of focus. The ability to resolve the small features in the group 9 objects was a test of the super resolving ability of FINCH as shown in our previous work [6]. However, the reconstructed image size was either smaller below the plane of focus or larger above the plane of focus. By using Eq. (1) we scaled the magnification of each image to the magnification at $\Delta z_s = 0$ by resampling. 3D stacks of images covering displacements of the USAF object over 30 microns in z_s are shown in Figure 3. The non-adjusted stack shows distortion due to the perspective effect of varying M_T , which

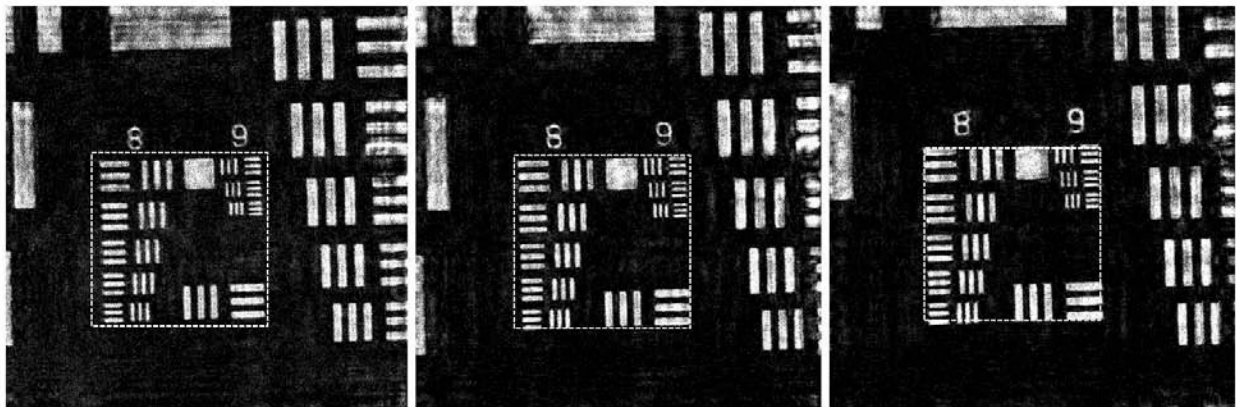


Fig. 2: The best focused reconstructed FINCH images from selected values of Δz_s . The dashed squares on the reconstructed images show that in reference to images calculated from the hologram captured at the focus of the objective (center image), the reconstructed images when the objective was 19 microns above focus (left) or 12 microns below focus (right) from the optical plane were either smaller or larger.

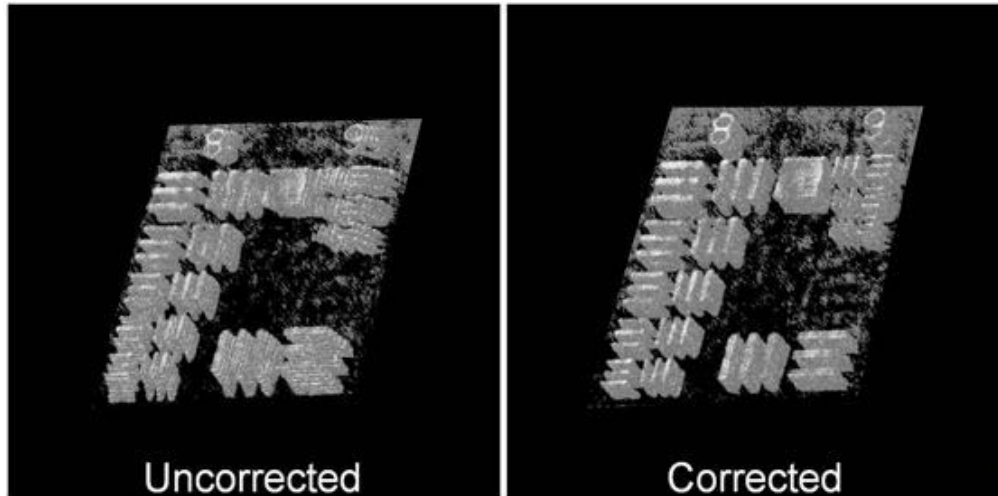


Fig. 3. 3D views (by direct volume rendering) of stacks of reconstructed images of the USAF pattern taken at z_s ranging from $30\ \mu\text{m}$ above f_0 to f_0 . The left image is the 3D view of images that have not been corrected for varying magnification. The right image is the 3D view of the reconstructed images that were resampled based on the ratio of magnifications as discussed in the text, and registered to lie directly over each other creating a clear well resolved 3D image. Notice that without correction, the smallest features in group 9 patterns are severely distorted, limiting resolution of 3D images.

makes the 3D reconstruction an inaccurate representation of the actual structure. The adjusted stack is free of the perspective effect and is thus a more clear and accurate representation of the object, an improvement that is even more significant when imaging very small objects. Note that by choosing as the M_T index the image with the highest M_T in the stack, the resampling of the lower- M_T images does not result in a loss of information.

4. Conclusions

We have shown FINCH imaging to resolve better than a corresponding widefield microscope both above and below the objective plane of focus, using a single FINCH configuration to capture images of a planar object translated with respect to the objective. It is possible, without loss of information, to adjust each image in a stack of reconstructed images from a FINCH hologram to match the size of the highest magnification image so that objects in 3D space can be reproduced with high resolution.

5. Acknowledgements

This work was supported by NIST ARRA Award No. 60NANB10D008 to GB, The Israel Ministry of Science and Technology (MOST) to JR and by Celloptic, Inc.

6. References

1. J. Rosen and G. Brooker, "Digital spatially incoherent Fresnel holography," *Opt. Lett.* **32**, 912-914 (2007).
2. J. Rosen and G. Brooker, "Non-scanning motionless fluorescence three-dimensional holographic microscopy," *Nat. Photon.* **2**, 190-195 (2008).
3. G. Brooker, N. Siegel, V. Wang, and J. Rosen, "Optimal resolution in Fresnel incoherent correlation holographic fluorescence microscopy," *Opt. Express* **19**, 5047-5062 (2011).
4. B. Katz and J. Rosen, "Could SAFE concept be applied for designing a new synthetic aperture telescope?," *Opt. Exp.* **19**, 4924-4936 (2011)
5. P. Bouchal, J. Kapitan, R. Chmelik, and Z. Bouchal, "Point spread function and two-point resolution in Fresnel incoherent correlation holography," *Opt. Express* **19**, 15603-15620 (2011).
6. J. Rosen, N. Siegel, and G. Brooker, "Theoretical and experimental demonstration of resolution beyond the Rayleigh limit by FINCH fluorescence microscopic imaging," *Opt. Express* **19**, 26249-26268 (2011).

Key to Authors and Presiders

A

Aegerter, Christof - BSu5A.6
Agnieszka, Suchwalko - BSu5A.5
Alfano, Robert - BSu5A.11
Andersson, Linda - BSu5A.2
Andersson-Engels, Stefan - BSu5A.2

B

Backman, Vadim - BSu5A.10
Bajaj, Shailesh - BSu5A.10
Bartels, Kenneth - BSu5A.12
Barzda, Virgis - BSu5A.4
Bigio, Irving - BSu5A.3
Brooker, Gary - DSu5B.5
Busch, David - BSu5A.7
Buzalewicz, Igor - BSu5A.5

C

Calabro, Katherine - BSu5A.3
Choe, Regine - BSu5A.7
Czerniecki, Brian - BSu5A.7

D

Davis, Scott - BSu5A.8
Demers, Jennifer-Lynn - BSu5A.8
DeMichele, Angela - BSu5A.7
D'Hollander, Antoine - BSu5A.1
Doleček, Roman - DSu5B.2, DSu5B.3
Durduran, Turgut - BSu5A.7

F

Feldman, Michael - BSu5A.7
Fredriksson, Sarah - BSu5A.2
Fuchs, Dieter - BSu5A.1

G

Gambhir, Sanjiv - BSu5A.13
Garcia-Sucerquia, Jorge - DSu5B.1
Ghielmetti, Giulia - BSu5A.6
Ghosn, Eliver - BSu5A.13
Gisselsson, Anna - BSu5A.2
Guo, Wensheng - BSu5A.7

H

Herzenberg, Leonore - BSu5A.13
Himmelreich, Uwe - BSu5A.1
Holyoak, G. Reed - BSu5A.12

I

in't Zandt, Rene - BSu5A.2

J

Jans, Hilde - BSu5A.1

K

Kiire, Tomohiro - DSu5B.4
Kim, Myung - Presider
Kjellman, Pontus - BSu5A.2
Kopecký, Václav - DSu5B.2

L

Lagae, Liesbet - BSu5A.1
Lédl, Vít - DSu5B.2, DSu5B.3
Li, Xingde - Presider
Liu, Haichun - BSu5A.2

M

Mies, Carolyn - BSu5A.7
Mo, Weirong - BSu5A.9
Monroy-Ramirez, Freddy - DSu5B.1
Morris, Michael - BSu5A.8
Mutyal, Nikhil - BSu5A.10

N

Nakadate, Suezou - DSu5B.4

O

Olsson, Fredrik - BSu5A.2

P

Piao, Daqing - BSu5A.12
Podbielska, Halina - BSu5A.5
Pogue, Brian - BSu5A.8
Prescher, Jennifer - BSu5A.13
Psota, Pavel - DSu5B.2, DSu5B.3
Pu, Yang - BSu5A.11

R

Radosevich, Andrew - BSu5A.10
Rallapalli, Harikrishna - BSu5A.13
Ritchey, Jerry - BSu5A.12
Rogers, Jeremy - BSu5A.10
Rohrbach, Daniel - BSu5A.9
Rosen, Joseph - DSu5B.5
Rosen, Mark - BSu5A.7
Rosenberg, Jarrett - BSu5A.13

Key to Authors and Presiders

Roy, Hemant - BSu5A.10

S

Sandkuijl, Daaf - BSu5A.4
Sawada, Shinya - DSu5B.4
Schnall, Michael - BSu5A.7
Shibuya, Masato - DSu5B.4
Siegel, Nisan - DSu5B.5
Smith, Bryan - BSu5A.13
Sordillo, Laura - BSu5A.11
Šulc, Miroslav - DSu5B.3
Sun, Yi - BSu5A.11
Sunar, Ulas - BSu5A.9
Svenmarker, Pontus - BSu5A.2

T

Tchou, Julia - BSu5A.7
Tokarz, Danielle - BSu5A.4
Tuer, Adam - BSu5A.4

U

Upadhye, Sudeep - BSu5A.10

V

Václavík, Jan - DSu5B.2, DSu5B.3
Vande Velde, Greetje - BSu5A.1
Vanspauwen, Bram - BSu5A.1
Vít, Tomáš - DSu5B.2

W

Wieliczko, Alina - BSu5A.5

X

Xu, Can - BSu5A.2

Y

Yang, Yuanlong - BSu5A.11
Yodh, Arjun - BSu5A.7

Z

Zhang, Anqi - BSu5A.12

**2012 OSA
TOPICAL MEETING
AND EXHIBIT**

Biomedical Optics and Three-Dimensional Imaging

Biomedical Optics (BIOMED)

Digital Holography & 3-D Imaging (DH)

OSA[®]

The Optical Society

2010 Massachusetts Ave., NW
Washington, DC 20036 USA

www.osa.org/meetings